

Experimental and Modelling Studies on Liquid-Liquid Slug Flow Capillary Microreactors

Zur Erlangung des akademischen Grades eines

Dr.-Ing.

vom Fachbereich Bio- und Chemieingenieurwesen der Universität Dortmund
genehmigte Dissertation

vorgelegt von

M.Tech-Ing. Madhvanand N. Kashid

aus

Sonand, India

Tag der mündlichen Prüfung: 26.03.2007

1. Gutachter: Prof. Dr. David W. Agar

2. Gutachter: Prof. Dr. Stefan Turek

Dortmund 2007

Dedicated to My Mother

Acknowledgement

It is a great pleasure for me to acknowledge all the people who helped me to accomplish this dissertation. First and foremost, I wish to express my deep felt gratitude towards my supervisors, Prof. Dr.-Ing. David W. Agar and Prof. Dr. Stefan Turek, for giving me an opportunity to work in their groups. I am highly indebted for their insights, advice, encouragement, easy accessibility and freedom for work which helped me to explore new ideas and to complete the work in time. I am thankful to both of them for sharing ideas on many varied issues such as report writing, time management, presentation techniques etc. which helped me to develop my personal skills as well. *Thank you for being wonderful teachers!* I would also like to thank chairman of the doctoral commission, Prof. Dr.-Ing. Jakob Jörissen, and members, Prof. Dr.-Ing. Karl Strauß and Prof. Dr.-Ing. Eugeny Kenig, for evaluating my work.

I am grateful to my colleagues from both groups (Institute of Reaction Engineering and Institute for Applied Mathematics), who ensured a technically stimulating, creative and pleasant working environment and helped in technical and non-technical matters. My special thanks to Frank for his erudite assistance, which was instrumental in the completion of my work. He always extended his friendly hand for all types of helps during my stay in Dortmund which may take more than 5 pages to acknowledge. *Vielen Dank Franky!* Oftenly, I had very nice discussions with Jaroslav, Abderrahim, Shuren, Otto, Mudassar, Simone and Ekkehard on technical and non-technical issues through which I learnt many things. *Thank you guys for giving nice company!* My sincere thanks to Alrun, Susanne and Anja for their help in all administrative work. The help of our laboratory staff, especially Michael and Julian, was very important to complete the experimental part of my work. *Danke schön Michael und Julian!*

It would have not been possible to complete the work without the help of my coworkers. I would like to thank Ingmar (currently working at University of Kyoto, Japan) for his experimental help and fruitful discussions in the early stages of the work. I thank my coworker and friend, Yogesh (currently working at ETH Zurich, Switzer-

land), for his help in carrying out experiments, for sharing lot of ideas about this research topic, and for making the weekends more enjoyable. *Thank you, Brother!* I would also like to acknowledge David (currently working at InSTEC, Habana, Cuba) for helping me to carry out some CFD simulations using levelset method. The help of Rohan and Aras in carrying out experimental studies on mass transfer and chemical reactions is highly acknowledged. The assistance of Ameya in the experimental work and Digpalsinh and Amit in the proof reading of the thesis was also important.

I am grateful to my Guru, Dr. Vivek V. Ranade, National Chemical Laboratory, India, for his eternal inspiration and guidance which propelled my career towards a successful chemical engineering researcher. *Thank you Sir!* I am thankful to my friends Vivek (and Shruti Vahini) and Praveen (and Esther) for taking my care during their stay in Germany, which made me feel like home. I also thank to my friends who are working around the globe, Hrishikesh, Prashant, Ajay, Mohan, Tukaram, Ravi, Anand, Shubhada, Trupti, Abhijeet, Nitin, Amol, Yogesh and Sachin, for their best wishes. Many thanks to Indian students in Dortmund, Prasad, Raghunadh, Surendra, Rajarajan and Gaurav, who made my stay enjoyable.

I would like to thank my father, brother, sisters and sister-in-law (Vahini) for their blessings and nephews and nieces for their wishes without which it would have been difficult to complete the work. I wish to express my dearest feelings towards my brother for his guidance, invaluable support and inspiration which has always been a very important part of my success. I also express my dearest feelings for my mother, who has been with me almost until end of my work but could not see the completed dissertation. I dedicate this dissertation with deepest gratitude to her for her love and countless sacrifices. She would be more proud of this achievement than any other person.

Finally, I am thankful to those who have assisted me directly or indirectly in the completion of this work. Their assistance is invaluable and shall always be held in high regards.

Contents

List of Symbols	IX
List of Figures	XIII
List of Tables	XXI
Summary	XXIII
Summary in German (Kurzreferat)	XXV
1 Introduction	1
1.1 Process Intensification	1
1.2 Microreactor Technology	2
1.3 Liquid-Liquid Contacting	5
1.3.1 Conventional contactors	5
1.3.2 Liquid-liquid slug flow	7
1.4 Background and Motivation	12
1.5 Objectives, Methodology and Present Work	13
1.5.1 Objectives	13

1.5.2	Methodology and present work	14
1.6	Outline of the Thesis	16
I	Experimentation	19
2	Hydrodynamics	21
2.1	Introduction	21
2.2	Experimentation	23
2.3	Results and Discussion	25
2.3.1	Slug flow generation	25
2.3.2	Flow regimes	27
2.3.3	Slug size measurement	30
2.3.4	Interfacial area	34
2.3.5	Pressure drop across Y-junction	37
2.3.6	Pressure drop along the length of capillary	43
2.3.7	Power input	47
2.4	Summary	47
3	Mass Transfer and Chemical Reaction	49
3.1	Introduction	49
3.2	Experimentation	52
3.3	Results and Discussion: Mass Transfer	55
3.3.1	Extraction efficiency	55
3.3.2	Mass transfer coefficients	58

3.3.3	Comparison with conventional contactors	64
3.3.4	Interfacial area and overall mass transfer coefficients	67
3.4	Results and Discussion: Chemical Reaction	68
3.4.1	Neutralisation reaction	68
3.4.2	Chemical method for interfacial area	73
3.5	Summary	77
4	Flow Splitting	81
4.1	Introduction	81
4.2	Experimentation	83
4.3	Results and Discussion	85
4.3.1	Effect of viscosity	86
4.3.2	Effect of flow rate, flow ratio and capillary size	89
4.4	Summary	94
II	Modelling	95
5	Modelling of Fluid Flow	97
5.1	Introduction	97
5.2	Single Phase Modelling	101
5.2.1	Internal circulations and mixing	101
5.2.2	PIV experimentation	104
5.2.3	CFD modelling	106
5.2.4	CFD particle tracing	108

5.3	Two Phase Modelling	110
5.3.1	Slug flow generation	110
5.3.2	Numerical mesh, boundary conditions and solution	112
5.4	Results and Discussion	114
5.4.1	PIV	114
5.4.2	CFD simulations	114
5.4.3	CFD particle tracing	120
5.4.4	Two phase modelling	123
5.5	Summary	126
6	CFD Modelling of Mass Transfer and Chemical Reaction	127
6.1	Introduction	127
6.2	Numerical Model	128
6.2.1	Problem definition	128
6.2.2	Fluid flow	131
6.2.3	Mass transfer	131
6.2.4	Chemical reaction	133
6.2.5	Numerical mesh, boundary conditions and solution	133
6.3	Results and Discussion	136
6.3.1	Fluid flow	136
6.3.2	Mass transfer	137
6.3.3	Chemical reaction	140
6.4	Summary	146

7	Conclusions and Future Developments	147
7.1	Conclusions	147
7.2	Open Questions	149
7.3	Future Developments	151
	Appendices	157
A	Pressure Drop Models	159
A.1	Pressure Drop - Without Film	159
A.2	Pressure Drop - With Film	160
B	Theory of Extraction Efficiency and Mass Transfer Coefficients	165
B.1	Physical Mass Transfer:	165
B.2	Mass Transfer with Chemical Reaction:	166
C	Theory of Chemical Method for Effective Interfacial Area	167
D	Physico-chemical Properties	171
	Bibliography	173
	Curriculum Vitae	183

List of Symbols

A	Cross-sectional area of the capillary microreactor, m^2
a	Specific interfacial area, m^2/m^3
C	Concentration, mol/L
Ca	Capillary number, -
Ct	Contamination, %
C_{ij}	Concentration of i^{th} species in j^{th} phase, mol/L
d	Characteristic length, m
D_R	Diffusivity ratio, -
D_{ij}	Molecular diffusivity of i^{th} species in j^{th} phase, m^2/s
d_s	Diameter of slug, m
E	Extraction efficiency, %
f	Forces acting on the system, N
F_{SF}	Continuum surface force vector, N
Fo	Fourier number, -
h	Film thickness, m
$H(x, y)$	Heaviside function
I	Ionic strength, mol/L
ID	Internal diameter of capillary, m
K	Rate constant, L/mol s
k_L	Overall mass transfer coefficient, m/s
$k_L a$	Volumetric mass transfer coefficient, $1/\text{s}$
K_s	Salting out parameter, L/mol
L	Length of the microreactor, m
l	Length of the slug, m
m	Distribution or partition coefficient, -
\mathbf{n}	Surface normal vector
p	Pressure, N/m^2
P_c	Capillary pressure, N/m^2
Pe	Peclet number, -
Q	Volumetric flow rate, m^3/s
R_c	Radius of capillary, m

R_s	Radius of the slug, m
r	Radial distance, m
r_{ik}	Rate of generation/disappearance of i^{th} solute in k^{th} phase, mol/Ls
r_0	Radial position of stagnant zone, m
Ra	Volumetric extraction rate, mol/L s
Re	Reynolds number, -
Sh	Sherwood number, -
T	Residence or total calculation time, s
t	Time, s
t_F	Slug generation time, s
$U(r)$	Velocity inside the slug at radial position r, m/s
\mathbf{u}	Velocity vector, m/s
V	Flow velocity, m/s
V_p	Particle velocity, m/s
V_s	Slug velocity, m/s
V'	Hypothetical flow velocity, m/s
X	Position of interface, m
x	Cartesian coordinate, m
y	Cartesian coordinate, m
Z	Initial position of the particle, m
Z'	Position of particle after time Δt , m

Greek

ΔP	Pressure drop, N/m ²
ΔP_i	Pressure drop along i^{th} branch of Y-junction, N/m ²
ΔP_H	Hydrodynamic pressure drop, N/m ²
Δt	Time step, s
Ω	Domain
α	Phase fraction, -
β	Ratio of base in aqueous to acid in organic phase, -
γ	Interfacial tension, N/m
θ_w	Wall contact angle, ⁰
κ	Curvature, 1/m
λ	Wavelength, nm
μ	Dynamic viscosity, Pa-s
μ_R	Viscosity ratio, -
ν	Kinematic viscosity, m ² /s
ρ	Density, kg/m ³
σ	Surface tension, N/m

τ	Circulation time, -
ϕ	Physical property

Superscript

0	time $t = 0$
*	saturation
<i>in</i>	inlet
<i>n</i>	number of time step
<i>out</i>	outlet
<i>T</i>	time $t = T$

Subscript

1,2	phase 1 and 2
<i>aq</i>	aqueous phase
<i>av</i>	average
<i>CH</i>	cyclohexane
<i>max</i>	maximum
<i>or</i>	organic phase
<i>U</i>	slug unit
<i>W</i>	water
<i>w</i>	with film
<i>wo</i>	without film

List of Figures

1.1	Benchmarking of microreactors	3
1.2	Experimental snapshot and schematics of flow patterns in liquid-liquid slug flow	7
1.3	Benchmarking of microreactor for liquid-liquid extraction	9
1.4	Methodology and contribution of the thesis	15
1.5	Outline of the thesis	17
2.1	Experimental set-up used to study hydrodynamics	26
2.2	Observed flow regimes in the capillary microreactor	27
2.3	Observed flow regimes for equal capillary and Y-junction internal diameters	29
2.4	Observed flow regimes for equal capillary and Y-junction internal diameters for different flow velocities	30
2.5	Observed flow regimes for different capillaries and similar Y-junction diameter	31
2.6	Observed flow regimes for different Y-junctions and similar capillary	31
2.7	Water slug size at equal flow rate of both phases	32
2.8	Slug size for similar Y-junction and capillary size	32
2.9	Slug size for different capillaries and similar Y-junction diameter	33

2.10	Slug size for different Y-junctions and similar capillary	34
2.11	Specific interfacial area for different capillary microreactor and Y-junction diameters.	35
2.12	Pressure drop across the Y-junction at equal flow rates of water and cyclohexane	38
2.13	Pressure drop in the vicinity of Y-junction at equal flow rates of water and cyclohexane	39
2.14	Pressure drop in the vicinity of Y-junction at unequal flow rates of water and cyclohexane	40
2.15	Pressure drop in the vicinity of Y-junction at unequal flow rates of water and cyclohexane	41
2.16	Experimental pressure drop along the length of the capillary microreactor for equal flow rates of water and cyclohexane.	42
2.17	Pressure gradient as a function of water to cyclohexane flow ratio. . .	43
2.18	Comparison of experimental and predicted pressure drop at equal volumetric flow rates of water and cyclohexane.	44
2.19	Comparison of experimental and predicted pressure drops for unequal flow rates of water and cyclohexane	46
3.1	Experimental set-up used to study mass transfer and chemical reaction	53
3.2	Concentration of NBF in aqueous phase as a function of slug flow velocity for different capillary lengths	55
3.3	Extraction efficiency as a function of slug flow velocity for different capillary lengths for the extraction of NBF from its saturated solution into distilled water, system I	56
3.4	Extraction efficiency as a function of slug flow velocity for different capillaries in the extraction of iodine from its aqueous solution into kerosene, system II	57

3.5	Extraction efficiency as a function of slug flow velocity for different capillaries in the extraction of succinic acid from its aqueous solution into n-butanol, system III	57
3.6	Extraction efficiency as a function of slug flow velocity for different capillaries in the extraction of acetic acid from kerosene into water, system IV	58
3.7	Extraction efficiency as a function of flow ratio of aqueous to organic flow rate for the extraction of succinic acid from its aqueous solution into n-butanol, system III	59
3.8	Extraction efficiency as a function of slug flow velocity for unequal phase flow rates for the extraction of succinic acid from its aqueous solution into n-butanol, system III	59
3.9	Volumetric mass transfer coefficient as a function of slug flow velocity for various capillary lengths for the extraction of NBF from its saturated solution into water, system I	61
3.10	Rate of extraction as a function of volumetric mass transfer coefficient for different capillary lengths for the extraction of NBF from its saturated solution into water, system I	61
3.11	Volumetric mass transfer coefficient as a function of slug flow velocity for various capillary internal diameters for the extraction of iodine into kerosene from its aqueous solution, system II	62
3.12	Volumetric mass transfer coefficient as a function of slug flow velocity for various capillary internal diameters for the extraction of succinic acid into n-butanol from its aqueous solution, system II	62
3.13	Volumetric mass transfer coefficient as a function of slug flow velocity for various capillary internal diameters for the extraction of acetic acid into water from kerosene, system II	63
3.14	Volumetric mass transfer coefficient as a function of slug flow velocity for equal residence times for extraction of iodine from its aqueous solution into kerosene, system II	63
3.15	Volumetric mass transfer coefficient as a function of flow ratio of aqueous to organic phase	65

3.16	Volumetric mass transfer coefficient as a function of slug flow velocity for unequal flow rates	65
3.17	Colour change distance for two different initial concentrations of NaOH: 0.25 and 0.4 mol/L	69
3.18	Slug length as a function of slug flow velocity	69
3.19	Colour change time for two different initial concentrations of NaOH: 0.25 and 0.4 mol/L	70
3.20	Comparison of empirical model time and measured time	71
3.21	Volumetric mass transfer coefficient for different capillary sizes and initial NaOH concentrations	72
3.22	Mass transfer coefficient for two cases: without film, k_{Lwo} and with film, $k_L w$	72
3.23	Outlet NaOH concentration as a function of volumetric flow rate	74
3.24	NaOH conversion as a function of slug flow rate	74
3.25	Danckwerts plot, $(Ra/C_{A,2}^*)^2$ vs outlet NaOH concentration for different initial concentrations, for various flow velocities	75
3.26	Danckwerts plot, $(Ra/C_{A,2}^*)^2$ Vs outlet NaOH concentration for different initial concentrations, for various flow velocities	75
3.27	Danckwerts plot, $(Ra/C_{A,2}^*)^2$ vs outlet NaOH concentration for different initial concentrations, for various flow velocities	76
3.28	Interfacial area by physical, without film (a_{wo}) and with film (a_w), and chemical method	77
3.29	Interfacial area by physical, without film (a_{wo}) and with film (a_w), and chemical method	78
3.30	Interfacial area by physical, without film (a_{wo}) and with film (a_w), and chemical method	78
4.1	Snapshots of experimental set-up and Y-splitter	84

4.2	Flow splitter configurations used in the study	85
4.3	Flow splitting mechanism	87
4.4	Flow splitting at a Y-splitter	90
4.5	Volume fraction of kerosene and water in steel and Teflon outlet, respectively	90
4.6	Average contamination as a function of flow rate for different capil- laries for water-kerosene system	91
4.7	Flow splitting for constant water and kerosene flow rates respectively	91
4.8	Volume fraction in steel outlet for constant water and constant kerosene flow rates respectively	92
4.9	Volume fraction in Teflon outlet for constant water and constant kerosene flow rates respectively	92
4.10	Average contamination as a function of water flow proportion for water-kerosene system	93
4.11	Effect of capillary ID on flow splitting	93
4.12	Volume fraction in steel and Teflon outlet for various capillaries . . .	94
5.1	Slug flow in the capillary microreactor	102
5.2	Experimental set up for PIV measurement	105
5.3	Numerical meshes used for the simulations	107
5.4	Boundary conditions used for the simulations	108
5.5	Cell refinement	109
5.6	Schematics of experimental set up and computational domain	113
5.7	Experimental snapshot and PIV velocity distribution within the slug	115
5.8	CFD simulated internal circulations within an aqueous and an organic slug, respectively	117

5.9	Parabolic velocity profile within the slug	117
5.10	Radial position of stagnant zone within the slug	119
5.11	Distance of stagnant zone centre from the back interface	120
5.12	Recirculation time within the liquid slug	121
5.13	Internal circulations by particle tracing in aqueous and organic slugs respectively	122
5.14	Flow simulation without wall adhesion in a microreactor of 1 mm diameter for oil-water system	123
5.15	Slug flow formation at Y-junction in a capillary microreactor of 1 mm diameter for oil-water system	124
5.16	Levelset simulations using FEATFLOW	125
6.1	Experimental snapshot, schematic representation of slug flow and computational domain.	130
6.2	Computational domain and mesh, showing more refined mesh in the vicinity of the interface and periodically connected interface	136
6.3	Flow development for different viscosities in a slug unit	136
6.4	Concentration profiles for different levels of refinement	139
6.5	Volumetric mass transfer coefficient, $k_L a$ and mass transfer coefficient, k_L for different levels of refinement	139
6.6	Representation of species for reaction	140
6.7	Variation of titration time with respect to levels of refinement	142
6.8	A typical plot of average concentrations of three species in water slug	143
6.9	Snapshots of concentration profile of acetic acid	144
6.10	Snapshots of concentration profile of NaOH	144
6.11	Snapshots of concentration profile of CH_3COONa	145

6.12	Plots of titration time vs flow speed and titration time vs slug length, respectively	145
7.1	Two stage counter-current extraction	153
7.2	Schematic of numbering-up of liquid-liquid slug flow capillary micro-reactor	155
A.1	Pressure drop along single slug unit. (a) without film and (b) with film	159
A.2	Velocity profiles for capsule (slug) flow in a pipe	161

List of Tables

1.1	Different types of contactors with their advantages and limitations . . .	6
1.2	Different types of microextractors	8
1.3	Important dimensionless numbers to characterise the liquid-liquid slug flow	10
2.1	Literature review on the hydrodynamics of liquid-liquid systems in the horizontal capillaries and chip reactors	24
2.2	Specific interfacial area for different capillaries and Y-junctions at equal and unequal flow rates of water and cyclohexane	36
2.3	Power input requirement for various liquid-liquid contactors	48
3.1	Literature review on the study of liquid-liquid systems for mass transfer and chemical reaction in the capillaries and chip reactors	51
3.2	Chemical systems and operating conditions used	54
3.3	$k_L a$ for different types of contactors	66
3.4	Volumetric mass transfer coefficient, $k_L a$, specific interfacial area, a , and mass transfer coefficient, k_L for different capillary internal diameters (ID) at equal flow rate of both phases for the case of without film (w_0) and with film (w) in the liquid-liquid slug flow capillary microreactor	67
4.1	Chemical systems, parameters and operating conditions used to study the flow splitting	85

4.2	The geometrical properties of the splitters employed	86
4.3	Flow splitting experiments for the both viscous and non-viscous- viscous systems	88
4.4	Flow splitting experiments with the system NBF - aqueous NaOH solution for equal flow rates of both phases	89
5.1	Literature review on mixing in drops or slugs in small scale geometries	99
6.1	Literature review on numerical models for mass transfer with and without chemical reaction in the liquid-liquid two-phase flow	129
6.2	Data used for mass transfer simulations	138
6.3	Data used for model validation	142
6.4	Mesh size and time steps used for model validation	143
D.1	Physical properties of the liquids used to study flow regime, slug size and pressure drop	171
D.2	Physical properties of the liquids used (Chapter 3)	171
D.3	Physico-chemical properties of the liquids used to investigate the in- terfacial area by chemical method	171
D.4	Physical properties of liquids used to study flow splitting (Chapter 4)	172

Summary

Microreactor technology, an important method of process intensification, offers potential benefits to the chemical process industries due to the well-defined high specific interfacial area available for heat and mass transfer, which increases transfer rates, and enhances safety resulting from low hold-ups. The liquid-liquid slug flow capillary microreactor intensifies the mass transfer in biphasic systems through internal circulation caused by the shear between continuous phase/wall surface and slug axis, which enhances diffusive penetration and consequently increases the reaction rates observed. This reactor concept has been exploited for mass transfer and chemical reaction without detailed hydrodynamics involved and it is this aspect which is the subject of the analysis of the research presented.

The present work highlights the hydrodynamics and mass transfer characteristics of the liquid-liquid slug flow capillary microreactors, which were investigated using complementary state-of-the-art experimental and computational techniques. Experiments were carried out to ascertain the extent of slug flow regime, to measure slug size and pressure drop and to investigate the mass transfer coefficients and effective interfacial areas. The results were compared with conventional contactors and it was found that such liquid-liquid microextractor-reactor offers superior performance and greater efficiency. A flow splitting element based on the preferential wettability of liquids with different solid materials was developed for the downstream separation of liquids and showed very good flow splitting providing precise contact time of biphasic mixture and thus accurate determination of mass transfer rates. Furthermore, CFD methodologies, developed to characterise internal circulations, to capture the slug flow generation mechanism and to study mass transfer with and without chemical reaction, improved the understanding and generated results showing that the processes relevant to this reactor concept can be studied using these methodologies.

Thus precise tuning of hydrodynamics and mass transfer together with easy downstream separation of liquids and the excellent accessibility for process modelling suggest that liquid-liquid slug flow in capillaries is a powerful laboratory technique for elucidating the processes involving biphasic mixture and for identifying asymptotic performance limits in such processes.

Kurzreferat

Die Mikroreakorteknik, eine wichtige Methode zur Prozessintensivierung, bietet die Möglichkeit, chemische Prozesse sicher und mit hohen Ausbeuten zu betreiben. In einem flüssig-flüssig Kapillarmikroreaktor liegt eine gut definierte Strömung mit alternierenden Pfropfen vor. Innerhalb der Flüssigkeits-Pfropfen befinden sich Rezirkulationsströmungen, die den Stoffaustausch an den Phasengrenzen erhöhen und damit zu höheren effektiven Reaktionsraten führen. Bisherige Arbeiten, die Stofftransport und Reaktionen im Kapillarmikroreaktor untersuchten, berücksichtigten keine Detailberechnung der Strömung. Die Hydrodynamik wird in der vorliegenden Arbeit vertieft untersucht.

Schwerpunkt der Forschungsarbeit war die Untersuchung der Hydrodynamik und der Stofftransportcharakteristik der Pfropfenströmung in einem flüssig-flüssig Kapillarmikroreaktor. Dies wurde mit Hilfe moderner experimenteller und simulationsbasierter Methoden erzielt. Die Experimente konzentrierten sich auf die Abgrenzung der Strömungsregime sowie auf die Ermittlung der Pfropfengröße, des Druckverlustes und Stoffübergangskoeffizienten und der effektiven Phasengrenzfläche. Beim Vergleich des Kapillarmikroreaktors mit herkömmlichen Apparaten wurde sowohl eine überlegene Leistung als auch eine größere Effizienz festgestellt. Weiterhin konnte eine Vorrichtung zur Trennung des zweiphasigen Gemisches entwickelt werden. Das Trennungselement befindet sich am Ende der Misch- und Reaktionsstrecke und nutzt gezielt die unterschiedlichen Benetzungseigenschaften der beiden Flüssigkeiten aus und hat sich in Versuchen sehr gut bewährt. CFD Simulationen wurden durchgeführt, um die Rezirkulationsströmung zu berechnen, und die Entstehung und Stabilität der Pfropfenströmung besser verstehen zu können. Bei der Untersuchung des Stoffübergangs wurde mit und ohne reaktiven Anteilen gerechnet. Die angewendeten CFD-Methoden haben sich insgesamt als gut geeignet erwiesen.

Zusammenfassend lässt sich sagen, dass mit dem Kapillarmikroreaktor eine genaue Einstellung der Hydrodynamik und des Stoffübergangs in Verbindung mit einer einfachen Phasentrennung und der ausgezeichneten Zugänglichkeit für Prozessmodellierung zur Verfügung steht. Damit können nun im Labor die limitierenden Einflüsse bzw. asymptotischen Leistungen von flüssig-flüssig Systemen aufgeklärt werden.

Chapter 1

Introduction

It is a sobering thought that if chemical engineers were given a free hand design to human digestive and metabolic system, our bodies would be much larger and require many kilowatts to operate them. On the other hand, nature operates unobtrusively with laminar flow in high density matrices (kidneys and lungs) on a semi-continuous basis, and copes with fouling problems by coughing. As a scientists and engineers we should not be too arrogant to learn a few lessons from the natural world.

- Prof. Colin Ramshaw

1.1 Process Intensification

In recent years, more and more efforts are being made to reduce emissions to the environment, in order to decrease global warming and halt the climate change. In this context it is important to develop a chemical industry based on sustainable technology. To this end, in addition to valorise the waste obtained in the process, the chemicals being used in the systems should be treated in such a way as to provide every molecule the same processing experience, yielding increased selectivity. This can be done by developing alternative synthesis and processing routes, which are based on highly selective catalysts (e.g. biocatalysts). The engineering solution to this problem is to improve the transport rates by increasing the specific interfacial area, which in turn reduces the diffusional path lengths and helps to enhance the safety by virtue of the lower hold-up and superior temperature control, even for strongly exothermic reactions. In addition, it is important to reduce the total energy consumption by better heat management and lowering the total pressure drop.

This overall development is often referred to as “Process Intensification”, which can be defined in various ways depending on the application involved. However, two terms, “innovative” and “substantial”, are common to practically all process intensification definitions [1]. The Institut für Mikrotechnik Mainz (IMM), Germany, gives broad definition referring to a process which is better (higher yield and/or selectivity), faster (enhanced space/time yield), safer and better for the environment (green chemistry with no high-risk process systems) and more cost effective (lower investment costs and/or total operational costs) [2].

Process intensification is a revolutionary development in chemical industry, which is being achieved by revisiting fundamentals of fluid dynamics, heat and mass transfer. The concept of process intensification was pioneered by Professor Ramshaw and his group at Imperial Chemical Industries (ICI), UK, in the late 1970’s, who considered how one might reduce equipment size by several orders of magnitude. However, in recent years, the objective of process intensification has broaden. In addition to reduction in size, different techniques are being exploited for process intensification, such as dynamic operation, special reaction media and the use of non-conventional energy sources, to name but a few. The opportunities that process intensification offers to a chemical company lie primarily in six areas: costs, safety, compactness, controlled well-defined conditions, time to the market, and company image [1]. It leads to substantially cheaper processes, particularly in terms of land usage (much higher production capacity and/or number of products per unit of manufacturing area), investment costs (smaller equipment, reduced piping, etc.), costs of raw materials (higher yields/selectivities), costs of utilities (in particular energy), and costs of waste processing (reduction in waste amounts).

1.2 Microreactor Technology

Among all methods of process intensification, reduction of size to the microscale or microreactor technology, offers considerable potential benefits to the process industries. Due to well-defined flow patterns and very high interfacial area, process intensification is possible in microstructured systems, which makes them an interesting option for enhancing the process performance. The benchmarking of microreactor for the demands, reaction, hydrodynamics and temperature control, is shown in Figure 1.1. As can be seen, the multitubular reactor works reasonably well for the chemical processes, however, the temperature control in this case is often difficult giving rise to considerable hot spots. In the microreactors, the reduced scale facilitates the temperature profiling giving an opportunity to maintain the temperature within any window required. The enhanced mass transfer due to very high

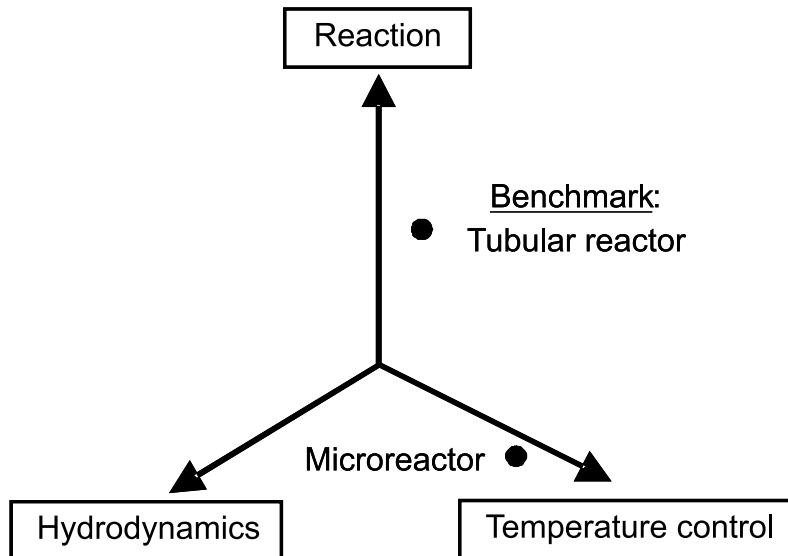


Figure 1.1: Benchmarking of microreactors

interfacial area increases reaction rates and thus reduces the total processing volume. Easy temperature profiling and enhanced mass transfer makes it possible to control highly exothermic and hazardous reactions. Additionally, microreactors can be simply bundled together for large scale production. This reduces the problem of scale-up arising in conventional reactors.

Different materials such as metals, glass, polymers and ceramic materials are used to fabricate the microreactors and various techniques such as etching, lithography, electroplating, molding, polymer microinjection molding, and embossing techniques are applied to make the microscale channels of different cross-sectional geometries (e.g. circular, rectangular, square, etc.). These fabrication techniques have been used in microelectronics to construct sensors and actuators and therefore a new field microelectromechanical systems (MEMS) has been started. Forschungszentrum Karlsruhe and the IMM, Germany, have been the first who fabricated multichannel microreactors, micromixers, and micro-heat-exchangers in metal by use of lithography, electroplating, and molding [3]. Some researchers have also used capillaries as microreactors [4] which are very easy to integrate in a set-up.

Though microreactor technology is in the primary stage, few micro-plants have been developed and successfully tested in the laboratory as well as in the commercial sites. In addition to university research, industries are working on microreactor research and manufacturing such as Cellular Process Chemistry Systems GmbH, IMM, Micronit Microfluidics, Ehrfeld BTS GmbH, Systanix, Inc., Styrris, are to name but a few. IMM, Germany, has made successful runs of a continuous microstructured nitroglycerine plant (capacity 15 kg/h) at the site of Xi'an Chemical Industrial Group

(HAC) in China. This plant consists of three main parts: the mixing of sulfuric acid with nitric acid (both highly concentrated fuming liquids), the reactor and the phase separation (washing and purification devices). On demand, glycerine and the acid mixture are fed separately into a microstructured reactor where mixing occurs within milliseconds. Such microreactor plant has also been developed for polymerisation of Methyl methacrylate by Iwasaki *et al.* [5] and showed significant improvement in the control of molecular weight due to superior heat transfer efficiency. The plant constructed by numbering-up eight tubes (microreactors), was continuously operated successfully for 6 days without any problem.

Microreactor technology is an important part of the decentralised mobile plant concept. Such plants have already been developed for biological applications (e.g. miniature analytical thermal cycling instrument, MATCI, to amplify and detect DNA via the polymerase chain reaction in real-time [6]). The objective behind chemical mobile plants is to reduce the risk associated with transporting hazardous chemicals. Rather than transporting hazardous chemicals, a distributed production strategy may be used with economic manufacturing on consumers site, as is currently being performed for oxygen and nitrogen [7]. Recently, a chemical plant has been developed by Ehrfeld Mikrotechnik BTS GmbH, Germany, in a briefcase which can be used for variety of applications.

Microreactor technology has several applications in pharmaceutical and fine chemicals where production amounts are often less than a few metric tonnes per year [8]. Most of the processes in these industries rely on batch or semi-batch mode of operation, which are often controlled manually. Using microreactor technology, these processes can be made continuous which have several advantages over the batch processes. Roberge *et al.* [9], a review on the benefits of microreactor technology to pharmaceutical industrial processes, cites that 50 % of the reactions in fine chemical/pharmaceutical industry could benefit from a continuous process based mainly on microreactor technology. In drug industry, there is always a strong time pressure to bring new molecules in the market to maximise the profitable manufacturing patent life of 20 years [7]. It also needs a quick approval from the regulatory authority for the production. This can be achieved by using microreactor based continuous process requiring short development time and eliminating approval for large scale production.

1.3 Liquid-Liquid Contacting

1.3.1 Conventional contactors

A wide variety of extraction equipment is available: mixer-settlers, centrifugal extractors and columns. A mixer settler consists of a mixer (agitated tank) in which the aqueous and organic liquids are contacted, followed by a gravity settling shallow basin called as settler where the liquids disengage into individual layer for separate discharge. In centrifugal extractors, two immiscible liquids of different densities are fed to a agitated tank and are rapidly mixed in the annular space between the rotor and the stationary housing. The high pressure feed and its intense mixing in the annular space alters the specific gravities of the liquids and thus the physical separation efficiency is very high in the centrifugal extractor than the mixer-settler. The third variety of extraction equipments, the columns, is commonly used in chemical industries in their countercurrent mode of operations. The columns are divided into two types: static columns (e.g. spray column, sieve plate column and packed column) and agitated columns (e.g. rotating disk contactor, Scheibel column, Kuhni column, Karr column and pulsed column). The advantages and limitations of the above mentioned contactors are summarised in Table 1.1.

Liquid-liquid extraction has been used in the laboratory for over a century. A number of books, review articles and research papers have been published on the topic over time on the experimental characterisation and mathematical modelling of extractive processes in the conventional contactors/reactors. A good review can be found in [10]. This extensive work has increased the understanding of the equipment performance and the application of mathematical models to describe the transport phenomenon which is a basis for equipment design. In the last decade, computational fluid dynamics (CFD) has also contributed a lot in understanding the transport phenomenon. However, due to complex hydrodynamics in most of the equipments presently employed in the industry, the interfacial area is often poorly defined. The scale-up from pilot plant data gives desired performance for the large scale production but the resulting design is far away from the optimum, and the design procedure can not be regarded as intellectually satisfied [11]. It shows that there is a need to change the equipment or technique which can improve space/time yield and reduce the costs associated with equipments.

A common drawback of conventional equipment is the inability to condition the drop size precisely and the non-uniformities that arise due to the complexities of the underlying hydrodynamics. This leads to uncertainties in extractor design and often imposes severe limitations on the optimal performance which can be achieved.

Table 1.1: Different types of contactors with their advantages and limitations

Contactors	Advantages	Limitations
Mixer settler	<ul style="list-style-type: none"> • Simplicity and low maintenance • Less number of stages required • Good contacting 	<ul style="list-style-type: none"> • High set-up cost • High operation cost • Design from first principle is not practicable
Centrifugal contactor	<ul style="list-style-type: none"> • Works at low density difference between two liquids • Less solvent volume required • Rapid mixing and separation can enhance product recovery and quality 	<ul style="list-style-type: none"> • Difficult to scale-up • Mechanical complexity and high maintenance cost
Static Columns	<ul style="list-style-type: none"> • Easy to operate • Satisfactory performance at lower cost 	<ul style="list-style-type: none"> • Performance completely rely on the packing/ internals • Good performance in limited range of flow rates
Agitated Columns	<ul style="list-style-type: none"> • Low investment cost • Better performance due to decrease in the mass transfer resistance with increased agitation 	<ul style="list-style-type: none"> • Difficult to provide right amount of mixing • Difficult to separate small density differences • Better performance for limited flow ratio

1.3.2 Liquid-liquid slug flow

Slug flow as a microextractor

Microreactors can be very efficiently used for liquid-liquid extraction, where they are called as microextractors. Some microreactor-extractors which are already developed and successfully tested in the laboratory are listed in Table 1.2. The detailed review of these extractors can be found in [3]. The pioneering work by Central Research Laboratory (CRL), UK, researchers showed that using small channels the mass transfer performance can be improved. Later on, a wedge-shaped parallel flow contactor was developed at the University of Newcastle upon Tyne by Professor Ramshaw and his group [12] and observed industrially competitive reaction rates for nitration of benzene. Furthermore, microchannel contactor separated by micromachined membrane and sieve like walls was developed at Pacific Northwest National Laboratory, Richland (PNNL), USA. A micromixer-settler fabricated at IMM was employed by BASF, Germany, for some extraction applications. All above mentioned contactors were tested in the laboratories with different aims. It shows that researchers are exploring various ideas in this area to show microreactor-extractor as an alternative to conventional extractors. Similarly, in this work, a new extractor concept, liquid-liquid slug flow capillary microreactors, has been explored.

Liquid-liquid slug flow in a capillary microreactor is a flow of two immiscible liquids, characterised by a series of liquid slugs (plugs) of one phase separated by the other. Since both phases move alternatively, each slug serves as an individual processing subvolume which are highly regular and guarantee well defined interfacial area for transfer process. A key feature of this type of microreactor is the ability to manipulate the two principle transport mechanisms: convection within the individual slug of each liquid phase and interfacial diffusion between adjacent slugs of different phases as shown in Figure 1.2.

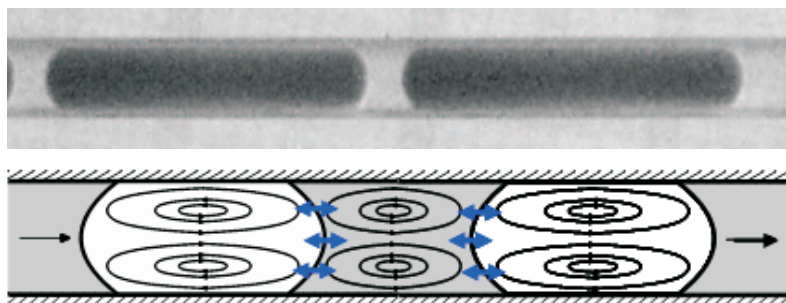


Figure 1.2: Experimental snapshot of liquid-liquid slug flow and schematics of slug flow showing internal circulation within each slug and interfacial diffusion between two adjacent slugs

Table 1.2: Different types of microextractors

Contactors	Systems studied	Developed/used at
Partially overlapping channels [13]	Xylene - Fe(III) - Water octan-1-ol - phenol - water	Central Research Laboratories (CRL), Middlesex, UK
Wedge shaped flow contactors [12]	Water - Kerosene (visual study) and Ni- tration of benzene	University of Newcastle upon Tyne and British Nuclear Fuels, Preston, UK
Microchannel separated by a mi- cromachined membrane [14]	Water - Cyclohexanol - Cyclohexane	Pacific Northwest National Laboratory, Richland, USA
Microchannels separated by a sieve like walls [3]	-	Institut für Mikrotechnik, Mainz, Ger- many
Micromixer-settler systems [3]	Water - Acetone - Toluene Water - Acetone - n-butyl acetate Water - Succinic acid - n-butanol Water - dl-pantolactone - Methyl-i- butyl-ketone	Institut für Mikrotechnik, Mainz and BASF, Ludwigshafen, Germany

In the liquid-liquid slug flow, the stable well-defined flow patterns and uniform interfacial areas permit a precise tuning of the mass transfer processes and make an *a priori* prediction of mass transfer coefficients feasible. Easy temperature profiling due to reduced scale helps in providing additional insights into the behaviour of a given reaction and in identifying the asymptotic performance which can be attained. It also offers fewer degrees of operational freedom and precludes detailed analytical monitoring over the course of reaction. Three fundamental operational parameters characterise the slug flow capillary microreactor: the pressure drop, the mass transfer rates and the residence time distributions.

The other major flow regime possible for a biphasic mixture in the capillary is parallel flow. Due to relatively low interfacial area and mass transfer only by diffusion, the parallel flow takes long time for higher throughput compared to slug flow. Besides, interfacial area can not be altered in parallel flow by varying speed which on the other hand is possible in slug flow - increasing flow velocity slug size decreases and thus increases the interfacial area. In addition, in the slug flow regime, increased flow rate intensifies internal circulations within the slugs which renew the interfacial surfaces with higher frequency enhancing the diffusive penetration. Finally, the slug flow shows very stable behaviour compared to parallel flow.

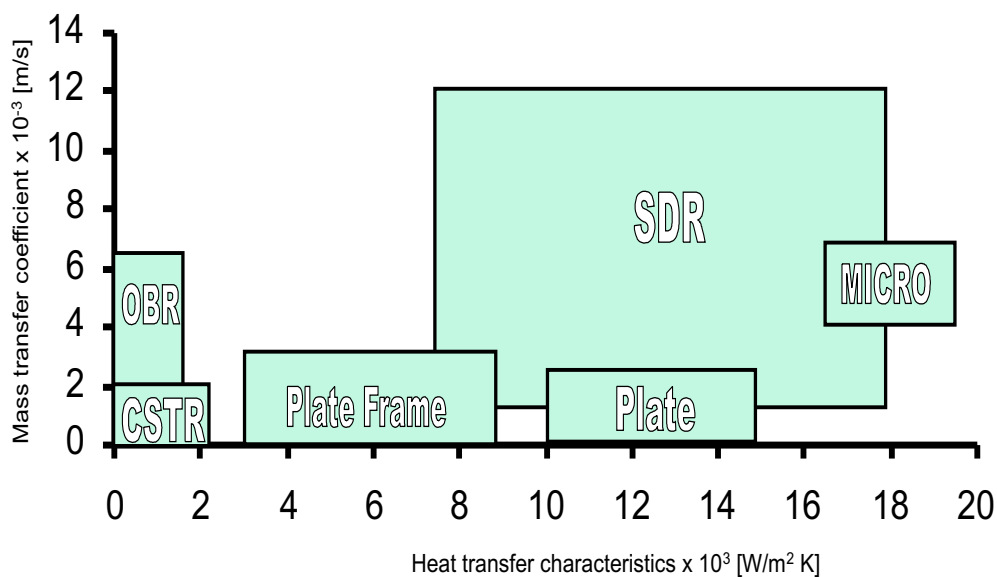


Figure 1.3: Benchmarking of microreactor for liquid-liquid extraction (from Prof. Jachuck, University of Clarkson [15])

The heat transfer and mass transfer characteristics of different types of contactors are shown in Figure 1.3 (from Professor Jachuck's homepage [15]). It shows that microreactors offer superior performance compared to conventional equipments. Oscillatory baffled reactor (OBR), Spinning disc reactor (SDR) and microreactors have

high mass transfer coefficients compared to CSTR, Plate and Frame and Plate reactors. However, SDR and microreactors are interesting options with respect to mass and heat transfer characteristics.

Characterisation of slug flow

Table 1.3: Important dimensionless numbers to characterise the liquid-liquid slug flow

Numbers	Definition	Significance
Reynolds number	$Re = \frac{\rho V d}{\mu}$	$\frac{\text{Inertial force}}{\text{Viscous force}}$
Capillary number	$Ca = \frac{\mu V}{\gamma}$	$\frac{\text{Viscous force}}{\text{Capillary force}}$
Viscosity ratio	$\mu_R = \frac{\mu_1}{\mu_2}$	$\frac{\text{Viscosity of phase 1}}{\text{Viscosity of phase 2}}$
Peclet number	$Pe = \frac{d_s^2 V_s}{Dl}$	$\frac{\text{Convective mass transfer}}{\text{Molecular diffusivity}}$
Fourier number	$Fo = \frac{tD}{R^2}$	$\frac{\text{Current time}}{\text{Time to reach steady state}}$
Diffusivity ratio	$D_R = \frac{D_1}{D_2}$	$\frac{\text{Diffusivity of solute in phase 1}}{\text{Diffusivity of solute in phase 2}}$
Distribution coefficient	$m = \frac{C_1^*}{C_2^*}$	$\frac{\text{Saturation conc. of solute in phase 1}}{\text{Saturation conc. of solute in phase 2}}$

It is customary to express the quantitative analysis of a problem in terms of dimensionless groups which reduces the number of independent variables and enhances the generality of results. The hydrodynamics and mass transfer in the liquid-liquid slug flow can be characterised using the dimensionless numbers and parameters mentioned in the Table 1.3. The definitions of those numbers for slug flow are based on flow of two alternate phases. However, in some cases, the surface properties are dominant which result in the formation of a film on the capillary surface. The liquid which forms a film is termed as carrier or continuous phase while the other is called as slug.

The important dimensionless number for characterisation of all types of flows is Reynolds number, Re , which relates the inertial force to the viscous force. In microreactors, due to low flow velocities and micrometer sizes, the Reynolds number is very low meaning viscous force is dominant over inertial force. Besides, the capillary force is also significant which is related to viscous force by capillary number, ratio of viscous force to the capillary force. In addition to this, viscosity ratio and density ratio are also important to characterise the system because large difference in the densities of the liquids make the flow patterns more complex due to influence of buoyancy force. Furthermore, the mixing within the slugs is characterised by Peclet number while the interfacial diffusion is characterised by Fourier number. The Peclet number relates convective and diffusive mass transport and Fourier number gives an idea about the progress of diffusive transport process. Finally, diffusivity ratio and partition coefficient gives an idea about the possible progress of the mass transfer.

Applications

At present, microreactor technology is considered as an efficient tool for kilogram scale synthesis in the continuous mode of operation and for processing hazardous reactions that do not allow scale-up in conventional reactors. Various disciplines such as chemistry, physics, chemical engineering, material science and mechanical engineering are involved to make it effective for different applications. The alternate flow of two liquid phases in a capillary shows wide range of applications in chemical industry from synthetic chemistry to chemical engineering. Each slug in this flow acts as a well-defined, individual processing subvolume and its individual handling leads to the possibility of realising serial processes.

As described above, extraction is the key unit operation which can be performed using liquid-liquid slug flow capillary microreactor. Liquid-liquid reactions are of extreme importance in several chemical engineering applications such as phase transfer catalysis, reactive extraction, nitration, polymerisation etc. It also shows applications in drug development (e.g. for testing of synergetic effects) and catalysis (e.g. catalysts screening) [16]. Köhler *et al.* [16] explained the concept of digital reaction technology which is an introduction of a digitalisation principle by use of a large number of small reaction volumes handled serially in a flow channel. This principle can be used for quantitative chemical analysis like titration (digital micro segment titration). Liquid-liquid slug flow could also be applied in modular synthetic chemistry, particularly in combinatorial chemistry so far as the reactants and products of single synthesis steps are compatible with two phase systems. The slug flow principle is of particular interest in biological applications as well (e.g. cell separation, DNA analysis [17], kinetic measurements [18] and protein crystallization [19]).

1.4 Background and Motivation

Process intensification via microreactor technology has remained an important strategy for many chemical processes. Though microreactor technology is relatively new area for engineers, several experimental and modelling studies have been carried out to identify the hydrodynamic flow regimes and their transitions for gas-liquid flows through various small-scale geometries (e.g. Paglianti *et al.* [20]; Mishima and Hibiki [21]; Triplett *et al.* [22]; Kreutzer [23], Simmons *et al.* [24]). Dispersion and mass transfer studies for gas-liquid flows have also been published (e.g. Thulasidas *et al.* [25]; Bercic and Pinter [26]; Elperin and Fominykh [27]). The recent experimental technique, particle image velocimetry (PIV) (e.g. Thulasidas *et al.* [28]), μ PIV (e.g. Devasenathipathy *et al.* [29]) and optical sensors (e.g. Kraus *et al.* [30]) have shown strong potential in characterisation of flow field in the microchannels. A few studies on characterisation of multiphase microreactors using CFD modelling for hydrodynamics and mass transfer have also published (e.g. Taha and Cui [31]; van Baten and Krishna [32]).

The use of slugs (capsules) in oil transportation, referred as pipeline flow of capsules, was studied experimentally by Hodgson and Charles [33] and reported flow regimes, slug velocities and pressure gradient for oil-water flow through a 1.04 inch diameter horizontal pipe. From the experimental snapshots, they revealed that the viscous or semi-rigid oil phase had been completely surrounded by less viscous water. Further, measurements of slug velocity and pressure gradient for laminar and turbulent flow conditions were deduced by Charles [34] with a suitable model. Three decades later, such flow scheme was exploited in a chip microreactor for intensification of rapid reactions by Professor Ramshaw and his group at University of Newcastle upon Tyne, UK. They developed a chip-based microreactor, 380 μm width channel, based upon the use of liquid-liquid slug flow and obtained mass transfer performance data for extraction of acetic acid from kerosene slugs (Burns and Ramshaw [35]). During the same period, Dummann *et al.* [4] carried out experiments for the production of nitrobenzene in a capillary microreactor using the same concept. The reaction was carried out in slug flow regime and focused on reduction in by-products formation. It was a successful effort as the by-product formation was reduced significantly. Some CFD simulations were carried out, leading to the conclusion that the enhancement of mass transfer can be interpreted in terms of an internal circulation flow within the slugs. Further, Harries *et al.* [36] developed a numerical model with general purpose CFD code and predicted internal flow patterns of slugs (which they referred as fluid segments) and the transfer of dissolved chemical species within the slugs and across the interfaces.

Furthermore, Professor Ismagoliv and his group from University of Chicago, USA, have carried out extensive work on understanding and controlling complex chemical and biological systems at critical times and locations using microfluidic chips. Their important contributions on hydrodynamics and mixing improved the understanding on the slug flow generation mechanism and mixing within the slugs ([37],[38]) and effect of viscosity on these phenomenon [39]. They also used the concept of segmented flow for several biological applications such as adsorption of nonspecific protein [9], measurement of kinetics of enzymatic reaction (kinetics of ribonuclease A [18]) using nanoliters of reagents, screening of protein crystallisation [19], nucleation of protein crystals [40], and determination of blood clotting time [41].

Meanwhile, Köhler *et al.* [16] have studied the concept of digital reaction technology with different combinations of flow fusion modules and segment fusion modules for the reorganization and recombination of serially flowing sequences of fluid segments. The segment splitting and thus cloning (biological term used for automated production of copies of whole sequence) of the segmented flow is also presented. Recently, Tanthapanichakoon *et al.* ([42] and [43]) have carried out 2D and 3D simulations to study mixing behaviour in the liquid slug of liquid-liquid slug flow and proposed a modified Peclet number for calculating the mixing within the liquid slugs.

The above mentioned work has demonstrated the potential of microreactor technology, in particular liquid-liquid slug flow in microreactors. It has also shown that the well-defined flow patterns arising in the slug flow capillary extractor/microreactor can be described very well using CFD tools. This liquid-liquid slug flow concept has so far been exploited for mass transfer with chemical reaction ([4];[35]) without much reference to the detailed hydrodynamics and mass transfer involved. Several issues such as pressure drop, slug size, interfacial area, extent of slug flow regime and mass transfer rates were not studied in detail in the previous work. Their understanding is inherently crucial for providing well-defined reaction conditions and identifying asymptotic performance limits, and therefore, it is a worthwhile subject for more rigorous analysis.

1.5 Objectives, Methodology and Present Work

1.5.1 Objectives

The objective of the thesis was to obtain fundamental understanding of the hydrodynamics and mass transfer with and without chemical reaction in order to design an appropriate reactor concept for the analysis of complex liquid-liquid processes us-

ing complementary state-of-the-art experimentation and computational techniques. The objectives of each subtopic are given as follows:

Hydrodynamics:

- Understand the mechanism of slug flow generation
- Investigate the extent of slug flow regime for different flow ratios, measure the slug size and interfacial area (physical method i.e. snapshot approach)
- Characterise internal circulations and investigate internal circulation time for development of first principle models
- Measure the pressure drop along the length of capillary and across the Y-piece mixing element to investigate the specific energy, power required per unit interfacial area

Mass transfer with and without chemical reaction:

- Investigate the mass transfer rates for different non-reacting systems in order to compare the performance of slug flow reactor with conventional contactors/reactors
- Study the mass transfer rates and reaction time scales for a simple mass transfer limited reaction
- Determine effective interfacial area for mass transfer using chemical method in order to demonstrate the presence of a wall film

Flow splitting:

- Demonstrate the online downstream separation of biphasic mixture in capillary microreactor

1.5.2 Methodology and present work

The methodology used in the present work is depicted in Figure 1.4. As can be seen, the thesis is divided into two parts: experimentation and modelling. Further, these

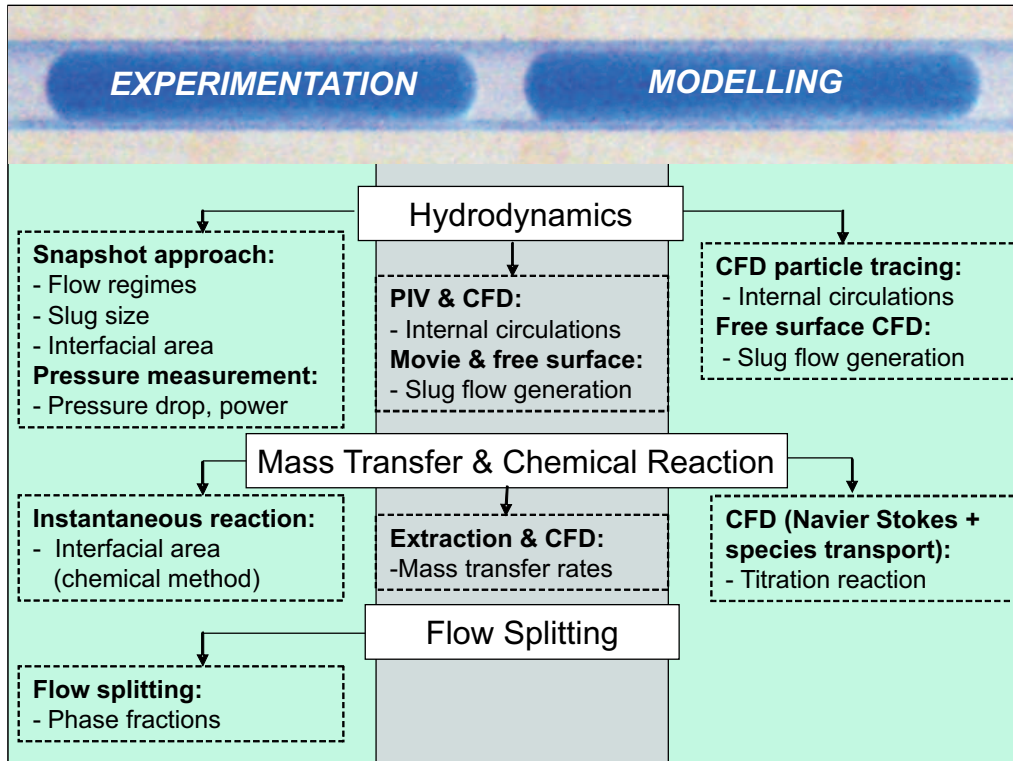


Figure 1.4: Methodology and contribution of the thesis

are divided into three sections: hydrodynamics, mass transfer with and without chemical reaction, and flow splitting.

The methodologies and contribution of the thesis are given as follows:

For the hydrodynamics study, the snapshots were taken with high speed camera to investigate the extent of slug flow regime and to measure the slug size for a non-reacting chemical system, water-cyclohexane. Experiments were carried out for different Y-junction mixing elements and various downstream capillaries. Further, the snapshots were used to investigate interfacial area and three phase contact angle. Pressure transducers were employed to measure pressures at different locations along the length of the capillary and across the Y-junction to investigate the pressure drop under various operating conditions. Based on the contribution of the Y-junction to the overall pressure drop, the power requirement was estimated and compared with various conventional equipments. The simplified theories were employed to determine the pressure drop along the length of the capillary which was then compared with the experimental results.

The internal circulations arise due to shear between slug axis and the capillary wall or continuous phase were characterised using PIV experiments and CFD simulations. The PIV experiments were carried out only for qualitative characterisation due to the

experimental set-up limitations while single phase CFD simulations were carried out for quantitative analysis. Further, a CFD particle tracing algorithm was employed to visualise the internal circulations. The effect of a wall film and other operating parameters such as flow velocity and slug length on internal circulations was studied. Also, location of stagnation zones in the slug and characteristic circulation times were calculated from the simulated results. Finally, a two-phase CFD methodology was developed to generate the slug flow using free surface CFD models: Volume of Fluid (VOF) and levelset.

In the mass transfer studies, the liquid-liquid extraction of four non-reacting systems were carried out: n-butyl formate from its saturated solution into water, succinic acid from its aqueous solution into n-butanol, iodine from its aqueous solution into kerosene, and acetic acid from kerosene into water. In this case, the outlet concentrations of the components in the extract and raffinate were determined using titrations as well as gas chromatography to predict the mass transfer rates. Further, a simple reaction of mass transfer limitation, neutralisation reaction, was studied and the mass transfer rates and base neutralisation times were investigated under various operating conditions for a kerosene (+ acetic acid) - water (+ NaOH) system.

The study of pressure drop in the capillary microreactor revealed the presence of an organic wall film in the capillary which is difficult to visualise with the help of snapshot at such a low scale. Therefore, the interfacial area was investigated by chemical method which uses Danckwerts theory of mass transfer with chemical reaction and both areas, physical (snapshot) and chemical, were compared. Finally, a CFD model comprising of Navier-Stokes equation with spatially resolved viscosities and densities and species transport equations for involved species was developed. The system of equations was solved using in-house developed finite element code, FEATFLOW (www.featflow.de).

Finally, a flow splitter based on wetting properties of the liquids and solid walls was developed for downstream separation of two phases. The effects of liquid viscosities and other operating conditions such as flow velocity, capillary diameter and flow ratio were studied.

1.6 Outline of the Thesis

The contribution of the thesis is arranged in two parts namely experimental (Chapter 2, 3 and 4) and modelling (Chapter 5 and 6) as shown in Figure 1.5. In some cases, the experimental results are presented in modelling part and vice versa for

their direct comparison. The thesis is summarised in Chapter 7. Each Chapter of both the sections is subdivided into three parts: firstly introduction containing short description of the particular topic and short literature review, secondly methodologies, results and discussion, and finally brief summary of the Chapter. Following details show the contents of each Chapter.

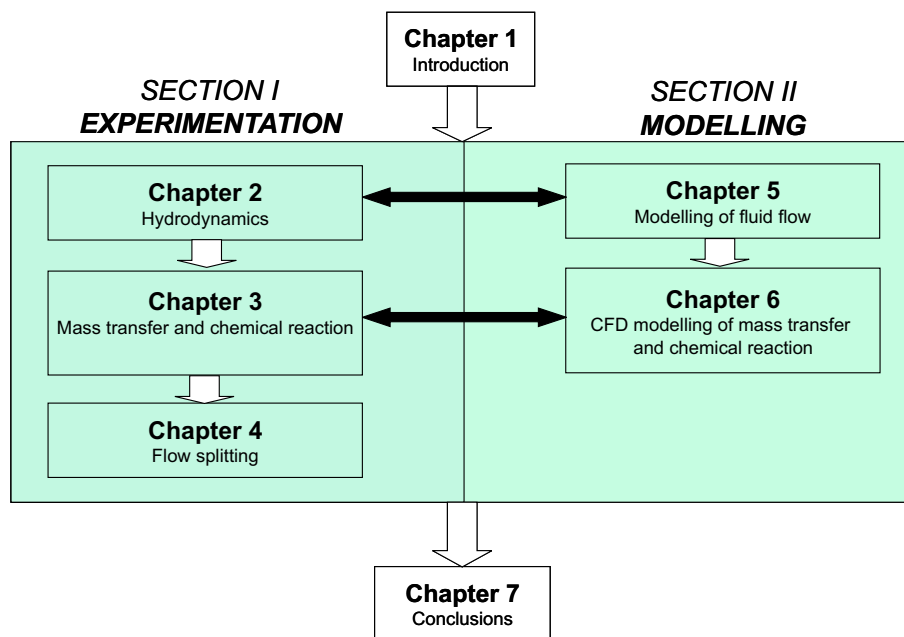


Figure 1.5: Outline of the thesis

Part I: Experimentation

Chapter 2: In this chapter, the experimental studies on hydrodynamics is presented. The experimental set-up, methodology and operating conditions used in this study are briefed. Further, the effect of various operating parameters on flow regimes, slug size, interfacial area and pressure drop are discussed. Finally, the experimental and theoretical pressure drop (derived in Appendix A) are compared and the power requirement was investigated.

Chapter 3: This chapter contains experimentation of mass transfer with and without chemical reaction for different chemical systems. The results obtained for four different systems used for mass transfer characterisation are presented in terms of extraction efficiency and mass transfer coefficients. The effect of various operating conditions such as flow rate, capillary diameter and flow ratio are discussed in detail. In addition, a mass transfer limited reaction and the methodology for investigation of interfacial area by chemical method along with their results is presented.

Chapter 4: This chapter is about the flow splitting for downstream separation of biphasic mixture. Different flow splitter configurations with effect of various operating conditions on splitting of different chemical systems are presented.

Part II: Modelling

Chapter 5: This chapter accounts different modelling aspects of liquid-liquid slug flow. In the first part, characterisation of internal circulations using simplified single phase CFD simulations, PIV experimentation and CFD particle tracing are presented. The effect of a wall film and other operating parameters like flow velocity and slug length on internal circulations is also discussed. The location and extent of stagnation zones within the slugs and characteristic circulation times calculated from simulated results are presented. In the second part, free surface CFD methodologies to generate the slug flow are described in detail. Effect of various operating parameters on slug flow generation is also discussed.

Chapter 6: A CFD model developed for mass transfer with and without chemical reaction in the liquid-liquid slug flow is presented in this chapter. The numerical model, its discretisation and method of solution are described. The effects of operating conditions on flow patterns, mass transfer and chemical reaction are discussed. Finally, the results are compared with experiments given in the literature.

Chapter 7: This chapter concludes the thesis. Besides, few open questions with few recommendations for future work are presented.

Part I

Experimentation

Chapter 2

Hydrodynamics

2.1 Introduction

Two fundamental operational parameters characterise the slug flow capillary microreactor: the mass transfer rates and the pressure drop. The mass transfer behaviour depends on the slug geometry and the circulation patterns, which vary with the physical properties of liquids as well as with operating parameters such as flow rates, mixing element (Y-junction) geometry and the capillary dimensions used. Burns and Ramshaw [35] have explained the performance for the obtained mass transfer data for the extraction of acetic acid from kerosene slugs in a glass chip-based reactor in terms of the prevailing slug lengths. Furthermore, Dummann *et al.* [4] studied the slug size distribution by measuring the dimensions of individual slug samples and calculating the corresponding slug volumes for a biphasic nitration reaction. They reported that the distribution of the slug size for the organic phase deviates only around 5 % from the mean value. The slug geometry not only defines the interfacial area but also the intensity of internal circulations which arise due to shear between slug axis and capillary wall. A simplified analysis of internal circulations using CFD simulations for different slug lengths of aqueous and organic slugs demonstrated that well-defined internal circulations arise in slugs having lengths greater than their diameters (for details, see Chapter 5). This regime of slug flow, which maximises the interfacial area and internal circulations within individual slug is not feasible under all operating conditions making it an interesting topic for investigation.

Different parameters were used to benchmark the technical reactors. The most important hydrodynamic parameter of practical relevance as a benchmark for technical reactors besides the interfacial area is the amount of energy required per unit in-

terfacial area i.e. specific energy. It can be investigated by measuring the pressure drop along the length of the capillary and across the Y-piece mixing element. Unlike single phase pressure drop under laminar flow regime, the two phase pressure drop has not understood well. The modelling of gas-liquid two phase is relatively easier than liquid-liquid two phase flow because the interaction of gas and liquid phases is neglected in most of the cases. In this case, the liquid phase flows as a continuous phase surrounding the gas phase in the form of bubbles (spherical or elongated) depending on the inlet flow ratio. A few studies have been published on the experimental determination and modelling of pressure drops in two phase gas-liquid flows in microchannels (e.g. [23]; [44]).

In the liquid-liquid slug flow the interaction between two liquid phases have significant effect on the overall performance of the slug flow reactor. There is a very little amount of work published on liquid-liquid flow in small channels and capillaries as shown in Table 2.1. Most of the previous studies were devoted for oil-water system with the aim of transportation of oil in the pipe using water which forms a wall film with the pipe/capillary material and gives lubricating action to the enclosed oil slugs. In this case, one phase flows as a continuous while the other as a discrete phase. Ousaka *et al.* [45] and Beretta *et al.* [46] have studied different flow regimes for oil-water system in the capillaries with size of 2 and 5 mm, and 3 mm, respectively. First study showed water-continuous and the inverted (oil-continuous) flow patterns, however, later study reported only water continuous flow patterns such as bubbly flow, slug flow and annular flow in a glass capillary.

If the surface tension between two liquids is lower than the capillary wall and discrete phase, then the two liquids show an alternate flow of one phase separated by the other as reported in [4], [35] and [47]. This makes both phases discrete and the hydrodynamics of such flow is not yet understood well. The nature of flow at this scale is highly dependent on the surface wetting properties. The pressure drop work, mostly carried out by physicists, in such systems have generally been interpreted in terms of two contributions: the pressure drop due to the individual phases (hydrodynamic pressure drop) and the pressure drop due to the capillary effects (capillary pressure) (e.g. [47]; [48] and the references cited therein). Further, Burns and Ramshaw [35] and Dummann *et al.* [4] carried out experiments for mass transfer and chemical reaction respectively and studied the effects of various parameters on slug size in the capillary.

Zorin and Churaev [48] have studied the liquid-liquid flow in hydrophilic and hydrophobic capillaries (0.01-0.04 mm diameter) and reported the presence of an organic wall film with hydrophobic material at such a low capillary size. Professor Ismagilov and his group ([38] and [39]), have studied the liquid-liquid slug flow in

the microfluidic chips and reported the slug flow formation mechanism and effect of viscosity on the slug flow. In the first case [38], they have used water-immiscible fluorinated fluid, PFD (10:1, perfluorodecalin and 1H,1H,2H,2H-perfluorooctanol). While in the later case [39], four combinations of immiscible liquids such as NV-A (24 %, m/m, glycerin in water) with NV-CF (10:1, v/v, fluorinated fluid and 1H,1H,2H,2H perfluoro-1-octanol, PFO), V-A (68 % glycerin in water) with V-CF (10:1, v/v, perfluoroper-hydrophenanthrene, PPP and PFO), NV-A with V-CF, and V-A with V-CF were used to study the effect of viscosity on the slug formation.

In this chapter, systematic experimental study on slug length and pressure drop has been presented on the chemically inert water-cyclohexane system. The existence of well-defined slug flow was investigated for different Y-junction mixing elements and various downstream capillaries. The slug length and contact angles were measured using a snapshot approach under similar operating conditions and corresponding interfacial area was determined. In addition to this, the pressure drop across different Y-junction mixing elements and along the length of each capillary was measured at various flow velocities. A simplified theory was employed to calculate the pressure drop along the length of capillary and the predictions were compared with experimental results. Based on the contribution of the Y-junction to the overall pressure drop, the power requirement was estimated and compared with values for conventional equipment.

2.2 Experimentation

Experimental Set-up: A schematic flowsheet of the experimental set-up for slug length and pressure drop measurement is depicted in Figure 2.1. It consists of two continuously operating high precision piston pumps to feed two immiscible liquids smoothly to a PTFE (Polytetrafluoroethylene) Y-junction mixing element with an angle of 120° between two inlet lines. The pumps with a throughput range of 1-999 ml/h each, are controlled with the help of computer which permits precise tuning of the flow rate down to 1 ml/h. An important characteristic of the Y-junction is that all three of its branches have equal dimensions. A transparent PTFE capillary, the capillary microreactor, is attached directly downstream of the Y-junction. The length of the capillary microreactor can be adjusted easily, and thus the set-up is very flexible with respect to the residence time. The photographic system comprises a commercial camera (Olympus E-20P with Macro extension lens WCON-08B) fitted at a length of 0.5 m downstream of the mixing element and a light source (2000 Watt). The transducers (range, 0-1 bar) to measure pressure drop were mounted at different locations including one on each inlet line at a distance of 0.25 m upstream

Table 2.1: Literature review on the hydrodynamics of liquid-liquid systems in the horizontal capillaries and chip reactors

System	Capillary size (mm)	Flow patterns	Reference
Dodecane - water	0.1, 0.26	Slug flow	Horvolgyi <i>et al.</i> [47]
Water - toluene, Tetradecane and Dibutyl phthalate (DBP)	0.01 - 0.04	Slug flow	Zorin and Churaev [48]
Oil - water	2.0, 5.0	Bubble, plug, slug, annular flow and inverted versions	Ousaka <i>et al.</i> [45]
Oil - water	3.0	Dispersed, slug, bubbly, plug and annular flow	Beretta <i>et al.</i> [46]
Kerosene - water	0.38	Slug flow	Burns and Ramshaw [35]
Water - PFD	0.05	Slug flow	Tice <i>et al.</i> [38]
NV-A - NV-CF	0.05 × 0.05	Slug flow	Tice <i>et al.</i> [39]
V-A - V-CF	0.15 × 0.1		
NV-A - V-CF and V-A - V-CF			

of the Y-junction, one at the Y-junction and one at a distance 0.5 m downstream of the Y-junction. Further, the positions of transducers were changed in order to measure the pressure gradient along the length of the downstream capillary. The transducers were attached to the capillaries with the help of PTFE T-junctions with the construction illustrated, while the transducer at Y-junction is attached to a similar port at the Y-junction.

Operating parameters and measurements: Experiments were carried out for different combinations of the Y-junctions having an internal diameter of 0.25 to 1 mm and with capillaries of internal diameters ranging from 0.25 to 1 mm. Water was used as an aqueous phase while cyclohexane constituted the organic phase. The physical properties of the liquids used in the present work are listed in Appendix (Table D.1). Two liquids were introduced at constant pressures and the volumetric flow rates were controlled precisely. The camera was adjusted so as to capture approximately 10 slugs in an exposure. Experiments were carried out with equal and unequal inlet flow rate combinations for each phase in the range of 5 to 200 ml/h for all capillaries. Four snapshots were taken under each set of flow conditions and the experiments were repeated twice in order to confirm the reproducibility of snapshots and pressure drop measurements. The snapshots for the contact angle measurement were taken under both flow and stationary conditions.

The snapshots were analysed using the Adobe Photoshop[®] and Image Tool software (developed by University of Texas Health Science Center San Antonio). The lengths were calibrated using the diameter of the slug and defined along the central axis of the slug. For a given snapshot maximum and minimum slug unit (i.e. a pair of aqueous and organic slugs) lengths and individual slug lengths were established, from which the average lengths, average slug size of each phase, interfacial area and standard deviations were then calculated. The three phase contact angle was also ascertained using the above-mentioned Image Tool software.

2.3 Results and Discussion

2.3.1 Slug flow generation

When two immiscible liquids are introduced into the Y-junction, one liquid initially flows downstream through the junction, while the other penetrates over to the opposite side of the junction, this mutual displacement process generates the characteristic alternating slug flow structure. This has been confirmed qualitatively

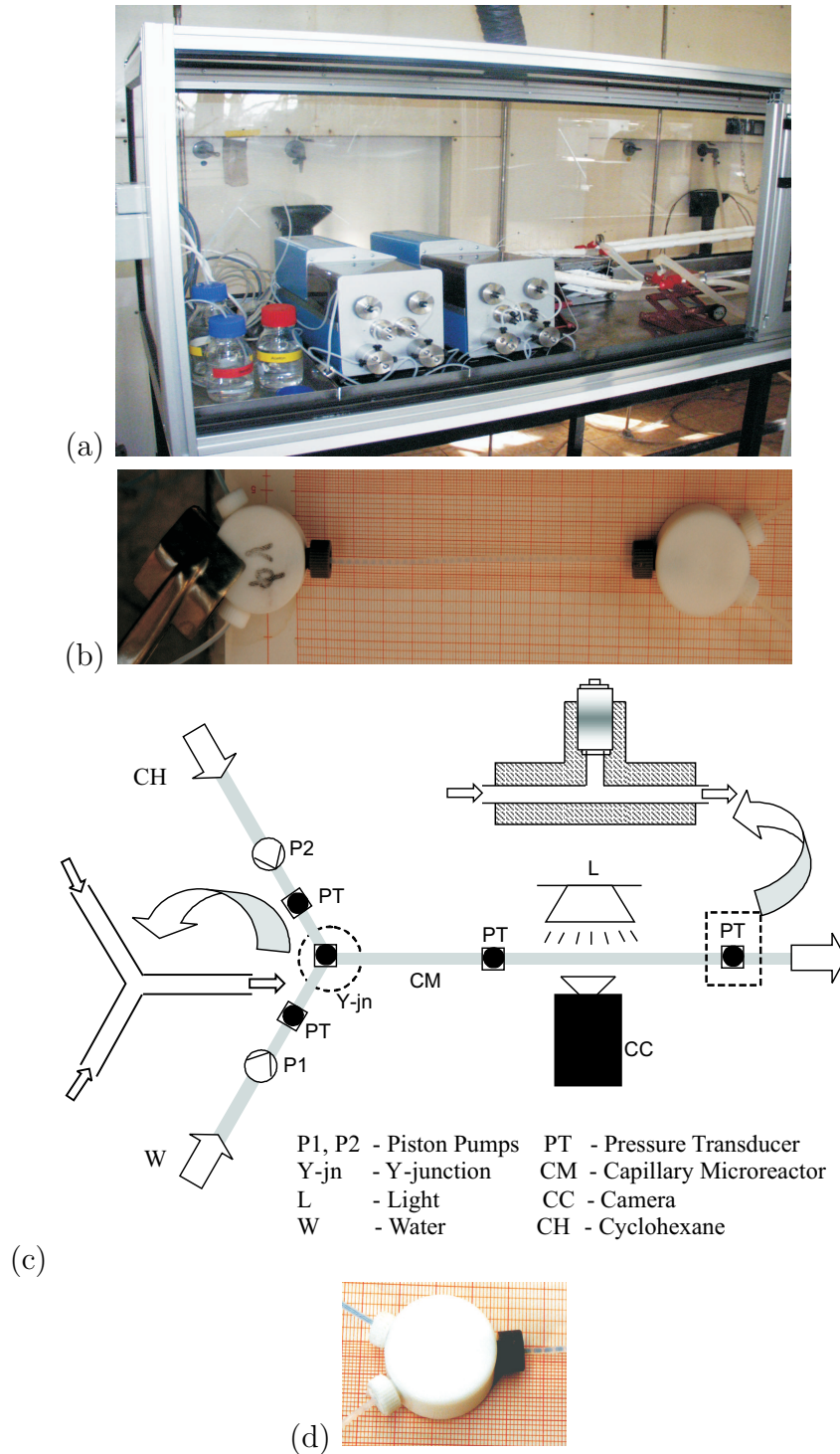


Figure 2.1: Experimental set-up used to study hydrodynamics: (a) Snapshot of experimental set-up, (b) Snapshot of Y-mixing element and Y-splitter (c) Schematic of whole set-up (d) Y-junction

by CFD simulations of the mixing behaviour. The literature shows different types of mixing elements to generate the slug flow in microreactor for different applications. The T and cross-type of elements were used to generate the slug flow in [35] and

reported that the comparison between these two devices shows no significant difference. Further, Y type mixing element was used for the production of slug flow in the capillary microreactor in [4] and reported that well defined slug flow was generated with the deviation of $\pm 5\%$ from mean slug size at same average flow velocity.

In order to distinguish two phases, the water phase was stained with a blue dye (brilliant blue) to appear darker than the colourless cyclohexane. The experimental results show that the water forms convex shaped slug while cyclohexane exhibits a concave geometry, as would be expected with the hydrophobic PTFE wall material. Experiments were carried out for capillary diameter ranging from 0.5 to 1 mm and observed well-defined slug flow in all capillaries. The experimental snapshots of prevailing flow regime of alternating two phase flow structures are shown in Figure 2.2a. The exact form of the slug and extent of slug flow regime depends on the inlet flow ratios and the capillary and Y-junction dimensions which is discussed in the next subsection.

2.3.2 Flow regimes

Flow Regime - the basic structure: In any multiphase reactor, interfacial area is governed by flow regimes. The experimental snapshots of prevailing flow regime of immiscible two phase flow structures are shown in Figure 2.2. One can easily recognise three distinct flow regimes: well-defined slug flow, drop flow and deformed interface flow. This characterisation refers to the behaviour of the water slug during flow and can be explained as follows.

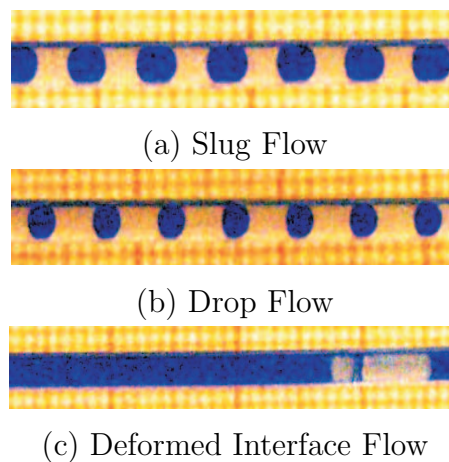


Figure 2.2: Observed flow regimes in the capillary microreactor. (Y-junction ID = 1 mm, Capillary ID = 1 mm)

1. Slug Flow: In this flow regime, the slugs of both phases have a length greater than their diameter. This flow pattern occurs at relatively low and approximately equal flow rates of both liquids. There is no coalescence or disintegration of the slugs and stable flow prevails as a consequence.
2. Drop Flow: In this regime, the water flows as small drops entrained in the organic phase due to the low water to cyclohexane ratio, while cyclohexane forms extended slugs of a length which increases with increasing cyclohexane flow rate.
3. Deformed Interface Flow: In the case of deformed slug flow, at high water to cyclohexane ratio (Q_W/Q_{CH}), water forms long slugs while cyclohexane is present as small droplets. This regime is less stable, because with increasing Q_W at constant Q_{CH} , the deformation of hemispherical caps of water slug becomes more pronounced and they tend to form bridges between adjacent water slugs, which may lead to the formation of still larger slugs by coalescence. Sometimes, it shows inverted flow patterns where water becomes continuous while cyclohexane flows in the form of enclosed slugs.

Liquid-liquid flow in horizontal pipe is characterised by different authors as shown in Table 2.1 and they observed more than three flow regimes. However, in the present work, experiments were carried out to identify the region where slug flow regime exists. Therefore two flow regimes drop flow and deformed interface flow which exists around the slug flow regimes are only presented. Two-phase gas-liquid flows in capillaries shows variety of flow patterns due to influence of buoyancy force. For liquid-liquid flows in the capillary, the small density difference results in weak gravity force and therefore patterns are usually much less complex.

Effects of capillary and Y-junction dimensions: The effect of equal capillary and Y-junction internal diameter on the flow regimes is depicted in Figures 2.3 and 2.4. The individual grid points in these figures correspond to the inlet volumetric flow rates of the two liquids into the Y-junction used for the experiments, while the bounded region indicates the conditions under which well-defined slug flow arises. As can be seen, the well-defined slug flow behaviour is observed at relatively low and approximately equal flow rates as discussed above and its extent varies with the capillary dimensions. In the case of a small capillary (ID = 0.5 mm), slug flow is observed for the same maximum flow rate of 70 ml/h for both liquids and beyond this point the flow was found to be completely unstable. However, for the larger capillaries (ID = 0.75 and 1 mm), the well-defined uniform slug flow was observed up to a maximum flow of 100 ml/h which is the maximum flow rate for both liquids

in the present study. Other investigations of the flow regime at unequal flow rates of both phases revealed that the transition of the slug flow to deformed interface flow and drop flow varies with the dimensions. The transition of slug flow to deformed interface flow occurs approximately in the Q_W/Q_{CH} range of 2.5 to 5, while the transition of slug flow to drop flow occurs in the Q_{CH}/Q_W range of 3 to 6. In the case of small capillary dimensions (ID = 0.5 mm), the transition to deformed interface flow takes place at Q_W/Q_{CH} equal to 2.5 while drop flow arises at the ratio of Q_{CH}/Q_W equal to 3 or higher. The difference between the ratios for the transition from slug flow to deformed interface flow and drop flow is thought to be due to the hemispherical caps of the water slug. The transition boundary broadens with increase in the capillary internal diameter.

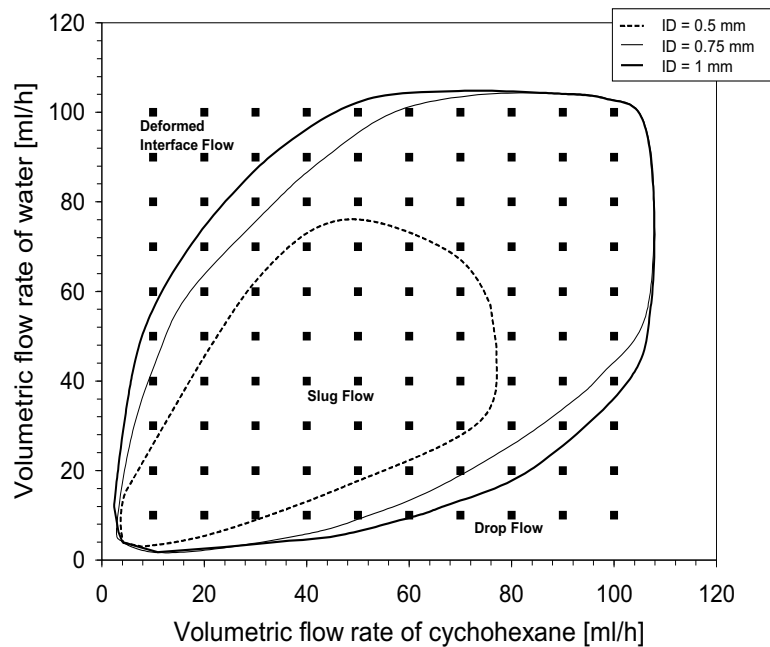


Figure 2.3: Observed flow regimes for equal capillary and Y-junction internal diameters

In order to study the effect of capillary and Y-junction dimensions on the flow regime separately, experiments were carried out for different capillaries with constant Y-junction dimensions and vice a versa. Figure 2.5 depicts the effect of different capillary dimensions on the flow regime for the same Y-junction. This figure is qualitatively similar to Figure 2.3 and shows no significant difference between constant and varying dimensions of the Y-junction. However, the different Y-junction for the same capillary diameter exhibit a considerable effect on the flow regime. Figure 2.6 depicts the effect of Y-junction dimensions (ID = 0.25 - 1 mm) on the flow regime for constant capillary internal diameter (0.75 mm). It shows that the well-defined slug flow occurs at all flow rates. In the case of a fine bore Y-junction (ID = 0.25 mm), the transition from slug flow to deformed interface flow occurs at

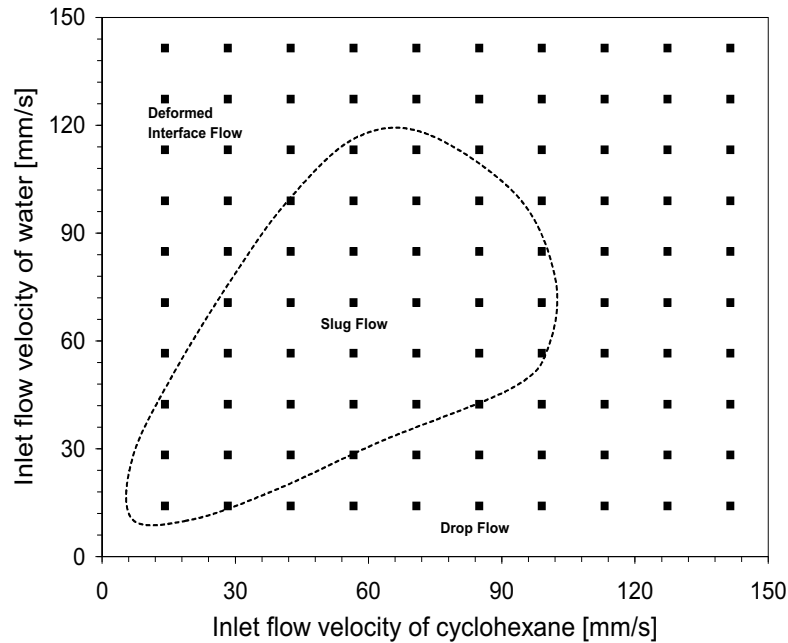


Figure 2.4: Observed flow regimes for equal capillary and Y-junction internal diameters for different flow velocities ($ID = 0.5$ mm)

a Q_W/Q_{CH} ratio of 2.5 and slug flow to drop flow at a Q_{CH}/Q_W of approximately 3. This transition boundary of the slug flow to the drop flow and deformed interface flow broadens with increasing internal diameter of the Y-junction for same capillary bore.

2.3.3 Slug size measurement

As discussed in the above section, the well-defined slug flow exists over a wide operating window, which guarantees a well-defined interfacial area for mass transfer. This information alone, of course, is not enough for *a priori* prediction of mass transfer and therefore the experiments were carried out to investigate the slug size in the well-defined slug flow regime. The effect of various operating conditions on the well-defined slug flow regime is discussed below.

Effect of slug flow velocity: The effect of slug flow velocity at identical flow rates of both phases and at equal Y-junction and capillary ID is plotted in Figure 2.7. Although the photographic evidence suggests that the slug flow is comprised of an alternating sequence of uniform slugs, the microscopic analysis reveals that the variation in slug size is by no means negligible. As illustrated in the Figure 2.7, the

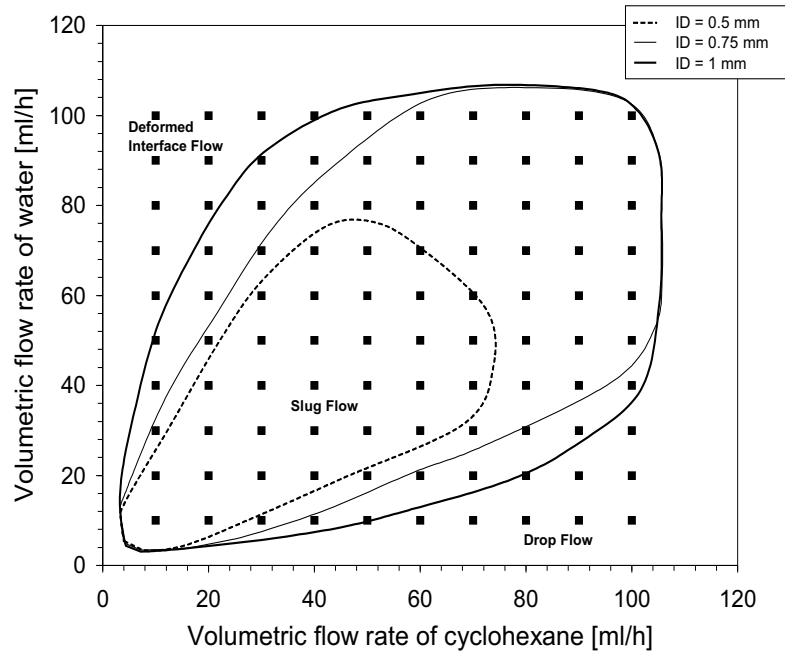


Figure 2.5: Observed flow regimes for different capillaries and similar Y-junction diameter (Y-junction ID = 0.5 mm)

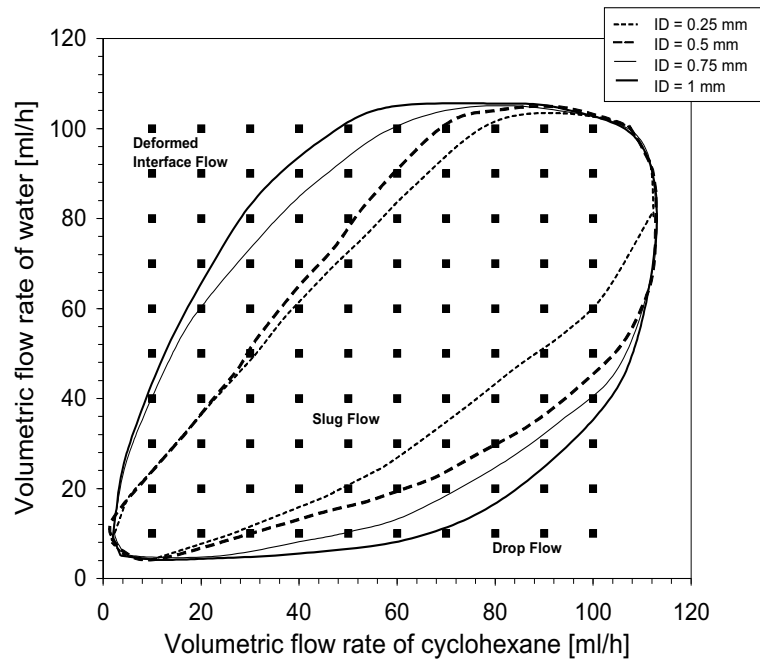


Figure 2.6: Observed flow regimes for different Y-junctions and similar capillary (ID = 0.75 mm)

slug size deviates from the mean value by 5 %. An advantage of high average flow velocity is that the slug size diminishes with increasing slug flow velocity. This is

due to the rapid penetration of one phase into other, which segregates the stream into a greater number of segments. One thus achieves higher specific interfacial areas and consequently increased mass transfer rates between adjacent slugs due to decrease in the volume of individual slugs for a given flow rate. An alternative

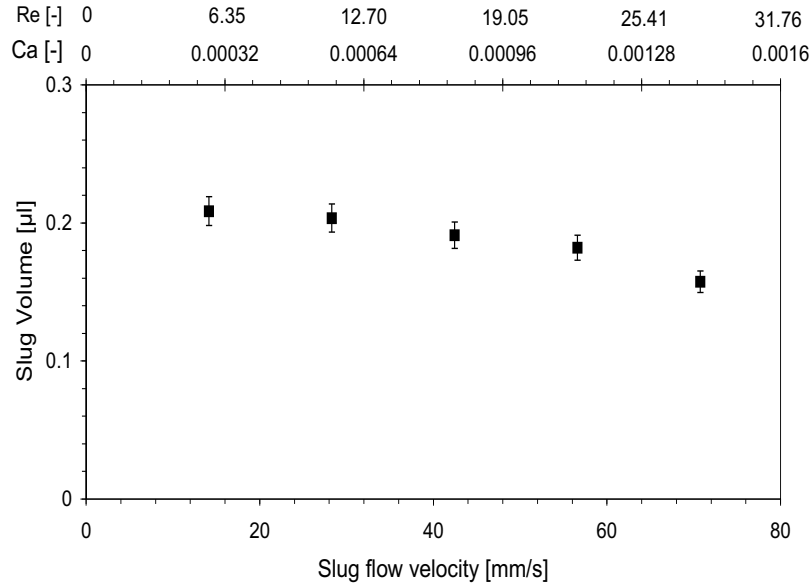


Figure 2.7: Water slug size at equal flow rate of both phases (Y -junction ID = Capillary ID, 0.5 mm)

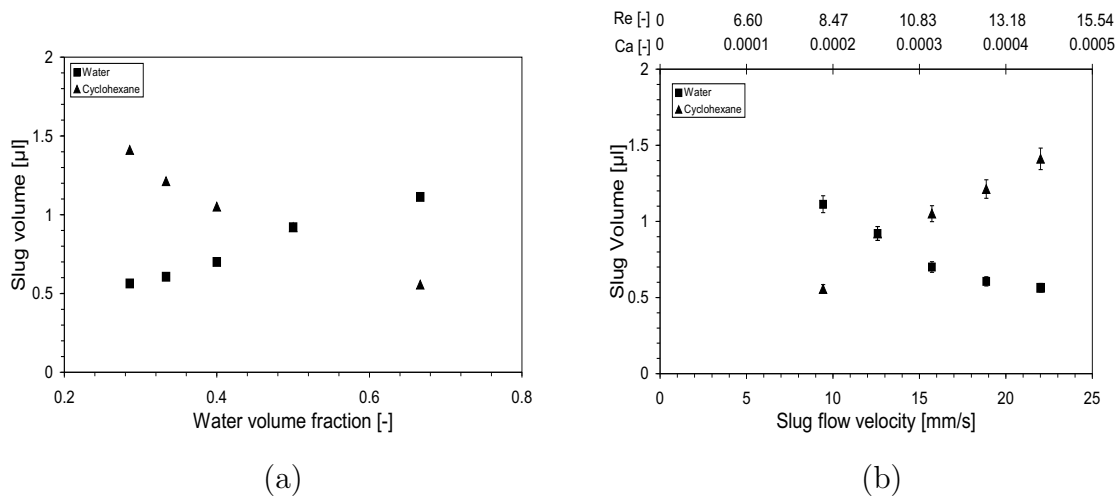


Figure 2.8: Slug size for similar Y -junction and capillary size. (a) Water and cyclohexane slug size as a function of water volume fraction (constant flow rate of water, 10 ml/h and ID = 0.75 mm), and (b) Water and cyclohexane slug size as a function of slug flow velocity, capillary number and Reynolds number (constant flow rate of water, 10 ml/h and ID = 0.75 mm) .

method to augment the interfacial area is to vary the ratio of inlet flow rates. In our experiments with variable flow rate ratios, which were carried out by keeping one liquid flow rate constant and varying the other, the volume of the slug phase with constant liquid flow rate decreases and slug volume of varying flow rate increases with increase in the flow rate as depicted in the Figure 2.8b - a not entirely unexpected result. However, the deviation of the slug size from mean remains the same.

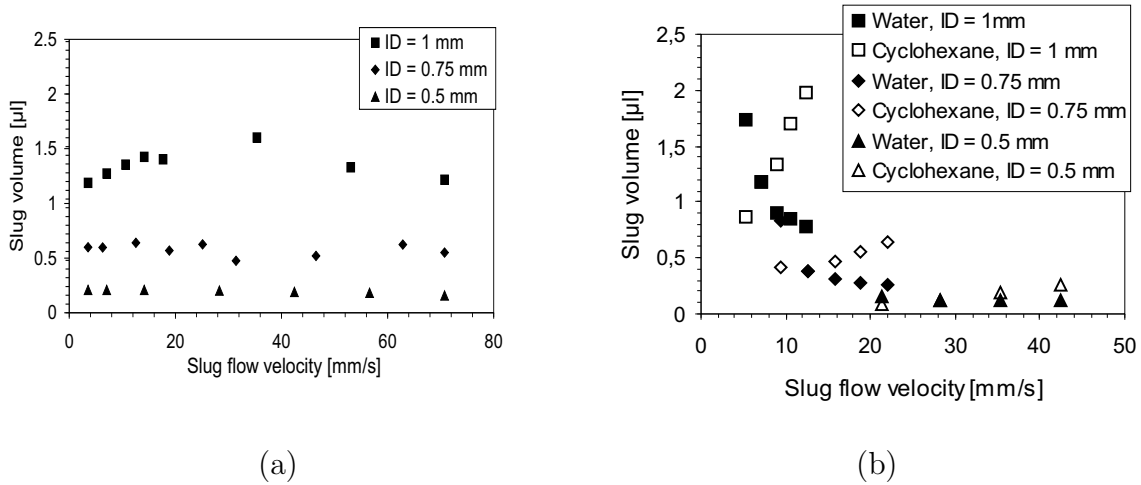


Figure 2.9: Slug size for different capillaries and similar Y-junction diameter. (a) for equal flow of both phases (Y-junction ID = 0.5 mm), (b) for constant flow rate of water (Y-junction ID = 0.25 mm).

Effect of capillary diameter: In order to study the effect of the capillary internal diameter on the slug size, experiments were carried out with different capillary diameters using the same Y-junction. The average slug volume for the aqueous phase is plotted as a function of slug flow velocity for identical inlet volumetric flow rates of both liquids for different capillaries and 0.5 mm ID Y-junction in Figure 2.9a. The slug size increases with an increase in the capillary ID for all slug flow velocities. As described above, for equal capillary and Y-junction ID, the slug size diminishes with increasing slug flow velocity. In the case of small differences between the capillary and the Y-junction dimensions (e.g., Y-junction with 0.5 mm ID and capillary with 0.75 mm), there is no significant difference in the trends. However, with further increase in the capillary ID, the trend of slug size with respect to flow velocity changes, which is in at variance with the results obtained for equal Y-junction and capillary ID. For a Y-junction with 0.5 mm ID and a capillary with 1 mm for instance, the slug size first increases with slug flow velocity. However, this trend is only temporary and beyond a flow velocity of 40 mm/s, the slug volume diminishes. This complex behaviour of slug volume for similar inlet flow rates is probably due to the different diameters affecting slug coalescence at low velocity. In addition to this,

different diameters for the Y-junction and capillary leads to increase in deviation of slug size from the mean value of around 10 % for the configuration described. The experiments with unequal flow rates of water and cyclohexane yielded similar results for increased capillary diameters as shown in Figure 2.9b.

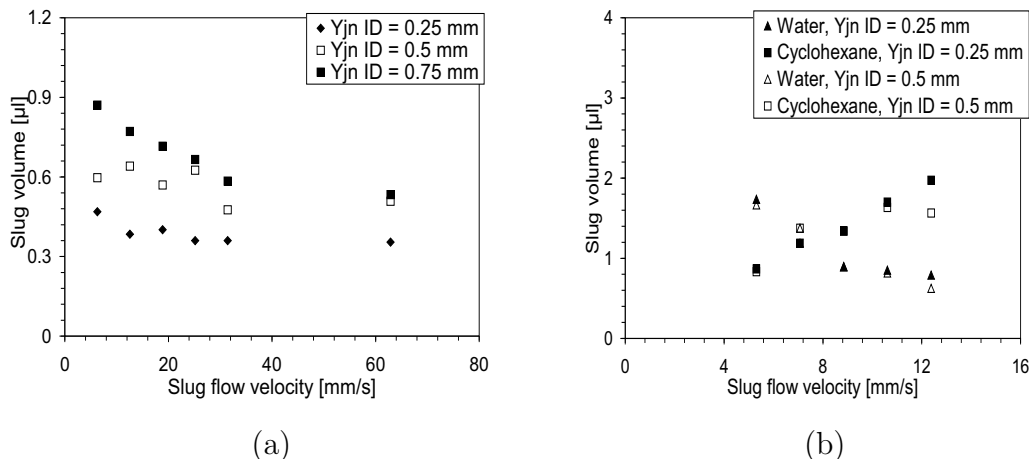


Figure 2.10: Slug size for different Y-junctions and similar capillary. (a) water slug size for equal flow rate of both phases ($ID = 0.75$ mm), (b) constant water flow rate ($Q_W = 10$ ml/h, $ID = 1$ mm).

Effect of Y-junction diameter: From the above discussion it is clear that the change in the capillary diameter exerts a major influence on the slug size. Similarly, a change in Y-junction ID also affects the slug size significantly. Increased Y-junction diameters yield larger slugs in comparison to smaller Y-junctions for the same capillary dimensions as shown in Figure 2.10a, which depicts slug size for different Y-junctions ranging from 0.25 -0.75 mm ID for a capillary with 0.75 mm. For all Y-junctions the slug size behaviour with respect to the flow velocity is the same, even though there is difference of 0.5 mm in capillary and Y-junction ID for the case of capillary with 0.75 mm and Y-junction with 0.25 mm ID. As expected, the same results were obtained for unequal flow rates as illustrated in Figure 2.10b.

2.3.4 Interfacial area

The well-defined flow patterns under slug flow regime make it possible to investigate the interfacial area from the experimental snapshots by simply measuring the size of aqueous and organic slug. Just as the slug size deviated to some degree from its mean value, a similar deviation was observed in the interfacial area. From the pressure drop studies (which are discussed in the next section), it was concluded

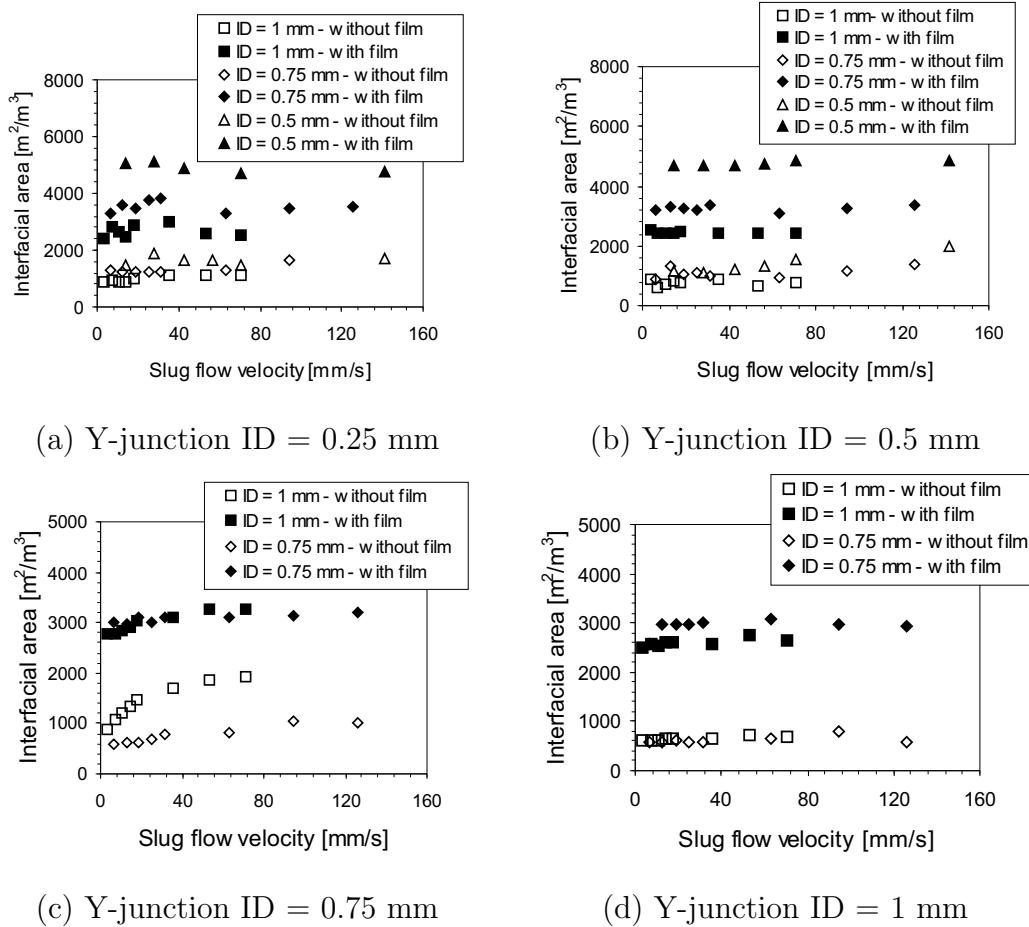


Figure 2.11: Specific interfacial area for different capillary microreactor and Y-junction diameters.

that an organic wall film is present. Two cases are therefore considered for the investigation of interfacial area: without film and with film. However, as it was difficult to visualise such a film with the resolution of our photographic equipment and the interfacial areas for the latter case were based on length of slug measured from experimental snapshots and film thickness calculated from Bretherton's law. For the case without film, only the hemispherical ends (caps) of the aqueous slug participate in the mass transfer process while in the latter case, with a wall film, the whole of the aqueous slug is involved, which of course enhances the overall transfer across the interface.

The interfacial area as a function of slug flow velocity for different capillaries and Y-junctions and for equal velocities of both phases is plotted in Figure 2.11. From the figure, one can appreciate that the presence of a wall film enhances mass transfer significantly, as increasing the interfacial area by a factor of 2-4 under all operating conditions. However, the range of interfacial area varies considerably with the capillary and Y-junction dimensions. The range of interfacial area for various operating

Table 2.2: Specific interfacial area for different capillaries and Y-junctions at equal and unequal flow rates of water and cyclohexane

Y-junction ID mm	Capillary ID mm	$Q_W = Q_{CH}$		$Q_W = 10$ ml/h		$Q_{CH} = 10$ ml/h	
		$a_{wo}, \text{m}^2/\text{m}^3$	$a_w, \text{m}^2/\text{m}^3$	$a_{wo}, \text{m}^2/\text{m}^3$	$a_w, \text{m}^2/\text{m}^3$	$a_{wo}, \text{m}^2/\text{m}^3$	$a_w, \text{m}^2/\text{m}^3$
0.25	0.5	1450 - 1680	4700 - 5100	1110 - 1905	4550 - 5100	1070 - 1480	4700 - 5130
	0.75	1220 - 1660	3300 - 3800	990 - 1220	3570 - 3720	930 - 1220	3540 - 3700
	1.0	860 - 1130	2430 - 2310	560 - 920	2550 - 2850	610 - 920	2550 - 2850
0.5	0.5	1080 - 1970	4500 - 4800	1085 - 1770	3660 - 4690	1085 - 1980	3300 - 4600
	0.75	880 - 1330	3200 - 3330	960 - 1330	2520 - 3300	1205 - 1334	2782 - 3310
	1.0	620 - 870	2400 - 2510	730 - 1025	1860 - 2440	750 - 1380	2024 - 3500
0.75	0.75	870 - 1686	2980 - 3190	540 - 630	2190 - 3010	620 - 990	3010 - 3560
	1.0	580 - 1040	2760 - 3090	490 - 1090	1710 - 2780	960 - 1410	2780 - 3170
1.0	0.75	560 - 780	2560 - 3080	580 - 620	1970 - 2440	510 - 580	1940 - 3400
	1.0	590 - 780	2510 - 2760	550 - 670	1750 - 2380	500 - 690	2520 - 3190

conditions is given in Table 4.4 which shows that increased capillary and Y-junction dimensions reduce the interfacial area. Recently, Dehkordi [49] has investigated a novel reactor referred to as a two-impinging-jets reactor which is characterised by a small reactor volume equipped with two simple nozzles directed towards each other in which interfacial area as high as $3500 \text{ m}^2/\text{m}^3$ were found, which is way above the values in a mechanically agitated reactor ($a \sim 500 \text{ m}^2/\text{m}^3$). The interfacial area was established assuming mass transfer with chemical reaction for a pseudo-first order heterogeneous liquid-liquid reaction. The directly measured interfacial area for the slug flow capillary reactor compares favourably with the impinging jet reactor. Besides, the presence of film in liquid-liquid slug flow offers 2 to 4 times more interfacial area under the same operating conditions. The interfacial area obtained can be manipulated precisely due to the well-defined flow pattern and one can thus regulate interfacial mass transfer.

2.3.5 Pressure drop across Y-junction

The power required to provide a unit interfacial area, a parameter of practical relevance as a benchmark for technical reactors, can be calculated from the contribution of Y-junction in the overall pressure drop. Therefore, experiments were carried out to measure the pressure drop across the Y-junction. Initially, several experiments were carried out in order to identify the most suitable pressure measurement points. This was done by taking sequential videos under various operating conditions and selecting four locations including two on the inlet lines at a distance 0.25 m upstream of the Y-junction, one at the junction itself and one at a distance 0.5 m downstream for mounting pressure transducers. The pressures were measured under various operating conditions and the differences between them are referred to as ΔP_1 , ΔP_2 and ΔP_3 as shown in Figure 2.12. As can be seen from the Figure, pressure drop increases with increase in the flow velocity. The major contribution to the pressure drop during slug generation is ΔP_3 , the pressure drop between a point on Y-junction and the point 0.5 m downstream in the capillary. The pressure drops between the inlet and Y-junction, ΔP_1 and ΔP_2 , are much lower and are more or less equal to the pressure drop for single phase flow through the capillary - i.e. the Hagen-Poiseuille pressure drop.

In order to observe the effect of the Y-junction on the pressure drop for equal inlet flow velocities, the variation of pressure along the length of the Y-junction and connected capillaries for equal inlet flow velocities is plotted in Figure 2.13a. The pressure loss due to the Y-junction is calculated by measuring ΔP_3 and the pressure gradient along the length of the capillary (discussed below). The results show that with increasing water inlet flow velocity, up to 25 mm/s, there is negligible pressure

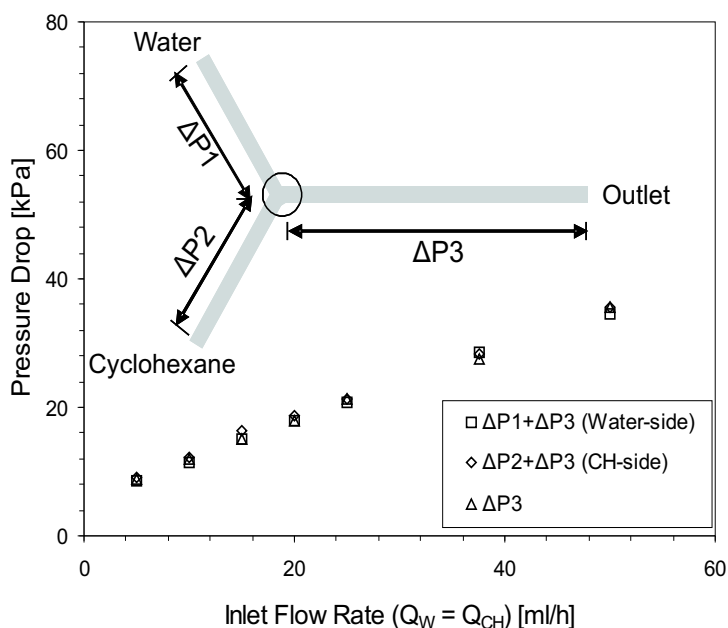
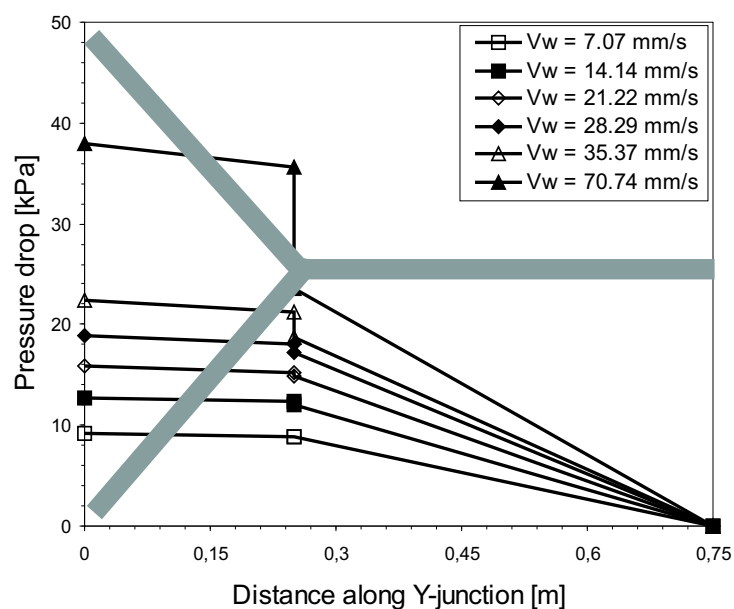


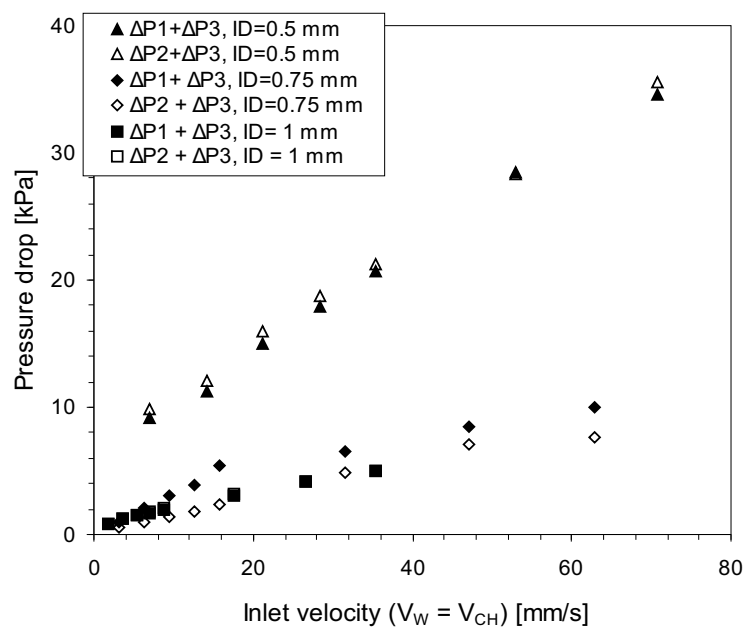
Figure 2.12: Pressure drop across the Y-junction at equal flow rates of water and cyclohexane. (Capillary ID = Y-junction ID, 0.5 mm)

drop while for further increase in it the losses become significant. At the transition boundary of the well-defined slug flow (the velocity beyond which the slug flow does not exist, 70 mm/s in this case), the pressure drop is about 12 kPa. Since the inlet velocity of water and cyclohexane is the same, similar pressure variations along the Y-junction were observed for different inlet velocities of cyclohexane. Further experiments were carried out to study the effect of capillary dimensions on the pressure drop across the Y-junction which was found to increase with decreasing capillary ID as shown in Figure 2.13b.

The introduction of unequal flow rates to Y-junction can affect the slug size and thus the interfacial area; and such asymmetric flow conditions will be the rule rather than the exception in chemical engineering processes. Therefore the measurements were carried out across the Y-junction for unequal flow rates of water and cyclohexane, i.e. done by keeping one of the flow rates constant and varying the other. The behaviour of the pressure drop in a capillary of internal diameter 0.5 mm along the Y-junction for various inlet flow ratios is plotted in the Figures 2.14a and 2.14b. As can be seen from the Figure 2.14a, at constant flow rate of water, the most significant effect was observed at a flow ratio of 0.66 ($Q_{CH} = 15$ ml/h), beyond which the slug flow disappeared. The same trends were observed at constant flow rate of cyclohexane, as shown in Figure 2.14b. Both figures indicate that the pressure loss contribution of the Y-junction rises with increasing total flow rate.



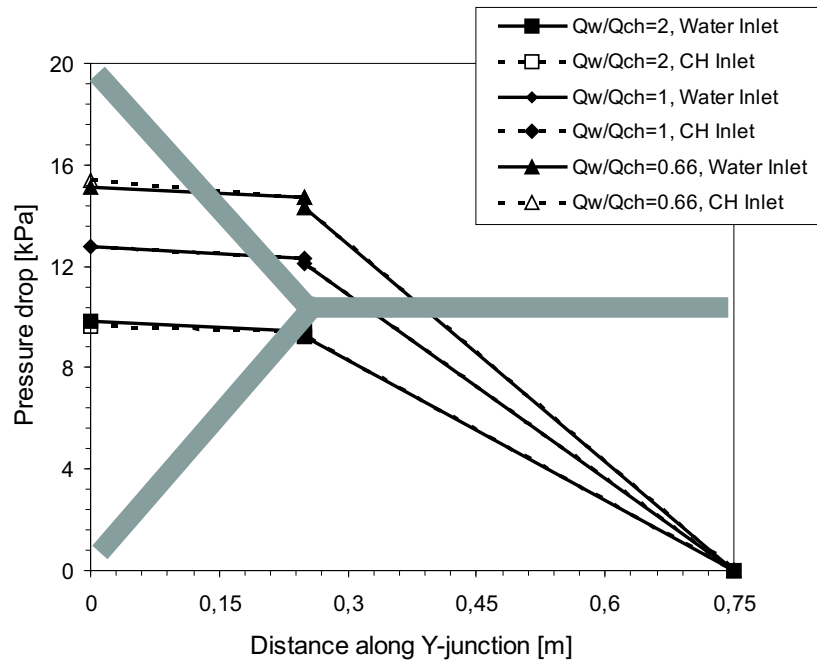
(a)



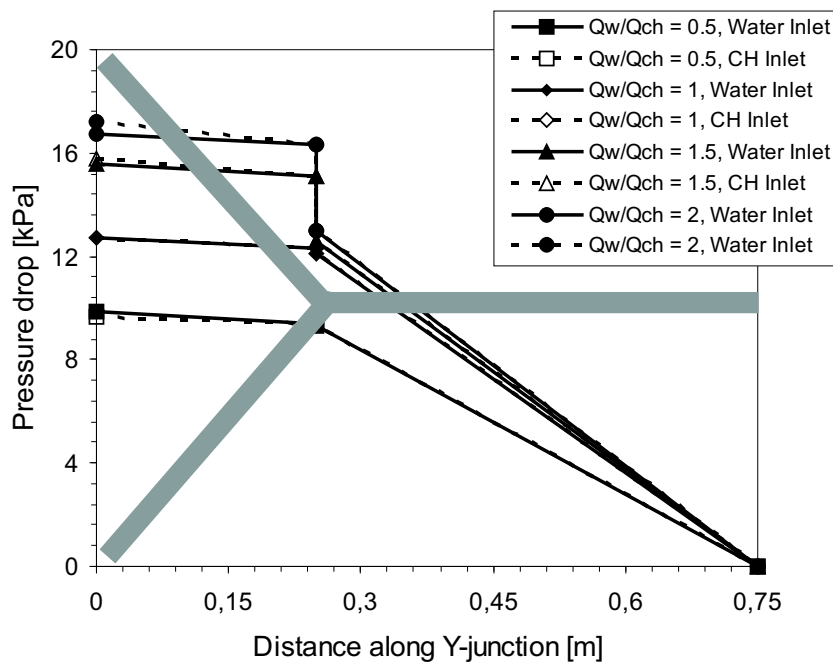
(b)

Figure 2.13: Pressure drop in the vicinity of Y-junction at equal flow rates of water and cyclohexane. (a) Behaviour of pressure along the length of Y-junction, and (b) Pressure drop for different internal diameters.

Further experiments were carried out under well-defined slug flow regime to establish the pressure drop across the junction ($\Delta P1 + \Delta P3$ and $\Delta P2 + \Delta P3$) at unequal flow rates of water and cyclohexane for both similar and dissimilar dimensions of

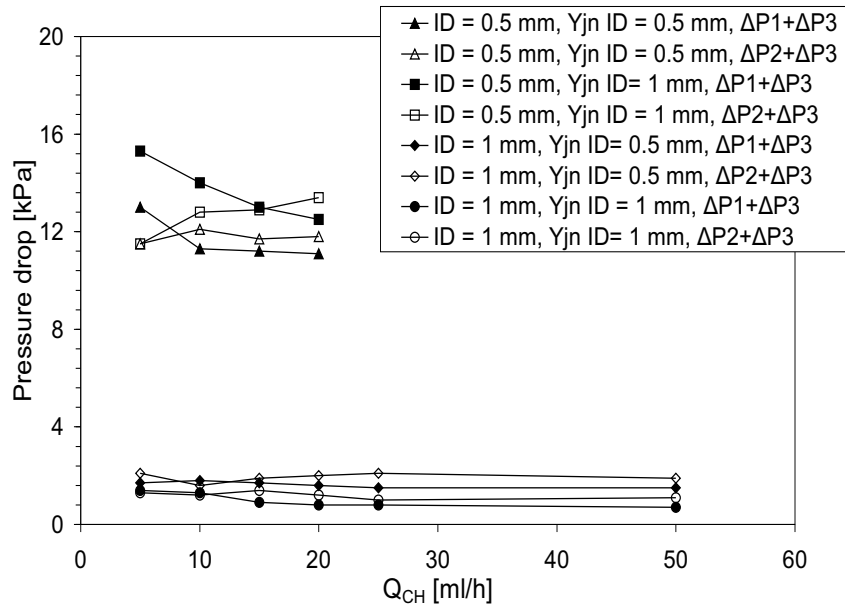


(a)

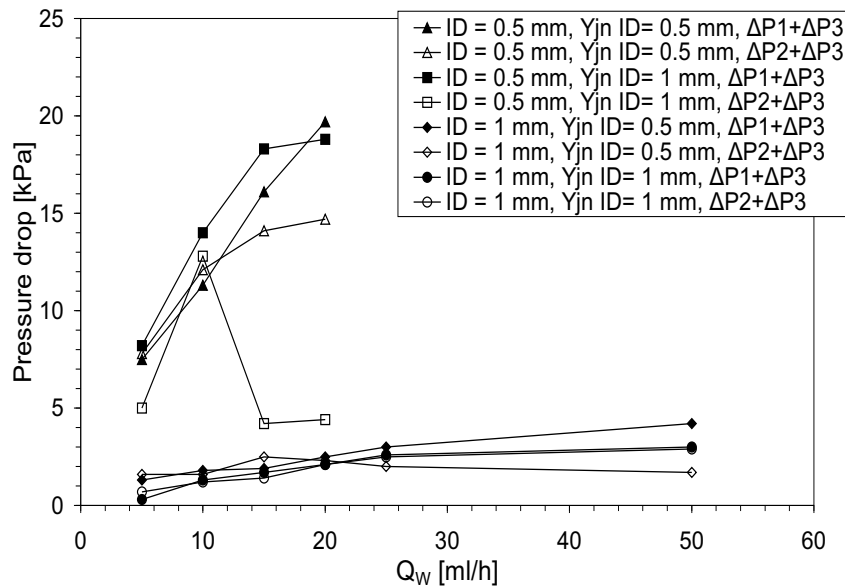


(b)

Figure 2.14: Pressure drop in the vicinity of Y-junction at unequal flow rates of water and cyclohexane. (a) Behaviour of pressure along the length of Y-junction at constant water flow rate, $Q_W = 10 \text{ ml/h}$, (b) Pressure drop for different internal diameter at constant cyclohexane flow rate, $Q_{CH} = 10 \text{ ml/h}$



(a)



(b)

Figure 2.15: Pressure drop in the vicinity of Y-junction at unequal flow rates of water and cyclohexane. (a) Pressure drop for different capillary internal diameter at constant flow rate of water, $Q_W = 10$ ml/h, and (b) Pressure drop for different capillary internal diameter at constant flow rate of cyclohexane, $Q_{CH} = 10$ ml/h

Y-junction and three downstream capillaries (see Figure 2.15). For similar internal diameter of capillary and Y-junctions, at constant flow rate of water, the water-side pressure drop ($\Delta P1 + \Delta P3$) decreases with increase in the inlet flow rate of cyclohexane, while the pressure drop on the cyclohexane side ($\Delta P2 + \Delta P3$) remains almost

constant. However, in the case of dissimilar internal diameters for the capillaries and Y-junctions (e.g. capillary ID = 0.5 mm and Y-junction ID = 1 mm), the water-side pressure drop ($\Delta P_1 + \Delta P_3$) decreases while the cyclohexane side pressure drop rises with increasing cyclohexane flow rate at constant water flow. However, in the case of larger capillary ID and smaller Y-junction bores, there is a significant effect of cyclohexane flow velocity on the pressure drop on both sides. The trends described are significantly different in the case of a constant flow rate of cyclohexane for increasing water flow rate.

In all cases of similar and dissimilar dimensions of capillaries and Y-junctions, the pressure drop increases markedly at higher water flow rates. This behaviour of pressure drop may be due to the presence of an organic wall film in the capillary, since in the absence of film the pressure drop should be approximately equal under both sets of conditions due to the similar properties of the liquids. In the presence of a film at constant flow rate of water, the slug size decreases significantly with increasing cyclohexane flow rates thereby reducing proportionately the overall film region which thus exerts a lower shear stress and exhibits no significant effect. On the other hand, for constant cyclohexane flow rate, the length of enclosed (water) slug increases with increasing water flow thus giving rise to a larger pressure drop.

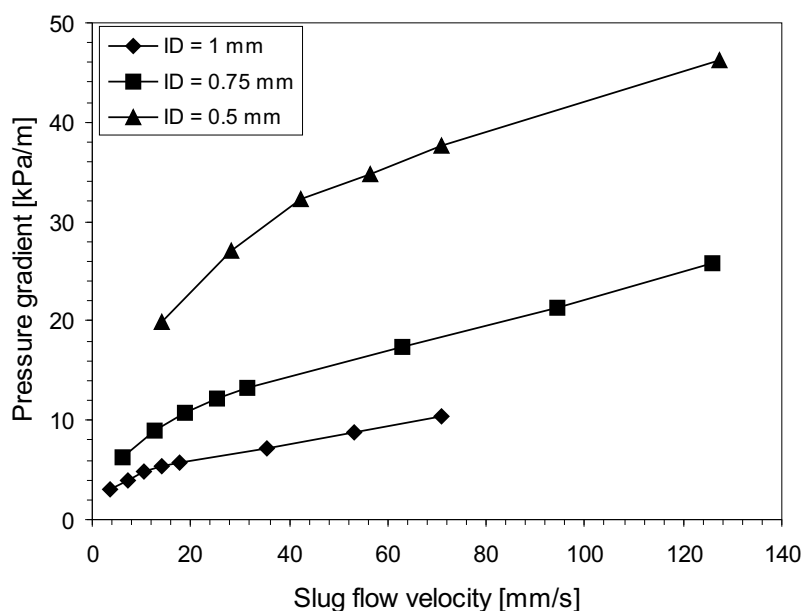


Figure 2.16: Experimental pressure drop along the length of the capillary microreactor for equal flow rates of water and cyclohexane.

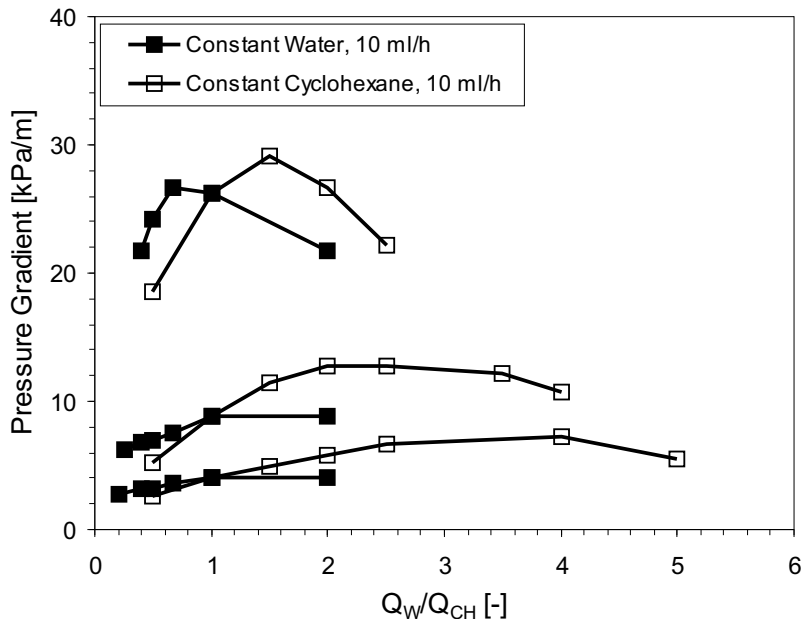


Figure 2.17: Pressure gradient as a function of water to cyclohexane flow ratio.

2.3.6 Pressure drop along the length of capillary

Experimental: The pressure drop across a given length of the liquid-liquid slug flow capillary microreactor was measured for different slug flow velocities and inlet flow ratios for various Y-junction and capillary dimensions. Figure 2.16 depicts the pressure drop behaviour observed for equal flow rates of both phases. The results show that for equal flow rates and for all capillaries, the pressure drop increases with increasing slug flow velocity and is furthermore a strong function of capillary ID as capillary effects dominate the behaviour at such small dimensions. As would be expected, the pressure drop was found to be larger for smaller capillary ID. In the experiments carried out with larger capillaries (ID = 1 mm) the pressure drop increased from the low values observed at slow flow up to a certain value and subsequently remained constant. For small capillaries (ID = 0.5 and 0.75 mm), on the other hand, the pressure drop increases with further in the same velocity range.

The pressure drop for different flow ratios (measured by keeping one of the flow rates constant and varying the other), illustrated in Figure 2.17, shows that the pressure drop increases with an increase in the flow ratio of water to cyclohexane but the trend is reversed beyond a certain flow ratio, and subsequently decreases. Alike pressure drop for equal flow rates, the capillary dimensions are decisive - pressure drop

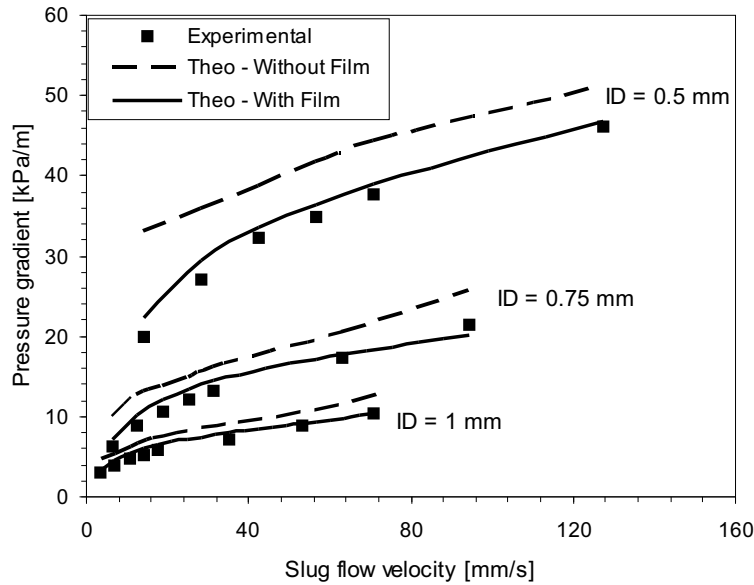


Figure 2.18: Comparison of experimental and predicted pressure drop at equal volumetric flow rates of water and cyclohexane.

increases with decrease in capillary size. Additionally an interesting phenomenon arises at constant velocities of water and cyclohexane. At low Q_W/Q_{CH} ratios, the pressure drop at constant flow rate of cyclohexane is less than at constant water flow rate and vice versa at higher Q_W/Q_{CH} flow ratio. The flow ratio corresponding to the maximum pressure drop is different for different capillary dimensions and flow rates. For a constant water flow rate, it is 0.65 for the capillary with 0.5 mm ID and 1 for the capillaries with 0.75 and 1 mm ID, while for constant flow rate of cyclohexane it is 1 for the 0.5 mm ID capillary and 2 and 2.5 for 0.75 and 1 mm ID respectively. The two pressure drop curves coincide at equal flow rates of water and cyclohexane.

As the slug size analysis shows, the Y-junction dimensions have strong influence on the slug length and thus size for the same capillary dimension. The pressure drop was also measured under the same operating condition and exhibited no effect of the Y-junction used for the same capillary. The results reveal the presence of a film, because in the absence of a film the pressure drop would be a strong function of the length of slug - a decrease in the length would enhance the capillary pressure and thus increase the overall pressure drop. However, the present study shows little effect of the slug size and only an influence of the flow ratio.

Theory - without film: In the previous sections, it has been conjectured that the organic liquid forms a wall film due to wetting properties of the two liquid phases and the capillary material. Since the film is probably only a few micrometer thick, it is virtually impossible to visualise it directly with the help of snapshots. We have therefore derived simplified models to provide evidence of the presence of a thin organic wall film which are described in detail in Appendix A. The final equation of the model, A.3, is given in the following;

$$\Delta P = \frac{L}{l_U}(\Delta P_W + \Delta P_{CH}) + \frac{2L - l_U}{l_U} P_C \quad (2.1)$$

The experimental results are compared with theoretical pressure drop without film in Figure 2.18. The theoretical pressure drop was calculated using the slug lengths and contact angles retrieved from the experimental snapshots. The contact angle was measured from the snapshot of static fluid. These values show reasonable agreement with the experimental results, although the discrepancy between the two increases with decreasing capillary diameter. In the experiments of Horvolgyi *et al.* [47] for very small capillaries (ID = 0.05 mm and 0.13 mm), it was observed that this theoretical pressure drop under-predicts the overall pressure drop and this was explained as a result of the capillary pressure term not being suitable to describe the two phase capillary flow in considerable section of the flow system.

In the present work, however, the analytical solution tends to over-predict of the pressure drop for all capillaries. This may well be due to the superior wetting properties of the organic phase on the capillary material, which results in the formation of a thin superficial film. This film provides a lubricating action on the embedded slug and yields annular flow behaviour exhibiting different pressure drop characteristics compared to the simplified model initially employed. Another possibility to explain the discrepancy is the internal circulations induced within each individual slug. When the slugs move through the capillary internal circulations arise within the slug, due to the shear between capillary wall and axis of the slugs, which reduces the thickness of the boundary layer and can eventually affect the capillary pressure. However, such circulations are of advantage in mass transfer because they enhance the diffusive penetration between two phases. It is thus important to implement the effect of film and internal circulations in the theoretical pressure drop calculations.

Theory - with wall film: Theoretical pressure drop with a wall film (derived in Appendix A) yields following equation for the pressure drop in a capillary;

$$\frac{\Delta P}{L} = \left(\frac{\alpha_W}{1 - k^4} \right) \left(\frac{\Delta P}{L} \right)_{CH} \quad (2.2)$$

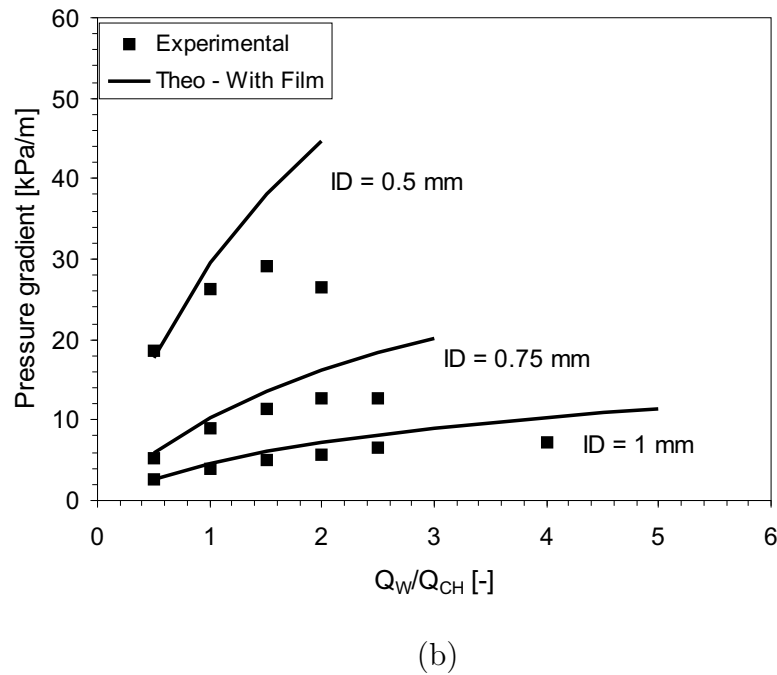
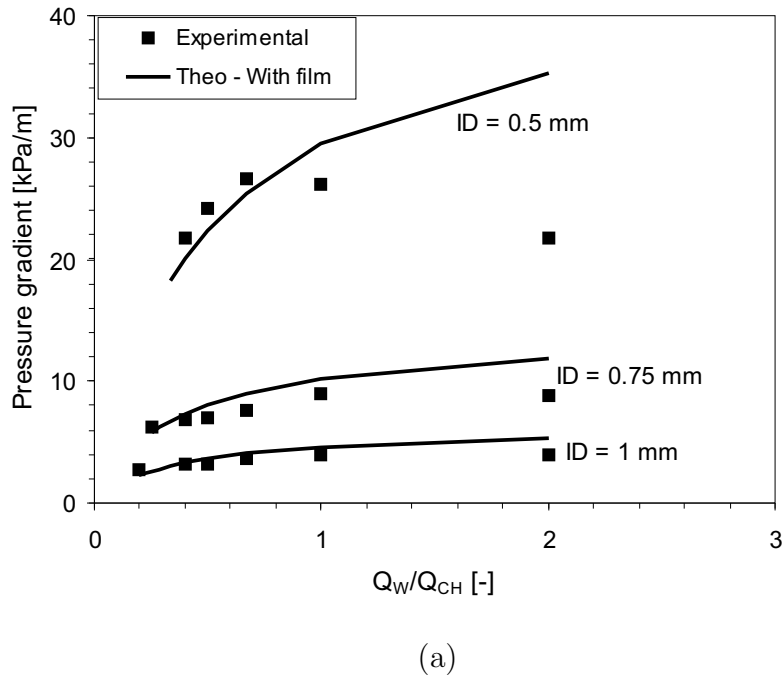


Figure 2.19: Comparison of experimental and predicted pressure drops for unequal flow rates of water and cyclohexane. (a) Constant flow rate of water, 10 ml/h and (b) Constant flow rate of cyclohexane, 10 ml/h

The experimental results and theoretical pressure drops are compared as shown in the Figure 2.18. It shows the comparison of theoretical pressure drop without and with film together with the experimental values at equal flow rate of both phases. The agreement between experimental and theoretical pressure drop is reasonably

good, especially in comparison to the model neglecting film formation. The film thickness calculated by Bretherton's law was in the range of 1-20 μm for all capillaries under the slug flow regime. Further predictions of the model at different Q_W/Q_{CH} flow ratios exhibit good agreement with the experimental values. The pressure gradient as a function of Q_W/Q_{CH} flow ratio is depicted in Figure 2.19. As with the pressure gradient at equal flow rates, the results show good agreement with the experimental values at the low ratio values. For larger capillary (ID = 1 mm), the agreement is good upto Q_W/Q_{CH} equal to 2 for constant water flow and Q_W/Q_{CH} equal to 4 for constant cyclohexane flow rate. However, the agreement between theoretical and predicted pressure drop worsens with decrease in the capillary diameter. For the small bore capillary (ID = 0.5 mm), it shows considerable deviation beyond a flow ratio 1 for constant flow rate of water and 1.5 for constant flow rate of cyclohexane. The disagreement between experimental and theoretical prediction at higher flow rates may be due to the transition of the slug flow regime into drop flow and deformed interface flow. Thus the prediction of pressure drop with the wall film shows that its presence can significantly alter pressure drop while the measurements of pressure drop along the capillary microreactor corroborates the presence of such a film.

2.3.7 Power input

Power input, an interesting parameter for benchmarking technical reactors, has been calculated from the pressure loss due to the Y-junction in the capillary microreactor. The results obtained were compared with various liquid-liquid contactors given in Dehkordi[49] as shown in Table 2.3. The comparison shows that the liquid-liquid slug flow capillary microreactor requires much less power than the alternatives to provide such a large interfacial area.

2.4 Summary

Experiments were carried out to investigate flow regime, slug size, interfacial area, pressure drop and power requirement under various operating conditions using different Y-junction mixing elements with various downstream capillaries. The capillary and Y-junction dimensions show a significant effect on slug size and thus interfacial area, which increases with decreasing dimensions. The pressure drop was measured across the Y-junction and along the length of slug flow capillary. A theoretical prediction for pressure drop along slug flow capillary was developed based on the

Table 2.3: Power input requirement for various liquid-liquid contactors

Contactator Type	Power Input, kJ/m ³ of liquid
Agitated extraction column	0.5 - 190
Mixer-settler	150 - 250
Rotating disk impinging streams contactor	175 - 250
Impinging streams	280
Impinging stream extractor	35 - 1500
Centrifugal extractor	850 - 2600
Liquid-liquid slug flow (Present work)	0.2 - 20

capillary pressure and hydrodynamics pressure drop without a wall film and compared with experimental results. The discrepancies were observed with this theory and the underlying reasons were identified. The presence of an organic wall film was one of the reasons and an improved model taking it into consideration showed good agreement with the experimental values. The power input was calculated using the pressure losses over the mixing element and it was found that slug flow capillary microreactor is superior to conventional equipment in the sense of providing more interfacial area with less power. In addition to this, precise tuning of interfacial area and thus mass transfer across the interface is possible in this reactor as a result of the well-defined flow patterns. These experimental findings will be helpful in devising a more detailed computational model for predicting the mass and heat transfer and reaction kinetics in liquid-liquid slug flow capillary microreactor.

Chapter 3

Mass Transfer and Chemical Reaction

3.1 Introduction

As discussed in Chapter 1, liquid-liquid extraction is an important unit operation for laboratory as well as industrial applications. Many studies, research papers (e.g. [50]), review articles and books (e.g. [11], [51]) have been published on the hydrodynamics, mass transfer and biphasic reaction in different contactors. Recently, for example, Dehkordi ([49], [52], [53]) has published series of articles on impinging stream contactors and compared their superior mass transfer performance with conventional contactors for various liquid-liquid systems.

When one considers the attention that has been paid on mass transfer in gas-liquid microreactors (e.g. [23], [25], [26], [27], [28], [32], [54]) the paucity of publications on microextractor technology is somewhat surprising. The liquid-liquid slug flow microreactor scheme was exploited for mass transfer and reaction engineering applications by Professor Ramshaw and his group at the University of Newcastle (UK). They developed a multiphase microreactor based upon the use of liquid-liquid slug flow and obtained mass transfer performance data for extraction of acetic acid from kerosene slugs [35]. Later on, they employed the same reactor for the nitration of benzene and toluene [55] and reported high reaction rates compared to conventional processes. During the same period, Dummann *et al.* [4] carried out experiments for the production of nitroaromatics in a capillary microreactor using the same concept. The reaction was carried out in slug flow regime and focused on reducing the formation of by-products. Some CFD simulations were carried out, leading to the

conclusion that the enhancement of mass transfer can be interpreted in terms of an intense internal circulatory flow within the individual slugs.

Liquid-liquid slug flow capillary microreactor can also be used to solve the problem associated with dispersion and mixing in the laminar flow. Song and Ismagilov [18] used liquid-liquid slug flow micro-fluidic equipment for measurement of millisecond kinetics of ribonuclease A to obtain single turnover rate constant. Each slug carried a mixture of two reagents and a stream of buffer injected into micro-fluidic chip and the mixing in the slugs were achieved by inducing chaotic flow inside the droplet.

As we know, an *a priori* knowledge of the effective interfacial area and the mass transfer coefficient is very important for appropriate design of an extractor. The interfacial area in the liquid-liquid contactors can be investigated using physical and chemical techniques for different chemical systems. The physical technique determines the local interfacial area, which can not be integrated for whole equipment to investigate the global interfacial area in the case of conventional contactors due to non-uniform flow patterns and therefore chemical method has been used extensively. On the other hand, microreactors provide well defined flow patterns and the local interfacial area can be integrated for the whole contactor. However, from the pressure drop study (see Chapter 2), it was revealed that due to superior wetting properties of capillary material and organic phase, the organic phase forms a wall film with capillary material which can not be seen with the help of laboratory camera. In this case, chemical method is useful as it gives global interfacial area available for mass transfer and its comparison with integrated physical interfacial area may give an idea about the presence of the wall film.

The major advantage of chemical method is that it determines global values of interfacial area in the heterogeneous system without disturbing the flow patterns. This method for investigation of interfacial area was developed by Westerterp *et al.* [56] for gas-liquid systems. Further, it was adapted for liquid-liquid systems by Nanda and Sharma [57] and numerous attempts have been made since then. They employed n-propyl formate and n-butyl formate to study the interfacial area in a spray column and proposed this method for rotating disc contactors, packed columns and agitated reactors. Later on, most of the studies were carried out for liquid-liquid systems in agitated column (e.g. [58], [59], [60], [61]). There are also studies published on spray columns [62] and packed extraction column [63]. Recently, Dehkordi [52] has used this method to investigate the interfacial area in an air driven impinging streams contactors.

The above work clearly demonstrate the potential of liquid-liquid slug flow capillary microreactor for mass transfer and chemical reaction. Also, the extensive use of

Table 3.1: Literature review on the study of liquid-liquid systems for mass transfer and chemical reaction in the capillaries and chip reactors

System	Capillary/chip size (mm)	Reaction	Reference
Kerosene (acetic acid) - Water (NaOH / KOH)	0.38	Neutralisation	Burns and Ramshaw [35]
Nitration acid (sulphuric acid + nitric acid) - Benzene, Toluene	0.127 - 0.3	Nitration	Burns and Ramshaw [55]
Nitration acid (sulphuric acid + nitric acid) - Aromatic (single ring aromatic)	0.5 - 1.0	Nitration	Dummann <i>et al.</i> [4]
RNase + buffer + RNaseAlert - fluorinated fluids	0.01 - 0.02	Enzymatic	Song and Ismagilov [18]

chemical method proves that it is a promising tool to investigate the interfacial area available for mass transfer in the liquid-liquid systems. In this chapter, experimental study on mass transfer with and without chemical reaction is presented. The chapter is outlined as follows. First part of the chapter presents the liquid-liquid extraction of four non-reactive systems: n-butyl-formate (NBF) from its saturated solution into distilled water (I), iodine from its aqueous solution into kerosene (II), succinic acid from its aqueous solution into n-butanol (III), and acetic acid from kerosene into distilled water (IV). The reason of choosing these four systems is that they used to investigate mass transfer rates in impinging stream contactors (system I - air driven contactor [52], and systems II, III, IV - jet contactors [49]). The objective was to compare the performance of liquid-liquid slug flow with the impinging stream contactor and other conventional contactors.

The second part of this chapter contains experimental study of mass transfer with chemical reaction for the extraction of acetic acid from kerosene into water using simple titration reaction. This reaction was chosen in order to obtain the information about the timescale required to perform mass transfer limited reactions. Further, results of the chemical method which was used to investigate the interfacial area are discussed in detail. The effects of various operating conditions such as flow rate, capillary diameter and flow ratio on both mass transfer and chemical reaction are also presented.

3.2 Experimentation

Experimental set-up: The experimental set-up used for mass transfer and chemical reaction is similar to the set-up presented in Chapter 2 which is briefed here with some additional elements. The set-up, Figure 3.1, illustrates that the two immiscible liquids (aqueous and organic from 1 and 2) are introduced by continuously operating high-precision piston pumps (3 and 4) to a symmetric 120° Y-piece mixing element made of Teflon (5). The capillary (6) contactor, is made of PTFE (Polytetrafluoroethylene) and was attached directly downstream of the Y-piece. At the end of the contacting stage, a flow splitter (7), which is discussed in detail in the next Chapter, was employed to separate the phases. The samples from two outlets of the splitter were collected in the sampling bottles (8 and 9) for further analysis.

Operating conditions and measurements: The operating conditions used for the experiments are given in Table 3.2 and physical properties of the liquids used are listed in Appendix (Table D.2). All experiments were carried out under the slug

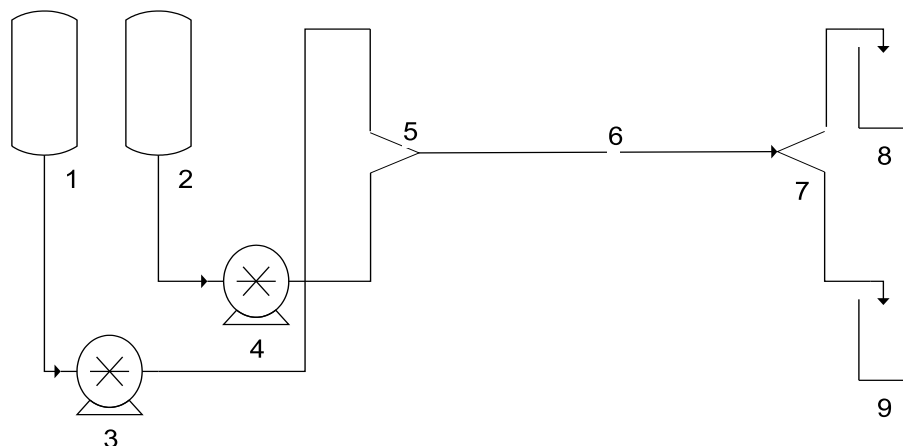


Figure 3.1: Experimental set-up used to study mass transfer and chemical reaction: (1,2) reservoirs containing aqueous and organic liquids; (3,4) feed pumps; (5) Y-junction mixing element; (6) slug-flow capillary; (7) flow splitter; and (8,9) sampling bottles

flow regime with both equal and unequal flow rates of the two phases. For each set of operating conditions, three samples were taken from each outlet stream of the splitter to ensure the reproducibility of the results. Quantitative analysis of the samples was performed using a simple saponification method for the determination of NBF concentration in aqueous phase in system I while acid-base titrations were carried out for others. Sodium thiosulphate was used as a titrant for iodine samples (system II) and a standard sodium hydroxide was used for succinic acid and acetic acid samples (system III and IV). The samples from each set of experiments were analysed and mean value was recorded. The accuracy of the analytical methods was checked using known samples. Before taking final measurements, several orientation experiments were carried out to identify appropriate lengths and residence times. Two sets of measurements were taken for each system: varying the flow rate at constant capillary length (i.e. varying residence time) and varying the flow rates in parallel with the length of the capillary (i.e. constant residence time). Various capillary and Y-junction sizes, 0.5, 0.75 and 1 mm, were used at different flow velocities and phase ratios to examine the dependence of microextractor performance on the operating conditions. The interfacial area was estimated using a snapshot technique as described in Chapter 2. The interfacial area thus determined was used to calculate the mass transfer coefficients under all operating conditions. Performance of the capillary micro-extractor was investigated using extraction efficiency and mass transfer coefficient.

In neutralisation reaction, the conventional pH indicator, phenolphthalein, was used to follow the reaction. First, the indicator was added to the distilled water and then this solution was used to make the aqueous solution of NaOH. The capillary was marked with the scale and the analysis of the titration was performed through

Table 3.2: Chemical systems and operating conditions used

Chemical systems:	
<i>Mass transfer:</i>	
Systems:	I, II, III and IV
Saturated concentration of NBF in water:	7.65 kg/m ³
Initial concentration of succinic acid in an aqueous solution:	10 kg/m ³
Initial concentration of iodine in an aqueous solution:	0.94 kg/m ³
Initial concentration of acetic acid in kerosene:	2 kg/m ³
<i>Neutralisation reaction:</i>	
System:	Kerosene (+ acetic acid) - water (+ NaOH)
Initial concentration of acetic acid in kerosene:	0.65 mol/L
Initial concentration of acetic acid in water:	0 mol/L
Initial concentration of NaOH in water:	0.25 and 0.4 mol/L
<i>Chemical method for interfacial area:</i>	
System:	NBF - water (+ NaOH)
Purity of NBF:	98%
Initial concentration of NaOH in an aqueous solution:	0.2 - 0.4 mol/L
Operating conditions:	
Flow rate (each phase):	5 - 80 ml/h
Capillary ID:	0.5, 0.75 and 1 mm
Y-junction ID:	0.5, 0.75 and 1 mm
Capillary length:	0.1 - 1.0 m

measurement of the distance from Y-junction to a point at which the pH indicator in the aqueous phase changed from pink to yellow i.e. neutralisation of the base by acid. The saponification method was tested by adding known amounts of NBF into distilled water. NBF was determined by hydrolysis by adding known amounts of NaOH ($C = 1$ mol/L). The change in NaOH concentration was found by acid-base titration with HCl ($C = 1$ mol/L). The average observed in this method was about

5 %. The saturation concentration of NBF in distilled water was determined by using a capillary with sufficient length to provide full extraction. The value found corresponds well with the data given in literature [64], 0.075 mol/L.

In the chemical method, which was used for investigation of interfacial area using instantaneous reaction of alkaline hydrolysis of NBF, the analytical grade NaOH and technical grade NBF (98 % pure) were used. The concentration of NaOH was analysed using acid-base titration.

3.3 Results and Discussion: Mass Transfer

3.3.1 Extraction efficiency

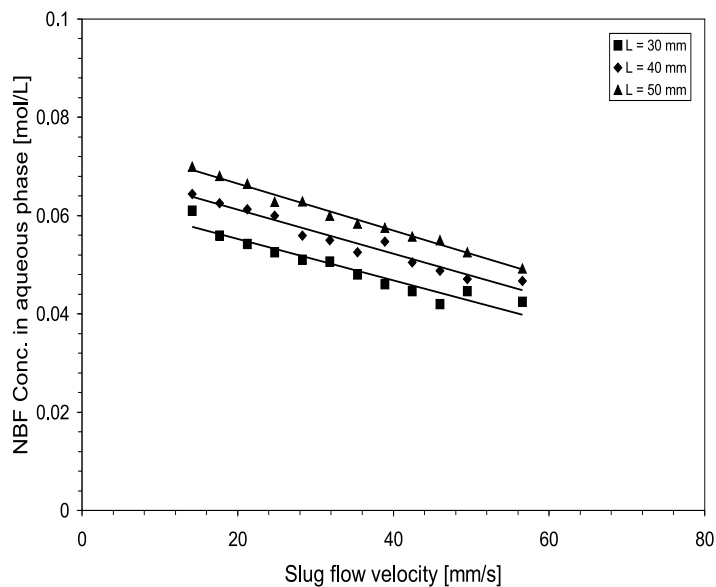


Figure 3.2: Concentration of NBF in aqueous phase as a function of slug flow velocity for different capillary lengths (Capillary ID = 1 mm)

The extraction efficiency is the ratio of the amount of material transferred to the maximum amount transferable. For a solute (A) transferring from one phase to another the extraction efficiency can be written as follows:

$$E = \frac{C_{A2}^{out} - C_{A2}^{in}}{C_{A2}^{*} - C_{A2}^{in}} \quad (3.1)$$

To calculate the extraction efficiency, the outlet concentrations of transferring species were measured. Figure 3.2 shows the concentration of NBF in the aqueous phase

for different capillary lengths. It shows linear relation with the slug flow velocity - decreases with increase in the flow velocity. Further, the extraction efficiencies of the systems I, II, III, and IV are plotted in Figures 3.3 to 3.6. The Figure 3.3 shows the extraction efficiency for different capillary lengths with same internal diameter (1 mm). As can be seen, with increase in the capillary length, the extraction efficiency increases due to increase in the residence or contact time of the fluids in the capillary. Different capillary lengths were used for all systems and the experiments were carried out to study the effect of flow velocity and capillary diameter in a length which shows extraction efficiency more than 90 %. Experiments were carried out in 100 mm length capillary for the systems, II and IV and in a 300 mm length capillary for system III. The results show that an extraction efficiency of greater than 90 % can be achieved in less than 5 seconds in the first case and in less than 20 seconds otherwise. They also show that with increase in the flow velocity for a given capillary, extraction efficiency decreases due to the decrease in the contact time, which indicates that mass transfer limitations dominate the system. With increasing flow velocity, the intensity of internal circulations within the slugs increases, which in turn enhances the convective mass transfer. However, the effect is overshadowed by the dependence of contact time.

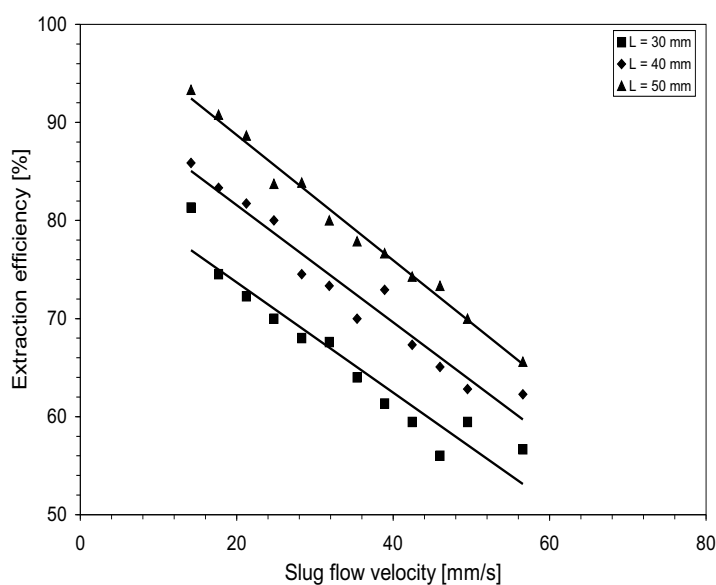


Figure 3.3: Extraction efficiency as a function of slug flow velocity for different capillary lengths for the extraction of NBF from its saturated solution into distilled water, system I (capillary ID = 1 mm)

The second set of experiment was carried out for different capillary diameters by keeping capillary length constant. The extraction efficiency shows significant effect of capillary diameter - decreases with increase in the capillary diameter due to the lower interfacial area as shown in Figures 3.4 to 3.6. Besides this, the extraction

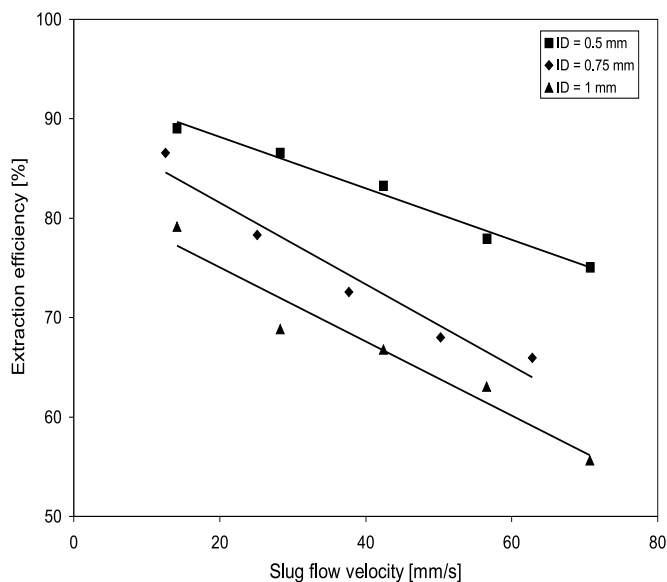


Figure 3.4: Extraction efficiency as a function of slug flow velocity for different capillaries in the extraction of iodine from its aqueous solution into kerosene, system II (capillary length = 100 mm)

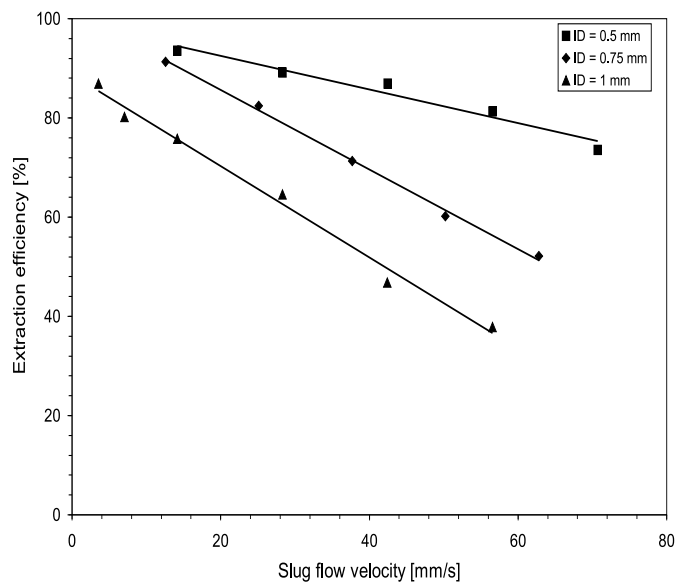


Figure 3.5: Extraction efficiency as a function of slug flow velocity for different capillaries in the extraction of succinic acid from its aqueous solution into n-butanol, system III (capillary length = 300 mm)

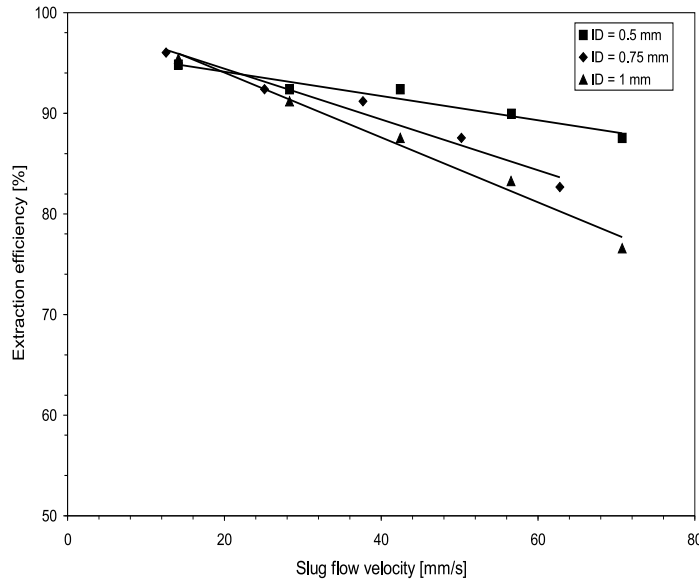


Figure 3.6: Extraction efficiency as a function of slug flow velocity for different capillaries in the extraction of acetic acid from kerosene into water, system IV (capillary length = 100 mm)

efficiency is also a function of inlet flow ratio. The experiments for unequal flow rates of both phases in the slug flow regime (Figure 3.7) show that extraction efficiency increases with an increase in the aqueous/organic (feed/solvent) flow ratio. In the case of a constant aqueous phase flow rate of 10 ml/h, the extraction efficiency increases significantly with decreasing solvent (n-butanol) flow rate, which indicates the effective use of the solvent. The same results are plotted as a function of slug flow velocity in Figure 3.8.

3.3.2 Mass transfer coefficients

The volumetric mass transfer coefficient and overall mass transfer coefficients are the characteristics parameters of a system (contactor and species) which are used to evaluate the performance of contactors and are given by following Equations (derived in Appendix B):

$$k_L a = \frac{1}{T} \ln \left(\frac{C_{A2}^{*} - C_{A2}^{in}}{C_{A2}^{*} - C_{A2}^{out}} \right) \quad (3.2)$$

$$k_L = \frac{1}{aT} \ln \left(\frac{C_{A2}^{*} - C_{A2}^{in}}{C_{A2}^{*} - C_{A2}^{out}} \right) \quad (3.3)$$

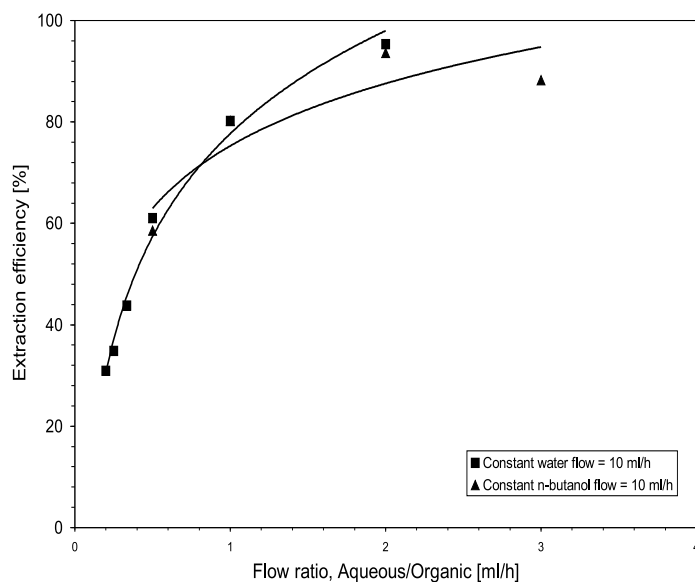


Figure 3.7: Extraction efficiency as a function of flow ratio of aqueous to organic flow rate for the extraction of succinic acid from its aqueous solution into *n*-butanol, system III (capillary length = 300 mm)

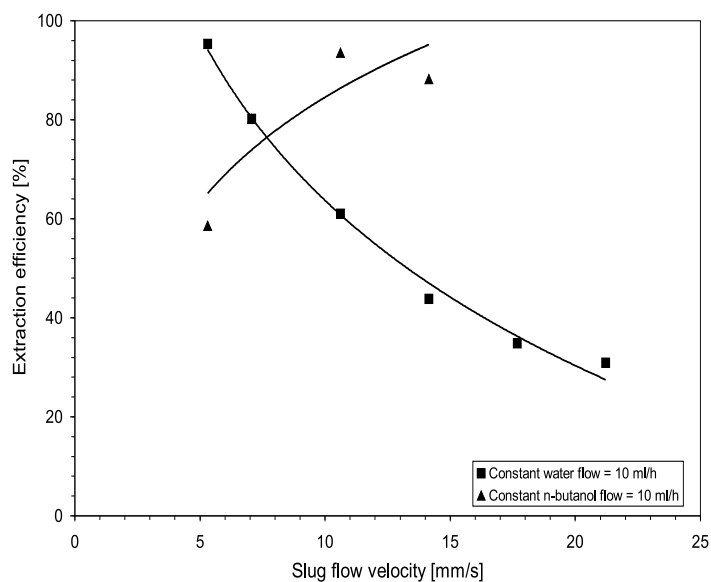


Figure 3.8: Extraction efficiency as a function of slug flow velocity for unequal phase flow rates for the extraction of succinic acid from its aqueous solution into *n*-butanol, system III (capillary length = 300 mm)

Effect of flow rates: The volumetric mass transfer coefficient as a function of slug flow velocity for the saturated NBF - water system is plotted in the Figure 3.9. As can be seen, the volumetric mass transfer coefficient is high for short capillaries due to low contact time. Further, the volumetric extraction rate, $R_A a$, is plotted as a function of volumetric mass transfer coefficient, $k_L a$, as shown Figure 3.10. It shows increased volumetric extraction rate with increase in the volumetric mass transfer coefficient. In addition, the performance of slug flow reactor shows that the flow velocity is a decisive parameter in dictating the rate of mass transfer. The volumetric mass transfer coefficients are plotted as a function of the slug flow velocity for equal flow rates of both phases in capillaries of 100 and 300 mm length in Figures 3.11 to 3.13. With increase in the flow velocity, the mass transfer coefficient increases over the entire slug flow regime. This is due to the increased interfacial mass transfer area and internal circulations with increased flow velocity.

Effect of capillary size: Different capillary diameters were employed to study mass transfer performance of the contactor. The volumetric mass transfer coefficients for different capillaries with respect to the flow rates for various chemical systems are plotted in Figures 3.11 to 3.13. It can be seen that for a given flow rate, the volumetric mass transfer coefficient increases with decreasing the capillary size. This is mainly due to the more extensive interfacial area with decreasing capillary size. Additionally, for the same flow rate, a smaller capillary induces very strong internal circulations, and therefore enhances the convective mass transfer. This convective flow inside the slugs renews the interfacial area which augments the concentration gradient of a species between two consecutive slugs, thus intensifying the diffusive penetration through the interface.

Effect of flow velocity for equal residence time: The experiments were also performed for equal residence time and the mass transfer coefficients observed are plotted in Figure 3.14. The only factor controlling the mass transfer in this case is the internal circulations within the slugs, which increase with increasing the flow velocity. At low flow velocities, it exhibits a relatively low mass transfer coefficient which increases with increasing flow velocity and then levels off. It can be concluded that beyond a certain flow velocity, the internal circulations are no longer governed by the flow velocity and no further effect is seen on the mass transfer coefficient.

Effect of flow ratio: An alternative technique for providing different interfacial areas and more effective use of solvent is to change the flow ratio of the aqueous and organic phases. The advantage of film-contacting technologies over more traditional

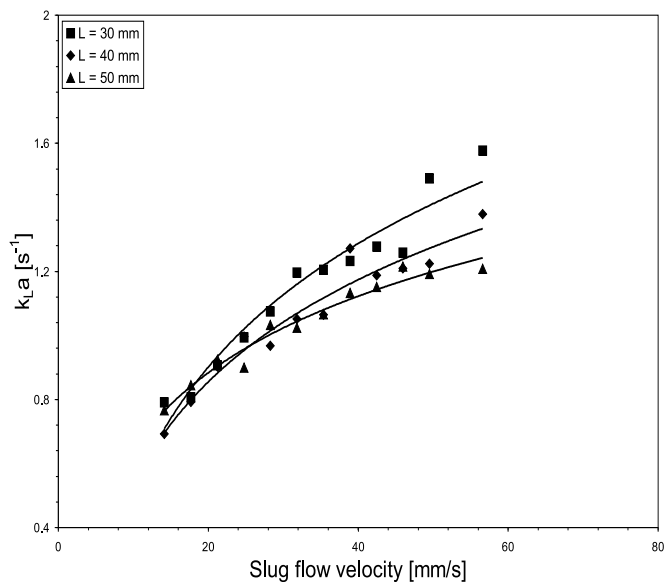


Figure 3.9: Volumetric mass transfer coefficient as a function of slug flow velocity for various capillary lengths for the extraction of NBF from its saturated solution into water, system I (capillary ID = 1 mm)

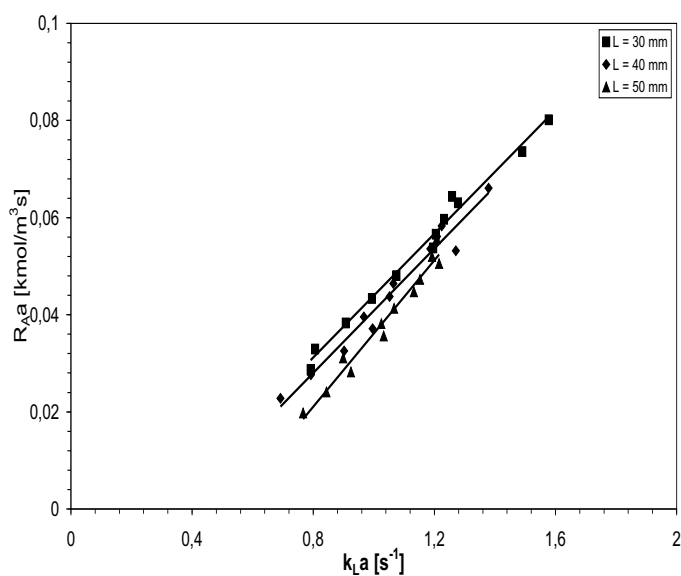


Figure 3.10: Rate of extraction as a function of volumetric mass transfer coefficient for different capillary lengths for the extraction of NBF from its saturated solution into water, system I (capillary ID = 1 mm)

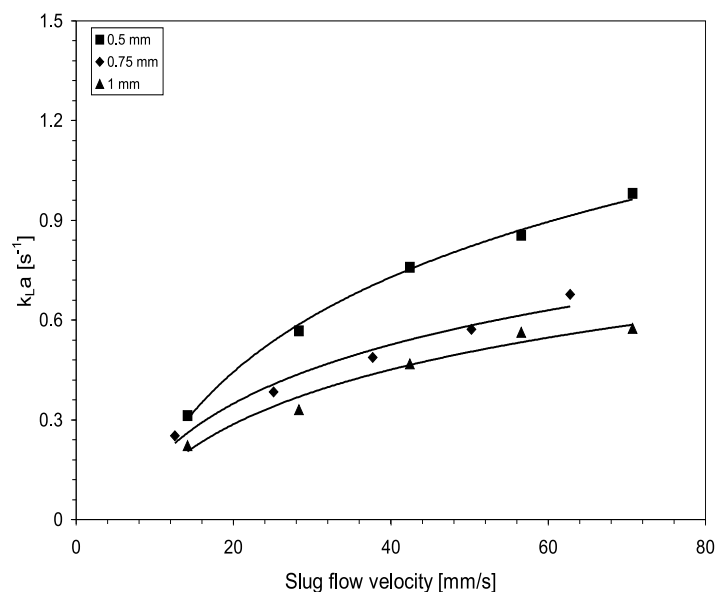


Figure 3.11: Volumetric mass transfer coefficient as a function of slug flow velocity for various capillary internal diameters for the extraction of iodine into kerosene from its aqueous solution, system II (capillary length = 100 mm)

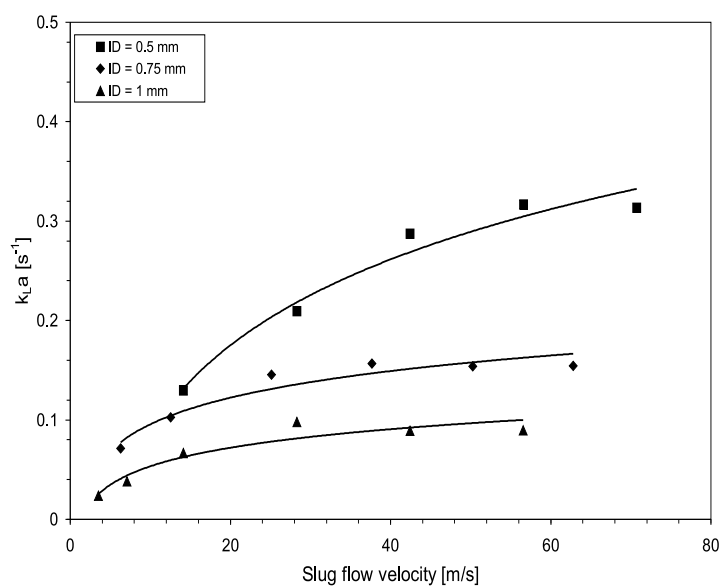


Figure 3.12: Volumetric mass transfer coefficient as a function of slug flow velocity for various capillary internal diameters for the extraction of succinic acid into n-butanol from its aqueous solution, system II (capillary length = 300 mm)

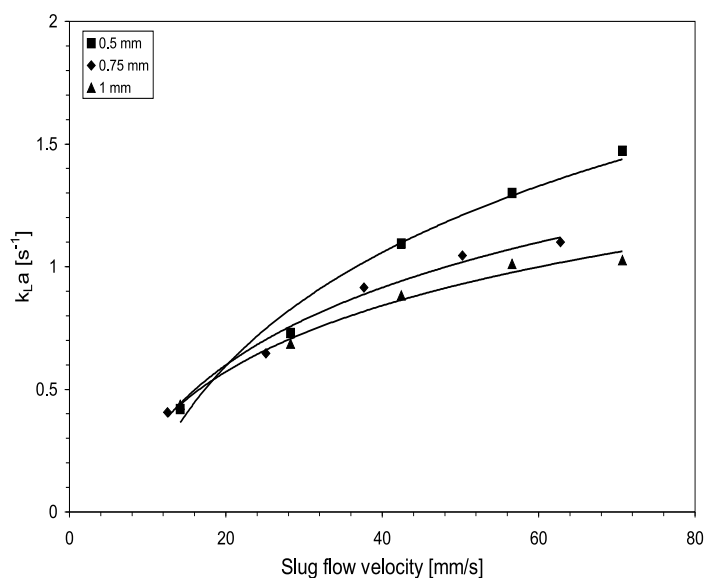


Figure 3.13: Volumetric mass transfer coefficient as a function of slug flow velocity for various capillary internal diameters for the extraction of acetic acid into water from kerosene, system II (capillary length = 100 mm)

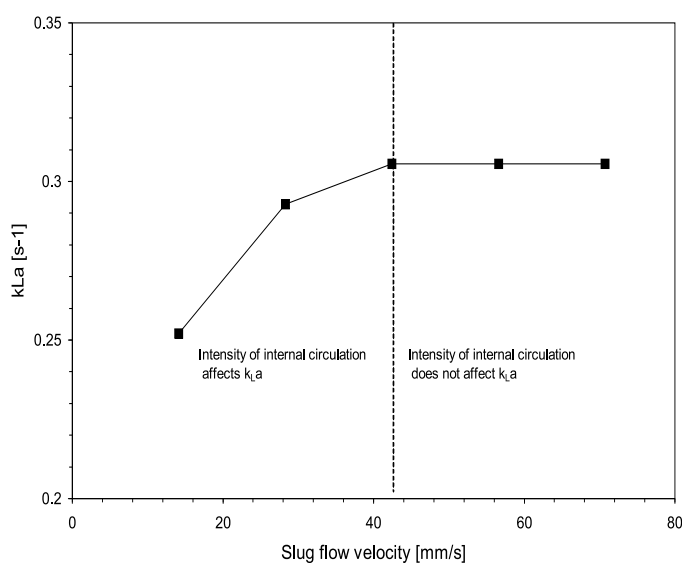


Figure 3.14: Volumetric mass transfer coefficient as a function of slug flow velocity for equal residence times for extraction of iodine from its aqueous solution into kerosene, system II (residence time = 7 s)

mixer-settlers lies in their ability to optimise the ratio of solvent to feed flow in order to reduce the solvent recovery costs[14]. The design of mixer-settlers becomes more difficult and mass transfer efficiency diminishes as the solvent-feed ratio becomes much less than one. However, film contactors can be designed and operated over a wide range of solvent-feed ratios which provide superior use of solvent, especially when the distribution coefficient of the solute is large. Liquid-liquid slug flow in the capillary shows well-defined and stable flow patterns at large flow ratios. From the previous Chapter on hydrodynamics of water-cyclohexane system [65] and the present studies of the four systems described, it was found that slug flow in the capillary was well-defined and stable over a wide range of organic to aqueous phase flow ratios (approximately, 4 to 5).

Experiments were carried out for various phase ratios, by keeping one flow constant and varying the other, and obtained promising results as plotted in Figures 3.15 and 3.16. Figure 3.15 illustrates that with increase in the flow ratio of aqueous (feed) to organic phase (solvent) at a constant solvent (kerosene) flow rate of 10 ml/h, very high mass transfer coefficients were observed, compared to the case of constant flow rate 10 ml/h of feed with varying solvent flows, as depicted in Figure 3.15. Such combinations of flow rates are useful for separation of solute having high distribution coefficient in the favour of solvent, which means effective use of the solvent and reduced cost for its regeneration. The dependence of the mass transfer coefficient on the slug flow velocity exhibits similar behaviour for the case of constant solvent flow rate. However, for the case of constant aqueous phase flow rate, the mass transfer coefficient diminishes with increasing slug flow velocity, as shown in Figure 3.16.

3.3.3 Comparison with conventional contactors

The volumetric mass transfer coefficients found in the liquid-liquid slug flow capillary contactor at various flow rates were compared with those for conventional equipment (Table 3.3). In the Table, c is the continuous phase while d is the dispersed phase and the substance in the middle is extracted in the direction from c to d except for kerosene-acetic acid-water, where the extraction is from d to c. It can be seen from the Table that the mass transfer coefficients found in the present work are way above those of conventional contactors and even higher than those obtained in the work on novel impinging streams contactor by Dehkordi cited earlier [49].

In the previous chapter, the pressure drop was measured across the Y-junction and the results obtained were used to investigate the amount of energy required to operate the set-up in slug flow regime which are compared with the energy required

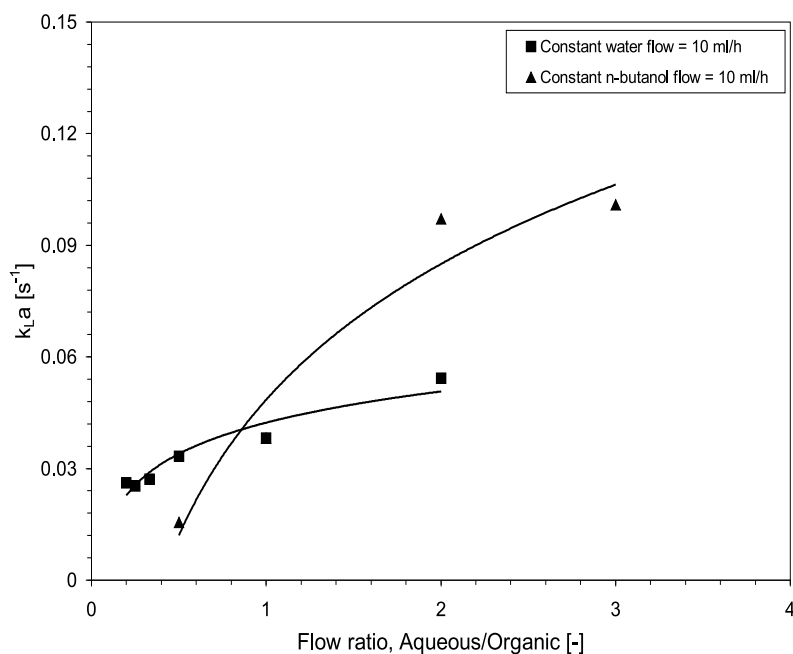


Figure 3.15: Volumetric mass transfer coefficient as a function of flow ratio of aqueous to organic phase (water - succinic acid - n-butanol, capillary length = 300 mm)

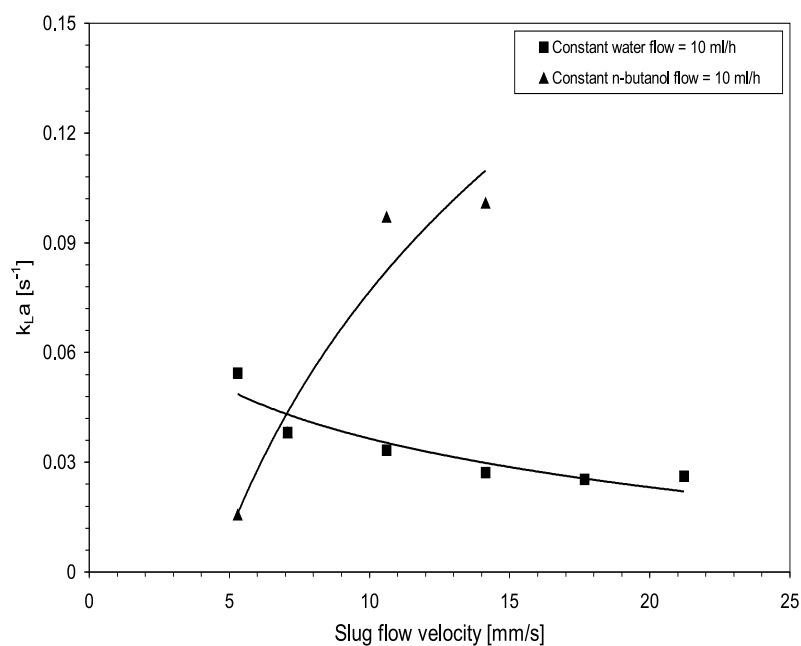


Figure 3.16: Volumetric mass transfer coefficient as a function of slug flow velocity for unequal flow rates (water - succinic acid - n-butanol, capillary length = 300 mm)

Table 3.3: $k_L a$ for different types of contactors

Contactors	Chemical system	$k_L a \times 10^{-4}$ [1/s]
Agitated vessel	Water (c) - iodine - CCl_4 (d)	0.16 - 16.6
	Sulphate ore (c) - uranium - kerosene (d)	2.8 - 17
Rotated disk contactor	Water (c) - succinic acid - n-butanol (d)	57
	Water (c) - acetic acid - methyl isobutyl ketone (d)	20 - 120
	Water (c) - acetone - DCDE (d)	63 - 266
Rotated agitated column	n-hexane(c) - acetone - water (d)	0.15
	Toluene (c) - acetone - water (d)	0.2 - 1.0
	Water (c) - furfural - toluene (d)	105
Spray column	Water (c) - acetone - benzene (d)	8 - 60
	Water (c) - adipic acid - ether (d)	20 - 70
	Water (c) - acetic acid - benzene (d)	17.5 - 63
	Water (c) - acetic acid - nitrobenzene (d)	7 - 32
Packed column	CCl_4 (c) - acetone - water (d)	7.4 - 24
	Kerosene (c) - acetone - water (d)	5.8 - 61
	Methyl isobutyl ketone (c) - uranyl nitrate - water (d)	14.7 - 111
	Toluene (c) - diethyl amine - water (d)	5 - 14.7
	Vinyl acetate (c) - acetone - water (d)	7.5 - 32
Perforated plate column	Water (c) - acetaldehyde - vinyl acetate (d)	28.5
Impinging streams	Water (c) - iodine - kerosene (d)	15 - 2100
	Kerosene (d) - acetic acid - water (c)	500 - 3000
	Water (c) - iodine - kerosene (d)	560 - 2000
Rotating disks impinging streams contactor	Water (c) - iodine - kerosene (d)	1187 - 3975
	Kerosene - acetic acid - water (c)	1364 - 4456
	Water (c) - succinic acid - n-butanol (d)	775 - 2500
Present work	Saturated NBF - water	7000 - 15000
	Water - iodine - kerosene	1311 - 9815
	Kerosene - acetic acid - water	4058 - 14730
	Water - succinic acid - n-butanol	200 - 3200

for several conventional contactors (see Chapter 2). From the Table 2.3, it can be seen that the liquid-liquid slug flow capillary extractor requires very small amounts of power compared to conventional contactors despite the extremely high rates of mass transfer attained. Thus in terms of the mass transfer coefficients per unit power input the capillary microreactor is far superior compared to the conventional contactors.

3.3.4 Interfacial area and overall mass transfer coefficients

As reported earlier, the interfacial area was measured by physical method (snapshot approach) and the mass transfer coefficients were estimated using Equation B.4. The interfacial area increases with increasing flow velocity and decreasing capillary diameter. The behaviour of slug size and interfacial area for various operating conditions can be found in Chapter 2. The ranges of the volumetric mass transfer coefficients, interfacial area and mass transfer coefficients for different capillaries are listed in Table 3.4. From this Table, it is apparent that with decreasing capillary diameter the interfacial area and the mass transfer coefficients are increasing. The increase in the interfacial area is due to decrease in the slug size with capillary diameter for a given volumetric flow rate, while increase in the mass transfer coefficients are due to strong shear forces experienced in the small capillaries. As mentioned above, in the presence of a wall film the whole slug surface participates in mass transfer which increases the interfacial area significantly (see Table 2.3 in Chapter 2). The slug flow in the presence of film offers 3 to 4 times higher interfacial area than without film, and the values are very high in comparison to conventional contactors (e.g., the benchmark agitated stirred tank offers interfacial area of only $500 \text{ m}^2/\text{m}^3$).

Table 3.4: Volumetric mass transfer coefficient, $k_L a$, specific interfacial area, a , and mass transfer coefficient, k_L for different capillary internal diameters (ID) at equal flow rate of both phases for the case of without film (wo) and with film (w) in the liquid-liquid slug flow capillary microreactor (water-iodine-kerosene)

ID [mm]	$k_L a$ [1/s]	a [m^2/m^3]		$k_L \times 10^{-4}$ [m/s]	
		a_{wo}	a_w	k_{Lwo}	k_{Lw}
0.5	0.31 - 0.98	1080 - 1970	4500 - 4800	2.75 - 6.29	0.66 - 2
0.75	0.29 - 0.64	870 - 1686	2980 - 3190	4.70 - 7.90	0.98 - 2
1	0.13 - 0.32	590 - 780	2510 - 2760	2 - 4.64	0.5 - 1.2

3.4 Results and Discussion: Chemical Reaction

3.4.1 Neutralisation reaction

Neutralisation time: In the present work, a simple titration reaction was chosen to investigate the timescale required for mass transfer and thus the rate of mass transfer. The same reaction can be carried out using a burette and a beaker with a magnetic stir bar which gives better mixing compared to internal circulations of the liquid-liquid slug flow. However, this reaction in the macroscale is single phase and it does not allow to measure mass transfer time and reaction time as the reaction is very rapid.

In this reaction, distance required for pH indicator to change the colour was measured [35] and corresponding parameters such as colour change time and mass transfer coefficients were investigated. The results for colour change distance for different capillary internal diameters for two chemical systems as a function of slug flow velocity were plotted in Figure 3.17. It shows that with increase in the slug flow velocity, more distance is required to change the colour. The relation between colour change distance and flow velocity is non-linear. It also shows that with increase in the capillary diameter the distance required to change the colour increases. In addition, it shows increased colour change distance for increase in NaOH concentration, from 0.25 to 0.4 mol/L, as expected.

As described in Chapter 2, the snapshots were taken for each operating condition and slug lengths were measured. Figure 3.18 shows that with increase in the flow velocity and decrease in the capillary size slug length decreases. There are two contributions to the overall colour change time in the capillary microreactor: slug flow generation time and residence time in the capillary until the colour change. Burns and Ramshaw [35] have explained the contribution of slug flow generation, i.e. end effects, in the colour change time but they had not considered this effect as it showed very less contribution in the total colour change time. It was calculated by dividing the slug flow velocity to the slug length as given by the following Equation:

$$t_F = \frac{l}{V_{av}} \quad (3.4)$$

The later contribution of residence time in the capillary for colour change was investigated by dividing colour change distance by average flow velocity. The total colour change time as a function of slug flow velocity is plotted in Figure 3.19. It shows that with increase in the flow velocity, the time required to change the colour decreases. With increase in the capillary diameter colour change time increases due to

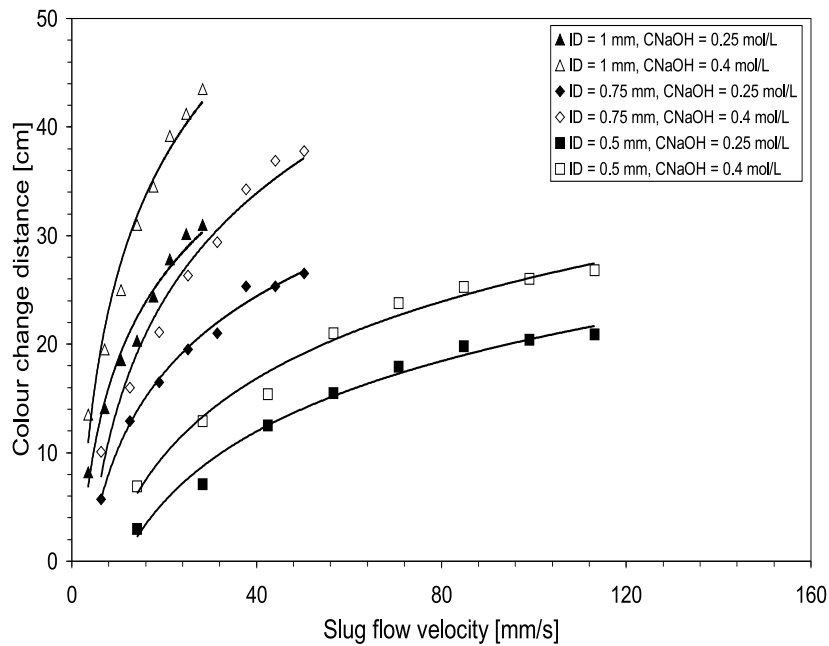


Figure 3.17: Colour change distance for two different initial concentrations of NaOH: 0.25 and 0.4 mol/L

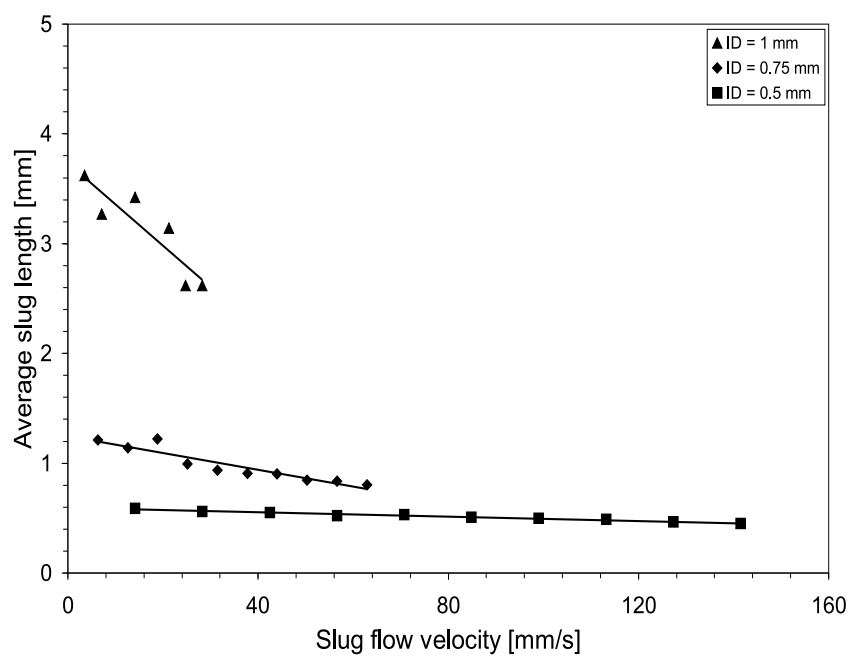


Figure 3.18: Slug length as a function of slug flow velocity

decrease in the interfacial area. It also shows that, for the chemical system with less initial concentration of NaOH requires less time compared to the other system with 0.4 mol/L initial concentration system. The slug flow generation time has relatively higher contribution for bigger capillaries at slow flow. For a capillary with internal diameter equal to 1 mm and flow velocity 3.5 mm/s, the slug flow generation time is about 1 s which is not significant contribution in the total colour change time of 25 and 39 s for 0.25 and 0.4 mol/L NaOH concentrations, respectively. However, with increase in the flow velocity and decrease in the capillary diameter slug flow generation time decreases.

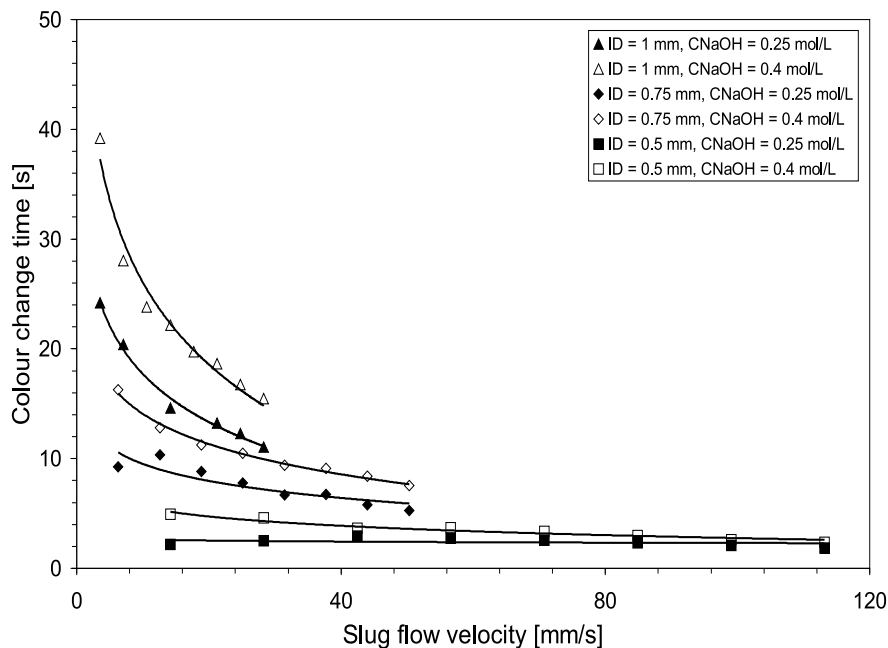


Figure 3.19: Colour change time for two different initial concentrations of NaOH: 0.25 and 0.4 mol/L

Burns and Ramshaw [35] have fitted their experimental data using linear regression and proposed an empirical model for the time required to change the colour as a function of proportion of acetic acid consumed (β), slug length (l) and flow velocity (V_{av}). Similarly, in the present work following correlation was fitted well with experimental data:

$$t = 3.41\beta^{0.67} \left(\frac{V_{av}}{V_0}\right)^{-0.19} \left(\frac{l}{l_0}\right)^{0.94} \quad (3.5)$$

The parameters V_0 and l_0 are the characteristic flow velocity and characteristic length which have values of 1 mm/s and 1 mm, respectively. The present work, for the liquid-liquid slug flow capillary microreactor shows best fit (92 %) as shown in

Figure 3.20. The difference in the present work and the work of Burns and Ramshaw (proportionality coefficient 4.67 instead of 3.41) is the diameter and material of the capillary. They have used a soda lime glass etched with rectangular channels having width and depth equal to 0.38 mm while the present work uses the PTFE capillaries with internal diameters equal to 0.5, 0.75 and 1 mm.

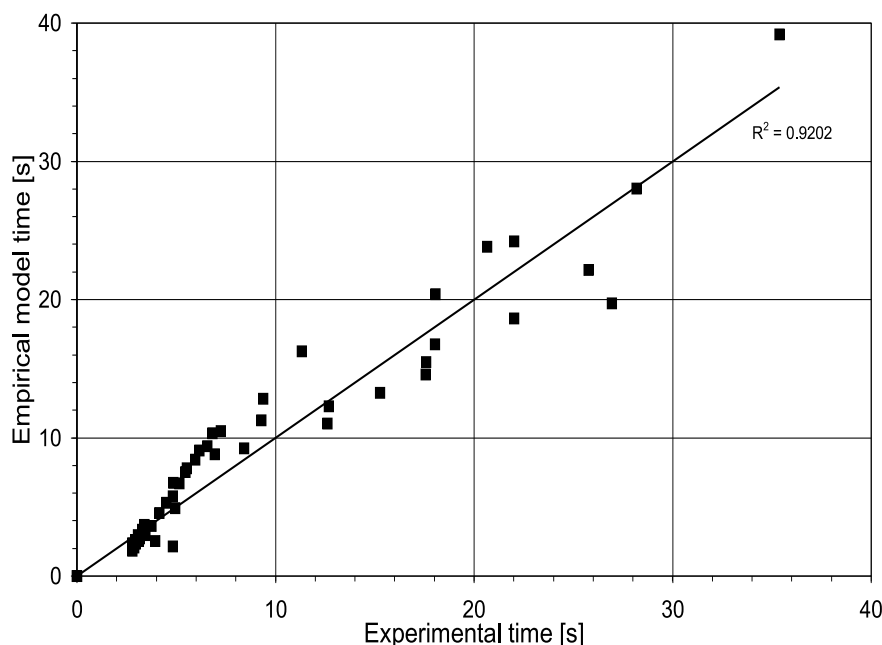


Figure 3.20: Comparison of empirical model time and measured time

Mass transfer coefficients: The mass transfer coefficients were investigated using Equation B.9. The volumetric mass transfer coefficients for two systems and for different capillary diameters as a function of slug flow velocity are given in Figure 3.21. It shows very high rates of mass transfer as the rapid reaction consumes acetic acid as soon as it enters the aqueous phase which produces high concentration gradient along the interface. The system with high initial concentration of acetic acid shows high rates of mass transfer.

Further, the overall mass transfer coefficients were investigated from the interfacial area measured. Two cases of without film and with film were considered. Overall mass transfer coefficient as a function of slug flow velocity is plotted in Figure 3.22 for a capillary having internal diameter 0.75 mm. As expected, the without film case shows more mass transfer coefficient compared to the case of with film. The presence of film offers higher interfacial area and therefore the overall mass transfer coefficients have less contribution in the volumetric coefficients.

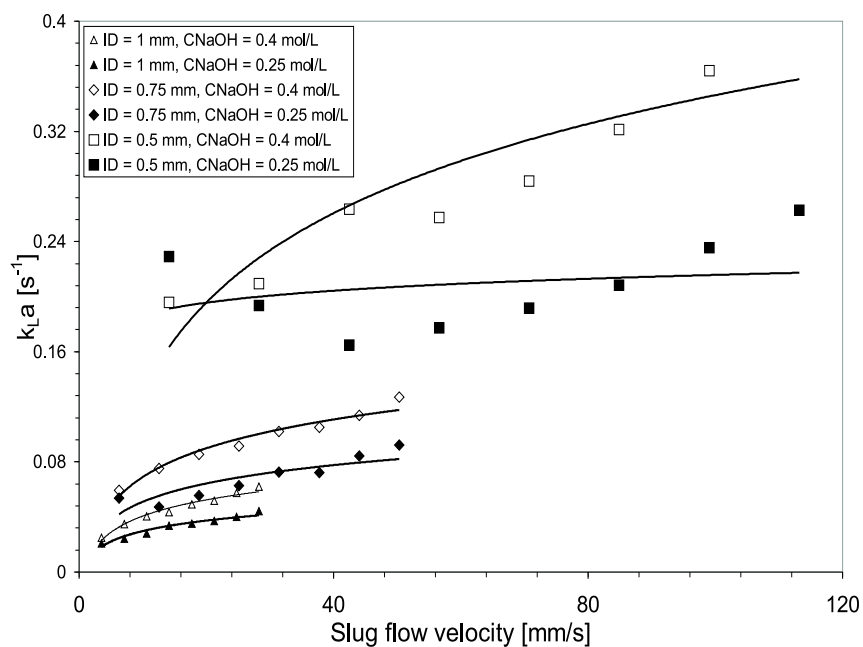


Figure 3.21: Volumetric mass transfer coefficient for different capillary sizes and initial NaOH concentrations

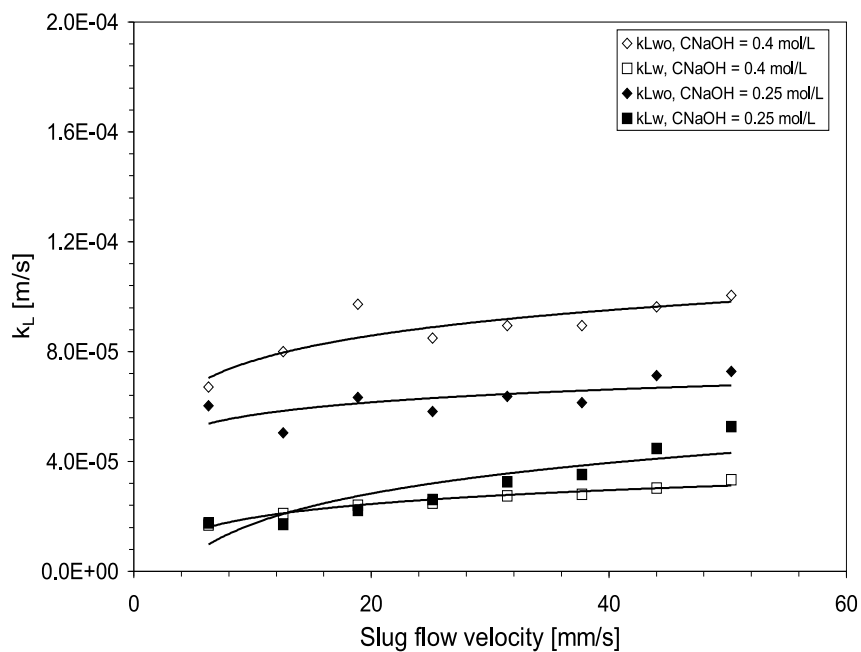


Figure 3.22: Mass transfer coefficient for two cases: without film, k_{Lwo} and with film, k_{Lw} (Capillary ID = 0.75 mm)

Comparison with diffusion-only case: Burns and Ramshaw [35] have compared the mass transfer performance of the microreactor with a simple diffusional process between two parallel two phase flow by solving a one dimensional diffusion equation. They used the solution provided by Crank [66] for the case of diffusion into a flat slab which is depending on the dimensionless Fourier number. The simulated results for 0.38 mm wide glass reactor showed that 62 % acetic acid transfer between the slugs is equivalent to a diffusive process with a path length of 0.2 mm which is about half of the channel width. It shows that slug flow provides an attractive method of multiphase contacting within a microreactor environment.

3.4.2 Chemical method for interfacial area

Danckwerts plot: In this work, chemical method is used to quantify the interfacial area using alkaline hydrolysis of NBF. NBF was contacted with various NaOH concentrations ranging from 0.2 to 0.4 mol/L to determine the values of extraction rate for the Danckwerts plots. As suggested by Dehkordi [52], lower concentration of NaOH was used in order to satisfy the condition for pseudo-first order reaction mechanism. The outlet concentration of NaOH was measured using acid-base titrations and is plotted as a function of volumetric flow rate for a capillary with 1 mm internal diameter and 30 mm length as shown in Figure 3.23. It shows that with increase in the flow rate the outlet concentration increases due to decrease in the residence time. From the outlet concentration, the amount of NaOH consumed was investigated and thus the conversion of NaOH. The NaOH conversion as a function of volumetric flow rate is plotted in Figure 3.24. As expected from the plot, it shows that the conversion of NaOH decreases with increase in the flow velocity.

The Danckwerts plots, $(Ra/C_{A,2}^*)^2$ as function of outlet concentration of NaOH, shows a straight line for all flow rates (Figures 3.25 to 3.27). It shows that with increase in the initial NaOH concentration, the volumetric extraction rate increases. At low flow rate values, the plot shows good fit to the straight line while with increased flow rate, it shows some deviation. From the slope of the line of each flow rate, the interfacial area was investigated using Equation C.5 and the physico-chemical properties given in Table D.3.

Comparison of interfacial areas: The interfacial area was investigated using physical (snapshot) and chemical method. In the physical method, two cases of without and with film are considered and the results of specific interfacial area without film (a_{wo}), specific interfacial area with film (a_w) and specific interfacial area by chemical method (a) for different capillaries as a function of slug flow rate

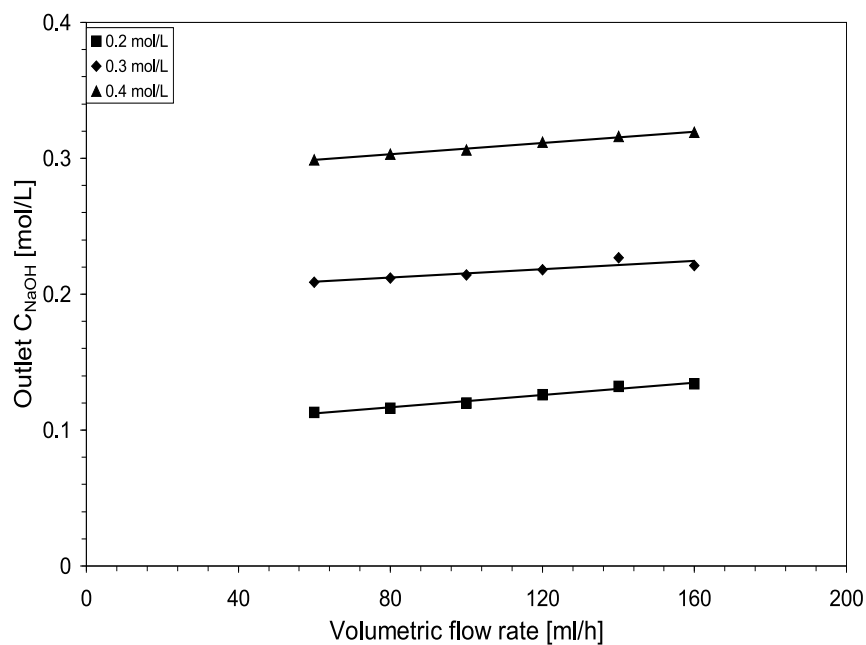


Figure 3.23: Outlet NaOH concentration as a function of volumetric flow rate (Capillary ID = 1 mm, capillary length = 30 mm)

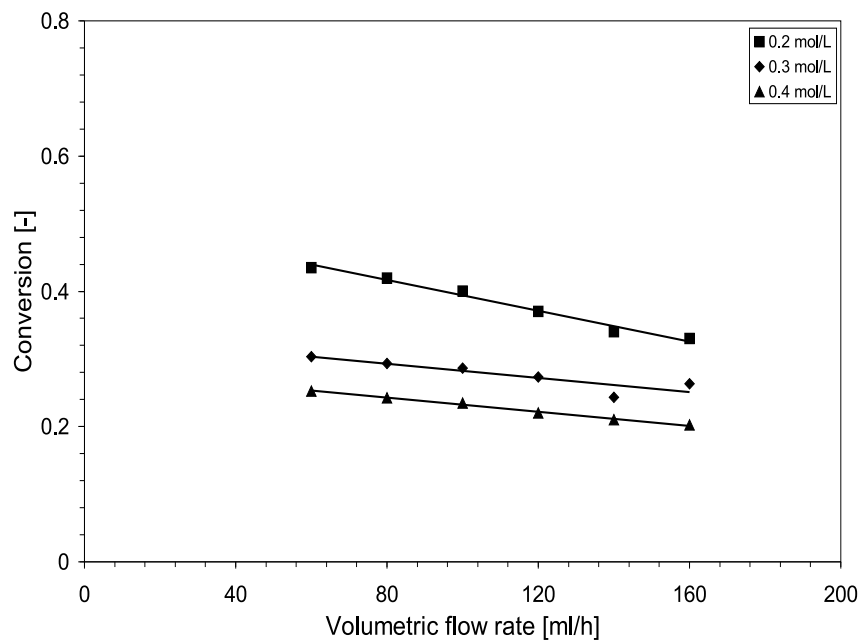


Figure 3.24: NaOH conversion as a function of slug flow rate (Capillary ID = 1 mm, capillary length = 30 mm)

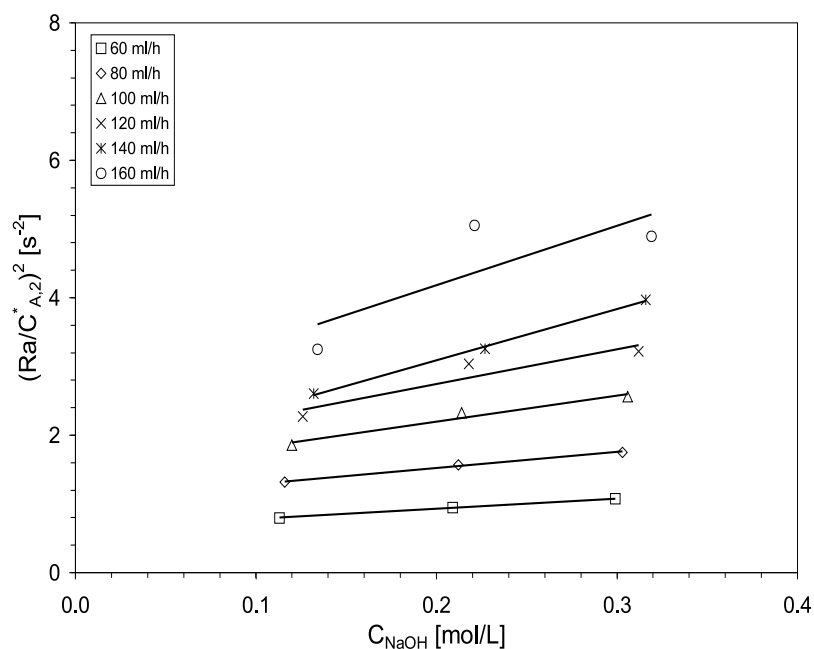


Figure 3.25: Danckwerts plot, $(Ra/C_{A,2}^*)^2$ vs outlet NaOH concentration for different initial concentrations, for various flow velocities (Capillary ID = 1 mm, capillary length = 30 mm)

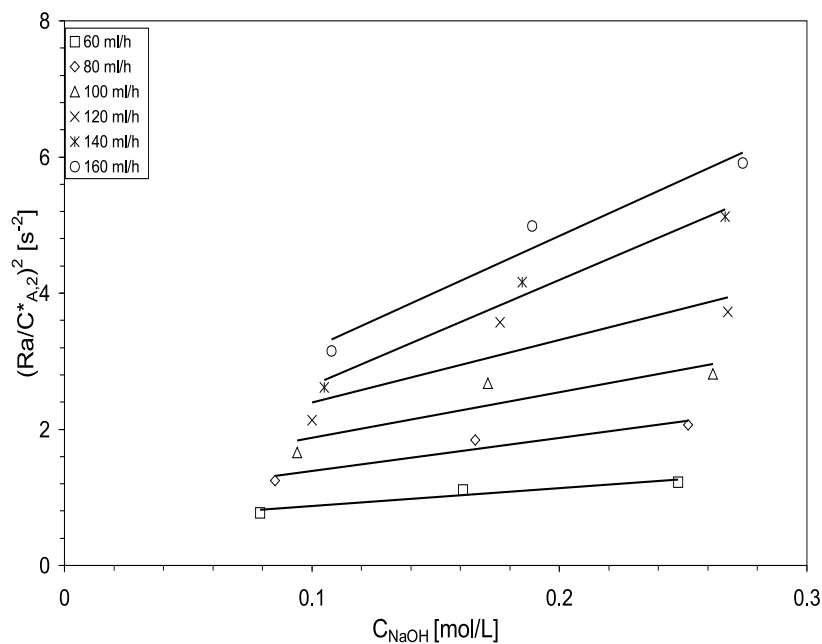


Figure 3.26: Danckwerts plot, $(Ra/C_{A,2}^*)^2$ Vs outlet NaOH concentration for different initial concentrations, for various flow velocities (Capillary ID = 0.75 mm, capillary length = 30 mm)

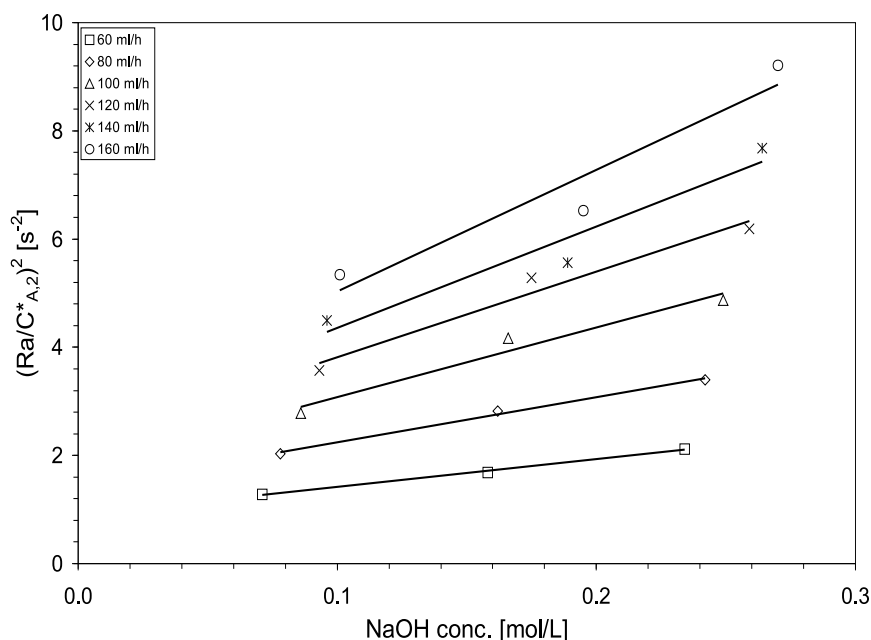


Figure 3.27: Danckwerts plot, $(Ra/C_{A,2}^*)^2$ vs outlet NaOH concentration for different initial concentrations, for various flow velocities (Capillary ID = 0.5 mm, capillary length = 30 mm)

are plotted in Figures 3.28 to 3.30. The Figures show that with increase in the flow velocity, the interfacial area without film increases while the interfacial area with film decreases. The increase in the interfacial area in the case of without film is due to decrease in the slug size with increased flow rate. However, slight decrease in the interfacial area with film is because of the increased film thickness with increased flow velocity as given by Bretherton's law [67] which narrows the enclosed slug. However, the accuracy of the interfacial area in this case rely on the accuracy of Bretherton's law for this system.

Further, the results obtained from Danckwerts plots were compared with physical specific interfacial area of without and with film. For all capillaries it shows that with increase in the slug flow rate, the chemical method interfacial area increases. In all capillaries, at low flow rates, the chemical method area is equal to the physical area without film. However, with increase in the flow rate interfacial area by chemical method increases and it was observed in some cases that it reaches to an asymptotic value (e.g. ID = 0.75 mm) which is very close to the interfacial area by chemical method. However, the other capillaries do not show asymptotic limits under the slug flow region as interfacial area increases with increase in the flow rate. In all, it can be concluded that the chemical method area is more than the physical area without film and therefore there is presence of an organic film. The conclusion is

due to the fact that the physical interfacial area without film is more accurate than with film as it does not use any correlation. It may also be possible that part of the capillary microreactor has a film and it grows with increase in the flow velocity. This issue can be resolved with more successor works.

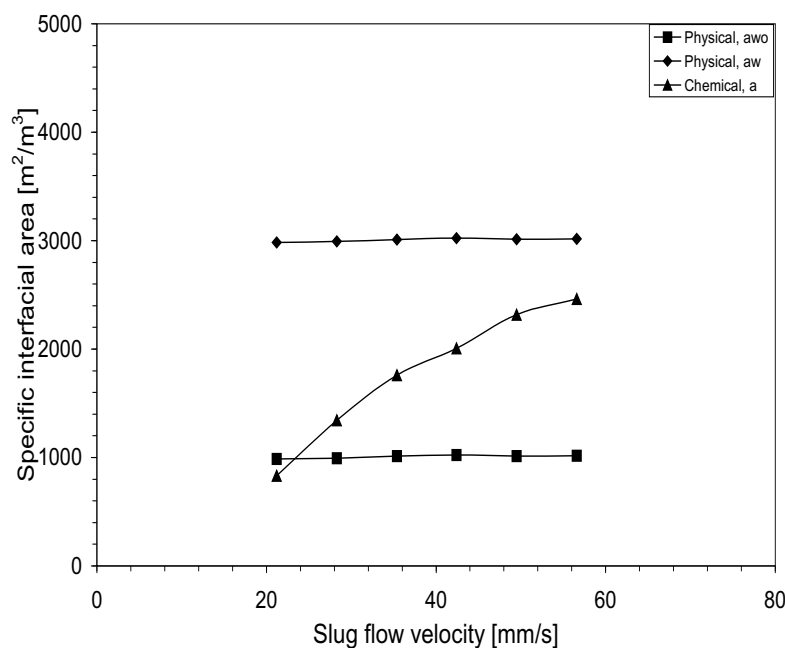


Figure 3.28: Interfacial area by physical, without film (a_{wo}) and with film (a_w), and chemical method (Capillary ID = 1 mm)

3.5 Summary

Experiments were carried out to investigate the mass transfer coefficients in the liquid-liquid slug flow capillary microreactor for four different non-reacting chemical systems. The mass transfer coefficients were compared with conventional contactors and it was observed that such liquid-liquid microextractor-reactors offer superior performance and greater efficiency in comparison to conventional equipment. The capillary microreactor provides very large specific interfacial areas in compared to other contactors, which enhances the mass transfer rates. Additionally, the internal circulations in the slugs, which arise because of the shear between slug axis and continuous phase or capillary wall, improve the mass transfer rate by surface renewal at the phase interface. A decisive feature, an organic wall film, was investigated using chemical method in the capillary offers very high interfacial area for mass transfer which can give much more rapid mass transfer. The ability to tune the mass transfer contributions precisely, to impose temperature profiles, to monitor

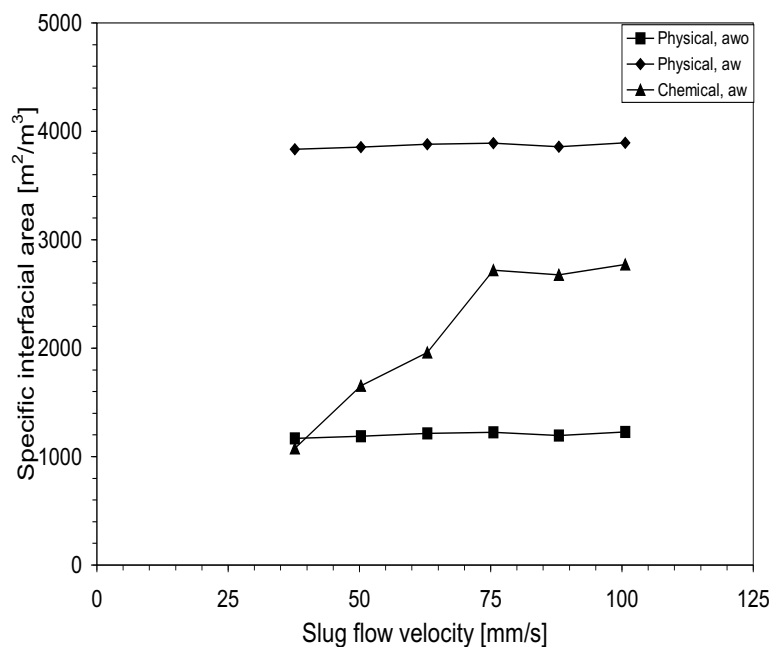


Figure 3.29: Interfacial area by physical, without film (a_{w0}) and with film (a_w), and chemical method (Capillary ID = 0.75 mm)

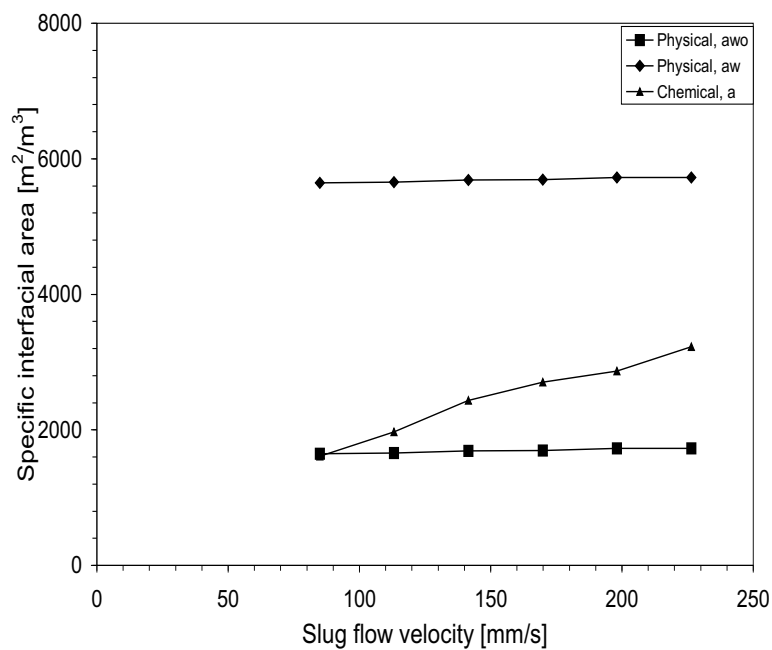


Figure 3.30: Interfacial area by physical, without film (a_{w0}) and with film (a_w), and chemical method (Capillary ID = 0.5 mm)

the progress of extraction and reaction together with the excellent accessibility for process modelling and to separate the downstream liquids easily suggest that the liquid-liquid slug flow in capillaries is a powerful laboratory technique for elucidating extraction and biphasic reactions. The results reported in the present work can also be used to identify the asymptotic performance limits in such systems, by permitting a precise evaluation of mass transfer effects.

Chapter 4

Flow Splitting

4.1 Introduction

Separation of two liquid phases after the mass transfer is an important step in the liquid-liquid extraction. Therefore, when designing an extraction unit, a question always arises as how to achieve the separation of two phases immediately following phase contact in the extraction zone. In conventional extraction equipment, the operations associated with mixing and separation of two liquids are usually at least partially distinct. Gravity based separation, based on the density difference between two phases, is the most commonly used method of separation. Difficulties that often occur in the separation of immiscible liquids include poor or slow phase separation, emulsion or rag layer formation and poor process control, especially in batch systems. Some liquid-liquid dispersions take hours to separate in conventional systems, which makes it difficult to determine the actual contact time and thus the mass transfer rates achieved. The usual remedy to stop extractive reactions, quenching, is similarly unsatisfactory and requires extensive control experiments. Some contactors, such as the mixer-settlers in their continuous mode of operation, separate the phases with fixed design parameters for a given flow rate ratio. However, changes in the flow ratio alter the performance of the separator and therefore designing and operating a unit for varying conditions is complicated.

Immediate separation after the mass transfer gives accurate contact time and thus precise mass transfer rates. This information is useful for *a priori* prediction of mass transfer rates while designing an extractor. The same is applicable for liquid-liquid biphasic reactions to extract precise kinetic parameters. The flow separation in liquid-liquid microreactor has already been achieved for parallel flow by Burns and Ramshaw [12]. They have developed a wedge shaped flow splitter to split parallel

flow and investigated the contamination in the outputs for a system, kerosene (+ dye) and aqueous solution of propylene glycol. Further, they carried out CFD simulations to study the performance of the flow splitter. In the model it was assumed that the liquids flow in the laminar region with flat interface between two phases and it was assumed that one of the outlets has single phase flow while the other with two phase flow and thus the contamination was estimated. Later on, based on the principle of wettability, a flow splitter was developed by Hoettges *et al.* [68] to separate two liquids flowing in a channel. Their methodology was to form a set of grooves on two surfaces having different surface chemistry (for example, one could be glass and the other an organic material) and to fix those surfaces on to each other so as to form channels in between them. The liquids tend to flow along the surface of the material to which they have the greatest affinity and thus separation is achieved. They performed experiments in a chip comprised of two layers and coated with polar (glass) and non-polar (a silicon monomer mix) substances for separating isooctane and water and achieved excellent results.

Numbering-up or scale-up of microreactors is very important to achieve throughput in the range of production scale. Microreactor technology achieves this target with numbering-up instead of scale-up - reduces the problems associated with scale-up. There are two key issues in numbering-up of microreactors: to achieve uniform distribution of flow in all channels and to separate the phases immediately after the mass transfer. Institut für Microtechnik, Mainz, Germany, have developed a single (liquid) phase flow splitting unit with three dampening tanks and six interdigital separation-layer micro mixers [69] and a minimum/maximum deviation of the 2-propanol/water distribution below 5 % and a standard deviation below 2 % was achieved. Further, they applied this single phase flow splitting element i.e. liquid distributor in the field of organic synthesis of n-butyl acetamide from the acid chloride in six parallel (numbering-up) micro reactors with an overall yield of 88 % and a purity in a range of 88 to 99 % [70].

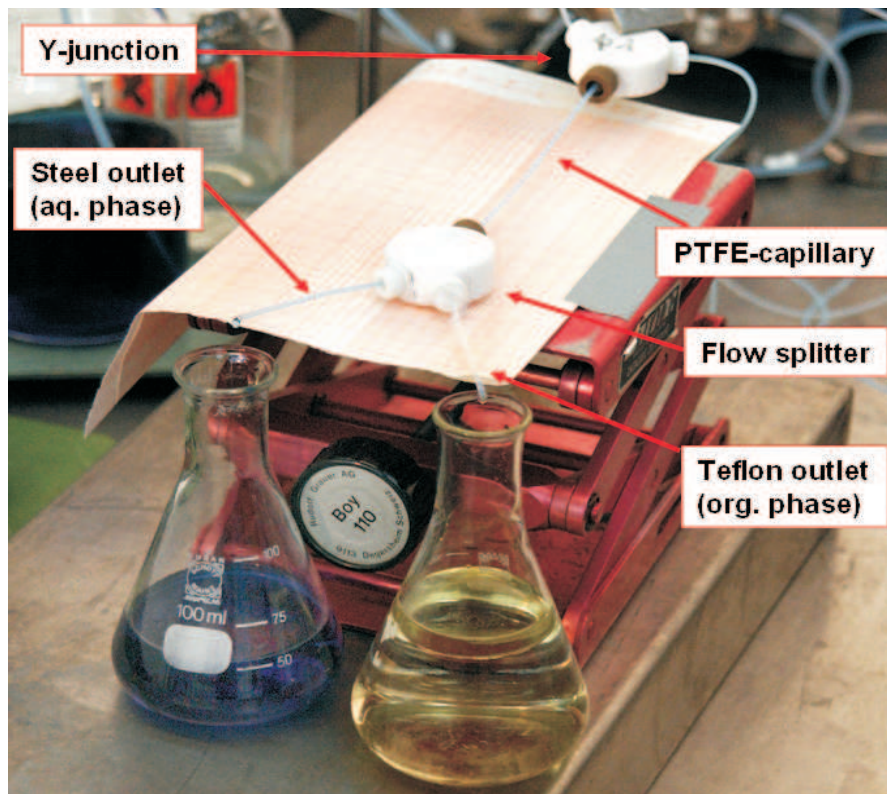
In addition to the single stage operation, as discussed above, multistage operations are common in liquid-liquid extraction for large scale production and effective use of chemicals. Depending upon the selectivity of the solvent and the amount of mass transfer required to achieve the desired solute recovery, several stages of extraction may be required. In this case, counter-current contact is the most efficient extraction method as it conserves the mass transfer driving force and therefore gives optimal performance. Most of the countercurrent operations in the laboratory practice uses batch processes and they are carried out using milliliter amount of feed and solvent in the flasks. Using the microreactors these processes can be made continuous. The important issue in making it continuous is the online separation of liquid phases being used in the systems.

Thus from the above discussion it is clear that there is a need to develop a liquid-liquid separation unit for the investigation of mass transfer rates precisely and for carrying out multistage operation. In this chapter, a microscale flow splitter which is developed based on the preferential wettability of liquids to the solid material, is presented. Different aqueous-organic systems, mostly laboratory benchmark systems for hydrodynamics and mass transfer, were used to study the effect of various operating conditions on the flow splitting.

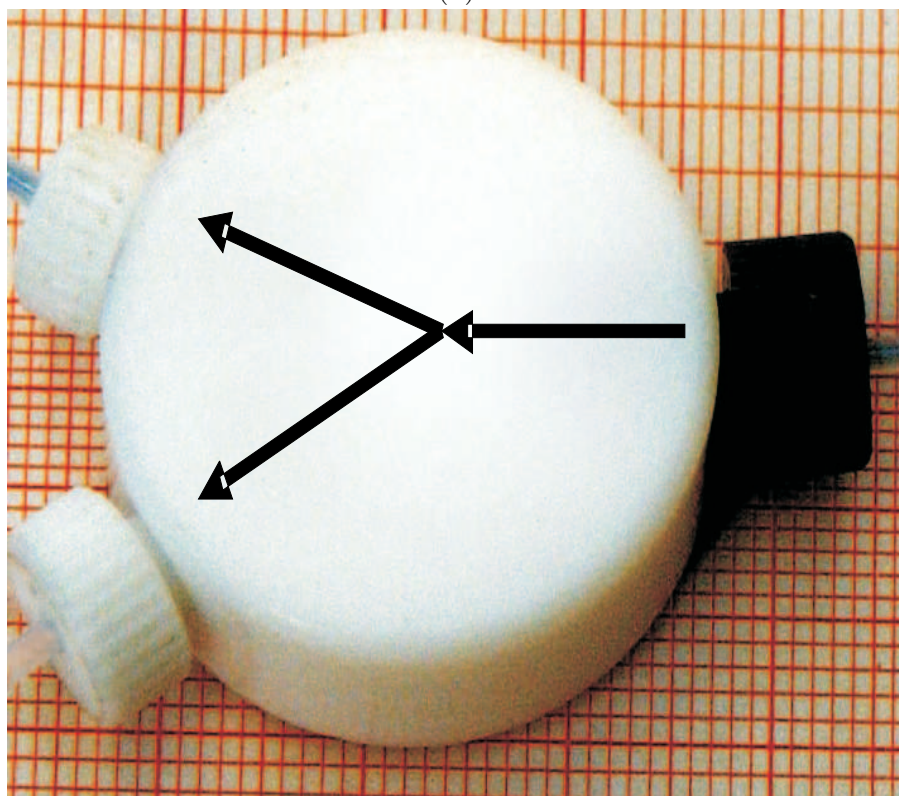
4.2 Experimentation

Experimental set-up: The experimental set-up used to study the flow splitting is already discussed in Chapter 3 and the set-up snapshot is shown in Figure 4.1. It shows that the splitter was connected to the capillary, capillary microreactor, at its end. The splitter, designed and fabricated in-house, is a Y-shape element with one inlet and two outlets to separate the two immiscible liquid phases (aqueous-organic) as shown in Figures 4.2. The splitter made-up of Teflon with a steel needle having an internal diameter equal to the Y-junction internal diameter is fitted into one of the outlets. The splitter works on the principle of preferential wettability of a liquid for a material. The aqueous phase has strong affinity towards steel while the organic phase has affinity towards Teflon. This difference in the affinity can be harnessed for the separation of the two phases. This technique is especially suitable for use in microscale equipment in which surface tension forces dominate rather than gravitational body forces. Furthermore, excellent separation can be achieved over a wide range of flowrates and phase ratios.

Operating conditions and measurements: The chemical systems, operating parameters and conditions used for flow splitting experiments are shown in Table 4.1. The physical properties of the chemical systems used are given in Table D.4. The systems studied were divided into three classes: both non-viscous (system I and II), non-viscous-viscous (system III-V) and both viscous (system V-VIII). The non-viscous liquid has viscosity less than 1 cP while the viscous system has viscosity more than 1 cP. In addition, depending upon the type of the systems, non-viscous-viscous or viscous-viscous, different flow splitter configurations having various angles between the outlets were used. The geometrical properties and type of splitter used are listed in Table 4.2. For a given flow rate, the liquid from each outlet was collected for a specific time and then the fraction of the total flow in the two outlets (steel and Teflon) and its composition (aqueous and organic phase) was determined.



(a)



(b)

Figure 4.1: Snapshots of experimental set-up and Y-splitter: (a) snapshot showing continuous phase separation (blue NaOH solution and colourless NBF) and (b) Teflon made Y-splitter

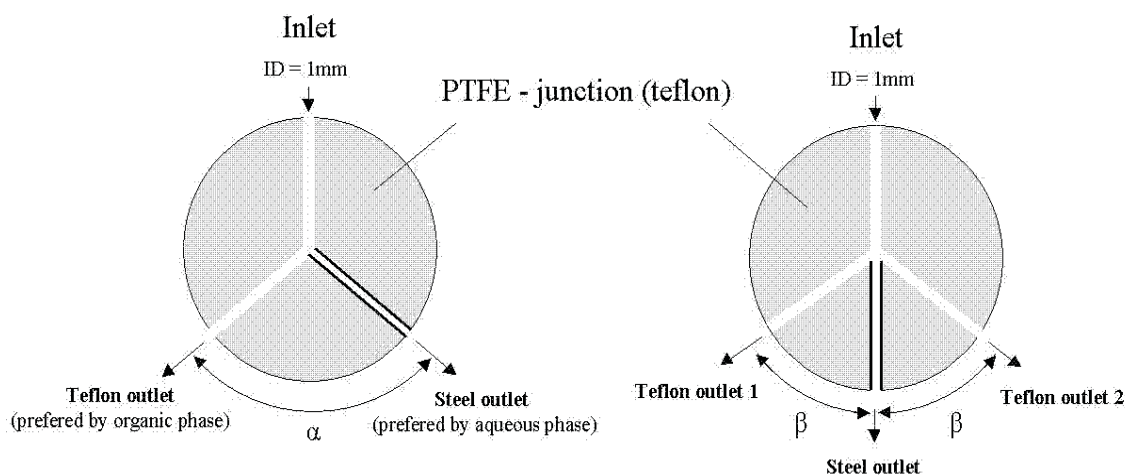


Figure 4.2: Flow splitter configurations used in the study

Table 4.1: Chemical systems, parameters and operating conditions used to study the flow splitting

Systems	Water - Kerosene (I) Water - n-butanol (II) Water - Cyclohexane (III) Water - n-butyl acetate (IV) Water - Saturated NBF solution (V) NBF - 0.2 M NaOH solution (VI) NBF - 0.3 M NaOH solution (VII) NBF - 0.4 M NaOH solution (VIII)
Flow rate (each phase)	5 - 80 ml/h
Capillary ID	0.5, 0.75 and 1.0 mm
Y-junction ID	0.5, 0.75 and 1.0 mm
Y-splitter ID	Inlet - 1.0 mm and outlets - 0.5 mm
Capillary length	1.0 m

4.3 Results and Discussion

In the present work, two types of flow splitters illustrated in Figure 4.2, were developed and tested in our laboratory. In these splitters, the angles between two outlets, α and β were varied according to the requirement which was 120° and 60° for most of the experiments. Due to the immediate separation achieved, a precise estimation of the contact time is possible facilitating the estimate of mass transfer rates with minimal error. A schematic diagram of the splitting mechanism in the

Table 4.2: The geometrical properties of the splitters employed

Splitter	No. of outlets	No. of Teflon outlets	Outlet ID [mm]	α	β
a	2	1	1.0	120°	-
b	2	1	1.0	90°	-
c	2	1	1.0	60°	-
d	3	2	0.5	-	60°
e	3	2	1	-	45°

Y-splitter with one steel and one Teflon outlet developed is shown in Figure 4.3. The Figure shows that when the slug flow touches the steel-Teflon junction point in the flow splitter, the aqueous phase proceeds along the steel branch due to its strong affinity towards this material, while the organic phase flows into the Teflon outlet. Although the slug flow consists of an alternating flow of one phase separated by the other, it was observed that the aqueous phase forms a bridge between the continuous flow in the steel outlet and aqueous slugs in the reactor as shown in Figure 4.3. In some cases it was observed that part of the organic phase is entrained in the aqueous phase in the form of very small droplets, which are trapped between the continuous flow in steel outlet branch and the slugs of aqueous phase and vice versa. In most of the experiments, it was observed that aqueous phase leads to a slight contamination with the organic phase. Nevertheless, in most of the chemical systems it was observed that at least one pure phase always proved possible.

The contamination in each outlet of the splitter was evaluated by collecting the liquid for a particular time and measuring the volume of each phase in both outlets using following equation:

$$Ct = \frac{\text{Volume of undesired phase}}{\text{Total volume collected}} \quad (4.1)$$

And the average contamination in two outlets is investigated by following equation:

$$Ct_{av} = \frac{1}{2} \left[\frac{V_{aq,T}}{V_{aq,T} + V_{or,T}} + \frac{V_{or,S}}{V_{or,S} + V_{aq,S}} \right] \quad (4.2)$$

4.3.1 Effect of viscosity

Both non-viscous and non-viscous-viscous systems: To study the effect of viscosity dependence of the systems, different system combinations such as both non-viscous, non-viscous-viscous and both viscous liquids were studied. In this case, the

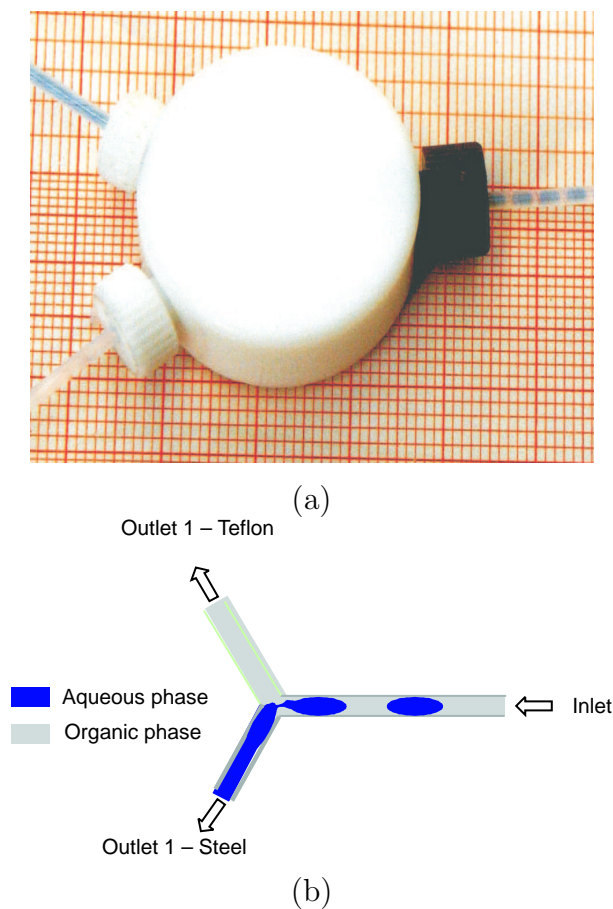


Figure 4.3: Flow splitting: (a) Snapshot of a flow splitter showing splitting of aqueous (water + brilliant blue dye) and organic (n-butyl formate) (b) Schematics of flow splitting mechanism

study was made qualitatively as all experiments were carried out for a given set of operating conditions using different combinations of liquids. Later on, the effects of different operating parameters such as flow rate, flow ratio and capillary size were investigated. First two systems (water-cyclohexane and water-n-butyl acetate) are both non-viscous, systems three to five (water-kerosene, water-n-butanol and water-n-butyl formate) are non-viscous-viscous and last three systems (NBF - 0.2 M NaOH solution, NBF - 0.3 M NaOH solution and NBF - 0.4 M NaOH solution) are both viscous.

In the experiments for both non-viscous and non-viscous-viscous systems, two types of flow splitters were employed, a flow splitter with two outlets having an angle of 120° (splitter A) in between them and a flow splitter with one steel needle in between two Teflon outlets (splitter D). The qualitative results for these combinations are listed in Table 4.3. The results are categorised into three types: average contamination less than 5 %, between 5 to 10 % and more than 10 %. It shows that for all

Table 4.3: Flow splitting experiments for the both viscous and non-viscous-viscous systems

Systems				Type of splitter	
Aqueous	Organic	$\Delta\mu$, cP	σ , N/m	A	D
Water	Cyclohexane	0.09	0.05	+	+/-
Water	n-butyl acetate	0.16	0.009	+	+/-
Water	Kerosene	21.11	0.05	+	+/-
Water	n-butanol	2.11	0.05	+	+/-
+: high splitting quality (average contamination less than 5 %)					
+/-: low splitting quality (average contamination between 5 to 10 %)					
-: poor splitting quality (average contamination more than 10 %)					

five systems, a flow splitter with one steel and Teflon outlet (splitter A) performs better than a flow splitter with one steel needle and two Teflon outlets (splitter D). Despite good performance of splitter A, splitter D was tested because in most of the cases, the aqueous phase showed contamination due to organic phase and therefore it was thought that more Teflon surface would reduce the total contamination.

Both viscous systems: To study the effect of both viscous liquids on the flow splitting, a system of NBF with different concentrations of NaOH was chosen. In this system, NBF is a viscous liquid. The other liquid, aqueous solution of NaOH, shows increased viscosity with increase in NaOH concentration to a value that the liquid property changes non-viscous to viscous. Initial experiments were carried out for the flow splitters which were employed for both viscous and non-viscous-viscous systems. The flow splitter A have shown good splitting, however, with increases in the NaOH concentration it showed increased contamination on both side. Therefore it was decided to change the contact angle between two outlets in both configurations and thus two types of flow splitters with five different configurations were chosen. The qualitative results obtained were divided into three categories as given above. The first system in this case was water-NBF which is non-viscous-viscous system which shows good flow splitting for all flow splitters. However, with increase in NaOH concentration from 0 to 0.2 M, the viscosity of water goes above 1 cP i.e. 1.05 cP which shows good splitting in all splitters except splitter A. Furthermore, increase in the concentration to 0.3 M NaOH, it shows good flow splitting in C and E. The final concentration of NaOH, 0.4 M, shows good splitting in splitter C only. Thus, it shows that viscosity of both phases also play an important role in the flow splitting.

Table 4.4: Flow splitting experiments with the system NBF - aqueous NaOH solution for equal flow rates of both phases

Systems				Type of splitter				
Aqueous	Organic	$\Delta\mu$, cP	σ , N/m	A	B	C	D	E
Water	NBF	5.41	0.0091	+	+	+	+	+
0.2 M NaOH	NBF	5.25	0.00919	+/-	+	+	+	+
0.3 M NaOH	NBF	5.17	0.00924	+/-	+/-	+	+/-	+
0.4 M NaOH	NBF	5.08	0.00928	+/-	+/-	+	+/-	+/-
+: high splitting quality (average contamination less than 5 %)								
+/-: low splitting quality (average contamination between 5 to 10 %)								
-: poor splitting quality (average contamination more than 10 %)								

4.3.2 Effect of flow rate, flow ratio and capillary size

Effect of flow rate: The flow splitting behaviour of liquids in the Y-splitter is shown in Figures 4.4 and 4.5. The dotted line shown in Figure 4.4 corresponds to ideal separation. The Figures 4.4 and 4.5 illustrate that the quality of splitting is almost independent of slug flow velocities for equal flow rates. For the results with the water-kerosene system, the incomplete phase splitting at equal flow rates is due to the presence of some organic phase in the aqueous phase. We further observed that this amount differs from system to system. The flow in the steel outlet was observed to be as high as 55 % of the total flow rate, which is assumed due to the stronger affinity of the aqueous phase for steel compared to the affinity of the organic phase for Teflon. It is thus always possible to obtain one pure phase for all flow rates at equal phase flow rates.

Further, the average contamination in the Y-splitter was investigated and plotted in Figure 4.6. As can be seen in the Figure, the average contamination is almost constant for all flow rates. The maximum contamination observed was less than 6 % which has major contribution in the steel side.

Effect of flow ratio: In order to study the effect of flow ratio on the flow splitting, experiments were carried out for unequal flow rates of two phases. This was done by keeping the flow rate of one phase constant and varying the flow rate of the other. The results obtained are plotted in Figures 4.7 to 4.9. It is evident from the Figures that the steel and Teflon branch fractions of total flow are in proportion to the fraction of the aqueous and organic phases fed to the splitter. At a constant flow rate of water of 10 ml/h and a variable flow rate of kerosene, a slightly higher

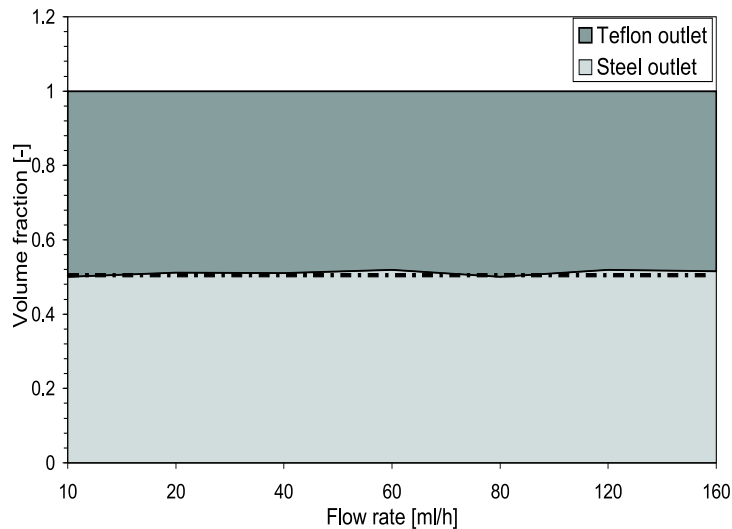


Figure 4.4: Flow splitting at a Y-splitter (Capillary ID = 1 mm, Y-junction ID = 1 mm, Y-separator ID = 1 mm, Flow ratio = 1)

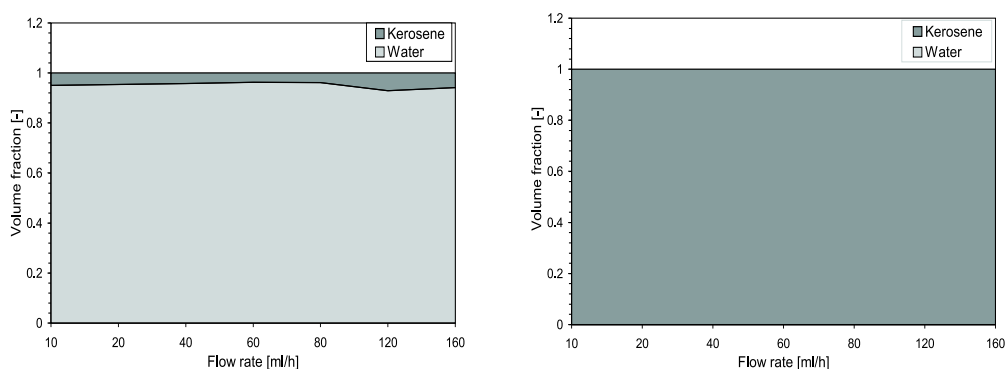


Figure 4.5: Volume fraction of kerosene and water in steel and Teflon outlet, respectively (Capillary ID = 1 mm, Y-junction ID = 1 mm, Y-separator ID = 1 mm, Flow ratio = 1)

volume fraction in the steel branch similar to the behaviour at equal flow rates was observed. The same results were found for constant kerosene flow rates whilst varying the water flow rate. For constant flow rate of water and constant flow rate of kerosene, the steel outlet branch shows about 5 % of organic phase contamination, except at higher flow rate of kerosene (above 50 ml/h), where the organic phase fraction is as high as 30 % (Figure 4.8). Similar results were observed in the Teflon outlet branch, where the aqueous phase content is as high as 30 % at high water flow rate (above 40 ml/h). This is due to the fact that at high flow rates with unequal flows the wetting forces for the lower flow rate liquid (e.g. aqueous phase in steel outlet branch) are dominated by the inertial flow forces and therefore the lower flow

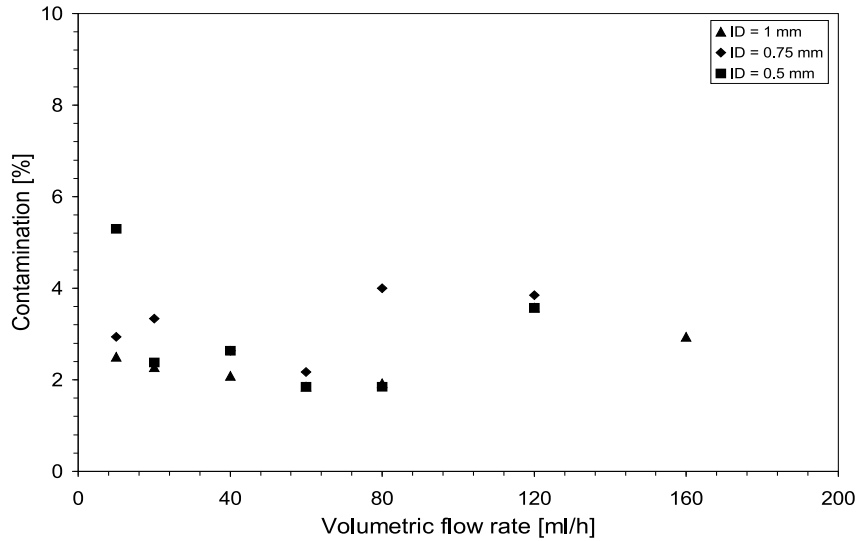


Figure 4.6: Average contamination as a function of flow rate for different capillaries for water-kerosene system ($Flow\ ratio = 1$)

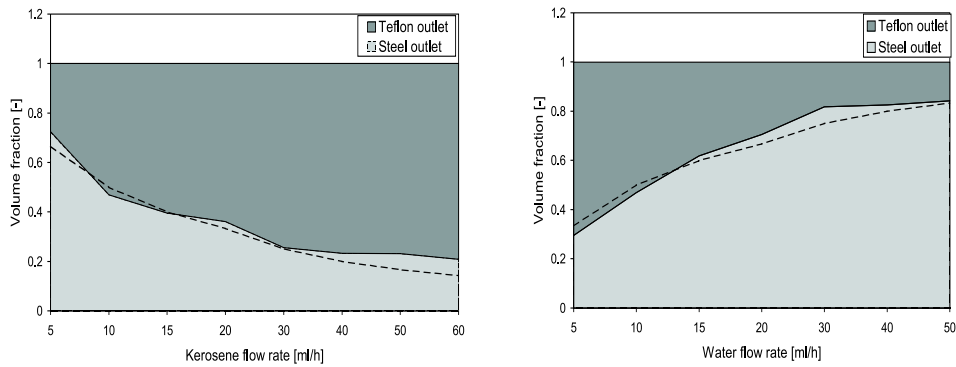


Figure 4.7: Flow splitting for constant water and kerosene flow rates respectively, (Capillary ID = 1 mm, Y-junction ID = 1 mm, Y-separator ID = 1 mm, constant flow rate of water = 10 ml/h and constant flow rate of kerosene = 10 ml/h)

rate outlet of the splitter receives part of high flow rate liquid.

The average contamination in both phases is plotted as a function of proportion of water flow rate in water-kerosene system. It shows that at very low proportion of water phase, the average contamination has very high value which is around 20 %. However, with increase in the water proportion it shows decrease in the contamination until the water proportion reaches 0.8. At equal flow rates of water and kerosene, water proportion equal to 0.5, it shows very less contamination. Thus, water proportion in the range of 0.2 to 0.8, the slug flow exists which shows that the splitting is very effective in slug flow region. However, in the first part, below

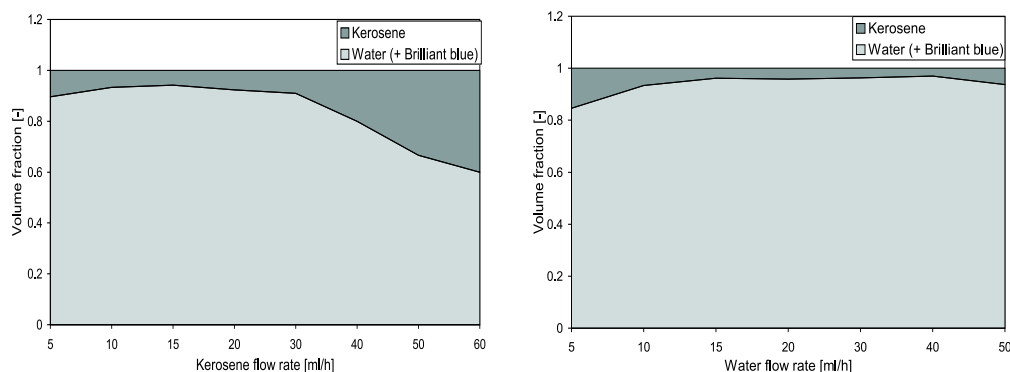


Figure 4.8: Volume fraction in steel outlet for constant water and constant kerosene flow rates respectively (Capillary ID = 1 mm, Y-junction ID = 1 mm, Y-separator ID = 1 mm, constant flow rate of water = 10 ml/h and constant flow rate of kerosene = 10 ml/h)

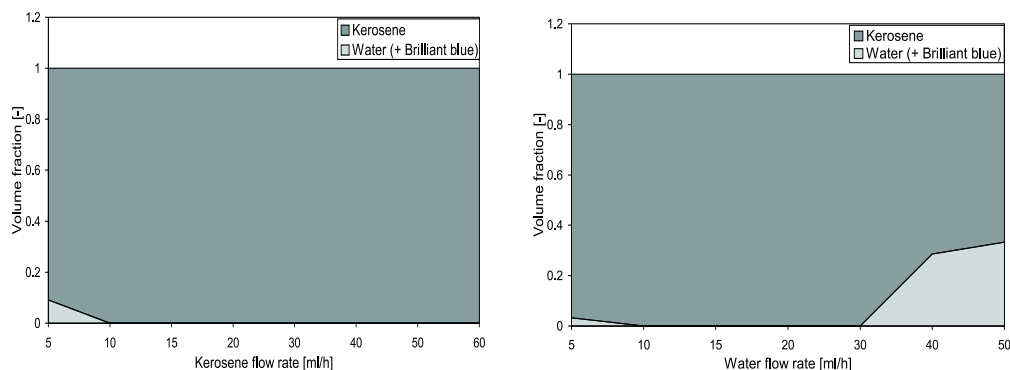


Figure 4.9: Volume fraction in Teflon outlet for constant water and constant kerosene flow rates respectively (Capillary ID = 1 mm, Y-junction ID = 1 mm, Y-separator ID = 1 mm, constant flow rate of water = 10 ml/h and constant flow rate of kerosene = 10 ml/h)

0.2 water proportion, it shows drop flow while above 0.8 it shows deformed interface flow.

Effect of capillary size: The effect of capillary internal diameter on the flow splitting is shown in Figure 4.11. It can be seen, there is no significant influence of the capillary diameter on the degree of flow splitting. For all capillaries studied, more than half of the flow goes to the steel outlet branch (approximately 5 %). For the capillary with an internal diameter of 0.75 mm, the fraction of the organic phase in the steel was found to be as high as 12 % (Figure 4.12). However, in all cases the Teflon outlet yielded pure organic phase except at very low flow rates for the capillary with internal diameter of 0.5 mm. The same effect can be seen in the average values of contamination given by Figure 4.6.

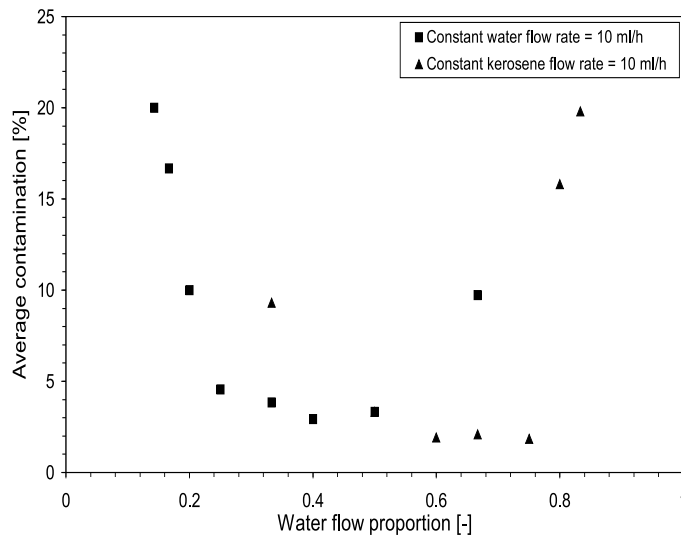


Figure 4.10: Average contamination as a function of water flow proportion for water-kerosene system

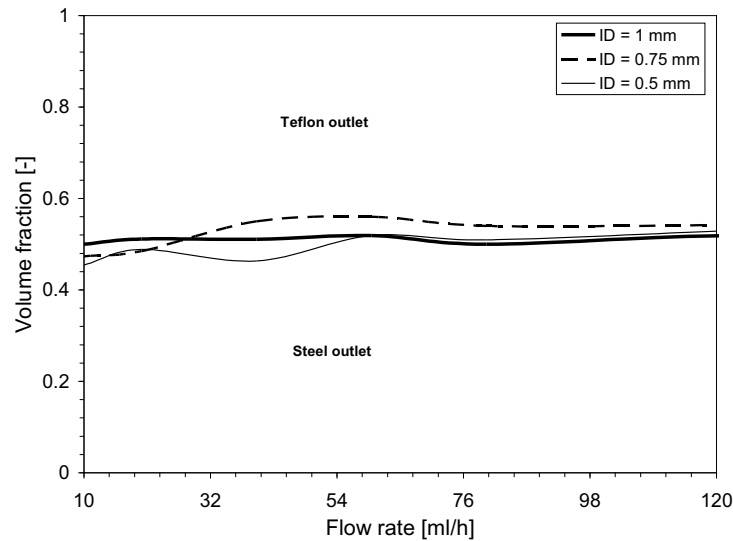


Figure 4.11: Effect of capillary ID on flow splitting (Flow ratio = 1)

The above results show that there is no significant effect of flow rate, flow ratio and capillary size on flow splitting for a given splitter under slug flow regime. The minor problems observed with phase cross-contamination could be resolved by cascading additional splitters downstream of the initial one.

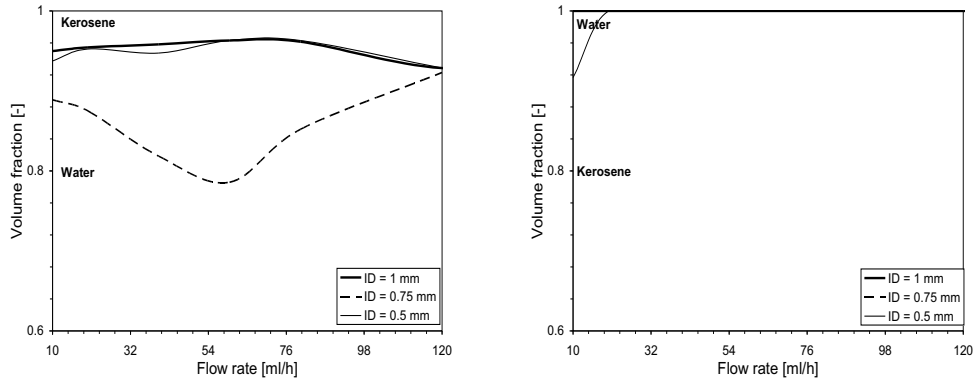


Figure 4.12: Volume fraction in steel and Teflon outlet for various capillaries (Flow ratio = 1)

4.4 Summary

The experiments were carried out to study the splitting of two liquid phases continuously. It was observed that the Y-splitter with one steel and one Teflon outlet yields better results than the splitter with a central steel and two lateral Teflon outlets. The fabrication of the splitter is very simple as a steel needle was fitted in one of the outlets. Different combinations of non-viscous and viscous liquids were studied and it was observed that all systems show best flow splitting with an average contamination less than 10 %.

Part II

Modelling

Chapter 5

Modelling of Fluid Flow

5.1 Introduction

In addition to the extent of slug flow regime, slug size, pressure drop and mass transfer rates, there are many other important issues in liquid-liquid slug flow microreactor such as circulation patterns within the slugs, effect of mixing element geometry on slug flow generation and stability of slug flow are to name but a few. These issues should be considered while designing such a reactor. In this reactor, both phases move alternatively and each slug serves as an individual processing subvolume which is highly regular and guarantees well defined interfacial area for transfer processes. The mass transfer takes place by two mechanisms: convection within the slug and diffusion between two slugs. The convection is due to the internal circulations within each slug because of the shearing action between slug axis and capillary wall or continuous phase while the diffusion is because of concentration gradients between two consecutive slugs. The first phenomenon depends on physical properties of fluids, slug geometry and flow velocity while the latter is depending on the interfacial area and concentration gradient between two consecutive slugs. In order to study all these phenomena, it is imperative that the fluid dynamics of the system has to be well understood. However, it is difficult to carry out experiments at all operating conditions in such a low scale. With the new developments in computational techniques, especially CFD, it is now possible to gain detailed insight into the flow through capillaries in order to tailor, monitor and optimize the performance.

For most of the applications in the microreactors, the mixing of the solute is purely by diffusion which is too slow. However, well defined internal circulations within the slugs of the liquid-liquid slug flow provide better environment for the reaction due to

intense mixing of the solutes. It also helps to solve dispersion problem which is commonly observed in conventional chemical reactors and single phase microreactors. Dispersion is a problem in the pressure driven laminar flow in microfluidic channels as the flow is parabolic, reagents move at different velocities across the width of the channel - slower along the wall and faster at the centre [71]. It also occurs by the diffusion of reagents along the channel. Turbulence and mixing by chaotic advection may reduce dispersion, but the localization of reagents in the droplets (slugs) removes the dispersion completely ([18]; [71]).

Few studies have already been published on dispersion and mixing in the multiphase flow in small geometries as given in Table 5.1. Thulasidas *et al.* [25] have studied dispersion in the gas-liquid flows in the circular and square capillaries. Furthermore, Handique and Burns [72] studied recirculation inside the discrete liquid drop in a slit type microreactor and presented the convection and diffusion dominated mixing behaviour of solute in a discrete moving drop. Furthermore, Professor Ismagilov (University of Chicago) and his group have published a series of articles on the mixing within the droplets (slugs) moving through microfluidic channels ([18];[38];[39] and [71]). Their first study, Song *et al.* [18], is about the experiments for scaling of chaotic mixing in a droplet moving in microfluidic channel. Later on, they have studied the effect of different initial solute distribution on mixing [38] and reported that steady internal circulatory flow is sensitive to distribution of the reagent during slug formation. Further, they have studied the effect of viscosity on the droplet formation and mixing and reported that the combining viscous and non-viscous reagents can enhance the mixing in droplets [39]. Aoki *et al.* [73] have developed a CFD model by using the principle of lamination segments for four types of reactions and reported the strong effect of the lamination width on yield of desired product. Sarrazin *et al.* [74] carried experiments to study the mixing and fast reactions in the micro-drops and presented control of drop coalescence and mixing behaviour. Recently, Tanthapanichakoon *et al.* [42] and [43] have carried out 2D and 3D simulations to study mixing behaviour in a liquid slug of liquid-liquid slug flow and have proposed a modified Peclet number for calculating the mixing in the liquid slugs [42]. They designed microfluidic slug mixing based on the correlation between a dimensionless mixing rate and a modified Peclet number [43].

Besides the computational techniques to visualise flow field, the recent experimental technique, PIV, has shown strong potential in flow field measurements ([76]; [77]). The PIV technique was used to establish the flow patterns within the liquid slugs of bubble train flow inside the capillaries by Thulasidas *et al.* [28] and shown to exhibit circulation patterns with a high degree of internal mixing. The recent developments in the PIV measurement for small scale geometries, μ -PIV, has been used to characterise the flow in the microscale (e.g. [78]; [79]; [80]).

Table 5.1: Literature review on mixing in drops or slugs in small scale geometries

Study	Capillary/chip size (mm)	Technique	Reference
Drop mixing in slit microchannel	0.05	a	Handique and Burns [72]
Scaling of mixing in microfluidic channels	0.01 - 0.1	b	Song <i>et al.</i> [18]
Mixing in straight microfluidic channel for different initial solute distributions	0.05	b	Tice <i>et al.</i> [38]
Effect of viscosity on mixing	$0.05 \times 0.05, 0.15 \times 0.1$	b	Tice <i>et al.</i> [39]
Effectiveness of lamination segments as a form of feed on mixing	0.2 and 2.0	c	Aoki <i>et al.</i> [39]
Mixing and fast reactions in micro-drops	0.05 and 0.1	b	Sarrazin <i>et al.</i> [74]
Design of mixing in microfluidic liquid slugs based on dimensionless number	0.05 and 0.25	c	Tanthapanichakoon <i>et al.</i> [42]
Design of mixing in microfluidic liquid slugs based on mixing rate and Peclet number	0.05 and 0.5	c	Tanthapanichakoon <i>et al.</i> [43]
Drop deformation and velocity field within the droplets	0.05 and 0.06	b, c	Sarrazin <i>et al.</i> [75]

a: Mathematical modelling

b: Experimental

c: CFD modelling

It is important to understand slug flow generation because the mass transfer contribution is very high at the time of slug generation. As discussed in the previous Chapters, the slug flow is generated using the Y-mixing element which was previously used by Dumann *et al.* [4]. Some studies used T-type mixing element for generation of slug flow in the microreactor (e.g. [18]; [35]). Both type of mixing elements shows qualitatively well slug flow generation. The pressure drop across the slug flow generation element has significant contribution to the overall pressure drop. In the case of Y-junction element the pressure drop is less compared to T-type mixing element as friction losses are less in Y-junction. In addition to this, the orientation of mixing element has an effect on the slug size and thus on the overall performance of the reactor. Extensive experimental work is needed to understand this effect which shows that there is a need to develop a model which would help to understand the slug flow generation and to characterise the slug size.

There are several CFD studies available on the behaviour of drops or bubbles in tubes (e.g. [81], [82]). These studies can be extended to slug flow microreactor by taking additional forces (e.g. capillary force) into account. Besides, most of the microreactors are made up of materials such as silicon, quartz, polymers and metals, and their interaction with liquids play important role on flow behaviour in the microreactor especially for multiphase flows. Therefore, it is necessary to know the wetting properties of respective solids and liquids before developing the CFD model. Few studies on single phase and two phase flow in the microreactor have been published (e.g. [83], [84], [85]). CFD simulations to study the hydrodynamics of bubble train flow have been carried out in Kreutzer [23] considering it as a single phase flow since the gas has very less density and viscosity compared to the liquid with which it is in contact. The simulations with reaction engineering models for liquid-liquid slug flow were carried out in Dumann *et al.* [4] and reported that increased flow velocity enhances the mass transfer by inducing stronger internal circulations within the slugs. Further, a numerical model was developed to predict the internal flow patterns of the fluid segments [36] and the transfer of the dissolved chemical species within and across the segments for liquid-liquid slug flow. The flow was represented by two stagnant and adjacent rectangular units which were linked at both ends to form a continuous loop. The model was validated with different sets of experimental results and showed accurate prediction of flow field and mass transfer.

The behaviour of interface has significant effect on the circulatory flow within the slugs and therefore free surface modelling is necessary. This is one of the challenging research areas for mathematicians with respect to providing an efficient solver. Volume of fluid (VOF) and levelset approaches belong to the two best possible implicit free surface reconstruction methods, while particularly VOF is relatively simple to

treat topological changes of the interface and is naturally conservative. This method was extensively used for many applications (e.g. [86], [87], [88], [89]). The velocity field and bubble profile in a vertical gas-liquid slug flow inside the capillaries have been obtained in Taha and Cui [31] and it was found to be in good agreement with published experimental measurements. In their study, the motion of single Taylor bubble rising in a flowing liquid was simulated using a finite volume discretisation. Furthermore, the mass transfer coefficients have been investigated from rising Taylor bubbles to liquid in circular capillaries using CFD simulations by considering bubble as void which was acting as a free surface with the surrounding liquid phase [32]. The simulations were performed over a unit cell by keeping the bubble stationary and moving the system with the average rise velocity. Recently, Sarrazin *et al.* [75] have carried out numerical simulations and experiments for liquid-liquid slug flow (referred as drop flow) using interface-capturing and μ -PIV techniques, respectively. The 3D simulations showed very good agreement with experimental data in a rectangular channel indicating that the obtained results are useful to study mixing as well as heat and mass transfer.

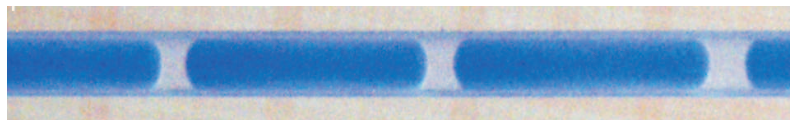
The above mentioned literature shows the potential of CFD methodology to characterise the mixing and flow behaviour in the immiscible fluids. In this chapter, a single phase CFD methodology to characterise the internal circulations within the liquid slugs of liquid-liquid slug flow is presented. The results obtained are qualitatively compared with the internal circulation results obtained by PIV measurements. In addition to this, a two-phase CFD methodology, free surface modelling, used to generate the slug flow is described in detail. Effects of various operating parameters on internal circulation and slug flow generation are discussed. The numerical challenges in the free surface modelling are also presented.

5.2 Single Phase Modelling

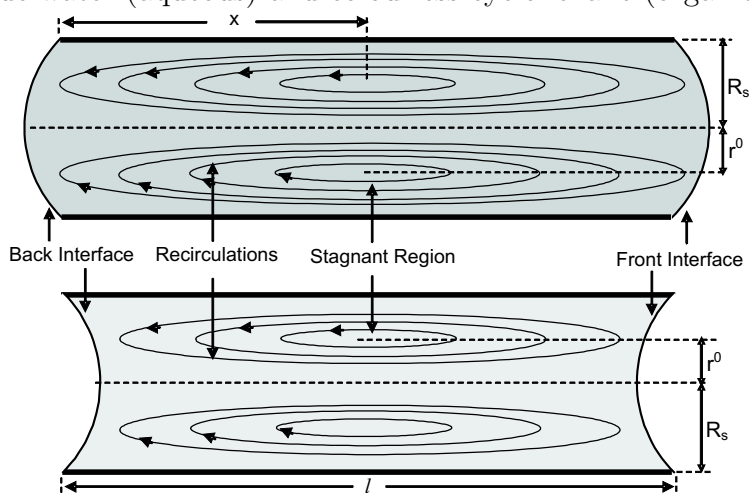
5.2.1 Internal circulations and mixing

The liquid-liquid slug flow in a capillary microreactor is shown in Figure 5.1a. When these slugs move through the capillary, depending on the prevailing physical properties and operating conditions, internal circulations within the slugs arise. The shear between the wall surface and slug axis produces internal circulations within the slug which reduce the thickness of boundary layer at the phase interface thereby enhancing the diffusive penetration. These circulations are illustrated schematically in Figure 5.1b which shows two zones: a recirculation zone at the centre of the

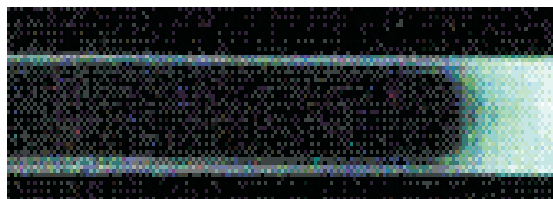
slug and a stagnant zone where the liquid velocity is effectively zero. Similar type of circulation inside liquid slugs of bubble train flow has been reported by several authors (e.g. Kreutzer [23]; Thulasidas *et al.*[28]; Gruber [54]).



(a) Liquid-liquid slug flow in a capillary microreactor showing alternate long blue water (aqueous) and colourless cyclohexane (organic) slug



(b) Schematic representation of internal circulations of aqueous and organic slug respectively.



(c) Liquid-liquid slug flow of water (+ fluorescence) - paraffin oil clearly showing the formation of paraffin oil film.

Figure 5.1: Slug flow in the capillary microreactor. (Y-junction ID = 1 mm, Capillary ID = 1 mm)

Experimental studies presented in previous chapters showed the presence of an organic wall film surrounding the aqueous slug due to superior wetting properties of the capillary wall material (Teflon). The same effect of film formation was observed (Figure 5.1c) during the lab on chip PIV experiments which are discussed in the following section. The significance of the film is that the whole slug surface takes part in the mass transfer thus increasing the mass exchange between two phases. The circulation within the slug with film thus exhibits a wall film zone in addition to the recirculation and stagnant zone. In this case, the liquid inside the slug is driven by the outer flow of wall film and slug displacement by enclosed slug. This wall film

is not stagnant since the liquid exerts considerable shear on it, which keeps the film moving at a low velocity. However, the enclosed slug moves with a velocity slightly greater than the average flow velocity. This velocity can be calculated by assuming a fully developed laminar velocity profile in the capillary as given in Chapter 2. The velocity of the slug (V_s) is considered as maximum velocity (plug flow behaviour) inside the capillary, and relates average velocity (V_{av}) inside the capillary by the following equation (5.1):

$$V_s = \frac{2}{1 + (R_s/R)^2} V_{av} \quad (5.1)$$

where R is the capillary radius and R_s is the radius of fast moving slug which depends on the wall film thickness (h). This in turn can be represented as a function of the capillary number (ratio of viscous forces and surface tension forces) according to the Bretherton law, Equation A.16 (Bico and Quere [67]). This calculation yields a film thickness approximately equal to the experimentally observed value. For the regulation of the mixing quality of such a slug flow reactor, the exact knowledge of the internal circulations as a function of the average flow rate is necessary. Thulasidas *et al.* [28] defined the circulation time in bubble train flow as time for the liquid to move from one end of the slug to the other end. Analogously, in liquid-liquid slug flow, the dimensionless recirculation time for slugs without film can be written as follows:

$$\tau_{wo} = \frac{l (r^0)^2}{2 \frac{l}{V_{av}} \int_0^{r^0} U(r) r dr} \quad (5.2)$$

In the case of wall film, the dimensionless recirculation time within the enclosed slug can be calculated from the above equation by replacing the average flow velocity (V_{av}) by slug velocity (V_s). However, the slug that forms the film (organic phase) keeps the part of the liquid circulating inside it. Considering the volumetric throughput for the stagnant zone radial position (r^o) to the recirculation boundary (r), the equation for the recirculation time can be expressed as:

$$\tau_w = \frac{l [r^2 - (r^0)^2]}{2 \frac{l}{V_s} \int_{r^0}^r U(r) r dr} \quad (5.3)$$

This parameter, recirculation time, represents the mixing timescale within the liquid slugs of liquid-liquid slug flow. Fluid mixing in the slugs have significant effect on yield and selectivity of reaction products in multiple reactions [73]. Two mixing regimes exist within liquid slugs of liquid-liquid slug flow: convection dominating mixing and diffusion dominating mixing. The characteristic is based on the

timescales required for the mixing. The convective transport timescale is proportional to the ratio of length of the slug to average flow velocity. Using the above dimensionless parameter, recirculation time, the equation for convective mixing time can be written as:

$$t_{conv} = \frac{\tau l}{V_s} \quad (5.4)$$

The diffusion within the liquid slug is in the radial direction and is proportional to d_s^2/D [42]. Using above equations the modified Peclet number, given by Tantha-panichakoon *et al.* [42], can be calculated as given in the following:

$$Pe = \frac{d_s^2 V_s}{D l} \quad (5.5)$$

The transport length is only horizontal length, length of slug, because the vertical velocity in the slug is almost zero in all parts except the vicinity of the front and back interface and therefore the convective transport in y-direction is negligible. From the definition of Peclet number, it is clear that for a given substance at high diameter and low flow velocity the mixing is diffusion dominating and at high velocity and low slug diameter the mixing is convection dominating.

5.2.2 PIV experimentation

From the transport phenomenon point of view, it is crucial to establish the recirculation patterns and stagnant zones. We employed the PIV method¹, a method for determining flow velocities in a two-dimensional measuring plane. Tracer particles were added to the fluid to visualize its flow. With the aid of a strong source of light - usually lasers are applied - a pulsed, two-dimensional light field is generated to illumine the measuring plane. The light that is scattered by the particles within the measuring plane is recorded by a camera as a sequence of frames. The image recording for the PIV data was carried in a Caliper[®] 42 Microfluidic Workstation which is schematically illustrated in Figure 5.2. This is a commercial product having a flow controller and an optical observation stand including a microscope (Nikon TE 300 Inverted Microscope) and electronic image recording (Cohu 1300 High Performance Colour CCD Camera).

The slug flow was generated by applying hydrodynamic pressure to a microfluidic glass chip (LabChip NS145) with T-contactor to a capillary width of 70 μm and depth of 12 μm . The LabChip capillary is illuminated as a whole using a mercury

¹The work has been carried out at ISAS - Institute for Analytical Sciences, Dortmund, Germany

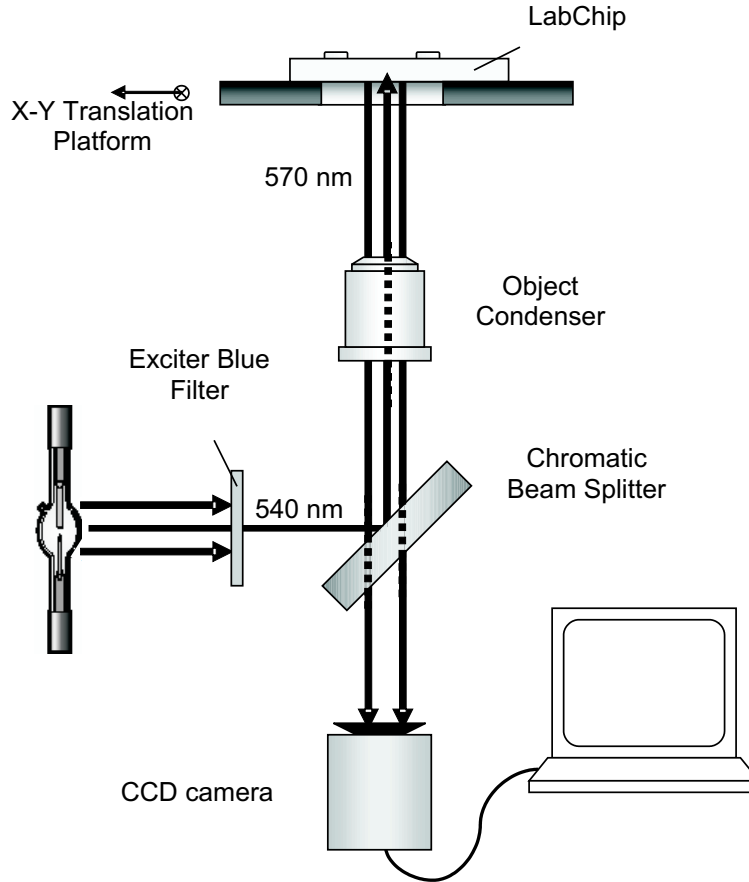


Figure 5.2: Experimental set up for PIV measurement

arc lamp. A light plane cannot be applied in these measurements, since the thickness of such a plane exceeds the depth of the capillary. The system examined was water-paraffin oil. The commercially available tracer particles (polystyrene microspheres, Sphero F_p-0856-2, density = 1.05 g/cm³) coated with a Fluorescing dye (Nile Red, $\lambda_{ex,max} = 510$ nm, $\lambda_{em,max} = 560$ nm) and with an average diameter of 0.84 μm were used. They were diluted with a Fluorescene solution (150 $\mu\text{mol/L}$) in a ratio of 1:8 to 1:12.

After generation of slug flow, the XY translation table of the microscope was manually synchronised with the slug motion thus maintains a constant position of the slug in the screen window. The screen window was then observed with the CCD camera at 10 \times magnification (objective lens NA = 0.3) and the video sequence was recorded with the help of a personal computer. Since the length of slug exceeded the screen width, only part of the slug was recorded. A complete transversing of a paraffin plug through a whole screen width was recorded at a fixed capillary position in order to observe the velocity difference between the two slugs.

Video processing is an important step in the PIV measurement. The recorded videos

were resolved into single frames and converted into grayscale pictures in Bitmap-format. These pictures were then processed with the aid of the software Dantec Dynamics[®] Multiphase ePIV² which determines the displacement vectors of each particle image by calculating a total sum correlation matrix. The maximum of this correlation matrix gives the maximal correlation of two frames for a certain displacement vector. The shape of the maximal peak of the correlation matrix indicates the quality of the calculated results for the displacement vectors. The sharper the peak the fewer different values for the displacements are detected in a single interrogation area. All results were analysed using the above correlation matrix.

5.2.3 CFD modelling

The CFD simulations were carried out for a system shown in Figure 5.1a. Each slug was considered separately as a two-dimensional, single phase domain and solved individually as a decoupled system. The length of the aqueous phase domain with and without film was assumed to be the same while the radius was modified considering the film thickness for aqueous slug with film. For organic slugs without film, the domain was considered as a closed geometry whereas for the film there was inlet and outlet flow via the wall film. The in-house developed open-source Finite Element CFD Tool, FEATFLOW [90], was used for all simulations considering the following assumptions:

- front and back interface of each slug were the same
- the slug size was the same for all flow velocities
- the problem was considered as two-dimensional and non-stationary
- the fluid in each slug was considered to be Newtonian, incompressible and isothermal

The FEATFLOW package solves the following incompressible Navier-Stokes equation with velocity constraints by projected and coupled approach (Turek [90]).

$$\begin{aligned} \nabla \cdot \mathbf{u} &= 0 \\ \frac{\partial \mathbf{u}}{\partial t} + \mathbf{u} \cdot \nabla \mathbf{u} - \nu \Delta \mathbf{u} + \nabla p &= f \quad \Omega \in \mathbb{R}^2 \times [0, T] \end{aligned} \quad (5.6)$$

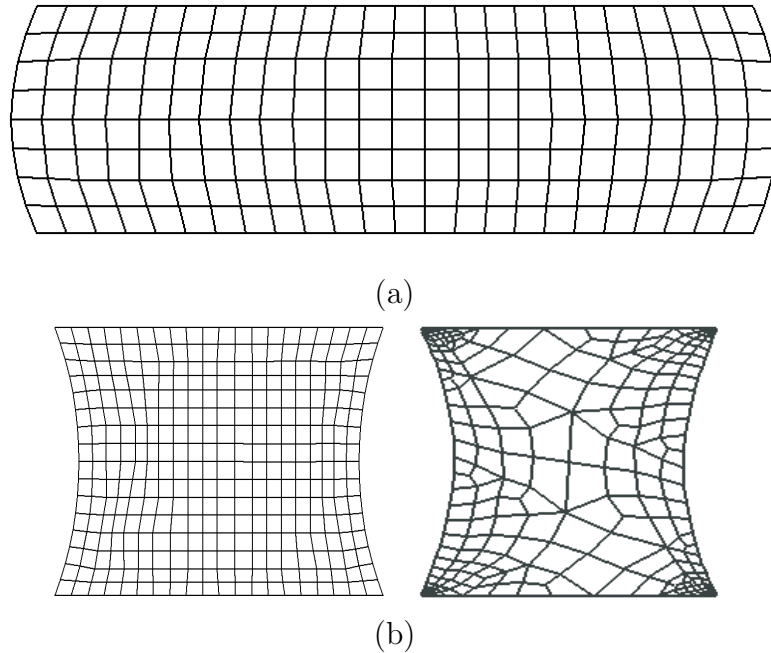


Figure 5.3: Numerical meshes used for the simulations: (a) aqueous slug and (b) organic slug (without and with film, respectively)

In this study, the geometry considered is shown in Figure 5.1b, with front interface being concave and the rear interface convex for the aqueous slug and vice-a-versa for the organic slug. The structured two-dimensional coarse grid was generated with the help of in-house developed Design and Visualisation Software Resource (DeViSoR 2.1) as shown in Figure 5.3 except for the organic slug with film. In the case of wall film, the unstructured grids were generated using commercial grid generator, GiD and was refined near the wall and corner of the geometry to improve the resolution. The Dirichlet type boundary conditions were used for the aqueous slug with and without film as shown in Figure 5.4a. The same boundary conditions were used for the organic slug without film as well since there was no inflow and outflow. For organic phase domain with film i.e. with film inlet and outlet flows, Neumann type boundary conditions were used. A negative x-velocity equal to average slug flow velocity was given to the capillary wall which moved it in negative direction while the slug remained stationary producing the internal circulations within the slugs. In the case of wall film inlet and outlet of organic slug, the slug was kept stationary and relative velocities for wall film flow inlets and walls were defined.

Initially, the simulations were carried out in order to make the solution grid independent using different levels of refinement. Stationary flow fields were achieved with

²Developed by the Chair of Fluid Mechanics, University of Dortmund

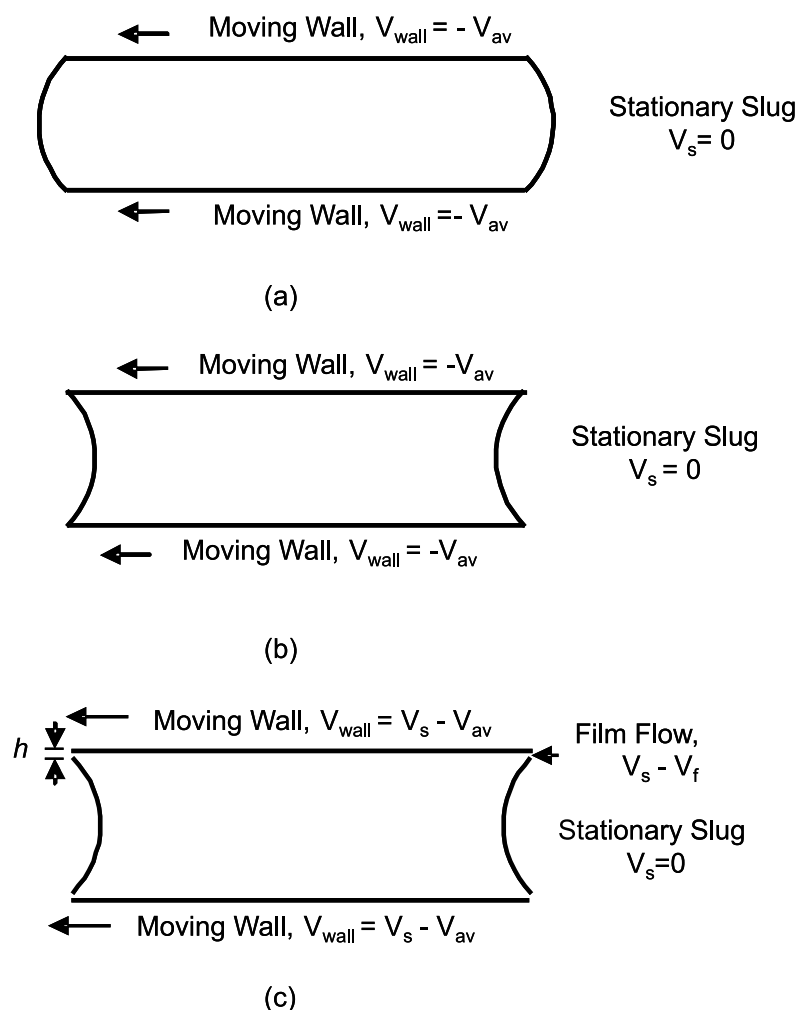


Figure 5.4: Boundary conditions used for the simulations: (a) aqueous slug with and without film, (b) Organic slug without film and (c) Organic slug with film

equidistant time stepping of 0.01 s and total time of 30 s for each slug. Similarly equidistant time stepping of 0.25 s was used for visualization of General Mesh Viewer (GMV) outputs. The GMV outputs were taken with the same level of refinement. The Sun-Fire-880 computer system with 900 MHz Sparcv9 processor was used for simulation. The total time required for a single simulation was 416 s (12288 cells) and 872 s (20480 cells) for aqueous ($L = 2.379$ mm) and organic ($L = 1.122$ mm) slug respectively.

5.2.4 CFD particle tracing

It is difficult to carry out experiments to visualise the flow field using PIV techniques at all operating conditions. We therefore used a method capable of calculating and visualising the convection resulting from a given stationary or non-stationary flow

called CFD particle tracing. This converts an Eulerian description of a flow into the corresponding Lagrangian description at selected particle location. Practically we define some particle sources that generate virtual massless particles once or on a regular basis which follow the path in the given flow field over time.

We have employed an in-house developed algorithm called GMVPT³ (General Mesh Viewer Particle Tracing) which does not carry out its own flow simulation, but imports flow fields from a series of CFD output files. The domain description is given by a coarse grid and can be refined down to the level of CFD refinement. These refinement levels are used to build up a hierarchical searching structure to determine in which cell each particle resides. Initially we define the position of a particle or particles and velocity. However, in most of the cases the velocity at the particle position chosen is not known and it has to be interpolated from the values at the grid nodes. So from the nodal information and the time step, we could determine the new position using the following simple relation:

$$Z' = Z + \Delta t \cdot V_p \quad (5.7)$$

First we have to determine the cell in which the particle resided and which node data we have to use for the interpolation. This was done by using the multilevel structure of the grids as shown in Figure 5.5. Ideally, full searches were made only at the coarse grid level and then only for the cells that were generated by refinement. However, this only works with cell hierarchies which have the property that all generated cells are included in the cells from where they are generated. For boundary cells this is not always true. Due to this, the cells which are outside of their parent cell have to be checked separately at each refinement level. For complicated domains with complex coarse grids, this method sacrifices some information and it is therefore planned to replace this method at a later date by a quad tree based approach.

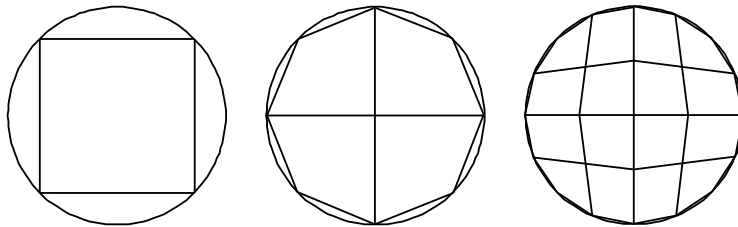


Figure 5.5: Cell refinement

The simulations for particle tracing were carried out with the result obtained from CFD simulations. The meshes with different levels of refinement were generated

³Developed by Institute for Applied Mathematics (LSIII), University of Dortmund

with the help of the in-house developed graphical pre-processing tool, TRIGEN2D, a tool for two-dimensional coarse triangulations and to write the corresponding data in special format onto a hard disc. A rectangular area of tracers with a constant frequency was inserted to simulate a constant stream of particles at various operating conditions.

5.3 Two Phase Modelling

5.3.1 Slug flow generation

A well defined and stable slug flow is suitable for investigations of two phase liquid-liquid reactions because it ensures a uniform interfacial area to fulfil the basic requirement for mass transfer. Slug flow generation by experimentation is discussed in Chapter 2 and the numerical experiments are discussed in this section.

To generate the slug by numerical experiments, a corresponding free surface methodology was developed. Different methods are available to model two immiscible fluids such as level set, VOF, marker particle, lattice boltzmann, front tracking and so on. A short review of these methods can be found in [91]. The description of the free surface is one of the challenging tasks and can be done by two approaches: Eulerian and Lagrangian. In liquid-liquid slug flow, the problem is relatively simple since the flow is quite stable while in the case of immiscible flow with large viscosity and density differences (e.g., air-water flow) the interface may undergo severe deformations and break up. The difference between the Eulerian and Lagrangian approach is that the mesh remains fixed with the flow moving through it in the first case while the mesh moves with the same speed of the fluid in the later case. In the Lagrangian approach the mesh distortion leads to limitations and thus only simple non-intersecting interfaces can be represented. So, we have followed the Eulerian approach which formulates the interface tracing by two methods: front tracking and volume tracking. The VOF methodology was developed [92] which relies on the fact that two or more phases are not interpenetrating and for each additional phase we add the volume fraction of the phase in the computational cell. In each control volume, the volume fractions of all phases sum to unity. This methodology has several advantages namely reasonable accuracy, relative simplicity and it can solve highly complex free surface flows. It solves the incompressible Navier-Stokes equations for velocity u and pressure p :

$$\nabla \cdot \mathbf{u} = 0 \tag{5.8}$$

$$\frac{\partial \mathbf{u}}{\partial t} + \nabla \cdot (\mathbf{u}\mathbf{u}) = -\frac{1}{\rho} [\nabla p - \nabla \cdot \mu (\nabla \mathbf{u} + [\nabla \mathbf{u}]^T)] + \frac{1}{\rho} F_{SF} \quad \Omega \in \mathbb{R}^2 \times [0, T] \quad (5.9)$$

where F_{SF} is continuum surface force vector. The above equation is dependent on the volume fractions of all phases through the properties ρ and μ . These properties were calculated by the following equations:

$$\rho = \sum \alpha_k \rho_k \quad (5.10)$$

and

$$\mu = \frac{\sum \alpha_k \rho_k \mu_k}{\sum \alpha_k \rho_k} \quad (5.11)$$

where α_k , ρ_k and μ_k are the volume fraction, density and viscosity of the k^{th} fluid, respectively. In a two-phase system, the following possibilities arises in a particular cell

$$\alpha_2 = \begin{cases} 0, & \text{(Fluid 1)} \\ 1, & \text{(Fluid 2)} \\ 0 < \alpha_2 < 1, & \text{(Interface between two fluids)} \end{cases} \quad (5.12)$$

The interface between two fluids was tracked by volume fraction function, α_k . It convects with the flow and conservation of this function can be represented with the help of interface mass balance conditions by pure convection equation:

$$\frac{\partial \alpha_k}{\partial t} + \mathbf{u} \cdot \nabla \alpha_k = 0 \quad (5.13)$$

The volume fraction for the primary phase was not solved and was obtained from the following equation:

$$\sum \alpha_k = 1 \quad (5.14)$$

In the case of level set free surface modelling approach, the basic equations are almost similar while the interface is tracked by a function which is zero at the interface, positive in the phase one and negative in phase two for biphasic fluids. The evolution of this function can be posed as a general transport problem as given in Equation 5.13 where u as a speed function dictating the rate of change of interface in normal direction [93]. In a capillary microreactor, modelling of surface tension and wall adhesion effects are important in addition to mass and momentum transfer. The surface tension is due to the strong intermolecular attractive forces between

molecules in a fluid which holds the molecules strongly and minimises the surface area of slug while the wall adhesion is due to the stronger attractive forces between liquid molecules and the wall and thus the fluid makes some contact angle with the wall. In the present work, the continuum surface force (CSF) model proposed in [94] was used to model surface tension. With this model, the addition of surface tension to the VOF calculation results in a source term in momentum equation. The surface curvature was computed from the local gradients in the surface normal at the interface. Thus, the source term in the momentum equation was specified as follows

$$F_{SF} = \sigma \kappa \mathbf{n} \left[\frac{\alpha_1 \rho_1 + \alpha_2 \rho_2}{\frac{1}{2}(\rho_1 + \rho_2)} \right] \quad (5.15)$$

where \mathbf{n} is the surface normal and κ is the curvature which are given as

$$\mathbf{n} = \nabla \alpha_2 \quad (5.16)$$

$$\kappa = -(\nabla \cdot \hat{\mathbf{n}}) = \frac{1}{|\mathbf{n}|} \left[\left(\frac{\mathbf{n}}{|\mathbf{n}|} \cdot \nabla \right) |\mathbf{n}| - (\nabla \cdot \mathbf{n}) \right] \quad (5.17)$$

The surface normal \mathbf{n} was evaluated in the cell where α_2 has value greater than 0 and less than 1 i.e. interface containing cell. The geometric construction scheme (Piecewise linear interface calculation, PLIC) was used to calculate the interface position in the cell. In the case of wall adhesion, rather than imposing the boundary condition at the wall itself, the contact angle that the fluid is assumed to make with the wall is used to adjust the surface normal in the cells near the wall. If θ_w is the contact angle at the wall then the surface normal at the live cell next to the wall is

$$\hat{\mathbf{n}} = \hat{\mathbf{n}}_w \cos \theta_w + \hat{\mathbf{t}}_w \sin \theta_w \quad (5.18)$$

where $\hat{\mathbf{n}}_w$ and $\hat{\mathbf{t}}_w$ are the unit vectors normal and tangential to the wall, respectively.

5.3.2 Numerical mesh, boundary conditions and solution

The geometry for the two-phase simulations is shown in Figure 5.6. The unstructured rectangular grid generated with the help of Gambit 2.2 (Fluent Inc., USA) was used for simulation. The grids were refined in the vicinity of Y-junction in order to improve the resolution. Two equal flow rates were given at the two inlets. In some simulations, those were used as constants while in others they were defined sinusoidal. At the outlet, the Neumann type boundary condition was used. The

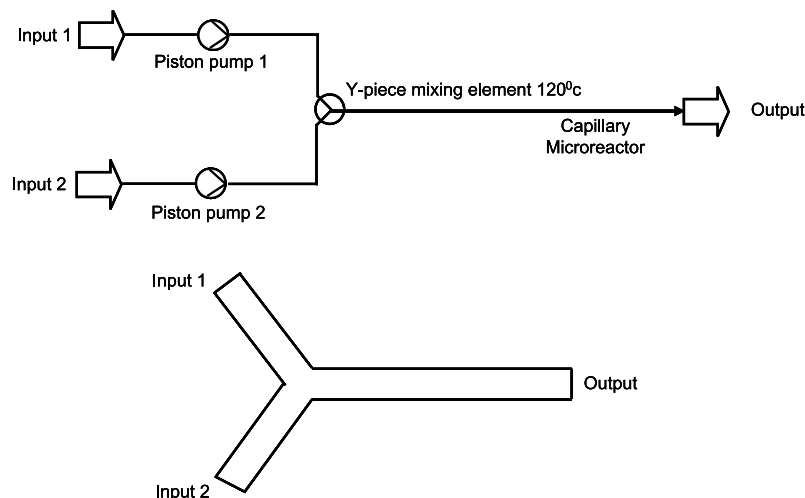


Figure 5.6: Schematics of experimental set up and computational domain

flow fields were achieved with equidistant time stepping of 3×10^{-5} s and with maximum time of 20 s. However, the other parameters were kept same like single phase simulations.

For the solid walls, rather than imposing the boundary conditions, the contact angle that the fluid assumed to make with the wall is used to adjust the surface normal in the cells near the wall. The contact angle values are taken from the experimental measurements and no-slip boundary conditions (zero velocity on walls) are used. The liquid-liquid-solid contact line moves along the wall, presenting a kind of singularity [95]. In this case, the velocity of the faces adjacent to wall are kept to zero and other parts (cell centre and other faces) have non-zero velocity. Such non-zero velocities influence volume fraction field and therefore position of the interfaces. Thus, such implementation realizes the movement of the liquid-liquid-solid contact line despite specifying no-slip boundary condition at the solid surface.

The above equations were solved with the help of finite volume (FVM) based commercial fluid flow solver FLUENT 6.1 (Fluent Inc., USA). Also the above systems of Equations for level set without wall adhesion was implemented in FEATFLOW [93].

5.4 Results and Discussion

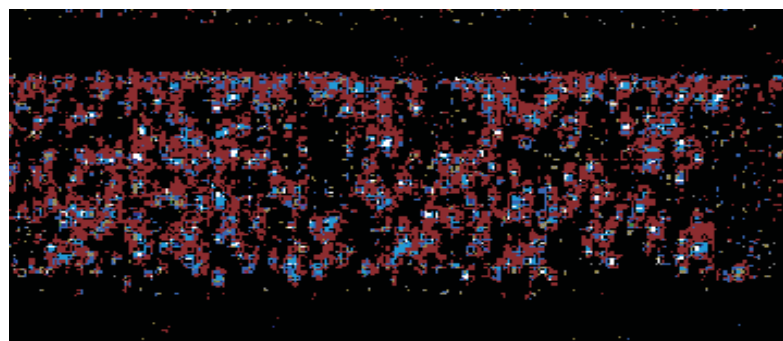
5.4.1 PIV

The experimental snapshot of fluorescence particles with PIV investigations in terms of velocity vectors for three different average velocities is shown in Figure 5.7. The experimental PIV measurements were carried out at very low flow rates due to experimental limitations while CFD simulations were carried out to study internal circulations over a wide operating window. In the PIV illustration of the velocity vectors, the green field indicates the correlation is in good agreement whereas the red background indicates less satisfactory correlation peaks. For the comparison of the vector fields it should be noted that the velocity vectors have been scaled differently in the illustrations presented.

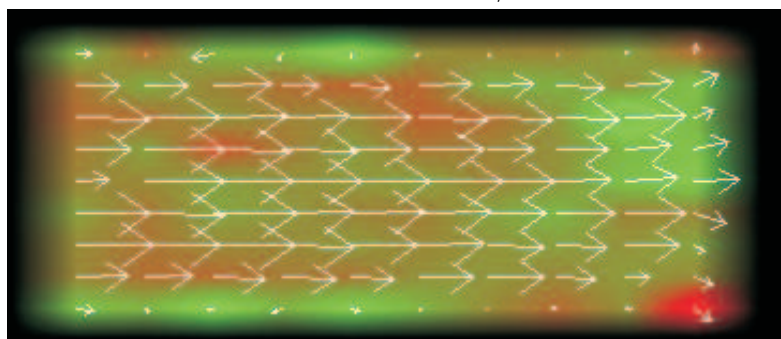
It can be seen from Figure 5.7 that the velocity of the back-flow increases in the vicinity of capillary wall relative to the flow rate close to the capillary symmetry axis. At the average flow velocity of 0.031 mm/s, particles in the vicinity of the wall flow in the reverse direction, but back-flow only occurs to a very limited extent. With increasing flow velocity to 0.072 mm/s, the back-flow of particles is not strongly pronounced. The illustration shows a similar relative velocity vector field. In the third PIV snapshot ($V_{av} = 0.086$ mm/s), one can observe internal circulations at the front end clearly while the rear interface is not visible. This shows that at extremely low flow velocities the particles are stagnant and start circulating over the slug length with increase in the flow velocity. Several videos were taken sequentially during this experimental study. It was observed that the wall film provides lubricating action to enclosed slug, whereby the slug surrounded by film moves with higher speed as compared to the average velocity.

5.4.2 CFD simulations

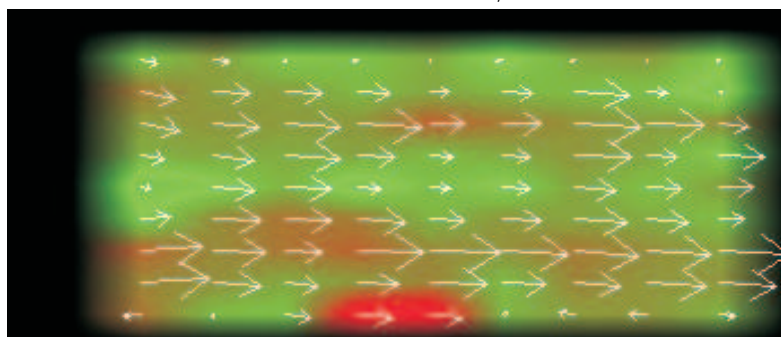
When the solute diffuses through the interface from one slug to another, it subsequently circulates within the slug. The solute moves towards the front end of the slug, part of it is retained in a quiescent zone at the front end, while the remainder recirculates along the wall to the centre of the slug at the rear end. Convective mass transfer takes place to a degree depending on the intensity of internal circulation, while interphase mass transfer depends on the intensity of flow at the end of both slugs. This recirculation is characterised by a recirculation time and recirculation patterns ascertained with the help of CFD simulations without mass transfer.



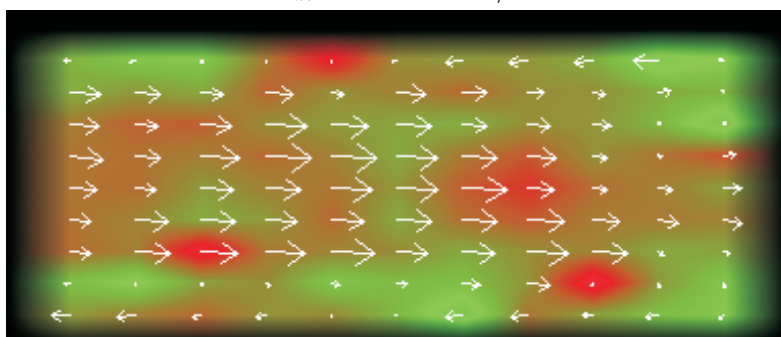
$$V_{av} = 0.031 \text{ mm/s}$$



$$V_{av} = 0.031 \text{ mm/s}$$



$$V_{av} = 0.072 \text{ mm/s}$$



$$V_{av} = 0.086 \text{ mm/s}$$

Figure 5.7: Experimental snapshot and PIV velocity distribution within the slug

The contours of the internal circulations (velocity vector magnitude) within the aqueous and organic slug indicating circulation patterns and stagnant zones (zero

vector magnitude) are shown in Figure 5.8. As can be seen, the maximum velocity is at the centre and minimum velocity at the wall, showing a fully developed parabolic (Poiseuille) profile. Two flow patterns were observed within each slug: a recirculation zone at the centre and in the wall proximity and two stagnant zones in between them. When the slug moves through the capillary, due to the shear between slug axis and capillary wall, the liquid in the centre moves to the front end of the slug, where it touches the front interface and returns back along the wall of the capillary while at the back end, liquid moves from the wall to the centre of slug and thus circulation takes place. Thus, the parabolic profile is bidirectional showing a maximum velocity at the centre of the slug, zero velocity at some radial position r^0 (stagnant zone) and negative velocity at the wall surface. The velocity profiles shown in Figure 5.9 were taken at the centre of the slug which shows fully developed parabolic velocity profile. The equation for x-velocity in the slug with respect to average slug flow velocity for slugs with closed geometry can be estimated from Hagen-Poiseuille law as

$$\frac{u(r)}{V_{av}} = 1.5 \left[1 - \left(\frac{r}{R} \right)^2 \right] - 1 \quad (5.19)$$

The above equation clearly shows that the average flow velocity has strong effects on the bidirectional profile or recirculation. With increase in the average flow velocity, internal circulation increases, and thereby enhances convective mass transfer. The above equation is not valid over whole slug region which is depending on the length of the slug. For longer slugs, it shows more area where the velocity profile is fully developed parabolic profile as given by the above equation. However, in the vicinity of the slug extreme ends of the slug the velocity profile changes.

These recirculation patterns are also strongly influenced by the slug geometry. With increase in the curvature of the extreme ends of the slug the circulation area within the slug decreases. In addition slug length plays an important role. If the length of the slug is less than its diameter (e.g. organic slug, $L = 0.561$ mm), the velocity patterns are totally different than the slugs with lengths greater than their diameters. In many chemical engineering studies, it is required to produce slugs with length less than its diameter. Therefore, many simulations were carried out to study such behaviour. In few simulations, dead zones rather than recirculation were observed. Sometimes they showed that the front part of the slug has dead zones and the back part has circulation at the corners only. Increasing the length of the slug, the velocity profile in the slug approached to parabolic (Poiseuille) profile. In the case of slugs with film, the aqueous slug has the same profile while in the organic slug it is slightly disturbed near the interface due to film inlet and outlet, however a fully developed profile was observed at the centre. The film thickness shows no strong effect on the velocity profile because it is very small as compared to the diameter

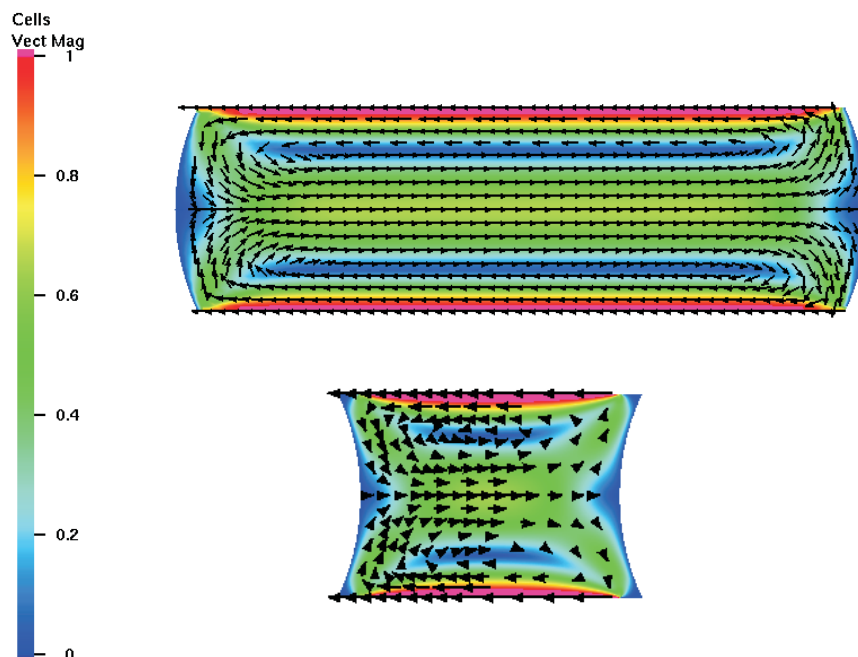


Figure 5.8: CFD simulated internal circulations within an aqueous and an organic slug, respectively

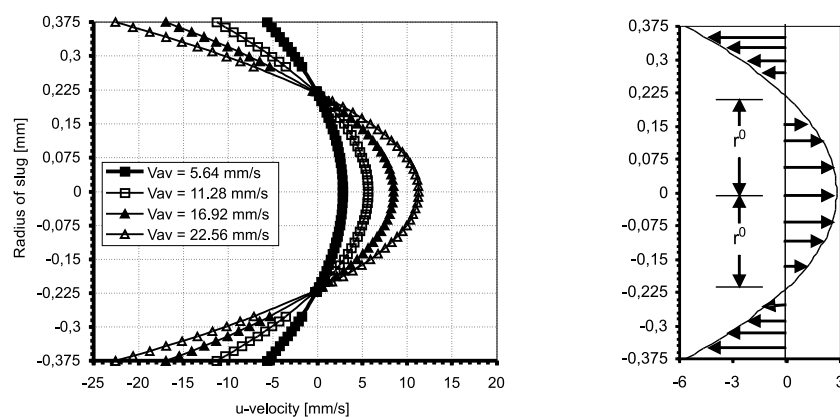


Figure 5.9: Parabolic velocity profile within the slug (aqueous slug, length = 2.379 mm and diameter = 0.75 mm)

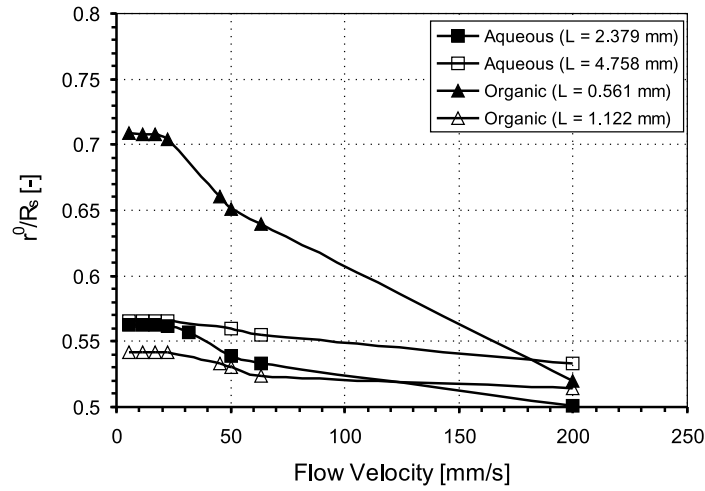
of the slug. Thus, from single phase simulations it was observed that for a slug with length greater than its diameter, intensity of internal circulation increases with increase in the average flow velocity and the film has no significant effect on it. The CFD circulations were observed at all flow velocities. However, the PIV results

show very less circulations compared to CFD results. This discrepancy with the PIV results is probably due to particle inertia.

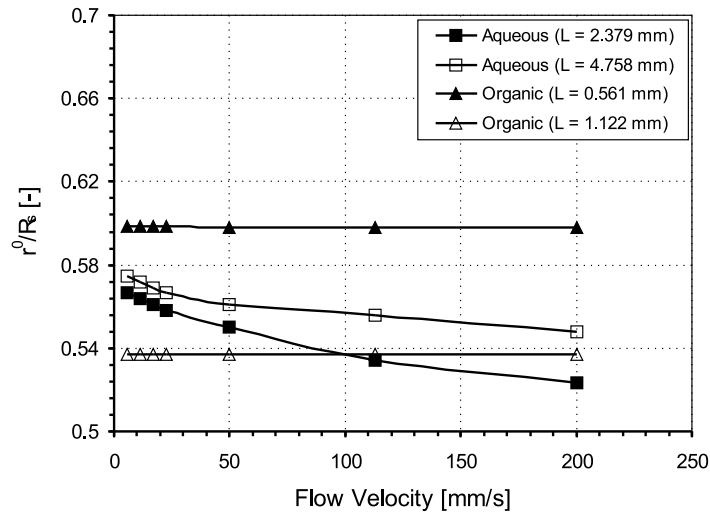
The liquid circulates around the two stagnant zones (see Figure 5.1b) showing a more intense recirculation at the centre of the slug and in between the two stagnant zones. In the stagnant zones the velocity is zero and the radial position was calculated by equating $u(r)$ equal to zero in the velocity profile equation. This radial position shows the area of available for upstream and downstream flows during recirculation. The dimensionless radial distance as a function of average flow velocity is plotted in Figure 5.10. As can be seen, for slugs with length greater than their diameter, the radial position (r^0/R_s) is located at roughly half the capillary radius and shifts slightly towards the centre of the slug with increasing liquid flow velocity. On the other hand, in the case of shorter slugs (i.e. organic slug $L = 0.561$ mm) the dimensionless radial position is 0.72 at low velocity and with increasing flow velocity the radial position diminishes rapidly, approaching 0.5 at 200 mm/s. The distance of the stagnant zone from the rear interface (x/L) indicating symmetry of the circulation, was also predicted from the simulated results and plotted in Figure 5.11.

At low flow velocities, the stagnant zone is at half of the length of the slug and with increasing velocity (~ 50 mm/s) the stagnant zone shifts towards the rear interface of the slug. In this case liquid circulates around the stagnant zone and exhibits intense circulation at the rear interface. For the slugs without film, with increasing length of the slug, the stagnant zone shifts more towards the rear side end of the slug. The same behaviour was also observed for an aqueous slug with film. In the case of the organic slug with a wall film, since there is inflow and outflow, the stagnant zone is at the centre of the slug at all flow velocities, and the intensity of recirculation is maximum at the centre line.

The average circulation time within the slug is calculated from simulated results (Equation 5.2 and 5.3) and plotted as a function of average flow velocities in Figure 5.12. Thulasidas *et al.* [28] reported recirculation time in gas-liquid flow with film and showed that at low capillary numbers the recirculation time inside the liquid slug is constant but increases at high capillary number (~ 0.1). In case of a slug without film, for a slug of sufficient length ($L > D$), the flow velocity has no significant effect on normalised circulation time. The dimensionless circulation time varies between 3 and 4, which indicates that a typical element inside the slug will move from one end of the slug to other end during the time the slug travels a distance 3 to 4 times its own length. For a slug with a length less than its diameter (e.g. organic slug with $L = 0.5616$ mm in Figure 5.12), at low liquid velocity the circulation time was constant, but with increasing the flow velocity, circulation time decreases and



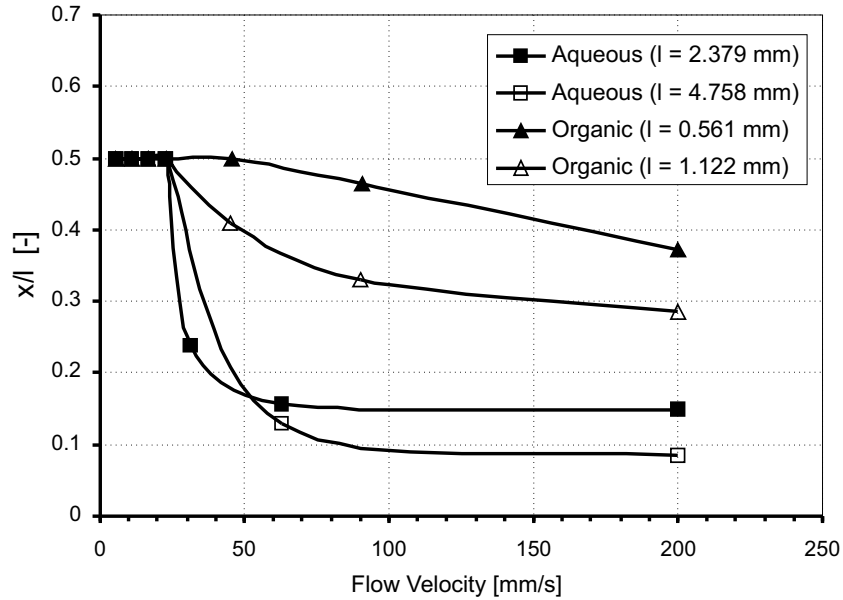
(a)



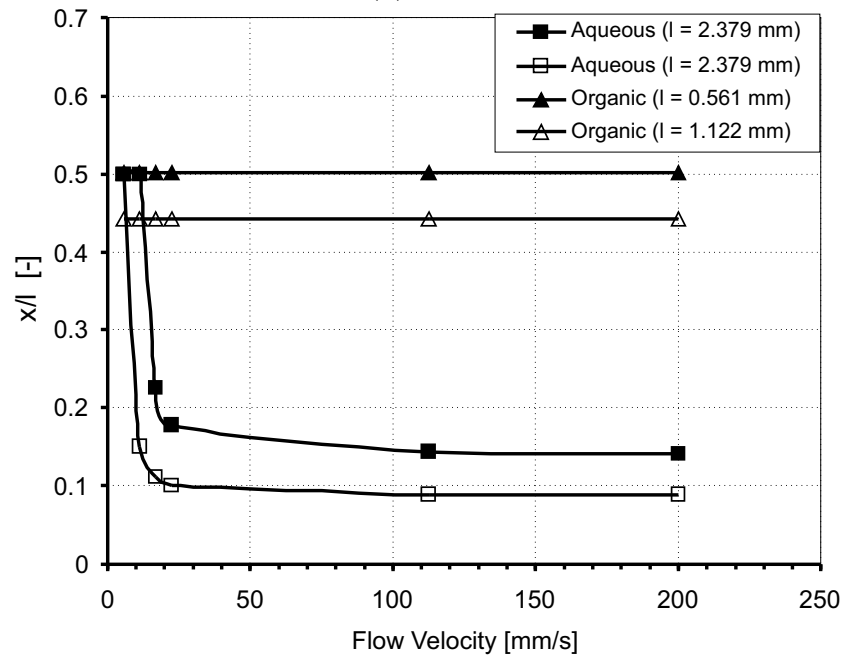
(b)

Figure 5.10: Radial position of stagnant zone within the slug (a) without film and (b) with film

subsequently remains constant. This indicates that at low flow velocity, the liquid circulates slowly and the circulation rate is enhanced with increasing flow velocity above 80 mm/s but further increase in velocity has no effect on recirculation time. With a wall film, for the aqueous slug the circulation time is slightly larger than the case of without film due to the decrease in the diameter of the slug and increase in slug velocity. It also decreases with increase in the flow velocity. For the organic slug, the circulation time is constant at all flow velocities due to wall film inflow and outflow. This information on the behaviour of internal circulation patterns and circulation time might be used in surface renewal model to calculate the mass transfer.



(a)

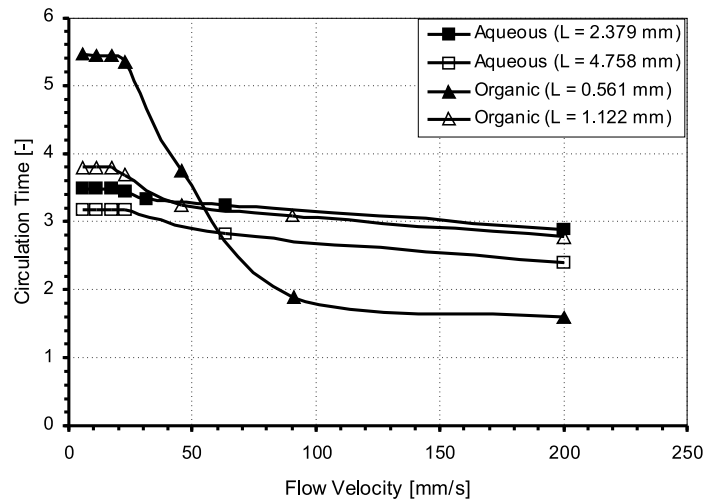


(b)

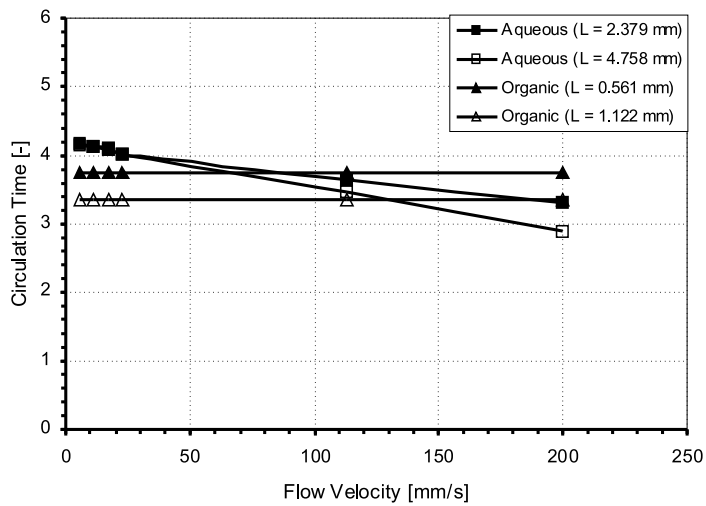
Figure 5.11: Distance of stagnant zone centre from the back interface (a) without film and (b) with film

5.4.3 CFD particle tracing

The simulations for particle tracing were carried out with the result obtained from CFD simulations. The meshes with different levels of refinement were generated with the help of the in-house developed graphical pre-processing tool, TRIGEN2D, a tool for two-dimensional coarse triangulations and to write the corresponding data



(a)



(b)

Figure 5.12: Recirculation time within the liquid slug (a) without film and (b) with film

in special format onto a hard disc. As mentioned before, a rectangular area of tracers with a constant frequency was inserted to simulate a constant stream of particles at various operating conditions.

Simulations were carried out with 2000 macro time steps and duration of 0.01 for both the slugs at different tracer block locations. The internal circulations inside aqueous and organic slugs using particle tracing observed at different times for a flow velocity of 5.64 mm/s are shown in Figure 5.13. As can be seen, at time zero a square block with 100×100 particles was introduced on the axis near the rear interface. With increasing time, the particles were swept along with the flow and

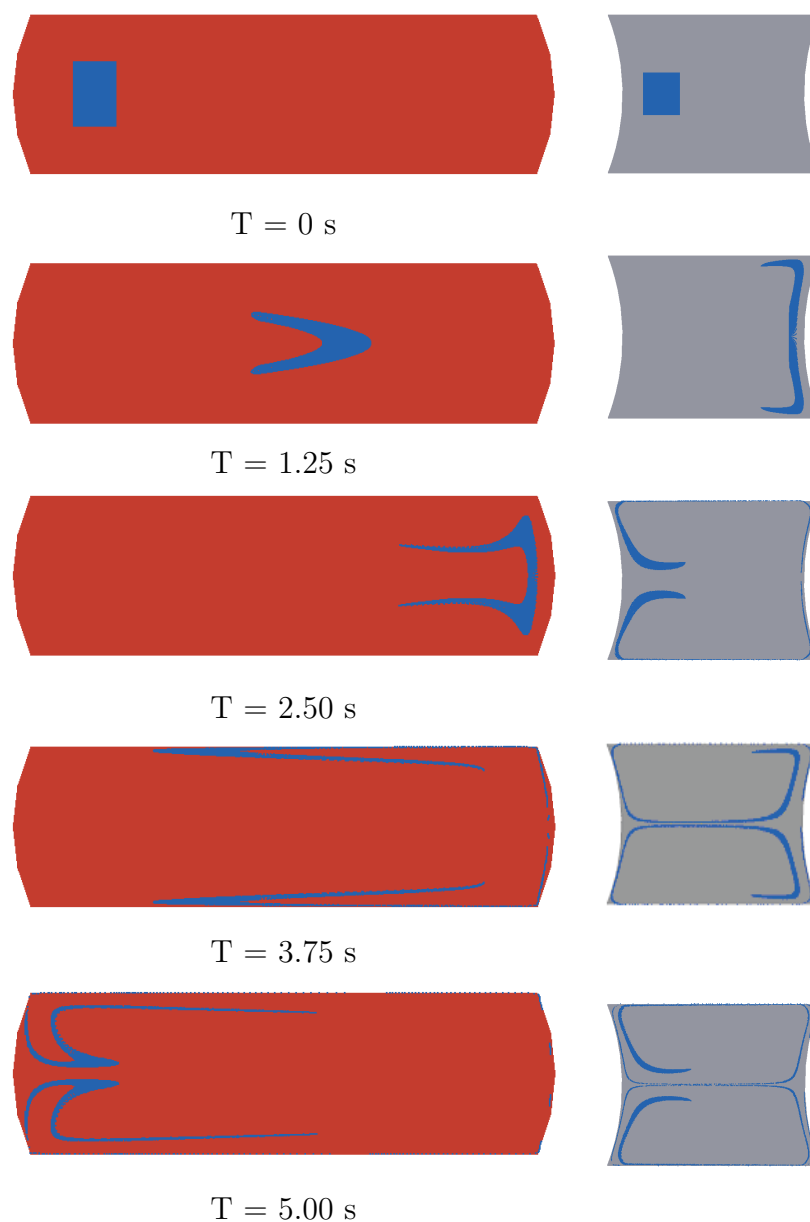


Figure 5.13: Internal circulations by particle tracing in aqueous and organic slugs respectively. ($V_{av} = 5.64 \text{ mm/s}$, $D = 0.75 \text{ mm}$)

reached the front end of the slug with a approximate time of 2.5 s (normalised time, 2.95) for aqueous slug and 1 s for organic slug. Many particle tracing simulations were carried out with different particle blocks for all slugs. The simulations with blocks of height equal to the diameter of the slug clearly show the circulations and the stagnant zone inside the slug. The particles in the stagnant zone remain at the same position while the others move around them due to recirculation. During recirculation some particles tend to remain at the front end of the slug even at finer level of mesh refinement. This seems to depend on the curvature of interface, which is a function of surface tension properties. This information is useful in

the design of a capillary slug flow microreactor in order to induce suitable internal circulations. Thus, the particle tracing provides a quantitatively good prediction of internal circulations inside the liquid slugs.

5.4.4 Two phase modelling

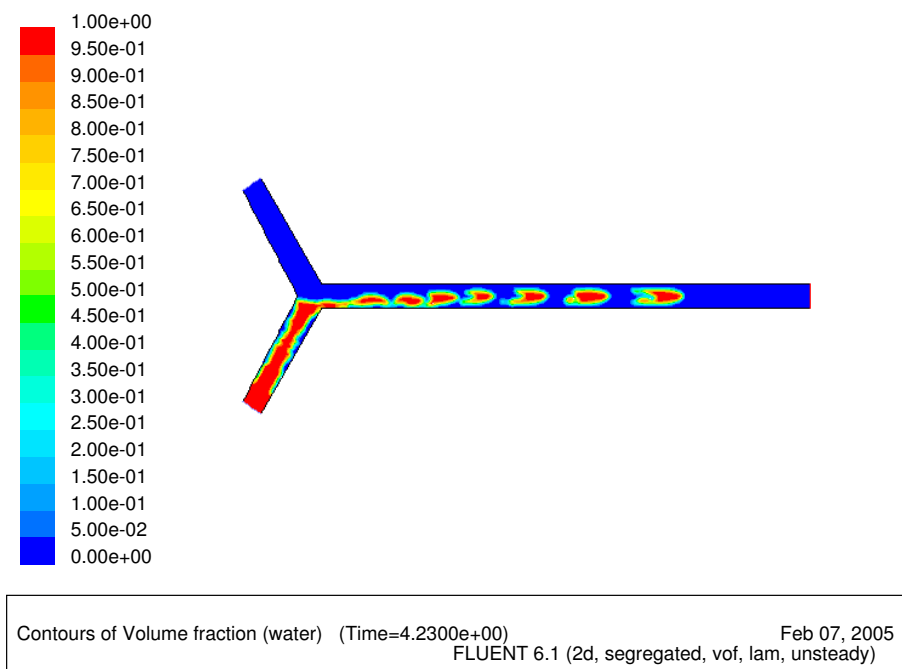


Figure 5.14: Flow simulation without wall adhesion in a microreactor of 1 mm diameter for oil-water system. ($u_1 = 10$ mm/s and $u_2 = 10$ mm/s)

The laboratory experiments were carried out for a cyclohexane-water system as presented in Chapter 2. In the case of gas-liquid pipe flow, the slug flow is generated from stratified flow [96] by natural growth of hydrodynamic instabilities and liquid accumulation is due to instantaneous imbalance between pressure and gravitational forces caused by pipe undulations. In order to generate the slug flow by CFD methodology, the simulations were carried out for the same experimental operating conditions using different immiscible fluid systems. As a first attempt, two sinusoidal inputs were given for two phases in order to understand if the hydrodynamics instabilities are one of the reasons to generate the slug flow. Initially, the simulations were carried out without surface tension and wall adhesion using FEATFLOW. In this case, at low flow velocities, both phases flow as parallel flow with wavy interface. With further increase in the flow velocities of both phases, the waves grow and finally they were as big as a slug. However, it shows deformed

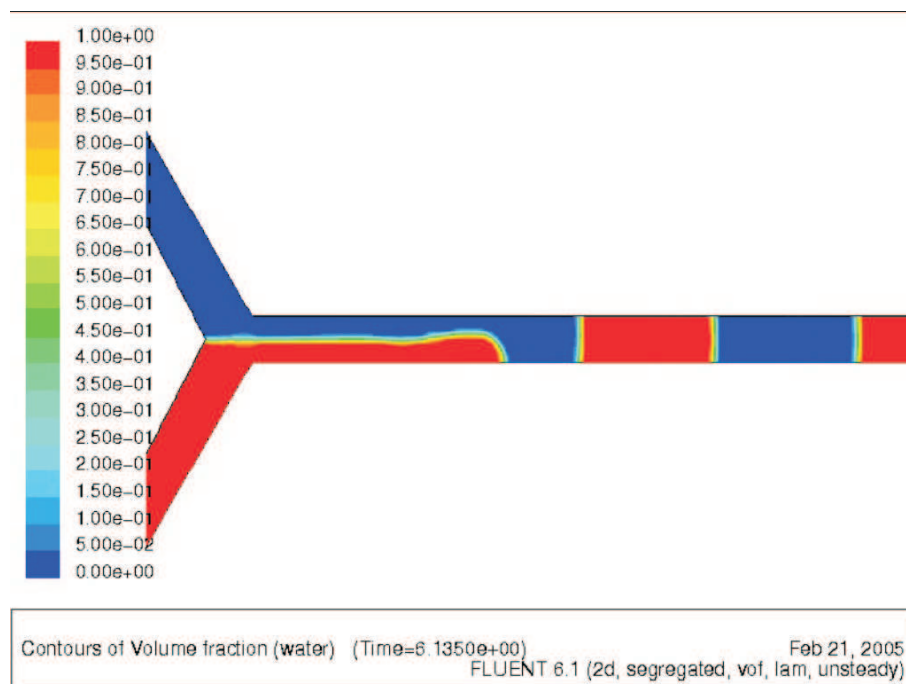


Figure 5.15: Slug flow formation at Y-junction in a capillary microreactor of 1 mm diameter for oil-water system. ($u_1 = 10$ mm/s, $u_2 = 10$ mm/s, $\theta_w = 90^\circ$)

interfaces which was connected to the bottom of other slug. The connecting layer between two slugs was found to be reduced along the length of the capillary. Then the surface tension was implemented and identical flow rates were given and it was observed that the secondary phase flows in the form of deformed drops and there is no interaction with the wall as shown in Figure 5.14.

Further, wall adhesion and surface tension was implemented in FLUENT solver and simulations were carried out. Refer to Gunjal *et al.*[97] for further details of surface tension and wall adhesion. The contact angle was given explicitly from the measured experimental values ($80 - 90^\circ$). The mesh was refined further to a size smaller than $0.001 \times$ slug diameter (capillary diameter). A time step of $1-5 \times 10^{-4}$ s used for simulations and well defined slug flow was observed. The well defined slug flow at inlet velocity of 10 mm/s for each phase is shown in Figure 5.15. As can be seen, the liquid travels through Y-junction as a parallel flow to a certain distance and due to wall adhesion the interface makes an angle with the wall and thus slug formation takes place. The size of the two consecutive slug is same because of equal input flow given at the inlet. Thus, it shows that wall adhesion plays an important role in slug flow generation. Also it was observed that wall adhesion influences the calculation of surface normal.

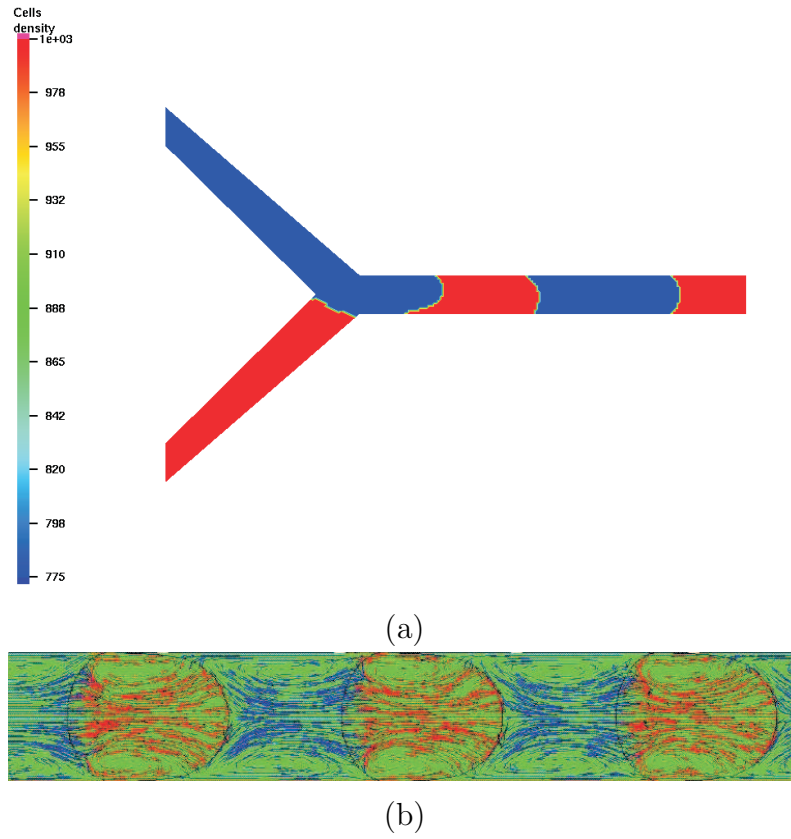


Figure 5.16: Levelset simulations using FEATFLOW: (a) Slug flow generation and (b) internal circulations

In the laboratory experiments, the slug flow was observed over a wide range of two phase flow (0 - 100 ml/h). Similar to this, the well defined slug flow was observed in the simulation with surface tension and wall adhesion for different immiscible fluid systems. Also, the simulations using FEATFLOW without wall adhesion showed qualitatively reliable, yet not perfect, results for slug flow generation. The slug flow generation and internal circulations by level set approach in this case are shown in Figure 5.16. It also shows well defined slug flow. However, both interfaces of a slug are deformed to one side due to the lack of adhesion effect in the FEM solver FEATFLOW. In addition, it also shows the well defined internal circulations within the slugs. This model can be extended for detailed characterisation of slug size, mass transfer and chemical reaction. It is also important to consider three dimensional effect in the slug flow generation. This target can certainly be achieved with more successor works.

5.5 Summary

Internal circulations within the slugs were studied using CFD simulations and the results were qualitatively realised with PIV measurements. A particle tracing algorithm was employed to visualise the flow patterns inside the slug. Further, a free surface CFD model was developed to understand the mechanism of slug flow generation. The PIV experiments show qualitatively reliable circulations at low flow velocities. The simulated results show that the position of the stagnant zone changes with changing flow velocity. At low flow velocities and for slug with sufficient length, the flow has no significant effect on the circulation time inside the slug but with increasing in flow velocity the circulation time decreases. The simulations reveal a slightly but important effect of the presence of a wall film on the circulation patterns and rates. The particle tracing methodology developed yields qualitative and quantitative information about the circulations and stagnant zones. The present two-phase flow methodology showed well defined slug flow which will be useful to study mass transfer and chemical reaction.

Chapter 6

CFD Modelling of Mass Transfer and Chemical Reaction

6.1 Introduction

In the liquid-liquid slug flow capillary microreactor, the phases are present as a series of alternating moving slugs, constituting a series of well-defined individual subvolumes which give an excellent accessibility for modelling. A number of theoretical models have been developed to describe mass transfer with and without chemical reactions between two immiscible liquid phases. However, the theoretical models do not give detailed information about the hydrodynamics involved as it governs the performance of the system. The recent developments in the CFD modelling have attracted chemical engineers for its use in the design of chemical equipment involving mass transfer and chemical reactions. Few CFD models are already developed and some of them are employed for a benchmark problem of modelling mass transfer between drops and continuous phase as listed in Table 6.1. Rieger *et al.* [98] were the first who developed a multi-dimensional two phase CFD model for liquid-liquid extraction using Euler-Euler and Euler-Lagrange approach. Later on, Piarah *et al.* [99] have developed a model for mass transfer between a single drop and an ambient flow to calculate the concentration fields inside and outside the droplet without assumption of turbulent inside the drop. Later on, Yang and Mao [100] have developed a free surface methodology, Level set method, for simulating the interphase mass transfer of single drops in immiscible liquid with resistance in both phases. They compared the results with the reported experimental data and observed good agreement.

Simulations with a simple reaction engineering model for liquid-liquid slug flow were carried out by Dummann *et al.* [4] and it was found that increased flow velocity enhances the mass transfer by inducing more intensive internal circulations within the slugs. Furthermore, a numerical model was developed to describe the internal flow patterns within the fluid segments and the transfer of the dissolved chemical species within and across the segments for liquid-liquid slug flow by Harries *et al.* [36]. The flow was represented by two stagnant, adjacent rectangular units which are linked at both ends to form a continuous loop. The model was validated with various sets of experimental results and showed good prediction of flow field and mass transfer.

In the previous Chapter, free surface methodologies for slug flow generation are presented. However, to solve the complete system for mass transfer with chemical reaction using these methods requires extensive computational resources. Therefore, a model is developed to study the mass transfer with chemical reaction in the liquid-liquid slug flow. Similar type of model has already been developed to study the reaction in the liquid-liquid slug flow by Harries *et al.* [36], however, they have used viscosity ratio equal to 1 while the present model is applicable for all viscosity ratios. The model equations are implemented in FEATFLOW. The objective was to develop a prototype model which can be used for any liquid-liquid system with fixed interface location for mass transfer with and without chemical reaction. The numerical model, its solution and the results obtained are discussed in the following sections. The effects of operating conditions on flow patterns, mass transfer and chemical reaction are presented in detail. Finally, the results were compared with the experimental and numerical results of Harries *et al.* [36].

6.2 Numerical Model

6.2.1 Problem definition

In the present work, unsteady flow behaviour and mass transfer with and without superimposed chemical reaction in slug flow is considered. Since the slug flow is an alternating flow of two immiscible liquid phases, it has two independent flow patterns in a single slug unit: a pair of two consecutive slugs. The following assumptions were considered to be reasonable for studying such a problem:

- Both slugs are comprised of Newtonian, viscous and incompressible fluids
- The shape of the slug and volume remains constant

Table 6.1: Literature review on numerical models for mass transfer with and without chemical reaction in the liquid-liquid two-phase flow

Study	System	Technique	Reference
Liquid-liquid extraction in rotating disk contactors	Residence time distribution using NaCl	A	Rieger <i>et al.</i> [98]
Mass transfer between a drop and an ambient flow	n-butyl acetate - acetone - water	B	Piarah <i>et al.</i> [99]
Mass transfer between drops and other immiscible liquid	Water - succinic acid - n-butanol	C	Yang and Mao [100]
Mass transfer with chemical reaction in segmented (slug) flow	Kerosene (+acetic acid) - water (+NaOH)	B	Harries <i>et al.</i> [36]
Mass transfer with chemical reaction between a drop and an ambient flow	Kerosene (+acetic acid) - water (+NaOH)	B	Pawelski <i>et al.</i> [101]

A: Euler-Euler and Euler-Lagrange

B: CFD modelling with fixed interface

C: CFD modelling, Level set approach

- The flow is laminar and the mass diffusivity is constant in both slugs
- There is no interfacial resistance to mass transfer
- The mass transfer and reaction does not affect the flow patterns within the slugs.

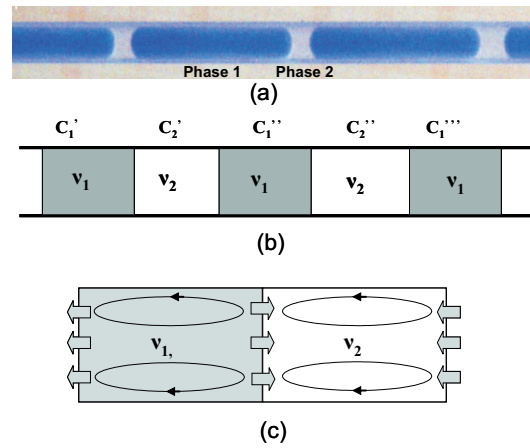


Figure 6.1: Liquid-liquid slug flow (a) Experimental snapshot, (b) schematic representation of the slug flow, and (c) computational domain

An experimental snapshot and the computational domain for this problem are depicted in Figure 6.1. The experimental snapshot shows well-defined slug flow consisting of alternate slugs of the two phases. This flow regime with mass transfer of single species can be schematically represented as shown in Figure 6.1b. Though the experimental snapshot shows that the interface between two slugs is curved, we have considered to be a straight line parallel to y-axis to simplify CFD problem formulation. $C_{A,1}$ and $C_{A,2}$ are the concentrations of species A in phase 1 and 2 having kinematic viscosities of ν_1 and ν_2 , respectively. Each slug has different species concentration depending on the residence time of the slug in the capillary microreactor. Since the microreactor comprises of the slugs of lengths ranging from μm to mm, the residence time difference between two consecutive slugs of one phase can be neglected. Therefore, it is considered that $c_{A,1}'$ is equal to $c_{A,1}''$ which implies that $c_{A,2}'$ and $c_{A,2}''$ are similar i. e. translational symmetry and the problem is reduced to a single slug unit (the pair of two slugs of two phases as shown in the Figure 6.1c) which can reduce the computational effort significantly. As shown in Figure 6.1c, the arrows indicate that each slug exchanges mass and momentum with its two neighbours.

6.2.2 Fluid flow

The computational domain shown in Figure 6.1c was considered as two dimensional. The velocity u and pressure p for this problem were solved by the following Navier-Stokes equation:

$$\nabla \cdot \mathbf{u} = 0 \quad (6.1)$$

$$\frac{\partial(\rho\mathbf{u})}{\partial t} + \rho\mathbf{u} \cdot \nabla\mathbf{u} - \nabla \cdot \mu (\nabla\mathbf{u} + [\nabla\mathbf{u}]^T) + \nabla p = f \quad \Omega \in \mathbb{R}^2 \times [0, T] \quad (6.2)$$

where ρ and μ are the density and dynamic viscosity respectively which are defined as follows:

$$\begin{aligned} \rho &= \rho_0 f(x, y) \\ \mu &= \mu_0 f(x, y) \end{aligned} \quad (6.3)$$

Two densities and viscosities were defined to represent the two phases in the same domain. However, there is an interface between the two slugs where the transport across it is due to diffusion only. This was represented by the concept of moving boundaries and the x-component of the velocity of interface containing cells was set to average slug flow velocity. In addition to this, there is a need to connect the two sides of the domain like a strip of paper wrapped around in a continuous loop. The connection was implemented using the concept of periodic boundary and interface boundary conditions were applied at this connection which is referred as the interface. Thus, the interface and periodically connected interface satisfies the following condition for momentum:

$$\mu_1 \frac{\partial u_1}{\partial \mathbf{n}_1} = \mu_2 \frac{\partial u_2}{\partial \mathbf{n}_2} \quad (6.4)$$

where μ_i , u_i and \mathbf{n}_i are the dynamic viscosities, velocities and unit normal to the interface in the i^{th} domain, respectively. Since the interface is parallel to the y-axis, the above equation can be written as follows:

$$\mu_1 \frac{\partial u_1}{\partial x} = \mu_2 \frac{\partial u_2}{\partial x} \quad (6.5)$$

6.2.3 Mass transfer

The transfer of species within the two phases is governed by the general convection-diffusion equations:

$$\frac{\partial C_{11}}{\partial t} + \mathbf{u}_1 \cdot \nabla C_{11} = D_{11} \Delta C_{11} \quad (6.6)$$

$$\frac{\partial C_{12}}{\partial t} + \mathbf{u}_2 \cdot \nabla C_{12} = D_{12} \Delta C_{12} \quad (6.7)$$

where C_{11} and C_{12} are the concentration of species 1 in phase 1 and 2, respectively. The natural boundary conditions were defined at the interface to satisfy the flux continuity at the interface by the following relation:

$$D_{11} \frac{\partial C_{11}}{\partial x} = D_{12} \frac{\partial C_{12}}{\partial x} \quad (6.8)$$

$$C_{12} = m C_{11} \quad (6.9)$$

where D_{11} and D_{12} are the diffusivities of species 1 in phase 1 and 2 respectively. In the above formulation, the species will transfer from the higher concentration to lower until equal concentration in both phases is achieved i.e. distribution coefficient (m) equal to 1. However, this is not always true and therefore the discontinuity was treated as given in Yang and Mao [100], who rendered the concentration field continuous across the interface by making following transformations:

$$\hat{C}_{11} = C_{11} \sqrt{m} \quad (6.10)$$

$$\hat{C}_{12} = C_{12} / \sqrt{m} \quad (6.11)$$

The concentration condition at the interface is:

$$\hat{C}_{11} = \hat{C}_{12} \quad (6.12)$$

Therefore, at the interface, the diffusion coefficients D_{11} and D_{12} are locally replaced by D_{11}/\sqrt{m} and $D_{12}\sqrt{m}$ to satisfy the original mass flux continuity. The interfacial boundary condition (Equation 6.8) becomes:

$$D_{11}/\sqrt{m} \frac{\partial \hat{C}_{11}}{\partial x} = D_{12}\sqrt{m} \frac{\partial \hat{C}_{12}}{\partial x} \quad (6.13)$$

Thus, the final equations for the species transport for two phases can be written as:

$$\frac{\partial \hat{C}_{11}}{\partial(\sqrt{m}t)} + \frac{1}{\sqrt{m}} \mathbf{u} \cdot \nabla \hat{C}_{11} = \frac{1}{\sqrt{m}} \nabla \cdot (D \nabla \hat{C}_{11}) \quad (6.14)$$

$$\frac{\partial \hat{C}_{12}}{\partial(\frac{1}{\sqrt{m}}t)} + \sqrt{m} \mathbf{u} \cdot \nabla \hat{C}_{12} = \sqrt{m} \nabla \cdot (D \nabla \hat{C}_{12}) \quad (6.15)$$

In general, the species transport equation takes the form of momentum equation given below:

$$\frac{\partial \hat{C}}{\partial t} + \mathbf{u} \cdot \nabla \hat{C} = \nabla \cdot (\hat{D} \nabla \hat{C}) \quad (6.16)$$

6.2.4 Chemical reaction

The chemical reaction in CFD formulation is represented as a source or sink term in the convection-diffusion equation depending on the kinetics of the reaction. So, in general, the convection-diffusion-reaction equation can be written as follows:

$$\frac{\partial C_{ik}}{\partial t} + \mathbf{u} \cdot \nabla C_{ik} = \nabla \cdot (D_{ik} \nabla C_{ik}) \pm r_{ik} \quad (6.17)$$

where, C_{ik} , D_{ik} and r_{ik} are the concentration, diffusivity and rate of reaction of i^{th} component in k^{th} phase.

The above equation is the generalised form of the equation 6.6 and 6.7 with additional reaction term. When the reaction takes place in just one of the phases, one or more species from non-reactive phase are transferred by diffusion to the reaction phase where the reaction takes place. This reaction creates the concentration gradient across the interface and enhances the rate of species transfer. As with mass transfer, it is physically possible that a entire species or more than the amount of species required for the reaction can pass into the other phase. This problem can be solved by carrying out the transformation discussed in the above mass transfer section.

6.2.5 Numerical mesh, boundary conditions and solution

The equations are first discretised using first order accurate, implicit Backward Euler (BE) scheme for time, which belongs to the *one – step – θ – scheme*, while a finite element (FEM) approach was used for spatial discretisation of the governing equations. The details of both discretisations are provided in Turek [90] and Ouazzi [102]. The set of resulting formulations are implemented in FEATFLOW.

For all simulations, the slug unit was kept stationary and the walls were moved with the average slug flow velocity and therefore the velocity of interface containing cells was set to zero. A no-slip boundary condition was implemented at the moving walls. The natural boundary conditions at the interface describes the transfer of momentum and species by diffusion across it according to the Equation 6.5 and 6.8, respectively. Similar boundary conditions were implemented to the periodically connected interface. For species transport, the Neumann type boundary condition (zero species flux) was implemented to the moving walls as shown in the following:

$$\hat{D} \nabla \hat{C} \cdot \mathbf{n} = 0 \quad (6.18)$$

For the reaction, the boundary conditions are similar to those used for mass transfer alone but it is important to identify the reactive phase. It varies from system to system and is discussed in detail with an example in the model validation section.

The FEATFLOW package gives the freedom to use two different approaches namely, a coupled approach and a projection approach to treat the discretised nonlinear system. The coupled approach solves for velocity and pressure simultaneously, providing the best stability behaviour, but requires greater numerical efforts, while the projection solver decouples velocity and pressure, reduces the problem to the solution of a sequence of scalar problems [90] and is well-suited for non-stationary configurations. So, in this study, the projected solver was deemed more suitable to simulate the flow field. The equations for mass transfer were solved using the projected solver in a manner similar to the momentum equations. The simulation were carried out in a transient manner i.e. first the steady state velocity and pressure profiles were established and then they were employed into mass transfer calculations.

The physical properties such as viscosities, densities and diffusivities are defined using Heaviside function, $H_\varepsilon(x)$ similar to Yang and Mao [100] as follows:

$$H_\varepsilon(x, y) = \begin{cases} 1, & \text{when } x \leq \mathbf{X} \\ 0, & \text{when } x > \mathbf{X} \end{cases} \quad (6.19)$$

where \mathbf{X} is the position of the interface. Using above function, the equation for any physical property, ϕ of the k^{th} phase, can be written as:

$$\phi = \phi_2 + (\phi_1 - \phi_2)H_\varepsilon(x, y) \quad (6.20)$$

However, in the case of partition coefficient (m), the gradients instead of values were scaled and thus the three terms in convection-diffusion Equation 6.16 can be written as:

$$\frac{\partial \hat{C}}{\partial t} = \frac{\partial \hat{C}_{12}}{\partial \left(\frac{1}{\sqrt{m}}t\right)} + \left(\frac{\partial \hat{C}_{11}}{\partial (\sqrt{m}t)} - \frac{\partial \hat{C}_{12}}{\partial \left(\frac{1}{\sqrt{m}}t\right)} \right) H_\varepsilon(x, y) \quad (6.21)$$

$$\mathbf{u} \cdot \nabla \hat{C} = \sqrt{m}u_2 \cdot \nabla \hat{C} + \left(\frac{1}{\sqrt{m}}u_1 \cdot \nabla \hat{C} - \sqrt{m}u_2 \cdot \nabla \hat{C} \right) H_\varepsilon(x, y) \quad (6.22)$$

$$\begin{aligned} \nabla \cdot (\hat{D} \nabla \hat{C}) &= \sqrt{m} \nabla \cdot (D_{12} \nabla \hat{C}) \\ &+ \left(\frac{1}{\sqrt{m}} \nabla \cdot (D_{11} \nabla \hat{C}) - \sqrt{m} \nabla \cdot (D_{12} \nabla \hat{C}) \right) H_\varepsilon(x, y) \end{aligned} \quad (6.23)$$

As we know, in most of the cases, more than one species participates in the chemical reaction, each additional species requires an appropriate convection-diffusion equation. In the present work, the convection-diffusion-reaction equations were solved using straight-forward operator splitting strategy described in [103] i.e. first of all scalar quantities are transported without taking the source/sinks into account. The convection-diffusion equations of each species are processed in parallel and the updated concentrations were used as initial data for a system of reaction ODEs, which describes the accumulation and consumption of a particular species. Thus, for the reaction calculation the generalised Equation 6.17 was splitted as:

$$\frac{\partial \hat{C}_{ik}}{\partial t} + \mathbf{u} \cdot \nabla \hat{C}_{ik} - \nabla \cdot (\hat{D}_{ik} \nabla \hat{C}_{ik}) = 0 \quad (6.24)$$

$$\frac{\partial \hat{C}_{ik}}{\partial t} = r_{ik} \quad (6.25)$$

It is important to note that the operator splitting strategy was applied locally in time, i.e. within each time step, $\Delta t_n = t_{n+1} - t_n$. The equidistant time stepping was used for all simulations and was refined for the mass transfer and reaction calculations. Since the multigrid solver was used for the simulations, the time step has to be refined with the level of mesh refinement. In most of the simulations a time step of 1×10^{-3} s was used for velocity, pressure and mass transfer with and without reaction calculations upto a mesh size of $0.03 \times$ slug diameter. However, with increased level of refinement, the time step for velocity and pressure was not reduced below 1×10^{-4} s while it was reduced by a factor of 2 with each level of refinement for mass transfer calculations. In order to maintain the positivity of the species concentration a conventional flux correction technique, upwinding, was applied.

The simulations with various parameters were carried out on a Sun-Fire-880 computer system with a 900 MHz Sparcv9 processor. The simulation time was noted for each operating condition and it was observed that the first part of simulations, hydrodynamic simulations took a very short time of several minutes, the mass transfer simulations took few hours while the reactions simulations took several hours to get the solutions for a mesh independent level of refinement.

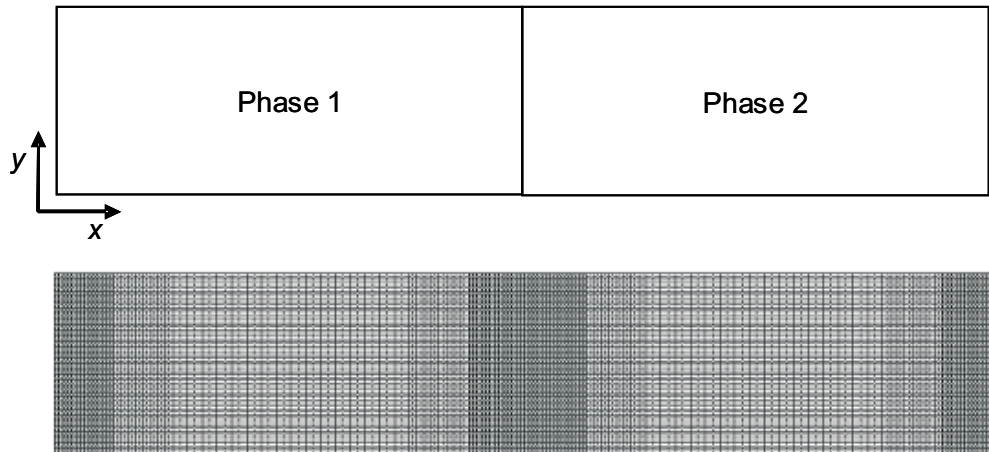


Figure 6.2: Computational domain and mesh, showing more refined mesh in the vicinity of the interface and periodically connected interface

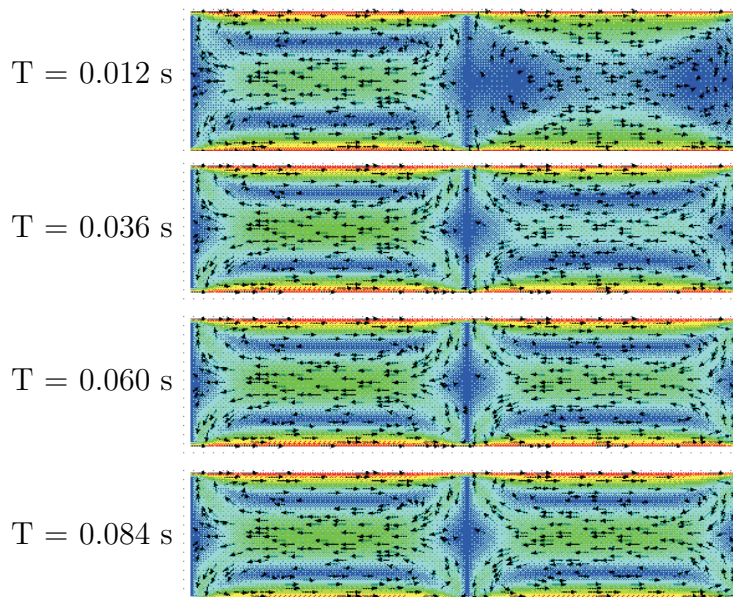


Figure 6.3: Flow development for different viscosities in a slug unit (Left slug kinematic viscosity = $0.3 \times 10^{-5} \text{ m}^2/\text{s}$ and right slug kinematic viscosity = $0.3 \times 10^{-3} \text{ m}^2/\text{s}$)

6.3 Results and Discussion

6.3.1 Fluid flow

Several simulations with different geometries and operating conditions and various viscosity combinations were carried out to study the flow behaviour within the slugs. The typical computational domain and its mesh, with more refinement near the

interface and periodically connected interface in order to capture the sharp gradients of the variables, especially species concentration, is shown in the Figure 6.2. The negative velocity was defined at the wall while the slug was kept stationary. Figure 6.3 shows a simulated snapshot of the velocity profiles in both slugs for a slug with 2 mm length and 0.5 mm width.

It was observed that a high viscosity fluid takes more time to achieve steady-state compared to a low viscosity fluid. Slug 1 contains the fluid with a kinematic viscosity of $0.3 \times 10^{-5} \text{ m}^2/\text{s}$ while slug 2 contains a fluid with $0.3 \times 10^{-3} \text{ m}^2/\text{s}$. The velocity vector plot shows that slug 1 has achieved steady state within a short time of around 0.012 s while slug 2 has taken 0.084 s at an average slug flow velocity of 0.01 m/s, which is typical capillary flow velocity. However, it is still not fully developed pressure field and pressure takes long time to achieve steady-state as compared to velocity.

Similar to single phase simulations, the steady-state velocity profile achieved shows a maximum velocity at the centre line and minimum velocity at the wall, with a fully developed parabolic (Poiseuille) profile. Two flow patterns were observed within each slug: a recirculation zone at the centre and in the interface proximity and two stagnant zones in between them. Though the slug ends show significant effect on flow patterns, the present work was restricted to flat interfaces.

6.3.2 Mass transfer

For mass transfer, the equations were solved in transient manner as discussed in the above section. Many simulations were carried out with different combinations of parameters to study the mass transfer in detail. As a test case, a slug unit with each slug having length of 1 mm with mass transfer of a species from phase 1 to 2 is presented here. The properties given in the Table 6.2 are defined corresponding to the extraction of succinic acid from its aqueous solution with n-butanol. The species is transported due to diffusion across the interface and keeps on recirculating due to internal circulations that arise. These circulations keep on renewing the interfacial concentration at the interface and increases the concentration gradient between two slugs which enhances the rate of mass transfer.

Before calculating the actual variables/parameters, several simulations were carried out to make the solution grid independent. The domain was meshed in different ways: uniform mesh and mesh refined in the vicinity of the interface. In the first case, more computational power was required to solve a problem, while the total number of cells could be reduced in the later case but it was necessary to optimise

Table 6.2: Data used for mass transfer simulations

Flow ratio (aqueous/organic)	1	-
Slug length	1	mm
Slug diameter(D)	0.5	mm
Slug flow velocity	1.41	mm/s
Density ratio (Phase 1/phase 2)	1.25	-
Viscosity ratio (Phase 1/phase 2)	0.27	-
Initial concentration of species in phase 1	0.084	mol/L
Initial concentration of species in phase 1	0	mol/L
Partition coefficient (m)	1.17	-
Smallest cell size	0.008ID	mm
Smallest time step for velocity and pressure	1 x 10 ⁻⁴	s
Smallest time step for mass transfer	1 x 10 ⁻⁵	s

the mesh. For a given number of cells in a domain, the mesh refined in the vicinity of the interfaces performs better and a significant difference in the concentration profiles was observed. Therefore, it was decided to use the refined mesh in the vicinity of the interface for further simulations.

The total concentration of the species in a particular region at each time step was determined by averaging it over the total number of nodes in that region. The volumetric mass transfer coefficient, $k_L a$, of a species, A, diffusing from phase 1 to phase 2 over the time period, t , from 0 to T is calculated as follows:

$$k_L a = \frac{1}{T} \ln \frac{(C_{A2}^* - C_{A2}^0)}{(C_{A2}^* - C_{A2}^T)} \quad (6.26)$$

where C_{A2}^* is the saturation concentration of the species in phase 2. The known specific interface area, a , enables calculation of overall mass transfer coefficient, k_L by the following equation:

$$k_L = \frac{1}{aT} \ln \frac{(C_{A2}^* - C_{A2}^0)}{(C_{A2}^* - C_{A2}^T)} \quad (6.27)$$

where

$$a = \frac{2}{l} \quad (6.28)$$

The total simulation time, which is the residence time of the species in the reactor can be calculated from the length of the capillary, L , and slug flow velocity, V_s .

$$T = \frac{L}{V_s} \quad (6.29)$$

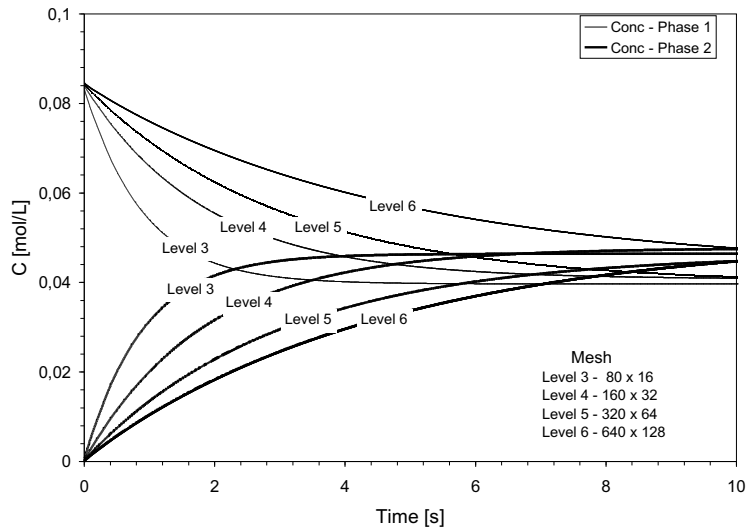


Figure 6.4: Concentration profiles for different levels of refinement

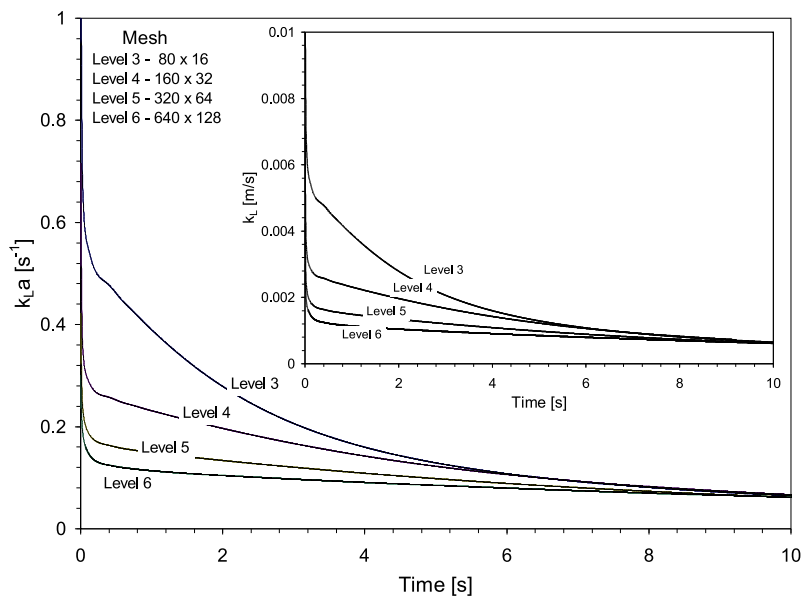


Figure 6.5: Volumetric mass transfer coefficient, $k_{L,a}$ and mass transfer coefficient, k_L for different levels of refinement

Figures 6.4-6.5 show the concentration profiles and mass transfer coefficients with respect to time for different meshes. With increase in the time, the concentration of species in phase 1 decreases while the concentration in the phase 2 increases. The saturation point, where the concentration curve of phase 2 remains constant, exhibit a slight difference for different levels of refinement while the concentration profiles before saturation shows a significant difference. The same effect of the mesh size was observed for mass transfer coefficients.

6.3.3 Chemical reaction (Model validation)

For the chemical reaction, a titration reaction system was chosen and the range of operating parameters was taken from the experimental results of Harries *et al.* [36]. The carried out CFD simulations and the results were compared with their experiments which were carried out in a glass microchannel. In this reaction system the acetic acid present in the kerosene phase is extracted using water where it reacts with the base, NaOH, producing salt and water. The representation of the system is shown in Figure 6.6. The partition behaviour studied experimentally have shown strong partition of acetic acid in favour of the aqueous phase (partition coefficient = 85). The reaction takes place in the aqueous phase and is extremely rapid as given by the following equation:

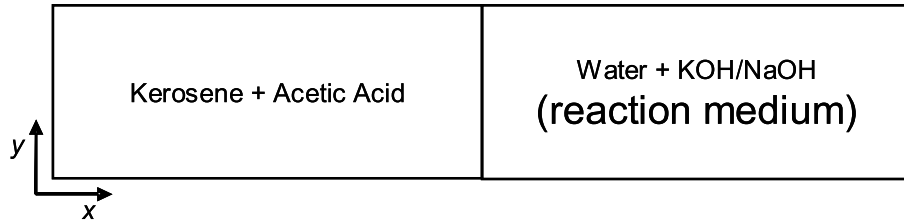
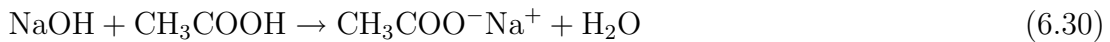


Figure 6.6: Representation of species for reaction



The same system of mass transfer equations need to be extended with additional source or sink term to represent the reaction. The reaction is second order and only takes place in the aqueous phase. The convection-diffusion-reaction equations for the species in the water phase are given as:

$$\frac{\partial C_{12}}{\partial t} + u_2 \cdot \nabla C_{12} = D_{12} \Delta C_{12} - K C_{12} C_{22} \quad (6.31)$$

$$\frac{\partial C_{22}}{\partial t} + u_2 \cdot \nabla C_{22} = D_{22} \Delta C_{22} - K C_{12} C_{22} \quad (6.32)$$

$$\frac{\partial C_{32}}{\partial t} + u_2 \cdot \nabla C_{32} = D_{32} \Delta C_{32} + K C_{12} C_{22} \quad (6.33)$$

$$\frac{\partial C_{42}}{\partial t} + u_2 \cdot \nabla C_{42} = D_{42} \Delta C_{42} + K C_{12} C_{22} \quad (6.34)$$

where C_{12} , C_{22} , C_{32} and C_{42} are the concentrations of CH_3COOH , NaOH , $\text{CH}_3\text{COO}^- \text{Na}^+$ and H_2O in phase 2 (water), respectively. However, as the acetic acid is present in both phases, it is governed by the Equations 6.14-6.15. Since the second reactant (species 2) and products are present in the aqueous phase only, their exclusion from the kerosene phase was restricted by setting diffusion coefficient equal to zero as well as by setting the velocity, u_1 equal to zero in the kerosene slug region. Therefore, species 2, 3 and 4 will not diffuse through the interface and will remain in aqueous phase alone.

The concentrations which were obtained in the solution of convection-diffusion equation were used as initial data for the solution of reaction ODEs, which are usually solved by explicit methods. However, this reaction is extremely rapid with the rate constant of 1.35×10^{11} L/mol.s and therefore, for a given time step it produces very high non-realistic value of the updated concentration of the products C_{32} and C_{42} . This problem could be solved using very small time step, but this is not feasible, because the computational time will increase significantly. Therefore an implicit treatment was employed and the solution of ODE from time t_n to t_{n+1} is updated for reactants and products in the following manner:

$$\begin{aligned} \text{Reactants :} \quad \hat{C}_{i2}^{n+1} &= -K \hat{C}_{12}^{n+1} \hat{C}_{22}^{n+1} \Delta t + \hat{C}_{i2}^n \\ \text{Products :} \quad \hat{C}_{i2}^{n+1} &= K \hat{C}_{12}^{n+1} \hat{C}_{22}^{n+1} \Delta t + \hat{C}_{i2}^n \end{aligned} \quad (6.35)$$

where, C_{i2} is the i^{th} species concentration in water phase and K is the rate constant of the reaction. This equation was solved and corresponding changes in the reactant and products were obtained for each node. Since the interface is represented by a straight line, it reduces the interfacial surface area for mass transfer and therefore an adjustment factor was applied to compensate the titration time i.e. the time required for complete disappearance of the base. The average values of the concentrations over the domains were obtained for mass transfer and titration time at an average concentration of reactant NaOH , C_{22} equals 5 % was used to compensate the titration time difference due to flat interface [36].

As mentioned in the earlier sections, the simulations were carried out in a transient manner for the operating conditions shown in Table 6.3. The steady-state velocity profiles were established and then species transport calculations were done.

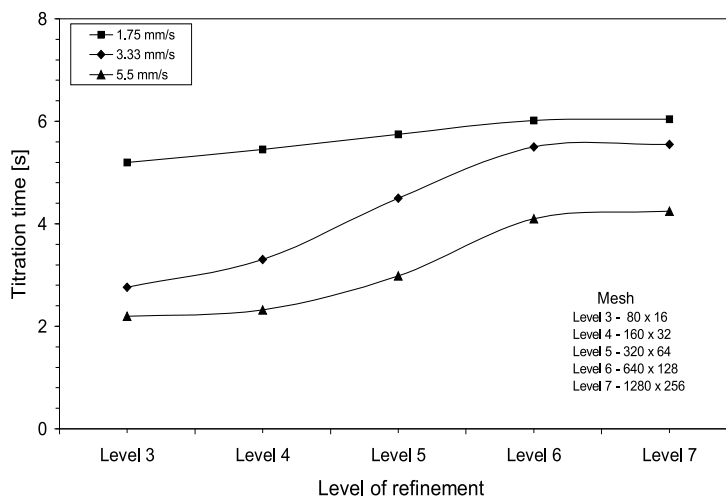


Figure 6.7: Variation of titration time with respect to levels of refinement

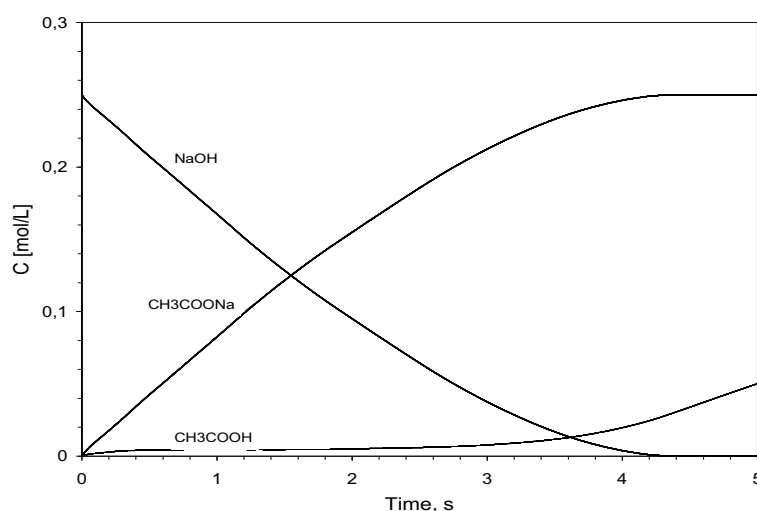
Initially, the simulations were carried out in order to confirm the solution grid independence by doing simulations for various refinement levels. Figure 6.7 shows how the titration time behaved with respect to the levels of refinement. In this case, the simulations were started at a relatively coarse mesh and were refined until the titration time difference between two consecutive levels becomes negligible. For this geometry, the coarse mesh was of size $0.25 \times$ slug diameter and the mesh independent solution was obtained for level 6, which is equal to $0.008 \times$ slug diameter.

Table 6.3: Data used for model validation

Flow ratio (aqueous/organic)	1	-
Slug length range	1.5 - 3.81	mm
Slug diameter	0.38	mm
Slug flow velocity range	0.6 - 16.6	mm/s
Density ratio (kerosene/water)	0.8	-
Viscosity ratio (kerosene/water)	1.82	-
Initial concentration of CH_3COOH in kerosene	0.5	mol/L
Initial concentration of CH_3COOH in water	0	mol/L
Initial concentration of NaOH in water	0.25	mol/L
Initial concentration of CH_3COONa in water	0	-
Partition coefficient for CH_3COOH (m)	85	-
Smallest cell size	0.008ID	mm
Smallest time step for velocity and pressure	1×10^{-4}	s
Time step for mass transfer and chemical reaction	1×10^{-5}	s

Table 6.4: Mesh size and time steps used for model validation

Level	Mesh size	Δt , u and p[s]	Δt , reaction[s]
Coarse	20×4		
2	40×8	1×10^{-3}	1×10^{-3}
3	80×16	1×10^{-3}	1×10^{-3}
4	160×32	1×10^{-3}	1×10^{-4}
5	320×64	1×10^{-3}	0.5×10^{-4}
6	640×128	0.5×10^{-3}	1×10^{-5}
7	1280×256	1×10^{-4}	1×10^{-5}

**Figure 6.8:** A typical plot of average concentrations of three species in water slug (slug length = 1.7 mm, slug flow velocity = 5.5 mm/s)

A typical plot of concentration profiles of two reactants, CH_3COOH and NaOH and a product, CH_3COONa in the aqueous phase for a slug with length 1.7 mm and flow velocity of 5.5 mm/s is shown in Figure 6.8. It shows that the concentration of CH_3COOH is very low in the aqueous phase which means that as it diffuses through the interface it reacts with the NaOH . Therefore the concentration of NaOH is decreases with time while the concentration of the product increases. When the entire NaOH in the water slug is consumed at time 4.15 s, the amount of CH_3COOH increases in the water slug due to its excess stoichiometric proportion. The same behaviour revealed from the simulation snapshots of concentration profiles of different species in both phases for a slug with length of 1.9 mm and flow velocity of 3.33 mm/s with time shown in Figures 6.9 to 6.11.

The simulated results are compared with experimental and numerical results (from the correlations) of Harries *et al.* [36]. The results show very good agreement

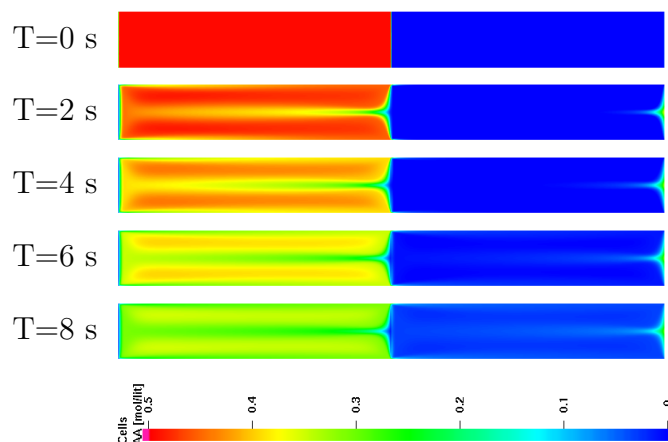


Figure 6.9: Snapshots of concentration profile of acetic acid (slug length = 1.9 mm, slug flow velocity = 3.33 mm/s)

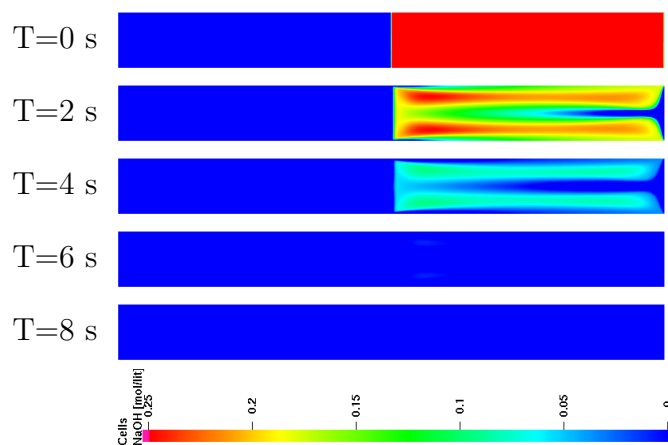


Figure 6.10: Snapshots of concentration profile of NaOH (slug length = 1.9 mm, slug flow velocity = 3.33 mm/s)

with both sets of values as shown in Figure 6.12. At high and intermediate flow velocities, it shows very good agreement while at low velocity it slightly overpredicts the results. The discrepancy in the experimental and simulation results (of Harries *et al.* and present model) is due to several possible reasons. One of them could be the assumption of flat interface which has strong effect on the velocity profile. The other may be the presence of a wall film in the microreactor used by Harries *et al.* [36]. In our laboratory experiments with PTFE capillary tube, it was demonstrated that, due to the superior wetting properties of the organic liquid phase on PTFE, an organic wall film is present.

The model showed improvement in comparison with the literature results for titration time as well the computational time requirement. In future studies, the model will be extended in order to incorporate free surface hydrodynamics. For curved

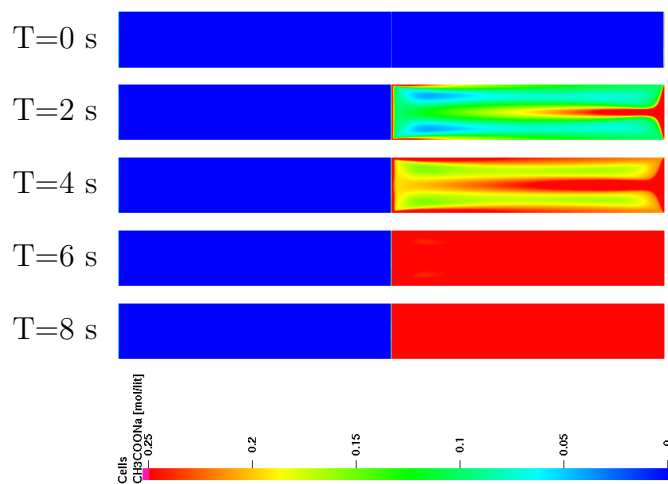


Figure 6.11: Snapshots of concentration profile of CH_3COONa (slug length = 1.9 mm, slug flow velocity = 3.33 mm/s)

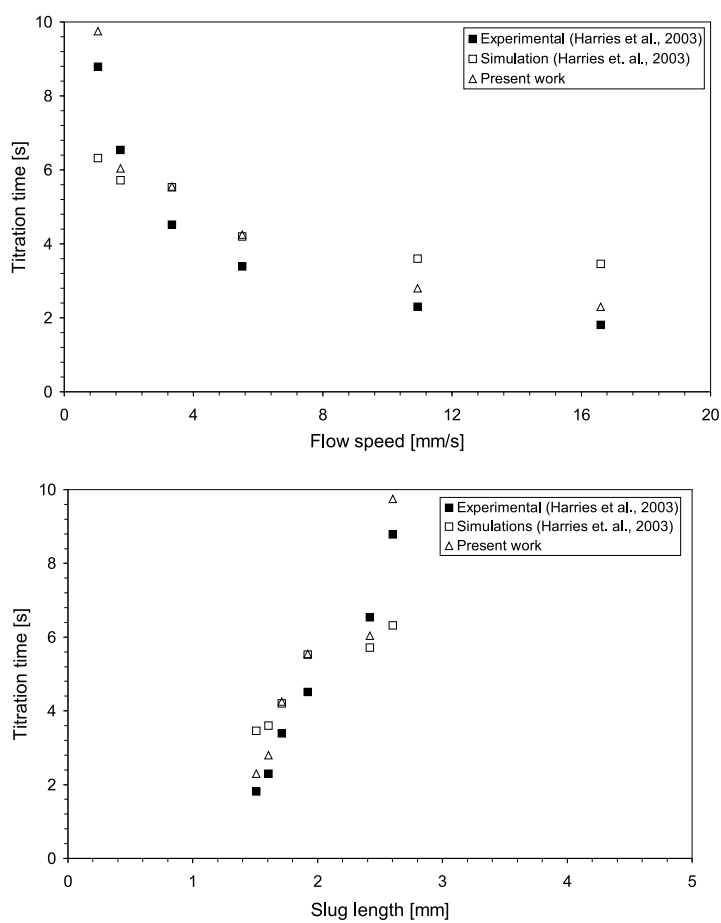


Figure 6.12: Plots of titration time vs flow speed and titration time vs slug length, respectively

interface, secondary circulatory flow generation takes place in the vicinity of the interface, which has significant effect on the hydrodynamics and thus on underlying mass transfer. In this case, a free surface simulation without mass transfer should be carried out first. The steady-state velocity profile obtained should then be incorporated into the present model. As mentioned above, the phenomenon of the organic wall film should also be included.

6.4 Summary

A CFD model was developed to simulate the mass transfer with and without chemical reaction for the liquid-liquid slug flow capillary microreactor. Several simulations were carried out to elucidate the fluid flow and mass transfer behaviour. Finally, the model was validated with a published example of titration reaction and it was observed that the experimental and simulated results presented in the literature are in very good agreement with it. This model can be applied for any liquid-liquid system with fixed interfacial location.

Chapter 7

Conclusions and Future Developments

7.1 Conclusions

The fluid dynamics, mass transfer and reaction characteristics of liquid-liquid slug flow capillary microreactors have been investigated in order to develop a new device for liquid-liquid extraction with and without chemical reaction. The characteristic feature of alternate liquid-liquid flow in capillaries is that it has an ability to couple two individual transport mechanisms: convection due to internal circulations in each individual slug and diffusion between two consecutive slugs. The active surface because of internal circulations within the slugs and well-defined very high interfacial area enhance the mass transfer. This concept differs from the conventional liquid-liquid contacting equipment in which the dispersed phase exists in the form of suspended drops in the continuous phase or a film of one phase is created on a moving or stationary surface by gravity or centrifugal forces. The interfacial area in these equipment is often poorly defined due to the complex hydrodynamics involved and the intensity of mass transfer is limited by the constraints imposed by the underlying buoyancy or gravitational effects being exploited.

The present work undertakes experimentation and modelling of liquid-liquid slug flow in capillary microreactors. It is demonstrated that liquid-liquid microextractor-reactor offers superior performance and greater efficiency in comparison to conventional equipment as it requires low power input, provides high interfacial area and gives high mass transfer rates. In addition, it has an ability to tune mass transfer contributions precisely, to impose temperature profiles easily and to monitor the

progress of extraction and reaction together with the excellent accessibility for process modelling. Thus liquid-liquid slug flow in capillaries is a powerful laboratory technique for elucidating extraction and biphasic reactions.

The individual topic can be concluded as follows:

Hydrodynamics: Experiments were carried out to investigate the extent of slug flow regime, to measure slug size and pressure drop, and to characterise the internal circulations. Further, a simplified theory was employed to investigate the pressure drop along the length of the capillary. Finally, CFD methodologies were developed to characterise the internal circulations within the slugs and to generate the slug flow.

The capillary and Y-junction dimensions showed a significant effect on slug size and thus interfacial area, which increases with decreasing dimensions. The pressure drop measured across the Y-junction and along the length of slug flow capillary showed increased value with increase in the volumetric flow rate and decrease in the capillary diameter. Theoretical predictions for pressure drop without a wall film along the length of the capillary based on the capillary pressure and hydrodynamic pressure drop showed discrepancies with experimental results and underlying reasons were identified. The presence of an organic wall film was one of the reasons and an improved model taking it into consideration showed good agreement with the experimental values. The power input which was calculated using the pressure losses over the mixing element showed that slug flow capillary microreactor is superior to conventional equipment as it provides very high interfacial area with less power. Also the PIV experiments showed qualitatively reliable circulations at low flow velocities.

The single phase simulation results depicted that the position of the stagnant zone within the slug changes with flow velocity. At low flow velocities and for slugs with sufficient length, the flow has no significant effect on the circulations but with increase in flow velocity the circulation time decreases. The simulations revealed a slightly but important effect of the presence of a wall film on the circulation patterns and intensity of slugs. This information is very useful to design mixing in the slug. The particle tracing algorithm employed yielded qualitative and quantitative information about the circulations and stagnant zones.

Mass transfer and chemical reaction: Experiments were carried out to investigate the mass transfer rates for different non-reacting systems. Further, a reaction system, neutralisation reaction, was chosen to study the mass transfer with chemical reaction in order to investigate the time scale required to complete the reaction.

To demonstrate the presence of a wall film, a reacting system was used to measure the interfacial area by chemical method. Finally, a CFD model comprising of Navier-Stokes equation with spatially resolved viscosities and densities and species transport equations for involved species was developed.

The mass transfer rates obtained were compared with conventional contactors and it was observed that such liquid-liquid microextractor-reactors offer superior performance and greater efficiency in comparison to conventional equipments. The surface renewal due to internal circulations and very large specific interfacial areas, in comparison with other contactors, enhanced the mass transfer rates. A CFD model developed to simulate the mass transfer with and without chemical reaction showed good agreement with the published example of titration reaction. This model is very useful for *a priori* predictions of mass transfer rates in the liquid-liquid slug flow capillary microreactor. It can also be applied for any liquid-liquid system with fixed interfacial location.

Flow splitting: To separate the two phases in order to investigate the precise mass transfer rates, a flow splitter based on wetting affinities of liquids with solid materials was developed and various systems with different combinations of non-viscous and viscous liquids were tested. From the different configurations of flow splitters it was observed that the splitting element with one steel and one Teflon outlet performs better even for unequal flow rates under slug flow regime. Better performance, easy fabrication and cheap material of construction (steel and Teflon) of the flow splitter facilitates its manufacturing in huge numbers for cascading as well as for numbering-up the reactors.

7.2 Open Questions

In the hydrodynamics study presented in Chapter 2, it was observed that with increase in the flow velocity, slug size decreases which in turn increases the interfacial area available for mass transfer. Different systems were studied and it was observed that the slug size depends on the physical properties of the system as well as on the interaction of capillary wall and liquids. In this case, the open question is how to correlate the slug size with physical properties of liquids and capillary wall. This model/correlation will directly give the interfacial area and thus *a priori* mass transfer rates.

A simplified pressure drop model developed for water-cyclohexane slug flow system

revealed that cyclohexane forms an organic wall film with PTFE capillary material. Similar results were observed in the investigation of interfacial area by chemical method presented in Chapter 3. However, in the latter case it showed transitional behaviour - no film at low flow velocity and a film with increased flow velocity. In the presence of a wall film, the whole enclosed slug takes part in the mass transfer providing higher interfacial area compared to the case of no film. Also it showed low pressure drop along the length of the capillary which means that presence of wall film is an advantage. Therefore the research should be directed on developing the understanding of wettability properties of the capillary materials and liquids. The properties should be tuned in such a way that one of the liquids should form a wall film.

In the flow splitting experiments it was observed that the flow splitter developed shows good separation with negligible contamination for equal flow rates. However, for unequal flow rates it showed more contamination which can be reduced by using flow splitters in series. It is arduous task to carry out experiments for each solid-liquid combination and therefore there is a need to develop a free surface CFD model - similar to the model developed for slug flow generation.

The internal circulations by simplified CFD simulations in Chapter 5 showed that intensity of internal circulations increases with increase in the flow velocity. The PIV experiments also showed qualitatively reliable circulations as the liquid within the slug circulates due to shearing action between the slug axis and continuous phase. However, due to the limitations of the experimental set-up, it was not possible to characterise the internal circulations quantitatively which is important in order to validate the CFD model and to study mixing in the slug.

Free surface 2D simulations showed well defined slug flow using commercial as well as in-house developed software. This model should be extended for 3D simulations in order to study the dimensional effect on slug flow generation. Finally, the results obtained from 2D and 3D simulations should be compared with experimental values. Also, the CFD model for mass transfer with and without chemical reaction showed very good agreement with experimental results. However, as discussed earlier, in the slug flow reactor an organic wall film was observed which should be taken into account. Also the model should be coupled with free surface models, in order to capture the complex hydrodynamics in the vicinity of the interface.

The above discussion shows some open questions in the characterisation of hydrodynamics and mass transfer. In addition, there are some recommendations on application front which are discussed in the following section.

7.3 Future Developments

Polymerisation reaction: The demand of polymeric materials is ever increasing because the higher strength polymers and composite materials are replacing the metals in automobiles, aircrafts and many other products. Some of the polymeric products are speciality chemicals which are manufactured in low volume with high product quality and are frequently used as copolymers. This is usually done in a batch reactor with the aim of manufacturing product with acceptable quality apart from a safe and economic operation. In this case, it is important to have precise tuning of the parameters in order to get the desired product. Microreactor is a powerful equipment to carry out such processes.

Liquid-liquid slug flow can be used for suspension polymerisation as it uses two immiscible liquids in which the monomer is initially dispersed in the continuous aqueous phase by the combined action of surface-active agents. The monomer and initiator(s) reside in the organic or oil phase. It is commonly used for producing a wide variety of commercially important polymers such as polystyrene and its copolymers (poly-vinyl chloride, poly-methyl methacrylate, poly-vinyl acetate). A commonly used equipment for suspension polymerisation is agitated stirred tank. The agitation intensity and the properties of the suspending agent determine the sizes of the dispersed monomer drops. The polymerisation occurs in the monomer droplets which become more sticky and viscous as conversion proceeds. Finally they are transformed into rigid, spherical polymer particles of size 50-500 μm [104] and the properties of the final particles depend on those of the initial drops which can be precisely tuned in the microreactors.

Industrial systems of kilogram scale production: There are several pharmaceutical and speciality chemicals which are manufactured in the range of kilogram per hour or even less than that. Conventionally, the chemicals are being manufactured using batch or semi-batch processes. A detailed review on the pharmaceutical processes, Roberge *et al.* [9], mentions that 50 % of the fine chemicals/pharmaceutical processes could be benefited from microreactor technology.

Now a days, some microreactor plants are being used for commercial production. One of the best examples is the production of nitroglycerine using a microreactor plant in the range of 15 kg/h [2] which is used as a drug for acute cardiac infraction. The process uses sulfuric and nitric acid, both highly concentrated fuming liquids, which are being handled well using microreactors. The high surface to volume ratio ensures an immediate transfer of heat released by the reaction. Thus, higher yield, better product quality, increased safety and reduction of environmental hazards are

the main advantages of using microstructured reactors.

The present work shows that liquid-liquid slug flow is far superior than conventional contactors. This work can be extended for the extractive processes which use batch processes to produce kilogram scale chemicals in the industry. Therefore the future work should be devoted to identify such processes and to make them continuous using microreactors.

Counter-current extraction: Multistage operations are common in liquid-liquid extraction for large scale production and effective use of chemicals. Depending upon the selectivity of the solvent and the amount of mass transfer required to achieve the desired solute recovery, several stages of extraction may be required. In this case, counter-current contact is the most efficient extraction method as it conserves the mass transfer driving force and therefore gives optimal performance. Most of the countercurrent operations in the laboratory practice uses batch processes which are carried out using milliliter amount of feed and solvent in the flasks. Using the microreactors these processes can be made continuous. The important issue in making it continuous is the online separation of liquid phases which is possible using flow splitters developed in the present work.

An illustration of two-stage countercurrent extraction is shown in Figure 7.1. The feed is fed from the reservoir 1 to the first stage with the help of high precision piston pump, 3. In the first stage, the feed is contacted with solvent rich phase coming from second stage which was fed from the reservoir 2 using pump, 6. In the first stage, the two phases form the slug flow and later they are separated with the help of flow splitter, 11. The solvent lean phase is passed to second stage while the solvent rich (extract) is taken out in the sampling bottle, 13. The solvent lean phase again contacts with fresh solvent in the capillary microreactor, 10 and is further splitted with the help of flow splitter, 12. The solvent lean (raffinate) phase is taken out after second stage in the sampling bottle, 14. Thus, two-stage counter-current extraction can be achieved.

Numbering-up: For large scale production, scale-up of microreactors is very important to achieve throughput in the range of industrial scale. Microreactor technology achieves this target with numbering-up instead of scale-up - reduces the problems associated with scale-up. There are two key issues in numbering-up of microreactors: to achieve uniform distribution of flow in all channels and to separate the phases immediately after the mass transfer. Uniform distribution of flow in all channels is very important as it decides the processing of the chemicals being used

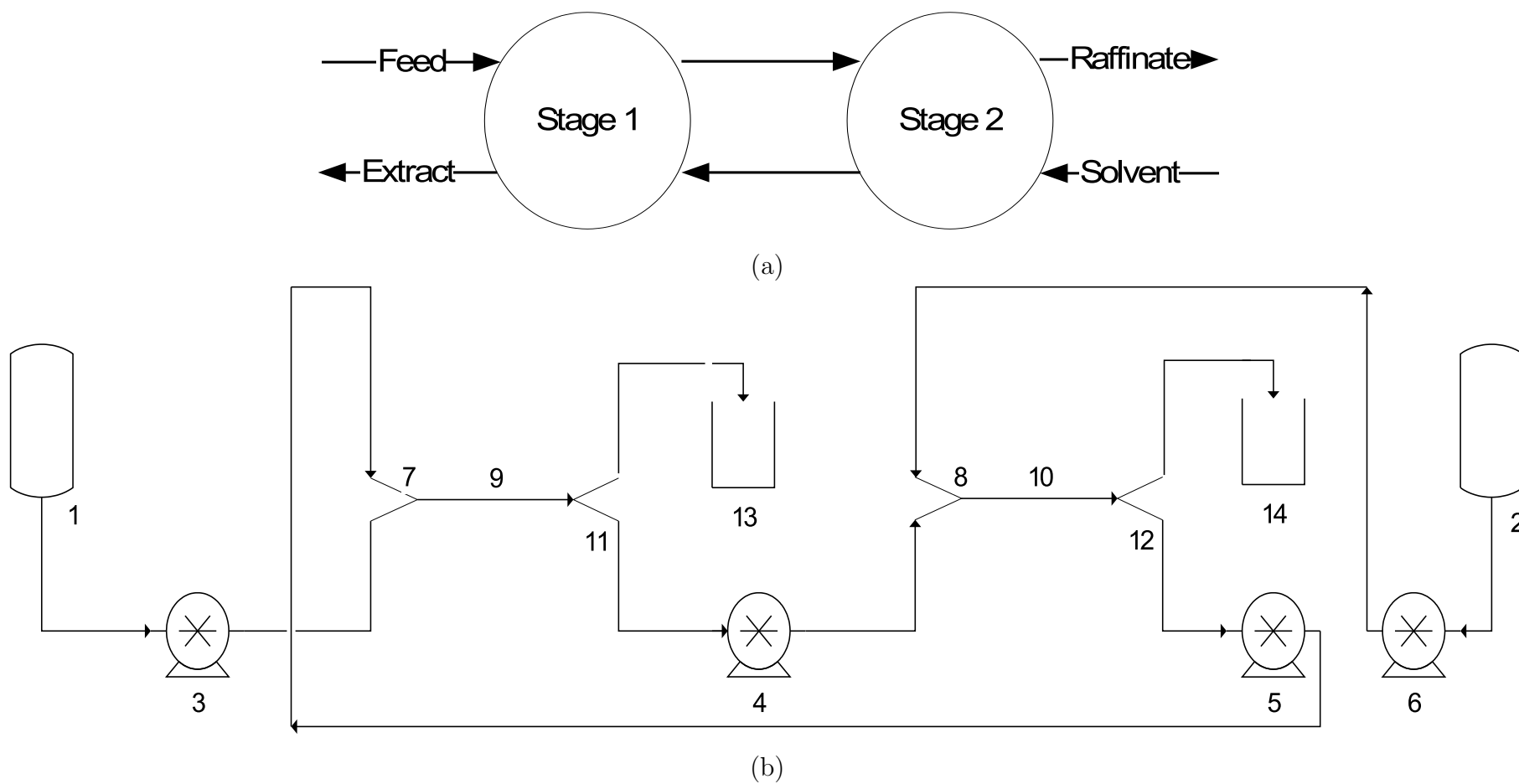


Figure 7.1: Two stage counter-current extraction: (a) Block diagram and (b) flow sheet: (1,2) reservoirs containing aqueous and organic liquids; (3,4,5,6) pumps; (7 and 8) Y-junction mixing element; (9,10) slug-flow capillary microreactors; (11,12) flow splitting elements and (13, 14) sampling bottles

in the process. This can be done by simply numbering-up the the same unit used in the present work. However, the cost associated with the set-up increases linearly which is not feasible due to high cost of the precision pumps. The alternative for this is to use a single distributor for all channels similar to those used for monolith reactors. IMM, Germany [69], have developed a single (liquid) phase flow splitting unit to split the liquids into different channels. Such distributors can be employed to distribute the liquid uniformly in all channels.

The Figure 7.2 shows an approach for numbering-up of liquid-liquid slug flow reactor for large scale production. Two liquids are fed to the six reactors arranged in parallel using two liquid distributors. Finally, the extract and raffinate from both splitters are collected in tanks 10 and 11.

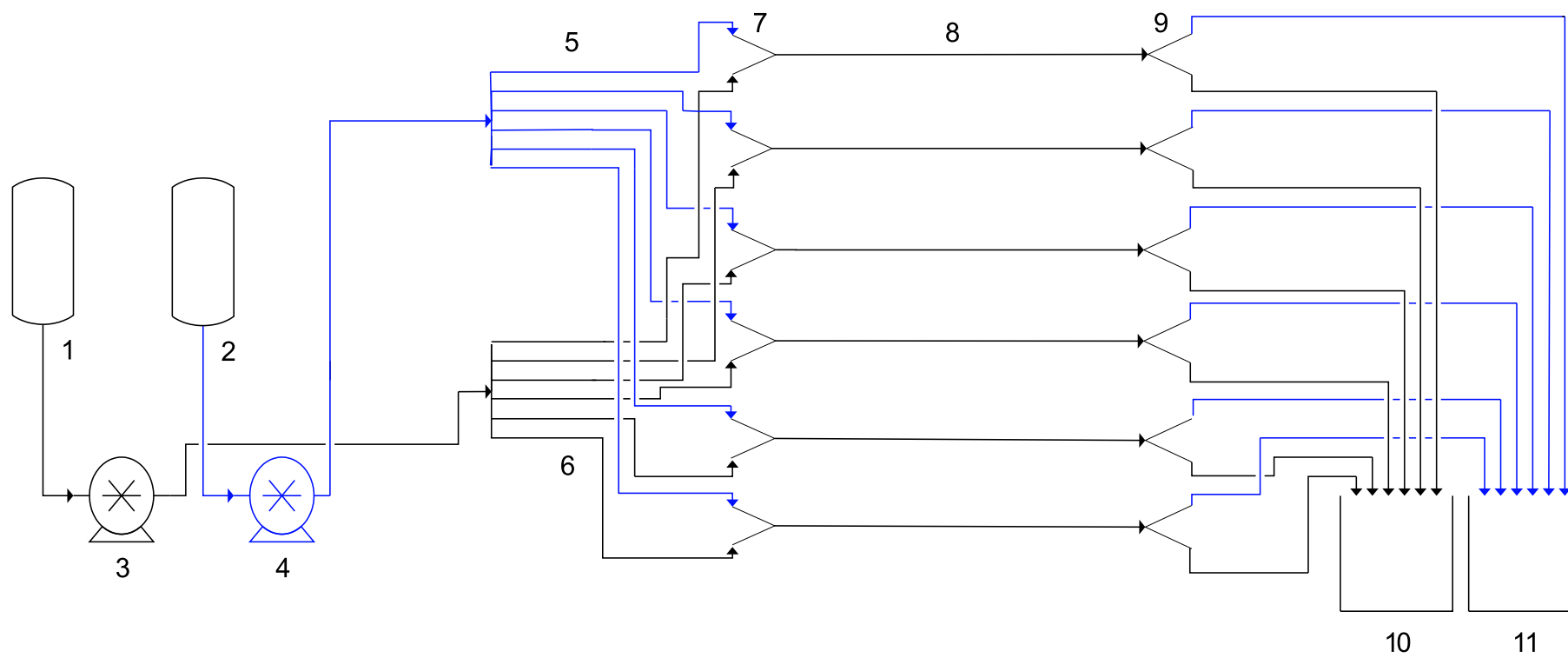


Figure 7.2: Schematic of numbering-up of liquid-liquid slug flow capillary microreactor

Appendices

Appendix A

Pressure Drop Models

A.1 Pressure Drop - Without Film

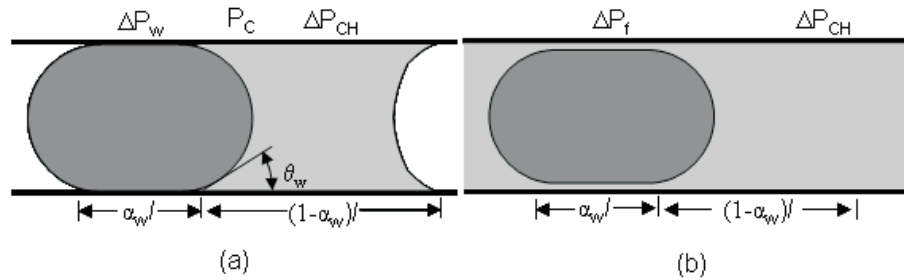


Figure A.1: Pressure drop along single slug unit. (a) without film and (b) with film

If we consider a single flow unit as shown in Figure A.1a, the overall pressure drop per length can be written as:

$$\begin{aligned}
 \Delta P_U &= \Delta P_H + P_C \\
 &= \Delta P_W + \Delta P_{CH} + P_C
 \end{aligned}
 \tag{A.1}$$

The hydrodynamic pressure drop can be calculated from the Hagen-Poiseuille equation, while the capillary pressure is obtained from the Young-Laplace equation for

a cylindrical tube [7] given by the following equations:

$$\begin{aligned}\Delta P_W &= \frac{8\mu_W V \alpha_W l_U}{r^2}; \\ \Delta P_{CH} &= \frac{8\mu_{CH} V (1 - \alpha_W) l_U}{r^2} \\ P_C &= \frac{2\gamma}{r} \cos \theta_w \\ \text{where, } V &= \frac{Q_W + Q_{CH}}{A}\end{aligned}\tag{A.2}$$

Assuming a constant dynamic contact angle and slug lengths with equal number of slugs of water and cyclohexane under similar operating conditions and neglecting end effects, the equation for pressure drop across the length of the capillary becomes:

$$\Delta P = \frac{L}{l_U} (\Delta P_W + \Delta P_{CH}) + \frac{2L - l_U}{l_U} P_C\tag{A.3}$$

A.2 Pressure Drop - With Film

Since the organic liquid has affinity towards the PTFE material, it was cyclohexane to form the wall film and water flows in the form of enclosed slugs. In this situation, the pressure drop in the film region is far higher compared to slugless flow (only cyclohexane flow). This is due to the constant velocity profile in the slug region (zero velocity gradient) and no-slip condition at the wall i.e. high velocity gradient in the film region. Therefore, for theoretical predictions, it is considered that the pressure drop along the length of the capillary is due to this region only.

The model for single phase flow through a pipe is very well established and the velocity distribution for laminar flow in a pipe is given by the following equations [105]:

$$V(r) = -\frac{\Delta P}{4\mu L} [R_c^2 - r^2]\tag{A.4}$$

Charles, 1963 [34] developed a model for pressure drop in the pipeline flow of capsules in the laminar flow regime assuming the pressure drop in the capsule flow is due to film region only. According to above equation, the velocity distribution in the film region, velocity at the film slug interface, slug velocity (V_s) and the velocity profile

in the slug region can be written as:

$$\begin{aligned}
 \text{Film region:} \quad V(r) &= -\frac{\Delta P}{4\mu L} [R_c^2 - r^2] \quad \text{for } R_s < r < R_c \\
 \text{Slug flow velocity:} \quad V_s &= -\frac{\Delta P}{4\mu L} [R_c^2 - R_s^2] \quad \text{for } r = R_s \\
 \text{Slug region:} \quad V(r) &= V_s \quad \text{for } 0 < r < R_s
 \end{aligned} \tag{A.5}$$

Equation A.5 gives velocity profile along the different regions such as film region, interface and slug region as shown in Figure A.2. It is represented as ADEC. Now, the volumetric flow rate in the film region can be obtained by integrating the velocity profile equation for the film region;

$$\begin{aligned}
 Q_f &= -\frac{\pi \Delta P}{8\mu L} [R_c^2 - r^2]^2 \\
 &= \frac{\pi}{2} V_s [R_c^2 - r^2]
 \end{aligned} \tag{A.6}$$

And the volumetric throughput of the slug region is;

$$Q_s = \pi R_s^2 V_s \tag{A.7}$$

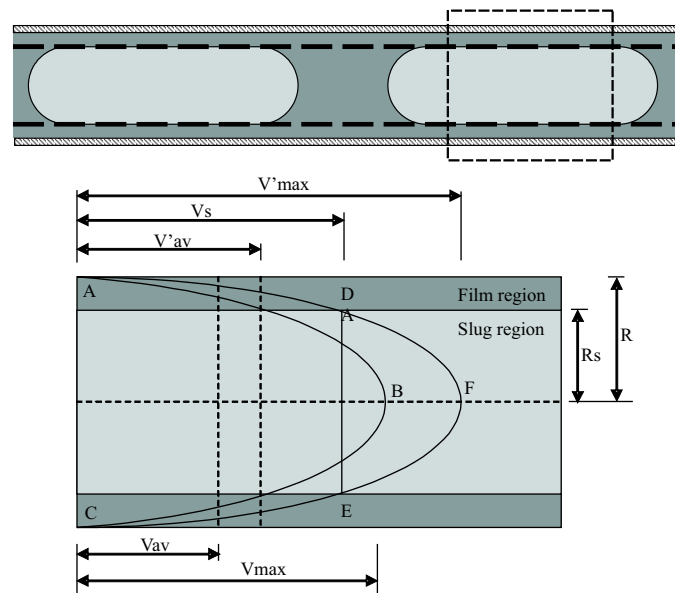


Figure A.2: Velocity profiles for capsule (slug) flow in a pipe given by Charles , 1963 [34]

The average flow velocity can be obtained by dividing the total volumetric flow rate by cross section area. Thus, from equation A.6 and A.7, the relation between

average flow velocity and slug flow velocity can be written as:

$$\begin{aligned}
 V_{av} &= \frac{Q_f + Q_s}{\pi R_c^2} \\
 &= \frac{R_c^2 + R_s^2}{2R_c^2} V_s \\
 \text{or} \\
 V_s &= \frac{2}{1 + (R_s/R_c)^2} V_{av} \quad \text{where } 0 \leq (R_s/R_c) \leq 1
 \end{aligned} \tag{A.8}$$

The relation, $0 \leq (R_s/R_c) \leq 1$, shows that the slug flow velocity is always greater than the average flow velocity.

Later, Charles (1963) has mentioned that the Reynolds number to be applied to the fluid flowing in the annular region is not based on V_{av} , but on V'_{av} which is the hypothetical average velocity of the profile ADFEC as shown in Figure A.2. So it is important to have relation between V'_{av} and V_{av} .

Similar to above equation for volumetric flow rates, the volumetric flow rate for the hypothetical average velocity profile ADFEC is given by:

$$Q_{ADFEC} = -\frac{\pi \Delta P}{8\mu L} R_c^4 \tag{A.9}$$

Therefore, the average flow velocity and slug flow velocity are given by:

$$\begin{aligned}
 V'_{av} &= \frac{Q_{ADFEC}}{\pi R_c^2} \\
 &= \frac{R^2}{2(R_c^2 - R_s^2)} V_s \\
 \text{or} \\
 V_s &= 2V'_{av}[1 - (R_s/R_c)^2] \quad \text{where } 0 \leq (R_s/R_c) \leq 1 \\
 &= V'_{max}[1 - (R_s/R_c)^2]
 \end{aligned} \tag{A.10}$$

From Equation A.8 and A.10, the relation between V_{av} and V'_{av} can be written as:

$$\begin{aligned}
 V'_{av} &= \left(\frac{1}{1 - k^4} \right) V_{av} \\
 \text{where, } k &= \frac{R - h}{R}
 \end{aligned} \tag{A.11}$$

In laminar flow the pressure gradient is proportional to the average flow velocity. Therefore, replacing the average velocities by respective pressure gradients in the above equation A.11, the equation for water-cyclohexane slug flow system can be written as:

$$\left(\frac{\Delta P}{L}\right)_f = \left(\frac{1}{1-k^4}\right) \left(\frac{\Delta P}{L}\right)_{CH} \quad (\text{A.12})$$

However, in the predictions of Charles [34], it was assumed that the capsules follow each other sufficiently close for the fluid between the capsules to be considered as part of the capsule stream. In the present case of liquid-liquid slug flow this assumption is usually not valid and will only apply when the water slugs have lengths several times greater than the cyclohexane slugs. The slug which forms the film may, however, be longer depending on the inlet flow ratio for both phases. It is therefore necessary to consider the phase fraction of both the liquids to calculate the pressure drop for a given length of the liquid-liquid slug flow capillary microreactor. In addition, the film thickness is very small compared to the radius of slug, which justifies the assumption that the length of the film region for a given length of capillary is nothing more than the water phase fraction times the total length. The pressure drop along the film region in the given pipe length can thus be written as:

$$\left(\frac{\Delta P}{\alpha_W L}\right)_f = \left(\frac{1}{1-k^4}\right) \left(\frac{\Delta P}{\alpha_W L}\right)_{CH} \quad (\text{A.13})$$

According to Hagen-Poiseuille equation, the single phase pressure drop per unit length is same for all lengths, i.e.

$$\left(\frac{\Delta P}{\alpha_W L}\right)_{CH} = \left(\frac{\Delta P}{L}\right)_{CH} \quad (\text{A.14})$$

Therefore, the Equation A.13 becomes:

$$\frac{\Delta P}{L} = \left(\frac{\alpha_W}{1-k^4}\right) \left(\frac{\Delta P}{L}\right)_{CH} \quad (\text{A.15})$$

To calculate the pressure drop using the above equation, the film thickness is crucial. It can be estimated using Bretherton's law, as a function of capillary number, given by the following equation [67].

$$\begin{aligned} h &= 1.34RCa^{2/3} \\ &= 1.34R \left(\frac{\mu_{CH} V_s}{\gamma}\right)^{2/3} \end{aligned} \quad (\text{A.16})$$

In the definition of capillary number the velocity used is called as velocity of film deposition and is considered as the velocity of the slug, which is slightly greater than the average flow velocity (see Equation A.8). Substituting h from Equation A.13 in A.16 and V_s from Equation A.8, the Equation A.16 will yield a non-linear equation which can be solved iteratively.

Appendix B

Theory of Extraction Efficiency and Mass Transfer Coefficients

B.1 Physical Mass Transfer:

Two parameters, extraction efficiency and mass transfer coefficient, can be used to compare the performance of the contactor. The extraction efficiency is the ratio of the amount of material transferred to the maximum amount transferable. For a solute transferring from one phase to another, the extraction efficiency can be written as follows:

$$E = \frac{C_{A2}^{out} - C_{A2}^{in}}{C_{A2}^* - C_{A2}^{in}} \quad (\text{B.1})$$

The mass transfer coefficient is a characteristic parameter of a system (contactor and species) used to evaluate the performance of contactors. The rate of mass transfer of species A from one phase to another, can be written as:

$$\frac{\partial C_{A2}}{\partial t} = k_L a (C_{A2}^* - C_{A2}) \quad (\text{B.2})$$

Upon integration equation B.2 in the time limit 0 to T and concentration limit from inlet to outlet, the residence time of the phases in the capillary, the above equation for volumetric mass transfer coefficient, $k_L a$, becomes:

$$k_L a = \frac{1}{T} \ln \left(\frac{C_{A2}^* - C_{A2}^{in}}{C_{A2}^* - C_{A2}^{out}} \right) \quad (\text{B.3})$$

With well-defined specific interface area, a , in a liquid-liquid slug flow capillary microreactor enables the precise calculation of the overall mass transfer coefficient,

k_L by the following equation:

$$k_L = \frac{1}{aT} \ln \left(\frac{C_{A2}^* - C_{A2}^{in}}{C_{A2}^* - C_{A2}^{out}} \right) \quad (\text{B.4})$$

B.2 Mass Transfer with Chemical Reaction:

A simple, rapid, acid-base reaction, titration reaction, was studied as it is a rapid reaction and its progress is controlled by the diffusion of the reactants within the slugs [35] i.e. mass transfer limited. In this case, acetic acid diffuses from kerosene into aqueous phase according to following reaction:



The mass transfer rate for rapid reaction can be investigated from the mass transfer equation B.2. Here, the rate of acetic acid transfer from kerosene to water depends on the concentration difference of acetic acid between two consecutive slugs as given by;

$$\frac{\partial C_{A1}}{\partial t} = k_L a (C_{A1} - C_{A2}) \quad (\text{B.6})$$

The reaction is rapid and as acetic acid diffuses through the interface into the aqueous phase it reacts with NaOH. Here the acetic acid is present in excess and therefore, the concentration differential between two slugs can be written as:

$$C_{A1} - C_{A2} \cong C_{A1} \quad (\text{B.7})$$

Therefore, the equation for mass transfer rates can be written as follows:

$$\frac{\partial C_{A1}}{\partial t} = k_L a C_{A1} \quad (\text{B.8})$$

Upon integration, above equation in the time limit 0 to T , the time to neutralise the base completely, and corresponding concentrations of solute A in phase 1, the above equation for volumetric mass transfer coefficient, $k_L a$, becomes:

$$k_L a = -\frac{1}{T} \ln \left(\frac{C_{A1}^{out}}{C_{A1}^{in}} \right) \quad (\text{B.9})$$

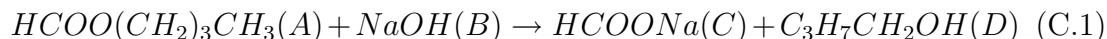
Appendix C

Theory of Chemical Method for Effective Interfacial Area

The extensive research on investigation of interfacial area by chemical method has developed the theory very well. It uses instantaneous heterogeneous reaction and there are limited chemical reacting systems which fulfill following requirements of chemical method [58]:

- The reaction is so fast that the reactant diffusing from the organic to the aqueous phase does not reach the bulk of the aqueous phase and reacts at the interface
- The solubility of the reactant present in the organic phase must be very low in the aqueous phase, so mass transfer limitations in the organic phase can be neglected
- The concentration of the reactant in the aqueous phase (bulk and interface) can be presumed constant during the process and therefore pseudo-first order reaction is assumed

Alkaline hydrolysis of ester can be used to determine both mass transfer coefficient and interfacial area of liquid-liquid contactors. Initially, this method was used by Puranik and Sharma [63] in a liquid-liquid contactor. Later on, Verma and Sharma [106], Sarkar *et al.* [107] and Dehkordi [52] used this method for packed columns, mechanically agitated columns and air driven impinging streams contactor, respectively. This method uses following theory:



In this case component A diffuses from a first phase into a second phase where it reacts with component B in the same phase with pseudo-first-order reaction mechanism. Nanda and Sharma [57] have given the characteristics of the selected system as follows:

- The solubility of the solute in the solvent phase should be preferably less than 10^{-4} gmol/cm³
- The first order or pseudo-first order rate constant should be of the order 1 to 300 s⁻¹, when the liquid side mass transfer coefficient varies from about 10^{-3} to 2×10^{-2} cm/s
- The analysis of the amount of solute reacted should be relatively simple

The volumetric extraction rate of component A, $R_A a$, can be defined using Danckwerts model by the following relation [108]:

$$R_A a = a C_{A2}^* (D_{A2} K_2 C_{B2} + K_L^2)^{0.5} \quad (\text{C.2})$$

The criteria for pseudo-first-order reaction is given by:

$$\left[1 + \frac{D_{A2} K_2 C_{B2}}{K_L^2} \right]^{0.5} \ll 1 + \frac{C_{B2} D_{B2}}{C_{A2}^* D_{A2}} \quad (\text{C.3})$$

Here, the extraction rate $R_A a$ and C_{A2}^* in the Equation C.2 are known, therefore the same equation can be used to analyse experimental data which can be arranged in following way:

$$(R_A a / C_{A2}^*)^2 = D_{A2} K_2 a^2 C_{B2} + (K_L a)^2 \quad (\text{C.4})$$

From Equation C.4, it is clear that a plot of $(R_A a / C_{A2}^*)^2$ vs C_{B2} known as Danckwerts plot should yield a straight line with a slope of $D_{A2} K_2 a^2$ and an intercept of $(K_L a)^2$. Thus, the equation for interfacial area can be written as:

$$a = \sqrt{\frac{\text{Slope}}{D_{A2} K_2}} \quad (\text{C.5})$$

Since the solubility of NBF in the aqueous NaOH solution differs from its solubility in water, the saturation concentration has to be obtained for the different concentrated solutions used. However, because of the irreversible reaction, the solubility can not be easily measured and has to be estimated. For this case, the solubility of NBF in

concentrated electrolyte solutions is estimated using the salting-out parameter, Ks , described by van Woezik and Westerterp [109]:

$$\log \left(\frac{C_{A2}^*}{C_{A2}} \right) = -KsI \quad (\text{C.6})$$

where, $Ks = i_+ + i_- + i_{ester}$ and the value of i_{ester} was obtained from the solubility data of NBF in an aqueous solution of sodium chloride as recommended by several authors (e.g. [57], [58], [59], [107], [110]). We have taken Ks as 0.1793 L/mol as given by van Woezik and Westerterp [109].

Appendix D

Physico-chemical Properties

Table D.1: Physical properties of the liquids used to study flow regime, slug size and pressure drop (Chapter 2)

Liquid	ρ [kg/m ³]	μ [kg/m·s]	σ [N/m]
Water	1000	0.001	-
Cyclohexane	780	0.000982	0.05

Table D.2: Physical properties of the liquids used (Chapter 3)

Liquid	ρ [kg/m ³]	μ [kg/m·s]	σ [N/m]
Water	1000	0.001	-
n-butanol	780	0.003	0.05 (with water)
Kerosene	810	0.0022	0.05 (with water)
NBF	894	0.0063	0.0091 (with water)
NaOH (0.2 M)	1007	0.0063	0.00919 (with NBF)
NaOH (0.3 M)	1012	0.0063	0.00924 (with NBF)
NaOH (0.4 M)	1016	0.0063	0.00928 (with NBF)

Table D.3: Physico-chemical properties of the liquids used to investigate the interfacial area by chemical method (Temperature = 25°C)(Chapter 3)

System	Ionic strength [mol/L]	Solubility [mol/L]	$D_{A,2}$ [m ² /s]	K_2 [L/mol·s]
NBF - water	0	0.075	0.88×10^{-9}	-
NBF - NaOH (0.2 M)	0.2	0.069	0.85×10^{-9}	23.6
NBF - NaOH (0.3 M)	0.3	0.066	0.83×10^{-9}	24.6
NBF - NaOH (0.4 M)	0.4	0.064	0.81×10^{-9}	25.6

Table D.4: Physical properties of liquids used to study flow splitting (Chapter 4)

Aqueous	Organic	ρ_{aq} [kg/m ³]	ρ_{or} [kg/m ³]	μ_{aq} [kg/m·s]	μ_{or} [kg/m·s]	σ [N/m]
Water	Cyclohexane	999	780	0.00089	0.000982	0.05
Water	n-butyl acetate	999	882	0.00089	0.00073	0.009
Water	Kerosene	999	810	0.00089	0.022	0.05
Water	n-butanol	999	780	0.00089	0.003	0.05
Water	NBF	999	894	0.00089	0.0063	0.0091
NaOH (0.2 M)	NBF	1007	894	0.00105	0.0063	0.00919
NaOH (0.3 M)	NBF	1012	894	0.00113	0.0063	0.00924
NaOH (0.4 M)	NBF	1016	894	0.00122	0.0063	0.00928

Bibliography

- [1] A. Stankiewicz and J. A. Moulijn. Process intensification. *Industrial and Engineering Chemistry Research*, 41:1920–1924, 2002.
- [2] *Institut für Mikrotechnik Mainz (IMM), Germany*, <http://www.imm-mainz.de/>.
- [3] W. Ehrfeld, V. Hessel, and H. Löwe. Microreactors. *Wiley-VCH Verlag GmbH, Weinheim, Germany*, 2000.
- [4] G. Dummann, U. Quittmann, L. Gröschel, D. W. Agar, O. Wörz, and K. Morgenschweis. The capillary-microreactor: a new reactor concept for the intensification of heat and mass transfer in liquid-liquid reactions. *Catalysis Today*, 79-80:433–439, 2003.
- [5] T. Iwasaki, N. Kawano, and J. Yoshida. Radical polymerization using microflow system: Numbering-up of microreactors and continuous operation. *Organic Process Research & Development A*, 10:1126–1131, 2006.
- [6] M. A. Northrup, B. Benett, D. Hadley, P. Landre, S. Lehew, J. Richards, and P. Stratton. A miniature analytical instrument for nucleic acids based on micromachined silicon reaction chambers. *Analytical Chemistry*, 70:918–922, 1998.
- [7] C. Ramshaw. Process intensification and green chemistry. *Green Chemistry*, 1:G15–G17, 1999.
- [8] K. F. Jensen. Microreaction engineering - is small better? *Chemical Engineering Science*, 56:293–303, 2001.
- [9] L. S. Roach, H. Song, and R. F. Ismagilov. Controlling nonspecific protein adsorption in a plug-based microfluidic system by controlling interfacial chemistry using fluorinated-phase surfactants. *Analytical Chemistry*, 77:785–796, 2005.
- [10] R. E. Treybal. Mass transfer operations. *McGraw-Hill Publishing Co.*, 3rd edition, 1980.

-
- [11] J. C. Godfrey and M. J. Slater. Liquid-liquid extraction equipment. *John Wiley and Sons*, 1994.
- [12] J. R. Burns and C. Ramshaw. Developement of a microreactor for chemical production. *Transaction of the Institution of Chemical Engineers*, 77A:206–211, 1999.
- [13] I. Robins, J. Shaw, B. Miller, C. Turner, and M. Harper. Solute transfer by liquid/liquid exchange without mixing in micro-contactors devices. in *Ehrfeld, W.(Ed.) Microreaction Technology, Proceedings of the 1st International Conference on Microreaction Technology; IMRET 1, Springer-Verlag, Berlin*, pages 35–46, 1997.
- [14] W. E. TeGrotenhuis, R. J. Cameron, M. G. Butcher, P. M. Martin, and R. S. Wegeng. Microchannel devices for efficient contact of liquids in solvent extraction. *Separation Science and Technology*, 34:951–974, 1999.
- [15] *Clarkson University, Department of Biochemical and Chemical Engineering, New York, USA, <http://www.clarkson.edu/chemeng/faculty/jachuck.html>*.
- [16] J. M. Köhler, Th. Henkel, A. Grodrian, Th. Kirner, M. Roth, K. Martin, and J. Metze. Digital reaction technology by micro segmented flow-components, concepts and applications. *Chemical Engineering Journal*, 101:201–216, 2004.
- [17] M. A. Burns, B. N. Johnson, S. N. Brahmaandra, K. Handique, J. R. Webster, M. Krishnan, T. S. Sammarco, P. M. Man, D. Jones, D. Heldsinger, C. H. Mastrangelo, and D. T. Burke. An integrated nanoliter DNA analysis device. *Science*, 282:484–487, 1998.
- [18] H. Song and R. F. Ismagilov. Millisecond kinetics on a microfluidic chip using nanoliters of reagents. *Journal of American Chemical Society*, 125:14613–14619, 2003.
- [19] B. Zheng, S. L. Roach, and R. F. Ismagilov. Screening of protein crystallization conditions on a microfluidic chip using nanoliter-size droplets. *Journal of American Chemical Society*, 125:11170–11171, 2003.
- [20] A. Paglianti, M. Giona, and A. Soldati. Characterization of subregimes in two-phase slug flow. *International Journal of Multiphase Flow*, 22(4):783–796, 1996.
- [21] K. Mishima and T. Hibiki. Some characteristics of air-water two-phase flow in small diameter vertical tubes. *International Journal of Multiphase Flow*, 22:703–712, 1996.

-
- [22] K. A. Triplett, S. M. Ghiaasiaan, S. I. Abdel-Khalik, and D. L. Sadowski. Gas-liquid two-phase flow in microchannels part I: two-phase flow patterns. *International Journal of Multiphase Flow*, 25:377–394, 1999.
- [23] M. Kreutzer. Hydrodynamics of Taylor flows in capillaries and monolith reactors. *Ph.D Thesis, Delft University Press, Netherlands*, 2003.
- [24] M. J. Simmons, D. C. Y. Wong, P. J. Travers, and J. S. Rothwell. Bubble behaviour in three phase capillary microreactors. *International Journal of Chemical Reactor Engineering*, 1:A30, 2003.
- [25] T. C. Thulasidas, M. A. Abraham, and R. L. Cerro. Bubble train flow in capillaries of circular and square cross section. *Chemical Engineering Science*, 50:183–199, 1995.
- [26] G. Bercic and A. Pinter. The role of gas bubbles and liquid slug lengths on mass transport in the Taylor flow through capillaries. *Chemical Engineering Science*, 52:3709–3719, 1997.
- [27] T. Elperin and A. Fominykh. Mass transfer during gas absorption in a vertical gas-liquid slug flow with small bubbles in liquid plugs. *Heat and Mass Transfer*, 33:489–494, 1998.
- [28] T. C. Thulasidas, M. A. Abraham, and R. L. Cerro. Flow pattern in liquid slugs during bubble train flow inside capillaries. *Chemical Engineering Science*, 52:2947–2962, 1997.
- [29] S. Devasenthipathy, J. G. Santiago, S. T. Wereley, C. D. Meinhart, and K. Takehara. Particle imaging techniques for microfabricated fluidic systems. *Experiments in Fluids*, 34:504–514, 2003.
- [30] T. Kraus, A. Günther, N. de Mas, M. A. Schmidt, and K. F. Jensen. An integrated multiphase flow sensor for microchannels. *Experiments in Fluids*, 36:819–832, 2004.
- [31] T. Taha and Z. F. Cui. Hydrodynamics of slug flow inside capillaries. *Chemical Engineering Science*, 59:1181–1190, 2004.
- [32] J. M. van Baten and Krishna R. CFD simulations of mass transfer from Taylor bubbles rising in circular capillaries. *Chemical Engineering Science*, 59:2535 – 2545, 2004.
- [33] G. W. Hodgson and M. E. Charles. The pipeline flow of capsules, part 1: Theoretical analysis of the concentric flow of cylindrical forms. *Canadian Journal of Chemical Engineering*, 41:43–45, 1963.

-
- [34] M. E. Charles. The pipeline flow of capsules, part 2: The concept of capsule pipelining. *Canadian Journal of Chemical Engineering*, pages 46–51, 1963.
- [35] J. R. Burns and C. Ramshaw. The intensification of rapid reactions in multiphase systems using slug flow in capillaries. *Lab on a Chip*, 1:10–15, 2001.
- [36] N. Harries, J. R. Burns, D. A. Barrow, and C. Ramshaw. A numerical model for segmented flow in a microreactor. *International Journal of Heat and Mass Transfer*, 46:3313–3322, 2003.
- [37] H. Song, M. R. Bringer, J. D. Tice, C. J. Gerdt, and R. F. Ismagilov. Experimental test of scaling of mixing by chaotic advection in droplets moving through microfluidic channels. *Applied Physics Letters*, 83:4664–4666, 2003.
- [38] J. D. Tice, H. Song, A. D. Lyon, and R. F. Ismagilov. Formation of droplets and mixing in multiphase microfluidics at low values of the Reynolds and the Capillary numbers. *Langmuir*, 19:9127–9133, 2003.
- [39] J. D. Tice, A. D. Lyon, and R. F. Ismagilov. Effects of viscosity on droplet formation and mixing in microfluidic channels. *Analytica Chimica Acta*, 507:73–77, 2004.
- [40] D. L. Chen, C. J. Gerdt, and R. F. Ismagilov. Using microfluidics to observe the effect of mixing on nucleation of protein crystals. *Journal of American Chemical Society*, 127:9672–9673, 2005.
- [41] H. Song, H.-W. Li, M. S. Munson, T. G. Van Ha, and R. F. Ismagilov. On-chip titration of an anticoagulant Argatroban and determination of the clotting time within whole blood or plasma using a plug-based microfluidic system. *Analytical Chemistry*, 78:4839–4849, 2006.
- [42] W. Tanthapanichakoon, N. Aoki, K. Matsuyama, and K. Mae. Design of mixing in microfluidic liquid slugs based on a new dimensionless number for precise reaction and mixing operations. *Chemical Engineering Science*, 61:4220–4232, 2006.
- [43] W. Tanthapanichakoon, K. Matsuyama, N. Aoki, and K. Mae. Design of microfluidic slug mixing based on the correlation between a dimensionless mixing rate and a modified peclet number. *Chemical Engineering Science*, 61:7386–7392, 2006.
- [44] A. Kawahara, P. M.-Y. Chung, and M. Kawaji. Investigation of two-phase flow pattern, void fraction and pressure drop in a microchannel. *International Journal of Multiphase Flow*, 28:1411–1435, 2002.

-
- [45] A. Ousaka, A. Kariyasaki, I. Morioka, M. Kiyota, and H. Takano. The flow characteristics of a nearly-equal-density oil-water two-phase flow in horizontal capillary tube. *ASME/JSME Joint Thermal Engineering Conference*, pages 113–118, 1995.
- [46] A. Beretta, P. Ferrari, L. Gabiati, and P.A. Andreini. Horizontal oil-water flow in small diameter tubes. flow patterns. *International Communications in Heat and Mass Transfer*, 24:223–229, 1997.
- [47] Z. Hórvölgyi, E. Kiss, and J. Pinter. Experimental studies on the control of slug flow by interfacial forces in silylated capillaries. *Colloids and Surfaces*, 55:257–270, 1991.
- [48] Z. M. Zorin and N. V. Churaev. Immiscible liquid-liquid displacement in thin quartz capillaries. *Advances in Colloid and Interface Science*, 40:85–102, 1992.
- [49] A. M. Dehkordi. Novel type of impinging streams contactor for liquid-liquid extraction. *Industrial and Engineering Chemistry Research*, 40:681–688, 2001.
- [50] L. A. Robbins. Liquid-liquid extraction: a pretreatment process for waste water. *Chemical Engineering Progress*, 76:58–61, 1980.
- [51] R. E. Treybal. Liquid extraction. *McGraw-Hill, New York*,, 2nd edition, 1963.
- [52] A. M. Dehkordi. Liquid-liquid extraction with an interphase chemical reaction in an air-driven two-impinging-streams reactor: effective interfacial area and overall mass transfer coefficient. *Industrial and Engineering Chemistry Research*, 41:4085–4093, 2002.
- [53] A. M. Dehkordi. Experimental investigation of an air-operated two-impinging-streams reactor for copper extraction processes. *Industrial and Engineering Chemistry Research*, 41:2512–2520, 2002.
- [54] R. Gruber. Radial mass transfer enhancement in bubble train flow. *Ph.D. Thesis, RWTH Aachen, Germany*, 2001.
- [55] J. R. Burns and C. Ramshaw. A microreactor for the nitration of benzene and toluene. *Chemical Engineering Communications*, 189:1611–1628, 2002.
- [56] K. R. Westerterp, L. L. van Dierendonck, and J. A. De Kraa. Interfacial areas in agitated gas-liquid contactors. *Chemical Engineering Science*, 18:157–176, 1963.
- [57] A. K. Nanda and M. M. Sharma. Effective interfacial area in liquid-liquid extraction. *Chemical Engineering Science*, 21:707–713, 1966.

-
- [58] S. Alwan, S. Hiraoka, and I. Yamada. Extraction rate of n-amyl acetate with alkaline hydrolysis in aqueous phase. *Chemical Engineering Communications*, 22:317–328, 1983.
- [59] J. B. Fernandes and M. M. Sharma. Effective interfacial area in agitated liquid-liquid contactors. *Chemical Engineering Science*, 22:1267–1282, 1967.
- [60] B. D. Prasher. Mass transfer coefficients and interfacial areas in agitated dispersions. *AIChE Journal*, 21(2):407–409, 1975.
- [61] B. Weinstein and R. E. Treybal. Liquid-liquid contacting in unbaffled, agitated vessels. *AIChE Journal*, 19:304–312, 1973.
- [62] M. M. Sharma and A. K. Nanda. Extraction with second order reaction. *Transaction of the Institution of Chemical Engineers*, 46:44–52, 1968.
- [63] S. A. Puranik and M. M. Sharma. Effective interfacial area in packed liquid extraction columns. *Chemical Engineering Science*, 25:257–266, 1970.
- [64] A. Alper. Effective interfacial area in the RTL extractor from rates of extraction with chemical reaction. *Chemical Engineering Research and Design*, 66(2):147–151, 1988.
- [65] M. N. Kashid and D. W. Agar. Hydrodynamics of liquid-liquid slug flow capillary microreactor: flow regimes, slug size and pressure drop. *Chemical Engineering Journal*, 131:1–13, 2007.
- [66] J. Crank. The mathematics of diffusion. *Clarendon Press, Oxford*, 2nd Edn, 1975.
- [67] J. Bico and D. Quere. Liquid trains in a tube. *Europhysics Letters*, 51:546–550, 2000.
- [68] K. F. Hoettges, D. Stevenson, K. P. Homewood, and R. M. Gwilliam. Liquid-liquid separation. *International Patent*, WO 03/082429:A2, 2003.
- [69] R. Schenk, V. Hessel, C. Hofmann, H. Löwe, and F. Schoenfeld. Novel liquid-flow splitting unit specifically made for numbering-up of liquid/liquid chemical micro processing. *Chemical Engineering and Technology*, 26:1271–1280, 2003.
- [70] R. Schenk, V. Hessel, C. Hofmann, J. Kiss, H. Löwe, and A. Ziogas. Numbering-up of micro devices: a first liquid-flow splitting unit. *Chemical Engineering Journal*, 101:421–429, 2004.
- [71] M. R. Bringer, C. J. Gerdtts, H. Song, J. D. Tice, and R. F. Ismagilov. Microfluidic systems for chemical kinetics that rely on chaotic mixing in droplets.

-
- Philosophical Transactions of The Royal Society of London Series A*, 362:1087–1104, 2004.
- [72] K. Handique and M. A. Burns. Mathematical modelling of drop mixing in a slit type microchannel. *Journal of Micromechanics and Microengineering*, 11:548–554, 2001.
- [73] N. Aoki, S. Hasebe, and K. Mae. Mixing in microreactors: effectiveness of lamination segments as a form of feed on product distribution for multiple reactions. *Chemical Engineering Journal*, 101:323–331, 2004.
- [74] F. Sarrazin, L. Prat, G. Casamatta, C. Gourdon, and M. Joanicot. Mixing characterization and fast reactions in micro-drops. *Proceedings of 6th international conference on process intensification published by BHR Group Limited, UK*, pages 199–207, 2005.
- [75] F. Sarrazin, K. Loubiere, L. Prat, C. Gourdon, T. Bonometti, and Magnaudet J. Experimental and numerical study of droplets hydrodynamics in microchannels. *AIChE Journal*, 52:4061–4070, 2006.
- [76] C. D. Meinhart, S. T. Wereley, and M. H. B. Gray. Volume illumination for two-dimensional particle image velocimetry. *Measurement Science and Technology*, 11:809–814, 2000.
- [77] C. T. Pan, H. S. Chuang, C. Y. Cheng, and C. T. Yang. Micro-flow measurement with a laser diode micro-particle image velocimetry. *Sensors & Actuators A*, 116:51–58, 2004.
- [78] M. R. Bown, J. M. MacInnes, and R. W. K. Allen. Micro-PIV simulation and measurement in complex microchannel geometries. *Measurement Science and Technology*, 16(3):619–626, 2005.
- [79] M. Hoffmann, M. Schlüter, and N. Rübiger. Experimental investigation of liquid liquid mixing in T-shaped micro-mixers using μ -LIF and μ -PIV. *Chemical Engineering Science*, 61:2968–2976, 2006.
- [80] D. M. Curtin, D. T. Newport, and M. R. Davies. Utilising μ -PIV and pressure measurements to determine the viscosity of a DNA solution in a microchannel. *Experimental Thermal and Fluid Science*, 30:843–852, 2006.
- [81] C. Pozrikidis. The buoyancy-driven motion of a train of viscous drops within a cylindrical tube. *Journal of Fluid Mechanics*, 237:627–648, 1992.
- [82] E. I. Shen and K. S. Udell. A finite element study of low Reynolds number two-phase flow in cylindrical tubes. *Journal of Applied Mechanics*, 52:253–256, 1985.

-
- [83] S. Hardt and F. Schonfeld. Simulation of hydrodynamics in multiphase microreactors. *Fifth world congress on computational mechanic, Vienna, Austria*, July 7-12, 2002.
- [84] I. Ming Hsing, R. Srinivasan, M. P. Harold, K. F. Jensen, and M. A. Schmidt. Simulation of micromachined chemical reactors for heterogeneous partial oxidation reactions. *Chemical Engineering Science*, 55:3–13, 2000.
- [85] B. Zou, M. P. Dudukovic, and P. L. Mills. Modelling of evacuated pulse micro-reactors. *Chemical Engineering Science*, 48:2345–2355, 1993.
- [86] D. Bothe, M. Koebe, K. Wielage, and H.-J. Warnecke. VOF-simulations of mass transfer from single bubbles and bubble chains rising in aqueous solutions. In *Proceedings of FEDSM'03: 4th ASME-JSME Joint Fluids Engineering Conference*, Honolulu, Hawaii, USA, 2003.
- [87] G. Cerne, S. Petelin, and I. Tiselj. Coupling of the interface tracking and the two-fluid models for the simulations of incompressible two phase-flow. *Journal of Computational Physics*, 171:776–804, 2001.
- [88] L. Chen and Y. Li. A numerical method for two-phase flows with an interface. *Environmental Modelling and Software*, 13:247–255, 1998.
- [89] J. Li and Y. Renardy. Numerical study of flows of two immiscible liquids at low Reynolds number. *Society for Industrial and Applied Mathematics (SIAM) Review*, 42(3):417–439, 2000.
- [90] S. Turek. Efficient solvers for incompressible flow problems: An algorithmic and computational approach. *Springer-Verlag, Heidelberg*, 1999.
- [91] M. van Sint Annaland, W. Dijkhuizen, N. G. Deen, and J. A. M. Kuipers. Numerical simulation of behaviour of gas bubbles using a 3D front tracking method. *AIChE Journal*, 52:99–110, 2006.
- [92] C. W. Hirt and B. D. Nichols. Volume of fluid (VOF) method for the dynamics of free boundaries. *Journal of Computational Physics*, 39:201–225, 1981.
- [93] S. Hysing. A new implicit surface tension implementation for interfacial flows. *International Journal of Numerical Methods in Fluids*, 51:659–672, 2006.
- [94] J. U. Brackbill, D. B. Kothe, and C. Zemach. A continuum method for modelling surface tension. *Journal of Computational Physics*, 100:335–354, 1992.
- [95] P. R. Gunjal. Flow modeling and mixing in packed bed reactor. *PhD Thesis, IIT Mumbai, India*, 2005.

-
- [96] R. I. Issa and M. H. W. Kempf. Simulation of slug flow in horizontal and nearly horizontal pipes with the two-fluid model. *International Journal of Multiphase Flow*, 29:69–95, 2003.
- [97] P. R. Gunjal, V. V. Ranade, and R. V. Chaudhari. Dynamics of drop impact on solid surface: experiments and VOF simulations. *AIChE Journal*, 51:59–78, 2005.
- [98] R. Rieger, C. Weiss, G. Wigley, H. J. Bart, and R. Marr. Investigating the process of liquid-liquid extraction by means of computational fluid dynamics. *Computers and Chemical Engineering*, 20:1467–1475, 1996.
- [99] W. H. Piarah, A. Paschedag, and M. Kraume. Numerical simulation of mass transfer between a single drop and an ambient flow. *AIChE Journal*, 47:1701–1704, 2001.
- [100] C. Yang and Z.-S. Mao. Numerical simulation of interphase mass transfer with the levelset approach. *Chemical Engineering Science*, 60:2643–2660, 2005.
- [101] A. Pawelski, A. R. Paschedag, and M. Kraume. Unsteady mass transfer in single droplets with a superimposed chemical reaction. *3rd international Berlin workshop on transport phenomena with moving boundaries, Germany*, pages 75–88, October, 2005.
- [102] A. Ouazzi. Finite element simulation of non-linear fluids with application to granular material and powder. *PhD Thesis*, University of Dortmund, 2006.
- [103] D. Kuzmin and S. Turek. Finite element discretization tools for gas-liquid flows. in: M. sommerfeld (ed.), *bubbly flows: Analysis, modelling and calculation*. *Springer-Verlag*, pages 191–201, 2004.
- [104] C. Kiparissides. Polymerization reactor modeling: A review of recent developments and future directions. *Chemical Engineering Science*, 51:1637–1659, 1996.
- [105] R. Byron Bird, W. E. Stewart, and E. N. Lightfoot. *Transport phenomena*. *John Wiley and Sons*, 2, 2002.
- [106] R. P. Verma and M. M. Sharma. Mass transfer in packed liquid-liquid extraction columns. *Chemical Engineering Science*, 30:279–292, 1975.
- [107] S. Sarkar, J. Mumford, and C. Philipps. Liquid-liquid extraction with interphase chemical reaction in agitated columns: 2. hydrodynamics and mass transfer in rotating disk and oldshue rushton contactors. *Industrial and Engineering Chemistry Process Design and Development*, 19:672–679, 1980.

- [108] P. V. Danckwerts. Gas-liquid reactions. *McGraw-Hill, New York*, 1970.
- [109] B. A. A. van Woezik and K. R. Westerterp. Measurement of interfacial areas with the chemical method for a system with alternating dispersed phases. *Chemical Engineering and Processing*, 39:299–314, 2000.
- [110] B. Ghosh, D. C. Mukherjee, S. Bhattacharjee, and B. Chaudhari. Alkaline hydrolysis of isoamylformate: effect of dissolved electrolytes on kinetics. *Canadian Journal of Chemical Engineering*, 79:148, 2001.

Curriculum Vitae

Personal data

Full Name: Madhvanand Namadeo Kashid
Birth Date: 15th February, 1980
Birth Place: Sonand (Dist - Solapur)
Permanent Address: Gherdi Road, Sonand (Dist - Solapur)
Maharashtra, India - 413 309
Present Address: Route de Vallaire 82
CH-1024 Ecublens, Switzerland

Education

- **Doctoral student in Chemical Engineering** (2003 - 2007)
Department of Biochemical and Chemical Engineering
University of Dortmund, 44221 Dortmund, Germany
- **Masters (M.Tech.) in Chemical Engineering** (2001 - 2003)
Dr. Babasaheb Ambedkar Technological University
Lonere-Raigad, India - 402 103
- **Bachelors (B.E.) in Chemical Engineering** (1997 - 2001)
Shivaji University (D. Y. Patil College of Engineering and Technology)
Kolhapur, India - 413 006

Experience

- **Scientific Collaborator** (Jun. 2007 - until now)
Group of Catalytic Reaction Engineering (GGRC)
Ecole Polytechnique Federale de Lausanne (EPFL)
CH-1015 Lausanne, Switzerland
- **Research Assistant** (2003 - 2007)
University of Dortmund, 44221 Dortmund, Germany
- **Project Assistant - II** (Mar. 2003 - Oct. 2003)
National Chemical Laboratory, Pune, India - 411 008